UNIVERSITE DE LIEGE
Faculté des Sciences

Laboratoire de Spectrométrie de Masse
Professeur E. DE PAUW

A STUDY OF NONCOVALENT INTERACTIONS BY ELECTROSPRAY MASS SPECTROMETRY

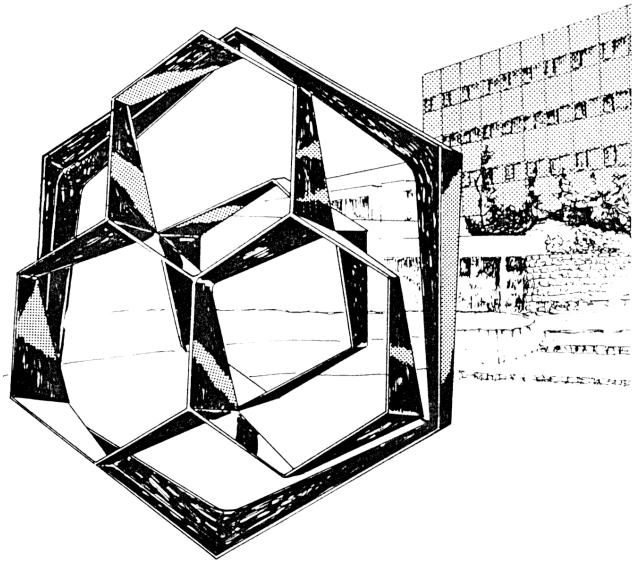

Dissertation présentée par

Valérie GABELICA

pour l'obtention du grade de
Docteur en Sciences
Année Académique 2001 - 2002

ABSTRACT

This work describes a study of noncovalent interactions by electrospray mass spectrometry (ES-MS). In particular, we studied DNA duplexes, DNA complexes with drugs and cyclodextrin complexes with aliphatic acids. ES-MS experiments were performed on a hybrid quadrupole-TOF instrument and on an ion trap instrument. Basically two kinds of information can be obtained on the complexes. First, the full scan mass spectra give information on the composition of the solution that is injected, and therefore on the solution-phase stability of the complexes. We compare the ES-MS data with the solution-phase data, and discuss the specificity of the observed complexes. The problem of nonspecific aggregation was encountered for the hydrophobic cyclodextrin complexes. We developed a new method for determining simultaneously the equilibrium association constant of [1:1] complexes and the ratio between the electrospray response factors of the complex and the free substrate. A change in the substrate conformation upon ligand binding can be detected by measuring the response factors of the complex and the free host. Second, the collision-induced dissociation of the complexes in the gas phase and the measurement of the amounts of fragments resulting from this dissociation give information on the gas-phase kinetic stability of the complexes. It is shown that different collision regimes allow the system to fragment via different pathways, and that fast activation conditions favor the noncovalent dissociation of the complex because this process is entropy-favored. The gas-phase kinetic stability measurements on series of homologous complexes suggest that intermolecular interactions like hydrogen bonding, electrostatic interactions, and stacking are conserved in the gas phase. Finally, on the basis of the results obtained on DNA duplexes, we propose a general multistep mechanism for the dissociation of noncovalent complexes.

RÉSUMÉ

Ce travail décrit l'étude des interactions non-covalentes par spectrométrie de masse couplée à l'électronébulisation (ES-MS). En particulier, nous avons étudié des duplex d'ADN, des complexes entre ces duplex et des drogues, et des complexes de cyclodextrines avec des acides aliphatiques. Les expériences ont été réalisées sur un spectromètre hybride quadripole-TOF et sur un spectromètre de type piège à ions quadripolaire. Deux types d'informations distinctes peuvent être obtenues sur les complexes. Premièrement, les spectres de masse simples renseignent sur les espèces présentes dans la solution injectée, et donc sur la stabilité en solution des complexes. Nous avons comparé les données en solution et les résultats obtenus en ES-MS pour discuter de la spécificité des complexes observés. Nous avons détecté une agrégation non-spécifique pour les complexes hydrophobes de cyclodextrines. Une nouvelle méthode a été établie pour déterminer simultanément la constante d'équilibre d'association d'un complexe [1:1] ainsi que le rapport entre les facteurs de réponse du complexe et du substrat libre. Le changement de conformation du substrat causé par la fixation du ligand se reflète dans les facteurs de réponse. Deuxièmement, la dissociation des complexes induite par collision et la mesure des intensités relatives des fragments en fonction de l'énergie collisionnelle donnent des informations sur la stabilité cinétique des complexes en phase gazeuse. Nous avons montré que des régimes de collision différents favorisaient des canaux de réaction différents, et que la dissociation du complexe non-covalent en ses ligands constitutifs était favorisée par un régime d'activation rapide, ce processus étant favorisé entropiquement. Les mesures de stabilité cinétique en phase gazeuse sur des séries de complexes homologues suggèrent que les interactions intermoléculaires telles les interactions électrostatiques, les liaisons hydrogène et les interactions d'empilement sont conservées dans les complexes isolés en l'absence de solvant. Enfin, sur base de différents résultats obtenus sur des duplex d'ADN, nous avons proposé un mécanisme multi-étapes pour rendre compte de la dissociation des complexes non-covalents en général.

ABBREVIATIONS AND ACRONYMS

A	Arrhenius pre-exponential factor
A	Adenine
BIRD	Blackbody infrared radiative dissociation
C	Cytosine
α-CD	α-Cyclodextrin
CD	Cyclodextrin
CID	Collision-induced dissociation
DNA	Desoxyribonucleic acid
DOF	Degrees of freedom
E_0	Threshold energy for dissociation
E_a	Arrhenius activation energy
E_r	Reverse energy barrier
ES	Electrospray
FTICR	Fourier transform ion cyclotron resonance
G	Guanine
ICR	Ion cyclotron resonance
MCP	Microchannel plate
MH	Maltohexaose

MS	Mass spectrometry
MS/MS	Tandem mass spectrometry
m/z	Mass-to-charge ratio
NMR	Nuclear magnetic resonance
$P(E)$	Internal energy distribution
QIT	Quadrupole ion trap
Q-TOF	Hybrid quadrupole – time-of-flight
RNA	Ribonucleic acid
RRK	Rice-Rampsberger-Kassel
RRKM	Rice-Rampsberger-Kassel-Marcus
T	Thymine
T_{cap}	Heated capillary temperature
TDC	Time-to-digital converter
T_{eff}	Effective temperature
TLO	Tube lens offset
T_m	Melting temperature
TOF	Time-of-flight
UV	Ultraviolet
V_{CS}	Capillary-skimmer voltage difference

1. NONCOVALENT INTERACTIONS

1.1. Supramolecular chemistry[1]

Molecular chemistry is the science of building molecular structures by breaking and forming covalent bonds between atoms in a controlled manner. Supramolecular chemistry deals with the next step in the complexity of life, after elementary particles, atoms and molecules: how do molecules interact with each other by noncovalent bonds to form complexes? Intermolecular interactions are responsible for highly specific processes of recognition, reaction, transport and regulation occurring in a living cell. The fundamental understanding of these noncovalent interactions is necessary to understand these specific biological processes.

1.2. Classification of the interactions

A compound problem

The need for understanding the nature of these noncovalent interactions automatically brought about the need for a rationalization by means of a decomposition of the overall effect into distinct components. Research areas like drug design can greatly benefit from predictive tools characterizing the *affinity* and the *specificity* of a potential ligand for its target. This leads to the “rational drug design” approach.

The *affinity* of a heteronuclear complex AB (eq. 1.1) is characterized by a binding constant, or association constant K_a (eq. 1.2) related to the standard free energy of association $\Delta G°_a$ (eq. 1.3), which has an enthalpic contribution $\Delta H°_a$ and an entropic contribution $\Delta S°_a$ (eq. 1.4). This can be expressed in an equivalent manner in terms of dissociation instead of association.

$$A + B \rightleftharpoons AB \tag{1.1}$$

$$K_a = \frac{[AB]}{[A][B]} = \frac{1}{K_d} \tag{1.2}$$

$$\Delta G°_a = -RT \ln K_a = -\Delta G°_d \tag{1.3}$$

$$\Delta G°_a = \Delta H°_a - T\Delta S°_a \tag{1.4}$$

The decomposition of the overall interaction into distinct contributions leads to a decomposition of $\Delta G°$ into a sum of terms, and of K in a product of terms[2-5]. A predictive tool based on such an approach takes the form of an incremental method. The contributions that are most often distinguished are electrostatic interactions, hydrogen bonding, Van der Waals forces and hydrophobic effects, but there are also some conformational changes, loss of translational and rotational degrees of freedom and creation of vibrational modes, induction forces, charge transfer, steric effects, stacking,[1,6-13]… The relative contribution of all these parameters to the observed binding constant is hard to establish, and the role of the solvent is a critical part of the problem. For example, a wide controversy exists on whether hydrogen bonds or hydrophobic interactions are responsible for the affinity and specificity of protein complexes[14-18].

Origin of the confusion

Two review articles, one by Connors on cyclodextrin complexes[7] and one by Janin on protein-protein recognition[8], are enlightening on the origin of the confusion that is encountered in so many papers. The thermodynamics of noncovalent interactions can be described at three different levels.

At the phenomenological level, pairwise (or higher level) interactions, such as solute-solute, solute-solvent and solvent-solvent, are identified and assigned quantitative roles. For a complex AB, the complexation reaction (eq. 1.1) can be rewritten, explicitly mentioning the solvation shell of the molecules:

$$\mathbf{A}.nH_2O + \mathbf{B}.mH_2O \rightleftharpoons \mathbf{AB}.xH_2O + (n+m-x)\,H_2O \qquad (1.5)$$

As thermodynamic parameters are measured in solution, their values reflect the overall process taking place in the given solvent (eq. 1.5), and not just the intermolecular interaction as in equation (1.1). The pure intermolecular interaction in the absence of solvent is identical to the interaction the partners would undergo in the gas phase. The gas phase and the solution phase association thermodynamics constants can be related by the appropriate thermodynamic cycle[19] including the transfer from the gas phase to the solution for each species (Figure 1-1).

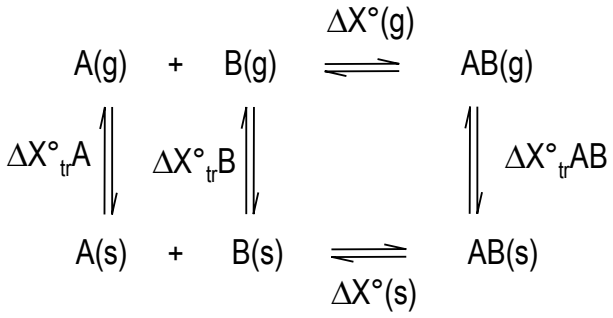

Figure 1-1. Thermodynamic cycle[19] for complex formation. ΔX stands for ΔH, ΔS or ΔG. The interaction in the gas phase (g) is purely intermolecular. The interaction in the solvent (s) depends on the intermolecular interaction and on the solvation of the species (tr = transfer between the two phases).

The interaction forces can also be described **at the physical level**. Electrostatic interactions include Coulombic forces (between two permanent multipoles), induction forces (between one permanent multipole and one induced multipole) and dispersion forces (Table 1-1). The term "Van der Waals forces" is generally used to describe all

forces with $1/r^6$ distance dependence, but this may differ from one author to another. All these interactions can be expressed classically[20]. Two non-classical terms are subsequently introduced in quantum calculations: an exchange interaction (global delocalization of the electrons on the supermolecule AB) and a charge transfer interaction (partial transfer of the electrons from A to B or vice versa)[21].

Table 1-1. Classical electrostatic interactions and their distance dependence.

COULOMBIC FORCES	
Ion-Ion	$1/r$
Ion-Dipole	$1/r^2$
Dipole-Dipole	$1/r^3$
Quadrupole-Quadrupole	$1/r^5$
INDUCTION FORCES	
Ion-Induced dipole	$1/r^4$
Dipole-Induced dipole	$1/r^6$
DISPERSION FORCES	
Induced dipole-Induced dipole	$1/r^6$

The third level, **the chemical level**, is entirely a consequence of the other two[7]. It embodies salt bridges, hydrogen bonding, hydrophobic interactions, π–π stacking, steric effects… This level is useful for the description of the complexation phenomenon because the interactions can be "visualized" easily in a given structure, and can provide reference marks for interpretations and predictions. The problem is

that mixing the three levels carries the potential for confusion as a result of "double counting".

Salt bridges are the ion-ion interactions between opposite charges. Hydrogen bonds are also of electrostatic nature (ion-dipole if the donor group is positively charged or dipole-dipole if it is neutral), but they are often distinguished from other interactions because they can be visualized easily in a structure. Stacking of aromatic molecules are sometimes represented as an overlap between out-of-plane p-based molecular orbitals, but their interactions are also of electrostatic nature. They are short range interactions (dipole-dipole or weaker), and are thus highly conformation-dependent[6,22,23].

Establishing the nature of hydrophobic interactions is a more difficult problem. In many articles, no definition of hydrophobicity is even given. We will adopt the following one[16]: "Hydrophobicity (…) is the operational process in which a nonpolar group is transferred from a polar or neutral phase to a nonpolar phase". The driving force is the solvent reorganization[24-27]: at hydrocarbon/water interfaces, water molecules form more highly ordered hydrogen-bonded structures than in the bulk solvent. Nonpolar groups have a preference for nonpolar phases. This minimizes the area of the hydrocarbon/water interfaces and therefore maximizes the entropy of the whole system. During complex formation, when the nonpolar groups of A and B come close to each other so that their Van der Waals surfaces are in contact, the area of the hydrocarbon/water interface decreases. The hydrophobic contribution to the complex formation can be correlated with the difference in solvent-accessible surface area (Δ_{SASA}) between the complex and in its separate constituents[6,14,28,29].

The role of the solvent in the complex formation is not limited to the hydrophobic effect, but it also affects other types of interactions, compared to the gas phase situation. Due to the high dielectric constant, the bulk solvent is shielding all electrostatic interactions. The same holds for the counter-ionic atmosphere (salts present in solution). At the microscopic level, water dipoles are strong competitors for forming electrostatic interactions, especially hydrogen bonds, with the substrates. This emphasizes the role of solute-solvent and solvent-solvent interactions in the phenomenological description of the complexation process.

1.3. Specificity of a complex

In a molecular recognition process, given substrate and ligand undergo noncovalent interactions with each other, some of which being impossible with other molecules than the partner, even if such molecules are chemically very similar. This discriminating quality is known as *specificity*[1]. The specificity of a complex depends on its affinity constant (an intrinsic parameter), but has to be defined in a context of competition with other interactions.[8,30] For a given substrate-ligand complex, competition can arise from different possible binding sites in the substrate, from different conformations of the complex (different orientations of the ligand in the binding site), or from competition with other ligands that are in the medium. The specificity depends on how more stable is the native state (the right ligand, in the right site, in the right position) compared to all other possible states.

1.4. Why studying noncovalent complexes by mass spectrometry?

There are two important issues that can be addressed adequately with mass spectrometric techniques. The first one is the analysis of the composition of complex mixtures. The different species can be identified by their masses. In traditional spectrophotometric methods, the signal detected results from the sum of the contributions of all the species present in solution (the complex of interest, plus the free ligands, the buffer, the solvent,…). This is especially important for the determination of the specificity, which is defined in a context of competition in the given medium. The second issue is the study of the different contributions to the binding affinity and specificity. Mass spectrometry has the unrivalled ability to study isolated molecules in the gas phase (in the absence of solvent, buffer,…), and therefore to study the sole contribution of the intermolecular interactions.

Noncovalent complexes are transferred in the gas phase by an electrospray source, which mechanism is described in Chapter 2. Some theoretical considerations on the dissociation kinetics in mass spectrometry are given in Chapter 3, and the current state of the art of noncovalent complex studies by mass spectrometry is reviewed in Chapter 4.

References

1. J.-M. Lehn *La Chimie Supramoléculaire*; De Boeck & Larcier s.a.: Paris, 1997.
2. S. Boresch, M. Karplus; The Meaning of Component Analysis: Decomposition of the Free Energy in Terms of Specific Interactions. *J. Mol. Biol.* **1995,** 254: 801.
3. H.-J. Schneider; Mechanisms of Molecular Recognition: Investigations of Organic Host-Guest Complexes. *Angew. Chem. Int. Ed. Engl.* **1991,** 30: 1417.
4. H.-J. Schneider, T. Schiestel, P. Zimmermann; The Incremental Approach to Noncovalent Interactions: Coulomb and Van Der Waals Effects in Organic Ion Pairs. *J. Am. Chem. Soc.* **1992,** 114: 7698.
5. H.-J. Schneider; Linear Free Energy Relationships and Pairwise Interactions in Supramolecular Chemistry. *Chem. Soc. Rev.* **1994,** 227.
6. C.A. Hunter; The Role of Aromatic Interactions in Molecular Recognition. *Chem. Soc. Rev.* **1994,** 101.
7. K.A. Connors; The Stability of Cyclodextrin Complexes in Solution. *Chem. Rev.* **1997,** 97: 1325.
8. J. Janin; Protein-Protein Recognition. *Prog. Biophys. Mol. Biol.* **1995,** 64: 145.
9. T. Hermann; Strategies for the Design of Drugs Targeting RNA and RNA-Protein Complexes. *Angew. Chem. Int. Ed. Engl.* **2000,** 39: 1890.
10. D.H. Williams, J.P.L. Cox, A.J. Doig, M. Gardner, U. Gerhard, P.T. Kaye, A.R. Lal, I.A. Nicholls, C.J. Salter, R.C. Mitchell; Toward the Semiquantitative Estimation of Binding Constants. Guides for Peptide-Peptide Binding in Aqueous Solution. *J. Am. Chem. Soc.* **1991,** 113: 7020.
11. M. Schapira, M. Totrov, R. Abagyan; Prediction of the Binding Energy for Small Molecules, Peptides and Proteins. *J. Mol. Recognit.* **1999,** 12: 177.
12. N. Horton, M. Lewis; Calculation of the Free Energy of Association for Protein Complexes. *Protein Sci.* **1992,** 1: 169.

13. J.B. Chaires; Dissecting the Free Energy of Drug Binding to DNA. *Anti-Cancer Drug Design* **1996,** 11: 569.

14. C. Chothia, J. Janin; Principles of Protein-Protein Recognition. *Nature* **1975,** 256: 705.

15. W.E. Stites; Protein-Protein Interactions: Interface Structure, Binding Thermodynamics, and Mutational Analysis. *Chem. Rev.* **1997,** 97: 1233.

16. G.D. Rose, R. Wolfenden; Hydrogen Bonding, Hydrophobicity, Packing and Protein Folding. *Annu. Rev. Biomol. Struct.* **1993,** 22: 381.

17. C.N. Pace; Evaluating Contribution of Hydrogen Bonding and Hydrophobic Binding to Protein Folding. *Methods Enzymol.* **1995,** 259: 538.

18. A.M. Davis, S.J. Teague; Hydrogen Bonding, Hydrophobic Interactions, and Failure of the Rigid Receptor Hypothesis. *Angew. Chem. Int. Ed. Engl.* **1999,** 38: 736.

19. J. Janin; Elusive Affinities. *Proteins* **1995,** 21: 30.

20. B. Honig, A. Nicholls; Classical Electrostatics in Biology and Chemistry. *Science* **1995,** 268: 1144.

21. A. van der Vaart, B.D. Bursulaya, C.L. Brooks, III, K.M. Merz, Jr.; Are Many-Body Effects Important in Protein Folding? *J. Phys. Chem. B* **2000,** 104: 9554.

22. J. Sponer, J. Laszczynski, P. Hobza; Hydrogen Bonding and Stacking of DNA Bases: a Review of Quantum-Chemical Ab Initio Stusies. *J. Biomol. Struct. Dyn.* **1996,** 14: 117.

23. P. Hobza, J. Sponer; Structure, Energetics, and Dynamics of the Nucleic Acid Base Pairs: Nonempirical Ab Initio Calculations. *Chem. Rev.* **1999,** 99: 3247.

24. B. Lee; Analyzing Solvent Reorganization and Hydrophobicity. *Methods Enzymol.* **1995,** 259: 555.

25. E. Grunwald, C. Steel; Solvent Reorganization and Thermodynamic Enthalpy-Entropy Compensation. *J. Am. Chem. Soc.* **1995,** 117: 5687.

26. R.U. Lemieux; How Water Provides the Impetus for Molecular Recognition in Aqueous Solution. *Acc. Chem. Res.* **1996,** 29: 373.

27. H.A. Sheraga; Theory of Hydrophobic Interaction. *J. Biomol. Struct. Dyn.* **1998,** 16: 447.

28. J. Janin; Angströms and Calories. *Structure* **1997,** 5: 473.

29. T. Ooi, M. Oobatake, G. Némethy, H.A. Sheraga; Accessible Surface Areas As a Measure of the Thermodynamic Parameters of Hydration of Peptides. *Proc. Natl. Acad. Sci. USA* **1987,** 84: 3086.

30. J. Janin; Quantifying Biological Specificity: the Statistical Mechanics of Molecular Recognition. *Proteins* **1996,** 25: 438.

2. THE ELECTROSPRAY MECHANISM

The electrospray process is described in detail in several excellent review papers[1-5], and only the key features will be described here.

2.1. Electrolytic vaporization of the solution

The solution containing the analyte is introduced in a capillary on which a high electric field is applied (Figure 2-1). The field causes a separation of the positive and negative charges in the solution. In the positive ion mode (when the capillary is the positive terminal), positive ions tend to move towards the counter-electrode and accumulate at the surface of the liquid at the tip. At a critical field the meniscus at the tip deforms into what is called the "Taylor cone", which continuously produces droplets enriched in positive ions. Reversing the polarity of the power supply can generate negatively charged droplets instead. As electrospray produces a continuous current, redox processes must occur at the capillary and at the counter electrode to avoid charge accumulation[6,7].

In practice, **standard electrospray** proceeds at flow rates of 1 to 100 µL/min. High flow rates are sometimes needed when coupled with separation methods like HPLC, depending on the column. At such flow rates the production of the droplets has to be assisted by a coaxial sheath gas or by ultrasounds (ionspray)[8]. The lower the flow rate, the lesser the need for spray assistance. **Nanospray**[9,10] (flow rate of a few nL/min) is the quintessence of electrospray: the electric field is sufficient to maintain the continuous production of charged droplets. It is also the most sensitive variant of electrospray.

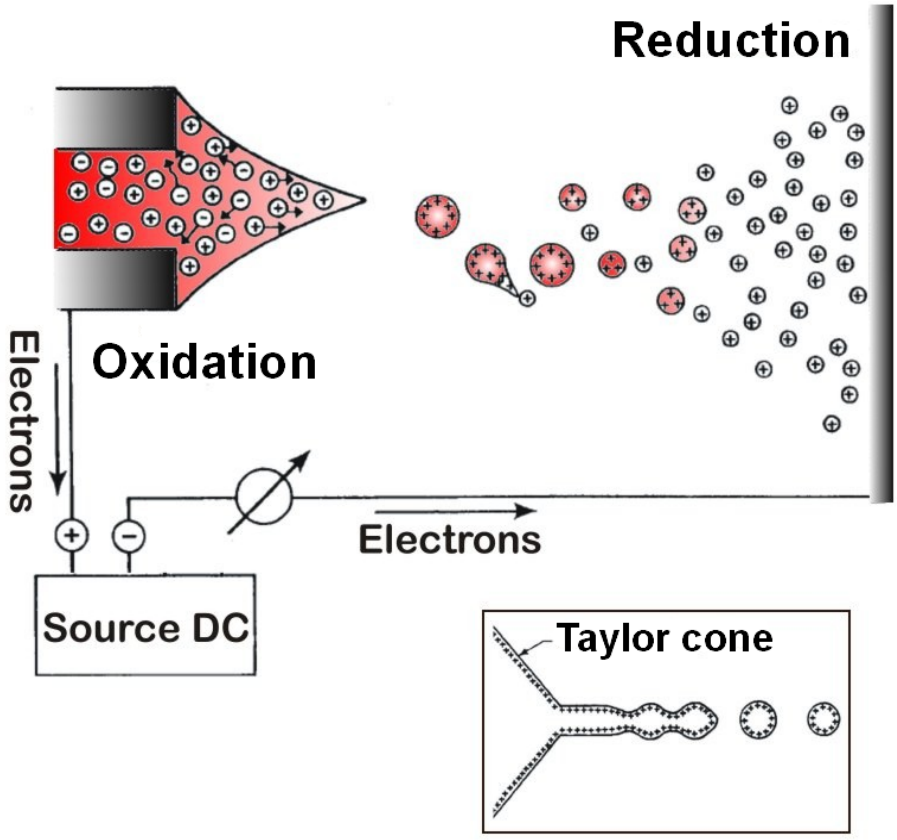

Figure 2-1. Production of charged droplets from the analyte solution. (adapted from reference 5)

2.2. Production of ions from charged droplets

Rayleigh fission of the droplets

Solvent evaporation occurs due to collisions with a neutral gas (heated or not). The radius of the droplet decreases at constant charge until being close to what is called the Rayleigh limit, where the Coulombic repulsion between the charges overcomes the cohesive forces. This leads to the Coulomb fission of the droplet (Figure 2-2): small offspring droplets are produced that carry about 2% of the mass and 15% of the charge of the parent droplet. As evaporation carries on, the daughter droplets undergo fission themselves. This is at the origin of the very rapid reduction in size and charge of the droplets.

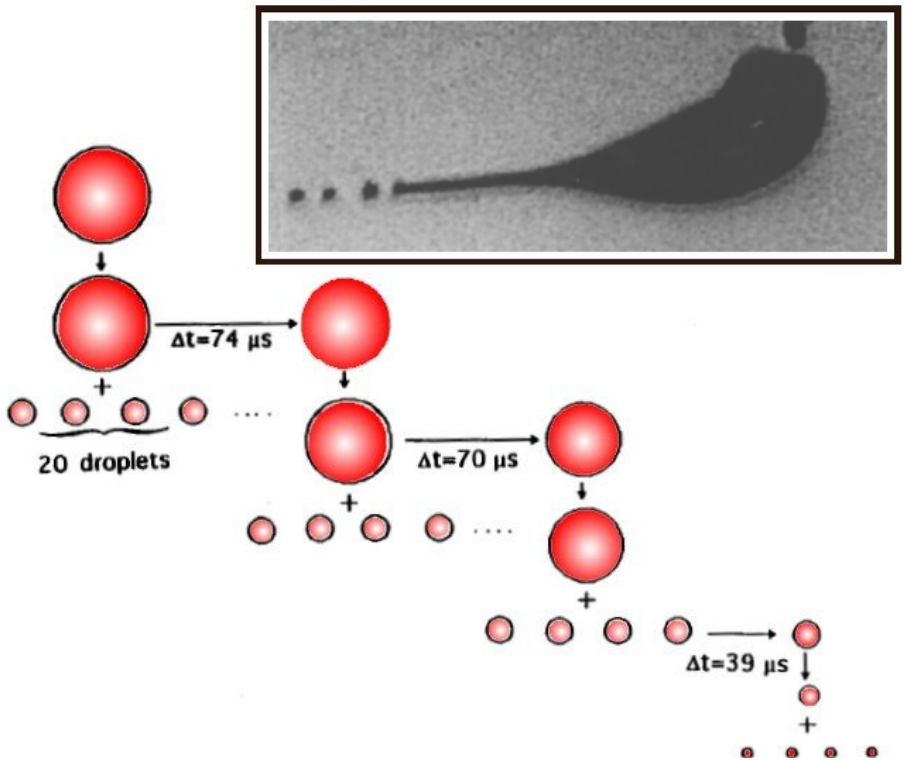

Figure 2-2. Droplet evolution scheme due to solvent evaporation at constant charge and Coulomb fissions at the Rayleigh limit (adapted from reference 5). The inset top right shows a flash shadowgraph of a droplet undergoing uneven Coulomb fission (from reference 11).

Production of desolvated ions

Two mechanisms can account for the production of desolvated ions in the gas phase: the ion evaporation model, proposed by Iribarne and Thomson[12-14] and the charged residue model proposed by Dole[15]. Historically, these models had been proposed before the droplet fission scheme presented in the above section was established. The two models therefore have to be restated as follows[5].

Ion evaporation model

According to this model, at an intermediate stage in the droplet's lifetime (critical radius larger than the Rayleigh limit), the electric field on the surface of the droplet is sufficiently high so that solvated ions are emitted directly from charged droplets. It is

now generally admitted that small ions (salts,…) are produced predominantly by this mechanism[16-18].

Charged residue model

This model assumes that the series of droplet fission events leads to a final droplet containing a single analyte molecule[19]. The last solvent molecules evaporate until the ion is completely desolvated. Large globular proteins are believed to be produced via this mechanism[3,20].

2.3. Transfer of the ions to the mass analyzer

Electrospray is an atmospheric pressure source, but the mass spectrometer must be operated at low pressures (10^{-3} to 10^{-10} Torr, depending on the analyzer). The pressure is usually reduced in multiple stages (differential pumping), the different vacuum chambers being separated by small orifices, or by skimmers (Figure 2-3).

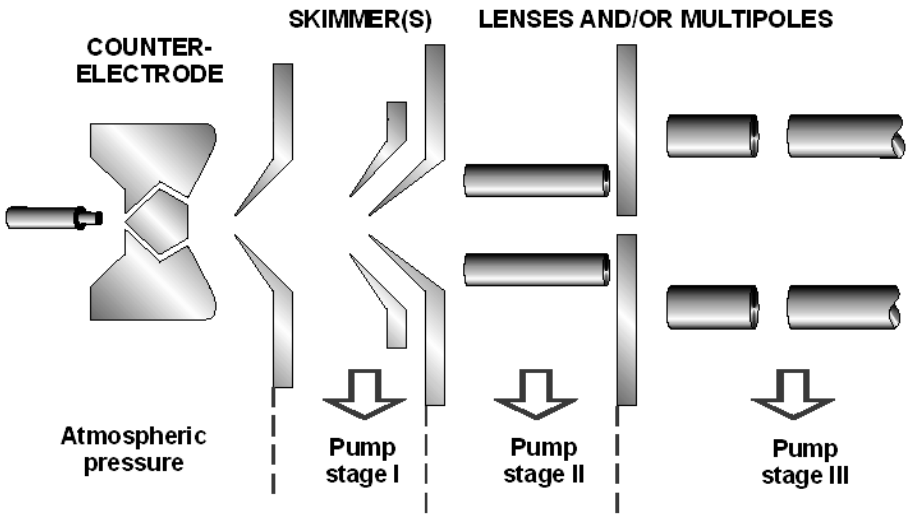

Figure 2-3. Typical instrument configuration for the transfer of the ions from the atmospheric pressure source to the analyzer region (adapted from the Micromass Q-TOF manual). In this case the counter-electrode has a pepperpot design, but this is not a general feature of ES sources.

The counter-electrode contains a hole for the ions to pass through. The skimmer is a cone-shaped metal piece. Voltage differences between the skimmer(s) and the other parts are responsible for the acceleration of the ions and/or of the charged droplets. Collision between the accelerated ions and the ambient gas in a high pressure region (atmospheric pressure or first pumping stage) increases the internal energy of the species: it favors the droplet evaporation and the fragmentation of the ions (collision-induced dissociation, see Chapter 3). The ion guiding system can include electronic lenses and/or RF-only multipoles.

2.4. Dependence of the sensitivity on the analyte

Of major concern to the mass spectrometrist (see Chapter 9) is whether the relative intensities in the MS spectra reflect the relative abundances of the analytes present in solution. The intensity of the signal corresponding to the analyte A^+ depends on its concentration. Its response is defined as R_A in:

$$I_{(A^+)} = R_A.[A^+] \tag{2.1}$$

Discrimination can arise from the mass analyzer, from the detector and from the electrospray process. The effect of the electrospray mechanism on the response of the analyte is discussed in this section in detail.

Ion evaporation model

This model assumes that the rate of evaporation of an ion from the droplet can be described by transition state theory (equation 2.2),

$$k_A = \left(\frac{kT}{h}\right) e^{-\Delta G_A^* / RT} \tag{2.1}$$

where ΔG^* is the free energy difference between the late transition state where an ion-solvent molecule cluster leaves the charged droplet and the initial intact droplet. To describe the analyte dependence of the sensitivity in ES mass spectrometry, Tang and Kebarle[21,22] proposed a model based on the hypothesis that the ion evaporation rate

depends on the concentration in the droplet. For two analytes A and B, the ratio between the intensities is given by:

$$\frac{I_{(A^+)}}{I_{(B^+)}} = \frac{k_A[A^+]}{k_B[B^+]} \tag{2.3}$$

The response factors are therefore proportional to the evaporation rates of the analytes. The comparison between the theoretical results and experiments could however not yet validate this model due to experimental difficulties and uncertainties on the calculation of ΔG*'s[2].

Surface-active analytes

In a paper published in 1993, Tang and Kebarle[22] also mentioned that the surface activity of the analyte should be taken into account, as the ions do evaporate from the surface of the droplet. The ion abundance is therefore proportional to the surface concentration and not on the bulk concentration This gives:

$$\frac{I_{(A^+)}}{I_{(B^+)}} = \frac{K_{S(A)} \cdot k_A[A^+]}{K_{S(B)} \cdot k_B[B^+]} \tag{2.4}$$

where K_S's are constants expressing the surface activity. As ion cluster solvation energies and surface activities are often closely correlated, it is difficult to attribute the relative responses either to the evaporation rate or to the surface activity effect. Moreover, the model does not explain the concentration dependence of the ion intensity on a broad concentration range[22].

Equilibrium partitioning model

In 1997, Enke[23] proposed a model to account for the concentration dependence of analyte response. The equilibrium partitioning model states that, whatever the exact mechanism, as the charges are located on the surface of the droplet, the molecules that are released as ions are those that are present at the surface of the droplet. The surface (which is charged due to an excess of ions of one polarity) is considered as a phase

separated from the neutral interior of the droplet. If the ion partitioning between these two phases is sufficiently rapid, one can define an equilibrium constant between the surface and the interior of the droplet. The concentration of excess charges on the surface of the droplet is determined by the experimental conditions. At low concentration, the surface is not saturated and all ions (for example A and B) can freely access the surface, independently of the equilibrium partitioning constants K_A and K_B. At high concentration, the surface is saturated and the different analytes are in competition for accessing the surface; the different responses will highly depend on K_A/K_B. The behavior at low and high concentration is therefore reconciled in a single model.

It must be emphasized that the surface activity effect can neither be related to the ion evaporation model, nor to the charged residue model. In the uneven Coulomb fission phenomenon, small offspring droplets are emitted from the surface of the parent droplet. Surface-active compounds will therefore be preferentially emitted in these offspring droplets and subsequently end up as free ions.

References

1. S.J. Gaskell; Electrospray: Principles and Practice. *J. Mass Spectrom.* **1997,** 32: 677.

2. P. Kebarle, M. Peschke; On the Mechanisms by Which the Charged Droplets Produced by Electrospray Lead to Gas Phase Ions. *Fres. J. Anal. Chem.* **2000,** 406: 11.

3. R.B. Cole; Some Tenets Pertaining to Electrospray Ionization Mass Spectrometry. *J. Mass Spectrom.* **2000,** 35: 763.

4. M.H. Amad, N.B. Cech, G.S. Jackson, C.G. Enke; Importance of Gas-Phase Proton Affinities in Determining the Electrospray Ionization Response for Analytes and Solvents. *J. Mass Spectrom.* **2000,** 35: 784.

5. P. Kebarle; A Brief Overview of the Present Status of the Mechanisms Involved in Electrospray Mass Spectrometry. *J. Mass Spectrom.* **2000,** 35: 804.

6. A.T. Blades, M.G. Ikonomou, P. Kebarle; Mechanism of Electrospray Mass Spectrometry. Electrospray As an Electrolysis Cell. *Anal. Chem.* **1991,** 63: 2109.

7. J. Fernandez de la Mora, G.J. Van Berkel, C.G. Enke, R.B. Cole, M. Martinez-Sanchez, J.B. Fenn; Electrochemical Processes in Electrospray Ionization Mass Spectrometry. *J. Mass Spectrom.* **2000,** 35: 939.

8. M.G. Ikonomou, A.T. Blades, P. Kebarle; Electrospray-IonSpray: a Comparison of Mechanism and Performance. *Anal. Chem.* **1991,** 63: 1989.

9. M. Wilm, M. Mann; Analytical Properties of the Nanoelectrospray Ion Source. *Anal. Chem.* **1996,** 68: 1.

10. R. Juraschek, T. Dülcks, M. Karas; Nanoelectrospray - More Than Just a Minimized-Flow Electrospray Ionization Source. *J. Am. Soc. Mass Spectrom.* **1999,** 10: 300.

11. A. Gomez, K. Tang; Charge and Fission of Droplets in Electrostatic Sprays. *Phys. Fluids* **1994,** 6: 404.

12. J.V. Iribarne, B.A. Thomson; On the Evaporation of Small Ions From Charged Droplets. *J. Chem. Phys.* **1976,** 64: 2287.

13. B.A. Thomson, J.V. Iribarne; Field Induced Ion Evaporation From Liquid Surfaces at Atmospheric Pressure. *J. Chem. Phys.* **1979,** 71: 4451.

14. J.V. Iribarne, P.J. Dziedzic, B.A. Thomson; Atmospheric Pressure Ion Evaporation-Mass Spectrometry. *Int. J. Mass Spectrom. Ion. Phys.* **1983,** 50: 331.

15. M. Dole, L.L. Mack, R.L. Hines; Molecular Beams of Macroions. *J. Chem. Phys.* **1968,** 49: 2240.

16. P. Kebarle, L. Tang; From Ions in Solution to Ions in the Gas Phase. *Anal. Chem.* **1993,** 65: 972A.

17. M. Gamero-Castaño, J. Fernandez de la Mora; Kinetics of Small Ion Evaporation From the Charge and Mass Distribution of Multiply Charged Clusters in Electrosprays. *J. Mass Spectrom.* **2000,** 35: 790.

18. G. Wang, R.B. Cole; Charged Residue Versus Ion Evaporation for Formation of Alkali Metal Halide Clusters in Electrospray Ionization. *Fres. J. Anal. Chem.* **2000,** 406: 53.

19. G. Schmelzeisen-Redeker, L. Bütfering, F.W. Röllgen; Desolvation of Ions and Molecules in Thermospray Mass Spectrometry. *Int. J. Mass Spectrom. Ion. Proc.* **1989,** 90: 139.

20. M. Gamero-Castaño, J. Fernandez de la Mora; Mechanisms of Electrospray Ionization of Singly and Multiply Charged Salt Clusters. *Fres. J. Anal. Chem.* **2000,** 406: 67.

21. L. Tang, P. Kebarle; Effect of Conductivity of the Electrosprayed Solution on the Electrospray Current. Factors Determining Analyte Sensitivity in Electrospray Mass Spectrometry. *Anal. Chem.* **1991,** 63: 2709.

22. L. Tang, P. Kebarle; Dependence of Ion Intensity in Electrospray Mass Spectrometry on the Concentration of the Analytes in the Electrosprayed Solution. *Anal. Chem.* **1993,** 65: 3654.

23. C.G. Enke; A Predictive Model for Matrix and Analyte Effects in Electrospray Ionization of Singly-Charged Ionic Analytes. *Anal. Chem.* **1997,** 69: 4885.

3. DISSOCIATION KINETICS IN MASS SPECTROMETRY

3.1. Internal energy

The internal energy of a single molecule is its total energy above its electronic, vibrational and rotational ground state[1]. A population of molecules is characterized by an internal energy distribution $P(E)$, which defines the probability of a species having a particular energy. The distributions $P(E)$ are normalized to unity. The most probable energy distribution characterized by a given mean energy is the Maxwell-Boltzmann distribution:

$$\frac{n_i}{\sum_i n_i} = \frac{\exp(-\beta E_i)}{\sum_i \exp(-\beta E_i)} \tag{3.1}$$

where n_i is the number of species in the state i of energy E_i, and β is the Lagrange parameter of the constraint on the mean energy. If the sum on the individual states i is replaced by an integral over all energies dE, the degeneracy (= the density of states $N(E)$) has to be considered. The constraint β can be expressed in terms of temperature if the mean thermal energy is fixed by energy exchanges with a bath at temperature T: $\beta = 1/kT$. This gives the following expression for $P(E)$ at a temperature T:

$$P(E;T) = \frac{N(E)e^{-E/kT}}{\int_0^\infty N(E)e^{-E/kT}\,dE} \tag{3.2}$$

3.2. The Lindemann-Hinshelwood mechanism

In 1922 Lindemann[2,3] suggested the separation of the dissociation reaction $A \longrightarrow B + C$ in two steps: (1) molecule A can be activated or deactivated by collisions with the bath gas M (with rate constants k_c and k_{-c}), and (2) an activated molecule (noted [A]*) can dissociate in a unimolecular process characterized by the rate constant k_{uni}. It is now well established that at low pressure in a mass spectrometer, activation and deactivation can also occur by radiative processes (gain or loss of a photon, with rate constants k_r and k_{-r})[4-6].

$$A \underset{k_{-c}[M] + k_{-r}}{\overset{k_c[M] + k_r}{\rightleftharpoons}} [A]^* \xrightarrow{k_{uni}} B + C \qquad (3.3)$$

The observed fragment formation rate $d[B]/dt = k_{obs}[A]$ depends on the relative values of the activation, deactivation and dissociation rates. Application of the steady state approximation to [A]* gives the following expression for the observed rate constant:

$$k_{obs} = \frac{k_{uni}(k_c[M] + k_r)}{k_{-c}[M] + k_{-r} + k_{uni}} \qquad (3.4)$$

At high pressure (when k_c[M] and k_{-c}[M] are higher than other rate constants), the observed rate is unimolecular. At intermediate pressures, the observed rate is bimolecular. At very low pressures, the radiative processes are predominant, and the observed fragmentation is again unimolecular[6].

The internal energy distribution $P(E)$ is built up by the activation/deactivation processes. In the Lindemann theory, each collision of [A]* results in deactivation; this is the strong collision assumption. However, the weak collision case is probably more appropriate in "slow heating" activation methods in mass spectrometry[4]. Activation and deactivation are in this case multi-step processes involving small increments, with up-steps balanced by down-steps at the steady state. In Section 3.4, we will show how to calculate the unimolecular dissociation rate constant k_{uni} as a function of the energy: $k(E)$.

3.3. Collisional energy transfer

In a binary collision, the maximal energy available for transfer into internal energy is the relative energy in the center-of-mass frame of reference (E_{rel}). A simple relationship between the laboratory collision energy (E_{lab}) and E_{rel} is given by equation (3.5):

$$E_{rel} = \frac{m_n}{m_n + m_i} E_{lab} \tag{3.5}$$

where m_n is the mass of the neutral target gas and m_i is the mass of the ion of interest. The collision is inelastic if part of E_{rel} is converted into internal energy[7,8].

In single collision conditions, the collision has to be activating. Part of the relative translational energy has to be converted into internal energy of the ion. In the experimental conditions used throughout this study ($E_{lab} \approx$ 10 to 100 eV and high mass ions), electronic excitation of the ions is usually ignored. Basically two mechanisms can account for the transfer of translational to vibrational energy[7].

The first mechanism is the formation of a long-lived complex between the ion and the target gas. In this case all the relative kinetic energy E_{rel} is present in the complex and redistributed. When the complex dissociates, the fraction of E_{rel} converted into internal energy of the ion depends on the lifetime of the complex (which increases with the depth of the interaction potential energy well, with the number of degrees of freedom of the complex, and decreases with E_{rel}), and on the fraction of the total number of degrees of freedom of the complex present in the ion. The energy transfer is very efficient but works well only for low E_{rel} values.

The second mechanism is called the “impulsive collision mechanism”. For large molecules, the collision can be viewed as inelastic with the whole molecule, but elastic with one subunit. The recoil of that subunit is responsible for the elongation of some bonds and the recoil energy is transferred to vibrational energy that can be subsequently redistributed. The efficiency of this mechanism is typically lower than for the mechanism of complex formation, but it is favored at higher E_{rel}. The interaction time between the target and the ion has to be in the order of a period of vibration.

The same mechanisms apply for each collision in the case of multiple collision conditions. This situation is encountered in the electrospray source, in MS/MS in the

quadrupole ion trap, and possibly in MS/MS in quadrupole collision cells. In the multiple collisions that an ion encounters during its lifetime, some can be activating and some can be deactivating. Hoxha *et al.*[9] have shown that multiple collisions in the electrospray source can lead ultimately to a Boltzmann-like internal energy distribution.

3.4. Unimolecular dissociation theory

RRKM theory of unimolecular dissociation: k(E)

The (Rice-Rampsberger-Kassel-Marcus) RRKM theory of unimolecular dissociation[3,10-14] is based on two assumptions: one is the existence of a transition state which irreversibly separates the reactant from the products of the reaction, and the other is the statistical redistribution of the total internal energy among the degrees of freedom of the reactant before the dissociation takes place[15-17]. RRKM is a statistical theory: the dissociation rate depends on the ratio between the number of favorable complexions (for which there is enough energy in the reaction coordinate to cross the transition state characterized by an energy barrier E_0) and the total number of complexions (all the possible ways of distributing the internal energy in the molecule). The microcanonical unimolecular rate constant is given by:

$$k(E) = \sigma \cdot \frac{G^{\ddagger}(E - E_0)}{hN(E)} = \sigma \cdot \frac{\int_0^{E-E_0} N^{\ddagger}(E_u) \cdot dE_u}{hN(E)} \tag{3.6}$$

where σ is the reaction path degeneracy, E_0 is the difference between the zero point energy of the transition state and the zero point energy of the reactant, $G^{\ddagger}(E - E_0)$ is the number of states of the transition state whose energy lies in the range $[0, E - E_0]$, h is the Plank constant, $N(E)$ is the density of states of the reactant at energy E, *and* $N^{\ddagger}(E_u)$ is the density of states of the reactant at energy E_u. Calculation of $k(E)$ requires the knowledge of E_0, the density of states of the reactant, and that of the transition state. The latter is the most difficult to evaluate because it requires the geometry and the frequencies of the transition state.

Substantial simplification of the RRKM equation is possible if the density of states is given by the classical approximation. This leads to the RRK equation:

$$k(E) = \nu_s \cdot \left(\frac{E - E_0}{E} \right)^{DOF-1} \tag{3.7}$$

where ν_s is a frequency factor and DOF is the number of degrees of freedom of the reactant. Though oversimplified, this equation is useful to help understanding some of the factors influencing the rate constant. The internal energy has to be higher than the barrier E_0 for the reaction to proceed (it there is no tunnel effect), and the higher the internal energy, the faster the reaction: there are more chances to have an energy $E > E_0$ in the particular degree of freedom which is the reaction coordinate s. Moreover, the larger the number of degrees of freedom in the reactant, the slower the reaction: there are more ways to redistribute the internal energy, and thus less chance for it to go in the reaction coordinate. The RRK formula is convenient to give an estimate of the rate constant.

The kinetic shift

Figure 3-1 shows a typical $k(E)$ curve. The reaction starts at the threshold E_0, and the rate constant increases as the available energy increases. The time scale of the experiment limits the range of k that are measurable and prevents from observing the reaction at the true threshold E_0. An example, adapted from reference 18, is given in Figure 3-1 for a quadrupole instrument. It was calculated that only the ions dissociating with a rate constant $\geq 10^4$ s^{-1} can be detected as fragments. This results in an apparent threshold E_{app} larger than the true threshold E_0. The difference between the E_{app} and E_0 is called the kinetic shift[1,19,20].

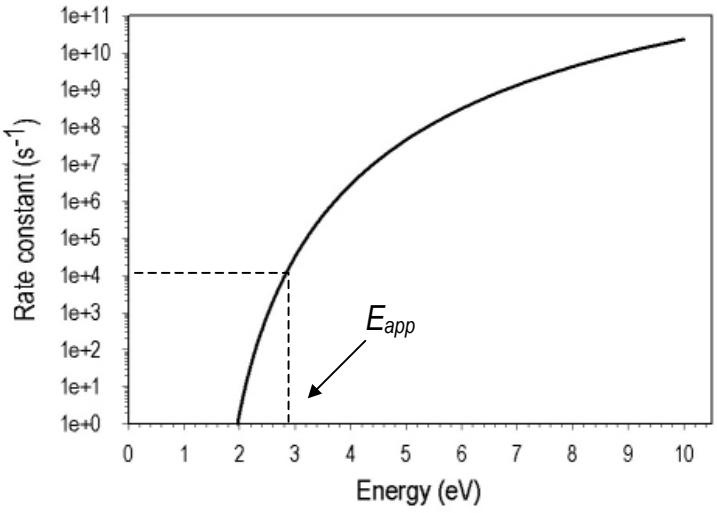

Figure 3-1. Typical k(E) curve: result of a RRKM calculation on p-CH_3 benzylpyridinium cation with E_0 = 1.6 eV and a loose transition state. The minimum rate constant that allows the observation of a fragment is 10^4 s^{-1}. The apparent threshold is therefore equal to 2.9 eV.

3.5. Dissociation kinetics of ions with an internal energy distribution

Here the ensemble is no more microcanonical, as the ion have an internal energy distribution $P(E)$, and not a single energy E.

The rapid energy exchange limit

When the activation/deactivation rates are higher than the dissociation rate, the internal energy distribution $P(E)$ is determined by the equilibrium established by activation/deactivation, and is not perturbed by the negligible contribution of the dissociation[4,5,21]. This limiting case is sometimes reached in multiple collisional activation or with blackbody radiative activation of large molecules at very low pressures. In multiple collision activation, the distribution $P(E)$ depends on the mean energy reached when activation and deactivation events occur at the same rate, and

$P(E)$ takes the form of a Maxwell-Boltzmann distribution. This distribution can be assigned a temperature, called the effective temperature[1,22-26] (T_{eff}): the term "effective" is used because this is not strictly a thermal equilibrium with a bath gas at temperature T.

In blackbody infrared radiation dissociation (BIRD), the temperature of the Boltzmann distribution is equal to the temperature of the walls of the reaction chamber. The observed dissociation rate constant (the canonical rate constant) is the average of the unimolecular rate constant $k(E)$ over the energy distribution $P(E)$:

$$k_{obs} = \int_{E_0}^{\infty} P(E)k(E)dE \tag{3.8}$$

and if k(E) is given by the RRKM equation (3.6) and $P(E)$ by the Maxwell-Boltzmann distribution (3.2), it can be demonstrated that the observed rate constant dependence on the temperature takes the form of the Eyring equation:

$$k_{obs}(T) = \frac{kT}{h}\exp\left(\frac{\Delta S^*}{R}\right)\exp\left(\frac{\Delta H^*}{RT}\right) \tag{3.9}$$

In practice, the experimental values of the rate constant as a function of temperature are fitted with the Arrhenius equation:

$$k_{obs}(T) = A.\exp\left(\frac{-E_a}{kT}\right) \tag{1.19}$$

A plot of $\ln(k_{obs})$ versus $1/T$ yields the activation energy E_a (slope) and the pre-exponential factor A (intercept). E_a is an experimental value that can be related to the true threshold E_0 by the Tolman theorem: the activation energy is the difference between the thermal energy of reacting molecules (thermal energy of the transition state + E_0) and the thermal energy of all reactant molecules[3,27]. In the rapid energy exchange limit, $E_a \approx E_0$, as the Boltzmann distribution is not perturbed by the dissociation[5,6,21].

The slow energy exchange limit

When the dissociation rate is higher than the activation/deactivation rates, the limiting step is now activation: as soon as a molecule has enough internal energy, it dissociates[4] and the energy distribution is depleted at high energies. The situation is

more complicated because the observed dissociation rate constant depends on the activation parameters, in addition to the characteristics of the transition state. Determination of the relationship between k_{obs} and the threshold E_0 requires modeling of the activation process. If the internal energy distribution can be characterized by a temperature, Arrhenius plots of experimental data give an experimental value of E_a and A, but the average energy of molecules undergoing reaction is lower due to the depletion of the distribution at higher energies: $E_a < E_0$, and the pre-exponential factor A is underestimated as well[21,28].

An interesting case to consider is the metastable decay of a population of ions characterized with an energy distribution $P(E)$. During metastable decay (during a time t), ions unimolecularly dissociate with k_{uni} depending on their initial energy, and no more activation/deactivation occurs. In this case, all parent ions with an energy $E \geq E_{app}$ (E_{app} depending on the time t and on $k(E)$, see Figure 1-5) will dissociate. After a time t, the starting internal energy distribution $P(E)$ is truncated for energies greater than E_{app}[5,28,29] (Figure 3-2).

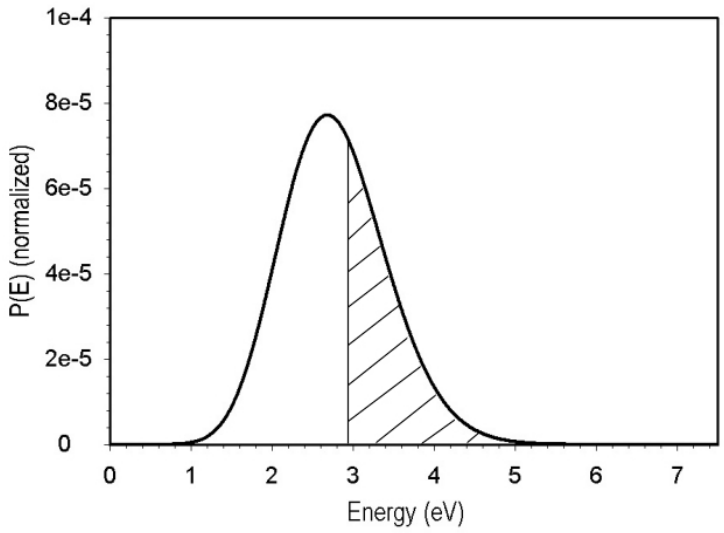

Figure 3-2. Typical Maxwell-Boltzmann internal energy distribution: $P(E)$ for p-CH_3 benzylpyridinium cation at T = 1000 K. If t = 10^{-4} s, E_{app} = 2.95 eV (see Figure 3-1). The fraction of parent ions that fragment before 10^{-4} s is given by the integral below the curve from E_{app} to infinite (hatched region).

Intermediate cases

In intermediate cases where activation, deactivation and fragmentation proceed on the same time scale, a detailed modeling of the activation/deactivation and dissociation processes by random walk simulations or master equation is required[6,20,21,29-32]. The probability and the energy step size of the activation and deactivation events must be known, and k_{uni} is calculated for each energy E by the RRKM formalism.

3.6. High mass ions

With single collision activation in beam-type instruments ($t = 10^{-4} – 10^{-6}$ s), observing dissociation is increasingly difficult when the mass of the parent ion increases. This is due first to the low relative kinetic energy that can be transferred to the ion during collision with a small neutral, and second to the large kinetic shift resulting from the high number of degrees of freedom (high density of states) of the molecule. Other techniques are therefore preferred for the study of high mass ion dissociation. Ion trapping (QIT or FTICR) instruments can be used to access longer reaction times ($t = 10^{-2} – 10^{2}$ s) and therefore to lower the kinetic shift. The number of collisions can also be increased: this is known as "slow heating"[4]. Moreover, for high mass ions, the thermal energy content of the ions before collision can become substantial as the number of atoms increases[33] and should not be neglected.

As the number of degrees of freedom increases, RRKM calculations and modeling of activation and deactivation processes in order to relate the observed rate constant to the true threshold E_0 become challenging. An elegant bypass is the BIRD method. For large molecules, as the density of states increases, radiative processes can become competitive at low pressures (typical of FTICR instruments). The reaction rates can be measured as a function of the temperature of the walls of the ICR chamber, and the activation energy is determined from an Arrhenius plot. A true thermal equilibrium is established within the reaction vessel, through IR photon absorption and emission. For other activation methods, a convenient way to describe the internal energy distribution of high mass molecules is by considering an effective temperature T_{eff}, which is the temperature of the Maxwell-Boltzmann distribution that would produce the same effect as the true distribution. However, deviation from the rapid energy exchange

limit is a major problem for relating k_{obs} to E_0. Moreover, the problem of how T_{eff} varies with the size of the ion in given activation conditions has not been established yet, so that the effective temperatures found for model small ions can not be transposed yet to high mass ions.

Finally, a more fundamental issue for high mass ions is whether they still behave statistically, i.e. whether the energy is redistributed on the whole molecule before dissociation occurs. It seems that energy transfer may be more efficient than for small molecules, or that energy transfer into some moiety of the molecule leads to dissociation before complete randomization[8]; this means that the RRKM formalism may not be valid. But the fact that internal energy may not be relaxed before dissociation takes place is not in contradiction with a statistical behavior of the whole population of molecules, as internal energy input by collision is a nonselective process which can lead to a statistical initial sampling of the molecular phase space.

References

1. K. Vékey; Internal Energy Effects in Mass Spectrometry. *J. Mass Spectrom.* **1996,** 31: 445.

2. F.A. Lindemann, S. Arrhenius, I. Langmuir, N.R. Dhar, J. Perrin, W.C. Lewis; Discussion. *Trans. Faraday Soc.* **1922,** 17: 598.

3. J.I. Steinfeld, J.S. Francisco, W.L. Hase *Chemical Kinetics and Dynamics*; Prentice Hall: New Jersey, 1999, Chapter 11, pp. 324-389.

4. S.A. McLuckey, D.E. Goeringer; Slow Heating in Tandem Mass Spectrometry. *J. Mass Spectrom.* **1997,** 32: 461.

5. R.C. Dunbar, T.B. McMahon; Activation of Unimolecular Reactions by Ambient Blackbody Radiation. *Science* **1998,** 279: 194.

6. W.D. Price, P.D. Schnier, R.A. Jockusch, E.F. Strittmatter, E.R. Williams; Unimolecular Reaction Kinetics in the High-Pressure Limit Without Collisions. *J. Am. Chem. Soc.* **1996,** 118: 10640.

7. S.A. McLuckey; Principles of Collisional Activation in Analytical Mass Spectrometry. *J. Am. Soc. Mass Spectrom.* **1991,** 3: 599.

8. A.K. Shulka, J.H. Futrell; Tandem Mass Spectrometry: Dissociation of Ions by Collisional Activation. *J. Mass Spectrom.* **2000,** 35: 1069.

9. A. Hoxha, C. Collette, E. De Pauw, B. Leyh; Mechanism of Collisional Heating in Electrospray Mass Spectrometry: Ion Trajectory Calculations. *J. Phys. Chem. A* **2001,** 105: 7326.

10. W. Forst *The Theory of Unimolecular Reactions*; New York, Londres, 1973.

11. R.G. Gilbert, S.C. Smith *Theory of Unimolecular and Recombination Reactions*; Oxford, 1990.

12. J.C. Lorquet; Whither the Statistical Theory of Mass Spectra. *Mass Spectrom. Rev.* **1994,** 13: 233.

13. T. Baer, P.M. Mayer; Statistical Rice Ramsperger Kassel Marcus Quasiequilibrium Theory Calculations in Mass Spectrometry. *J. Am. Soc. Mass Spectrom.* **1997,** 8: 103.

14. W.L. Hase; Some Recent Advances and Remaining Questions Regarding Unimolecular Rate Theory. *Acc. Chem. Res.* **1998,** 31: 659.

15. I. Oref, B.S. Rabinovitch; Do Highly Reactive Polyatomic Molecules Behave Ergodically ? *Acc. Chem. Res.* **1979,** 12: 166.

16. B.K. Carpenter; Dynammic Behavior of Organic Reactive Intermediates. *Angew. Chem. Int. Ed. Engl.* **1998,** 37: 3340.

17. D. Boyall, K.L. Reid; Modern Studies of Intramolecular Vibrational Energy Redistribution. *Chem. Soc. Rev.* **1997,** 26: 223.

18. C. Collette, L. Drahos, E. De Pauw, K. Vékey; Comparison of the Internal Energy Distributions of Ions Produced by Different Electrospray Sources. *Rapid Commun. Mass Spectrom.* **1998,** 12: 1673.

19. C. Lifshitz; Time-Resolved Appearance Energies, Breakdown Graphs, and Mass Spectra: the Elusive "Kinetic Shift". *Mass Spectrom. Rev.* **1982,** 1: 309.

20. R.C. Dunbar; New Approaches to Ion Thermochemistry Via Dissociation and Association. *Adv. Gas Phase Ion Chem.* **1996,** 2: 87.

21. W.D. Price, E.R. Williams; Activation of Peptide Ions by Blackbody Radiation: Factors That Lead to Dissociation Kinetics in the Rapid Energy Exchange Limit. *J. Phys. Chem. A* **1997,** 101: 8844.

22. P.D. Schnier, J.C. Jurchen, E.R. Williams; The Effective Temperature of Peptide Ions Dissociated by Sustained Off-Resonance Irradiation Collisional Activation in Fourier Transform Mass Spectrometry. *J. Phys. Chem. B* **1999,** 103: 737.

23. K.G. Asano, D.E. Goeringer, S.A. McLuckey; Thermal Dissociation in the Quadrupole Ion Trap: Ions Derived From Leucine Enkephalin. *Int. J. Mass Spectrom.* **1999,** 185/186/187: 207.

24. D.E. Goeringer, K.G. Asano, S.A. McLuckey; Ion Internal Temperature and Ion Trap Collisional Activation: Protonated Leucine Enkephalin. *Int. J. Mass Spectrom.* **1999,** 182/183: 275.

25. K.G. Asano, D.J. Butcher, D.E. Goeringer, S.A. McLuckey; Effective Ion Internal Temperatures Achieved Via Boundary Activation in the Quadrupole Ion Trap : Protonated Leucine Enkephalin. *J. Mass Spectrom.* **1999,** 34: 691.

26. L. Drahos, R.M.A. Heeren, C. Collette, E. De Pauw, K. Vékey; Thermal Energy Distributions Observed in Electrospray Ionization. *J. Mass Spectrom.* **1999,** 34: 1373.

27. D.G. Truhlar; Interpretation of the Activation Energy. *J. Chem. Educ.* **1978,** 55: 309.

28. R.C. Dunbar; Kinetics of Low-Intensity Infrared Laser Photodissociation. The Thermal Model and Application of the Tolman Theorem. *J. Chem. Phys.* **1991,** 95: 2537.

29. R.C. Dunbar; Kinetics of Thermal Unimolecular Dissociation by Ambient Infrared Radiation. *J. Phys. Chem.* **1994,** 98: 8705.

30. D.E. Goeringer, K. Asano, S.A. McLuckey; Ion Internal Temperature and Ion Trap Collisional Activation: Protonated Leucine Enkephalin. *Int. J. Mass Spectrom. Ion. Proc.* **1998,** 182/183: 275.

31. K. Asano, D.E. Goeringer, S.A. McLuckey; Thermal Dissociation in the Quadrupole Ion Trap: Ions Derived From Leucine Enkephalin. *Int. J. Mass Spectrom. Ion. Proc.* **1998,** 185/186/187: 207.

32. L. Drahos, K. Vékey; MassKinetics: a Theoretical Model of Mass Spectra Incorporating Physical Processes, Reaction Kinetics and Mathematical Descriptions. *J. Mass Spectrom.* **2001,** 36: 237.

33. L. Drahos, K. Vékey; Determination of the Thermal Energy and Its Distribution in Peptides. *J. Am. Soc. Mass Spectrom.* **1999,** 10: 323.

4.

ELECTROSPRAY MASS SPECTROMETRY OF NONCOVALENT COMPLEXES

The capability of electrospray ionization mass spectrometry for detecting a noncovalent complex has been first demonstrated in 1991[1]. Since then, the literature concerning supramolecular complex analysis by ES-MS is constantly growing. The complexes studied to date include synthetic systems (cation-macrocycle, supramolecular assemblies,…), and complexes of biochemical interest (protein-protein, protein-ligand, protein-DNA, protein-RNA associations, etc…), and this list is not exhaustive. The goal of this chapter is not to make a comprehensive literature overview, but to classify the various information electrospray ionization mass spectrometry can provide about supramolecular complexes.

4.1. Information on the species present in solution

Determination of the stoichiometry of the complexes and identification of their constitutive ligands

The great advantage of mass spectrometry for the characterization of noncovalent complexes is of course the possibility to measure the masses of the species, and thus to allow a rapid and unambiguous assignment of the stoichiometry of the observed complexes. Their constituents can also be identified by their masses, and if necessary by MS/MS or MS^n experiments. MS^n is useful for the identification of a constituent by its fragmentation after the breaking of the complex in a first MS/MS step.

The critical point when starting the study of a new system is to determine whether or not the observed complexes reflect the specific interactions occurring in solution. Are all the complexes in the solution detectable by MS (aren't there false negatives)? Are all the detected complexes really present in solution (aren't there false positives)?

Whether mass spectrometry accurately reflects the composition of the solution depends on the experimental parameters. Smith *et al.*[2,3] have suggested a series of tests to discriminate between specific and nonspecific complexes:

(i) Specific molecular recognition results in complexes of well-defined stoichiometries, with defined binding constants. However, nonspecific aggregation, often driven by electrostatic interactions, results in random association. Experimental conditions must be tuned to minimize random aggregation and to allow only the observation of the specific complexes of well-defined stoichiometries[4]. One way to do so is to investigate the influence of the dilution of the sample: if few molecules are present per droplet, electrostatic aggregation upon evaporation of the solvent is minimized.

(ii) According to Smith *et al.*[2,3], the lability of a complex may also be indicative of its specificity: a specific complex is supposed to be more stable in the gas phase than a nonspecific one. It will thus survive longer to collisional activation in the source of the spectrometer. A fine tuning of the cone voltage of the source is necessary to disrupt the nonspecific complexes while keeping intact the specific ones, achieving nevertheless a sufficient desolvation of these species.

(iii) The composition of the solution is also a very important parameter: biological complexes are often stable only in a narrow range of solution pH and ionic force, and do rarely tolerate the addition of organic co-solvents. These conditions are unfortunately not ideal for electrospray ionization mass spectrometry. Adding organics like methanol or acetonitrile in the solution to obtain a stable spray, changing the pH to enhance the ionization yield, often result in a denaturation of the complex. However, this can be used to test the specificity of the observed complex. When performing the analysis in denaturing solution conditions, no more complex should be observed, as it is no more present in the solution.

(iv) The specificity of an observed ligand-substrate complex can also be unambiguously proved by comparison with a solution in which the ligand (or the substrate) has been replaced by a molecule of homologous structure, but which is known not to bind to the substrate (or to the ligand). For that test solution, no

complex should be observed in ES-MS because none is present in solution, all other parameters being the same.

Determination of relative and absolute binding constants in solution

While the position of the peaks on the *m*/*z* scale allows the identification of the species, their intensities can be related to the concentrations in solution. Electrospray ionization mass spectrometry thus offers the possibility of an alternative method for determining binding constants in solution. The validation of such new method of course implies the comparison of the results with constants determined in solution by proven traditional methods (fluorescence, UV or NMR titration, titration calorimetry,…).

Establishing for one of the ligands a calibration of the intensity (number of counts) as a function of the solution concentration allows the determination of the concentration of free ligand upon titration of a known quantity of substrate by that ligand. The concentration of bound ligand is calculated by the difference between the total amount of ligand added and the free ligand concentration determined using the calibration curve. A Scatchard plot[5] of the results of the titration gives access to the stoichiometry and the association constant of the complex[6,7].

Another method for determining K_a (eq. 1.4) is to measure the relative intensity of the peaks corresponding to the complex AB and to the free substrate A (or B), and to calculate the ratio of the concentrations by equation (4.1), assuming that the response factors of A and AB are identical:

$$\frac{I(AB)}{I(A)} = \frac{[AB]}{[A]} \tag{4.1}$$

The association constant can be determined with a single mass spectrum[8-12] or by fitting data obtained by a titration experiment[13-15]. This methodology can be applied to the case of complexes with multiple stoichiometries[15] or when different ligands are in competition for binding to a given target[10,12,16]. The assumption that the response factors of the complex and the free ligand are the same, has been validated by comparison with independent solution-phase data in the case of vancomycin-peptide

complexes[10]. This has been attributed to the fact that the peptide is imbedded in the complex and that the conformation of vancomycin does not change.

An important factor worth to mention is the strong influence of the ion activation in the electrospray source. The ideal case is when the specific complexes are sufficiently stable to reach the detector. If not, it will cause an underestimation of the binding constant[10].

A method for determining the ratio between the response factors of the complex and the free ligands is to perform two independent measurements in which the equilibrium was shifted completely to the left, then to the right, by using appropriate media. In one study of the dimer ⇔ hexamer equilibrium of citrate synthase[17], a correction factor of 0.77 was determined, and the equilibrium association constant in the solution of interest could be determined subsequently. Such a procedure to determine the ratio of the response factors is rigorous, but not of general applicability.

The determination of binding selectivities by measuring the ratio of two complexes when two ligands are in competition (equimolar mixture) for a given substrate[18-28], mainly applied to cation-crown ether complexes, is also based on a similar approximation: the response factors of the two complexes have to be the same. Application of this method for the screening of a library of ± 250 synthetic peptides for a given receptor has been reported[29]. The quantification and identification of the ligands were made by MS/MS and MS^n in a FTICR mass spectrometer.

By comparison of the mass spectrometric results with the theoretical intensities (calculated from known association constants[19,20,22,23] or determined experimentally by shifting the equilibria to the right by adding an excess of reactant[18,30]), the approximation was proven to be valid when comparing complexes of the same host with different guest cations, but not in the opposite situation[19,20,22,23]. When trying to generalize the results, we see that the response factor is very sensitive to both the conformation and the charge of the considered molecule. The question is how sensitive is the method to conformational variations, and how to predict in which cases the method will (or won't) give acceptable results.

A method avoiding any approximation on the response factors has been recently proposed by Kempen and Brodbelt[31]. It consists in monitoring the intensity of a reference complex before and after the addition of a competing host or guest. The calibration curve of the intensity of the reference complex requires the knowledge of the equilibrium association constant K_a of that complex.

Study of the conformation of the complexes in solution

The conformation of the complexes in solution can also be studied by hydrogen/deuterium exchange with a detection by high resolution mass spectrometry[9,32,33]. In this case, if the complex is formed quantitatively in solution, there is no more requirement for maintaining the complex intact in the mass spectrometer. The subunits can be studied separately if they come from the dissociation of the specific complex, provided that no rearrangement of the deuterium atoms occurs in between.

4.2. Study of noncovalent complexes in the gas phase

Measurement of equilibrium constants in the gas phase

Measuring equilibrium constants in the gas phase is very difficult experimentally. For example, for the equilibrium (4.2), the determination of the equilibrium constant requires the measurement of the ratio of the charged species (given by the relative intensities of these charged species), but also the ratio between the partial pressures of the neutrals, which are not detected by the mass analyzer.

$$[\text{Ligand1} + \text{M}^+] + \text{Ligand2} \rightleftharpoons [\text{Ligand2} + \text{M}^+] + \text{Ligand1} \qquad (4.2)$$

$$K_{eq} = \frac{[Ligand2 + M^+] \cdot p_{Ligand1}}{[Ligand1 + M^+] \cdot p_{Ligand2}} = \frac{I_{(Ligand2+M^+)}}{I_{(Ligand1+M^+)}} \cdot \frac{p_{Ligand1}}{p_{Ligand2}} \qquad (4.3)$$

This method is only applicable to sufficiently volatile ligands (for example small crown ethers and cryptands[34-37], or small organic molecules complexed by charged cavitands[38,39]), and the relative pressures of the neutrals are measured by indirect ways like their relative protonation yields. This is of course the major source of error. The most suitable instrument allowing equilibration for a sufficiently long time is the FTICR-MS.

The comparison between the solution phase and the gas phase equilibrium constants revealed very interesting features. Macrocyclic[34] and cryptate effects[35] persist in the gas phase: they are thus not only due to the effect of the solvent, but the pre-

arrangement of the donor groups intrinsically play a role in the stability of the complex. However, the "best fit" principle, according to which the most stable complexes in solution are obtained when the closest match between the cation size and the ligand cavity is achieved, is not verified in the gas phase. The gas phase affinity depends directly on the number of donor atoms in the ligand, and on the charge density of the cation. In solution, the smallest cations are also the most solvated ones, and there is competition between the solvent and the ligand for binding the cation.

Dissociation of the complexes in the gas phase

In all the methods mentioned below, some internal energy is given to the complex, which causes its unimolecular dissociation in the gas phase. As only the dissociation occurs, it is not an equilibrium like in the previous case. The dissociation can be monitored in time, but most often the dissociation time is fixed, either by instrumental constraints, or by the experimentalist.

Collision-induced dissociation (CID)

Internal energy is given by collisions, either in the electrospray source (source-CID)[40-44] or in MS/MS experiment[45-48]. In MS/MS, the complex is mass-selected before CID. In source-CID, all ions produced by electrospray undergo collisional activation, but it allows the study of very large complexes (too high *m/z* to be selected for MS/MS[42]).

Most papers report the dissociation as a function of the collision energy in the laboratory frame of reference, or more simply as a function of the experimental parameters as tuned directly on the mass spectrometer (orifice-skimmer voltage in electrospray source, activation amplitude in SORI-CID, …). Only few papers report the energy in the center-of-mass frame of reference[44,45], which is particularly important when comparing complexes of different masses. The discussion of the results is always based on the qualitative comparison between the resistance to dissociation in the gas phase and the stability in solution. These comparisons are sometimes made via a parameter E_{50} or V_{50}, which is the energy or voltage at which 50% of the complex is fragmented.

Threshold CID

Armentrout and co-workers[49-51] have developed experimental and theoretical tools to determine the threshold energy E_0 from CID experiments. There are many constraints in that method: collision energies should be well-defined, the ion internal energy before collision has to be known (ions are usually not produced by electrospray), extrapolation to zero pressure is needed to extrapolate to single collision conditions, and the collision gas should provide efficient energy transfer. The data analysis involves an RRKM modeling of the experimental data. The method therefore requires to know all sources of internal energy, and to calculate the vibrational modes and the reaction pathways at a high level of accuracy. The kinetic shift has to be taken into account. The method has been applied to polyether-metal complexes, which are small enough to allow for such a data treatment.

Kinetic method

The kinetic method[52,53] can be used for noncovalent ternary complexes involving two neutral ligands and one cation. The method consists in the comparison between two competitive dissociation pathways of a single, mixed complex in which two ligands are bound to the same substrate.

$$[\text{Ligand1} - \text{X}^+ - \text{Ligand2}] \begin{cases} \nearrow [\text{Ligand1} - \text{X}^+] + \text{Ligand2} \\ \searrow [\text{Ligand2} - \text{X}^+] + \text{Ligand1} \end{cases} \qquad (4.4)$$

The relative intensities of the products indicate which reaction pathway has the lower barrier, and thus which ligand is the most tightly bound to the substrate denoted X^+. The only requirement is that the activation entropy is the same for the two reactions. The method has been applied mainly for polyether-metal complexes[54-56].

BIRD

As explained in Chapter 3, BIRD experiments allow the determination of the Arrhenius parameters E_a and A for the dissociation. This is also applicable to the noncovalent dissociation of a complex[57-59].

The dissociation of the heme-myoglobin complex was investigated[57]. The complexes generated from a pseudo-native solution showed larger activation energy and pre-

exponential factors ($E_a \approx 0.9$ eV and $\log A \approx 8$-9) than complexes issued from a denaturing solution.

The dissociation kinetics of a series of oligonucleotide DNA duplexes was also studied[58]. The values of E_a and A for the dissociation of the duplex into the monomers are gathered in Table 4-1. In addition to the noncovalent dissociation into the monomers, the authors also observed some covalent fragmentation, mainly neutral base loss. The activation energies are correlated to the number of hydrogen bonds in the duplex, and thereby to the solution-phase behavior.

Table 4-1. Activation energy and pre-exponential factors for the dissociation of duplex DNA into single strands[58].

Base sequence	log(*A*)	E_a (eV)
$(TGCA)_2^{3-}$	18.2	1.41
$(CCGG)_2^{3-}$	19.7	1.51
$(AATTAAT)_2^{3-}$	15.5	1.44
$(CCGGCCG)_2^{3-}$	16.5	> 1.65
$A_7 \cdot A_7^{3-}$	14.8	1.39
$T_7 \cdot T_7^{3-}$	17.1	1.40
$A_7 \cdot T_7^{3-}$	19.2	1.68

Recently, the study of the thermal decomposition of a large multiprotein complex (a pentamer) was reported[59]. The pentamer dissociates into a monomer plus a tetramer, the charge-to-mass ratio of the monomer being much higher than that of the tetramer. This is a widely encountered behavior in the dissociation of multiprotein complexes[60,61]. The E_a and A parameters have been determined for the reaction $B_5^{n+} \longrightarrow B^{p+} + B_4^{(n-p)+}$ for different values of n and p. It was found that when the charge state of the parent ion increases, E_a and A decrease (from $E_a \approx 3.5$ eV and $\log A \approx 40$ for $n = 11$ to $E_a \approx 1.5$ eV and $\log A \approx 18$ for $n = 14$). This is attributed to the Coulombic

repulsion between the fragments. For a given parent ion charge state, the activation energy and pre-exponential factors increase when the charge of the monomer fragment increases (for $n = 14$: $E_a = 1.41$ eV and $\log A = 16.2$ for $p = 4$, $E_a = 1.48$ eV and $\log A = 17.3$ for $p = 5$ and $E_a = 1.67$ eV and $\log A = 19.7$ for $p = 6$).

It must also be mentioned that not all complexes are suitable for a BIRD analysis. It was shown for example that cyclodextrin-peptide complexes underwent covalent fragmentation of the peptide (one part remaining attached to the cyclodextrin) instead of noncovalent dissociation of the complex[62]. The determination of Arrhenius parameters by BIRD requires the dissociation channel of interest to be the major one observed on the time scale of the measurement.

Heated capillary dissociation

This method uses a heated capillary in the transfer region of the electrospray source (see for example the source of the LCQ in Figure 7-1) to activate the ions and cause their dissociation[63-68]. The temperature dependence of the fragmentation can be monitored to gain information on the gas-phase kinetic stability of the complexes[66-68]. He *et al.*[67] tried to infer Arrhenius parameters from the temperature dependence of the dissociation, but the physical basis for this treatment remains unclear. The residence time in the capillary was estimated at about 0.01 ms[67], and the ions can dissociate after leaving the capillary. These two factors suggest that the rapid energy exchange limit is not attained. The Arrhenius parameters are thereby called "apparent"[67].

Comparison between resistance to CID and solution phase stability

Complexes of alkali cations with crown ethers have been extensively investigated[49,54-56,69]. The lability in the gas phase reveals that the size of the cation (or, more precisely, its charge density) plays the major role in the absence of solvent, differing from the behavior in solution in which the "best fit" principle prevails. The same conclusions arose in the above-mentioned studies of the gas phase equilibrium constants.

For other complexes of biochemical interest, the results can be summarized as follows. There is a good agreement between the solution and the gas phase behavior for complexes of which the main interactions are electrostatic and hydrogen bonds[40,46,58], but care is necessary if protonation or deprotonation during the electrospray process induces a change in the structure compared to the native one[70]. Stacking[48] and steric[46] effects have also been noted in the gas phase. However, the contribution of the solvent (hydrophobic effect) is obviously not present in the gas phase anymore[40,45,48].

Study of protein conformation in the gas phase

The conformation of proteins (secondary and ternary structure) is driven by intramolecular noncovalent interactions, and their study in the gas phase will also give insight into the problem of the conservation of specific noncovalent interactions in the gas phase. The two techniques which allow the study of conformations in the gas phase are ion mobility mass spectrometry[71-74] (determination of the collision cross section of the molecule by measuring the time of flight in a drift tube filled with a collision gas) and hydrogen/deuterium exchange in the gas phase[75-77] (reaction with D_2O vapor in an ICR cell).

One or several distinct conformations can be distinguished, depending on the electrospray conditions (solvent, temperature, voltage on the instrument) and on the charge state. The latter is very important because of Coulombic repulsion, favored in the gas phase due to the absence of shielding dielectric medium. The conformation(s) in solution (which can be varied by changing the solvent or the pH) influences the conformation(s) that are observed in the gas phase[78]. However it has been shown that the gas phase conformation(s) were different from the solution one(s)[72,77,79]. It is suggested that the high number of collisions in the drift tube allows the system to evolve towards other low energy conformations, stable in the absence of solvent[72,80]. Secondary structures like α-helices, stabilized by hydrogen bonds, will likely be maintained *in vacuo*[79]. Interactions with the solvent, however, will probably be replaced by "intramolecular solvation" of the protein by itself[77,80], and this will cause dramatic changes in the overall conformation.

References

1. B. Ganem, Y.-T. Li, J.D. Henion; Detection of Non-Covalent Receptor-Ligand Complexes by Mass Spectrometry. *J. Am. Chem. Soc.* **1991,** 113: 6294.

2. R.D. Smith, K.J. Light-Wahl; The Observation of Non-Covalent Interactions in Solution by Electrospray Ionization Mass Spectrometry: Promise, Pitfalls and Prognosis. *Biol. Mass Spectrom.* **1993,** 22: 493.

3. R.D. Smith, J.E. Bruce, Q. Wu, Q.P. Lei; New Mass Spectrometric Methods for the Study of Non-Covalent Associations of Biopolymers. *Chem. Soc. Rev.* **1997,** 26: 191.

4. N. Potier, L.J. Donald, I. Chernushevich, A. Ayed, W. Ens, C. Arrowsmith, K.G. Standing, D.C. Duckworth; Study of a Non-Covalent Trp Repressor: DNA Operator Complex by Electrospray Ionization Time-of-Flight Mass Spectrometry. *Protein Sci.* **1998,** 7: 1388.

5. G. Scatchard; The Attraction of Proteins for Small Molecules and Ions. *Ann. N. Y. Acad. Sci.* **1949,** 49: 660.

6. J.A. Loo, P. Hu, P. McConnell, W.T. Mueller, T.K. Sawyer, V. Thanabal; A Study of SH2 Domain Protein-Phosphopeptide Binding Interactions by Electrospray Ionization Mass Spectrometry. *J. Am. Soc. Mass Spectrom.* **1997,** 8: 234.

7. H.-K. Lim, Y.L. Hsieh, B. Ganem, J.D. Henion; Recognition of Cell-Wall Peptide Ligands by Vancomycin Group Antibiotics: Studies Using Ionspray Mass Spectrometry. *J. Mass Spectrom.* **1995,** 30: 708.

8. X. Cheng, R. Chen, J.E. Bruce, B.L. Schwartz, G.A. Anderson, S.A. Hofstadler, D.C. Gale, R.D. Smith; Using Electrospray Ionization FTICR Mass Spectrometry to Study Competitive Binding of Inhibitors to Carbonic Anhydrase. *J. Am. Chem. Soc.* **1995,** 117: 8859.

9. C.V. Robinson, E.W. Chung, B.B. Kragelund, J. Knudsen, R.T. Aplin, F.M. Poulsen, C.M. Dobson; Probing the Nature of Noncovalent Interactions by Mass

Spectrometry. A Study of Protein-CoA Ligand Binding and Assembly. *J. Am. Chem. Soc.* **1996,** 118: 8646.

10. T.J.D. Jorgensen, P. Roepstorff, A.J.R. Heck; Direct Determination of Solution Binding Constants for Noncovalent Complexes Between Bacterial Cell Wall Peptide Analogues and Vancomycin Group Antibiotics by Electrospray Ionization Mass Spectrometry. *Anal. Chem.* **1998,** 70: 4427.

11. T.J.D. Jorgensen, T. Staroske, P. Roepstorff, D.H. Williams, A.J.R. Heck; Subtle Differences in Molecular Recognition Between Modified Glycopeptide Antibiotics and Bacterial Receptor Peptides Identified by Electrospray Ionization Mass Spectrometry. *J. Chem. Soc., Perkin Trans. 2* **1999,** 1859.

12. K.A. Sannes-Lowery, J.J. Drader, R.H. Griffey, S.A. Hofstadler; Fourier Transform Ion Cyclotron Resonance Mass Spectrometry As a High Throughput Affinity Screen to Identify RNA Binding Ligands. *Trends Anal. Chem.* **2000,** 19: 481.

13. M.J. Greig, H. Gaus, L.L. Cummins, H. Sasmor, R.H. Griffey; Measurement of Macromolecular Binding Using Electrospray Mass Spectrometry. Determination of Dissociation Constants for Oligonucleotide-Serum Albumin Complexes. *J. Am. Chem. Soc.* **1995,** 117: 10765.

14. R.H. Griffey, K.A. Sannes-Lowery, J.J. Drader, V. Mohan, E.E. Swayze, S.A. Hofstadler; Characterization of Low-Affinity Complexes Between RNA and Small Molecules Using Electrospray Ionization Mass Spectrometry. *J. Am. Chem. Soc.* **2000,** 122: 9933.

15. K.A. Sannes-Lowery, R.H. Griffey, S.A. Hofstadler; Measuring Dissociation Constants of RNA and Aminoglycoside Antibiotics by Electrospray Ionization Mass Spectrometry. *Anal. Biochem.* **2000,** 280: 264.

16. A.J.R. Heck; Ligand Fishing by Mass Spectrometry. *Spectroscopy Europe* **1999,** 11/6: 12.

17. A. Ayed, A.N. Krutchinsky, W. Ens, K.G. Standing, D.C. Duckworth; Quantitative Evaluation of Protein-Protein and Ligand-Protein Equilibria of Large Allosteric Enzyme by Electrospray Ionization Time-of-Flight Mass Spectrometry. *Rapid Commun. Mass Spectrom.* **1998,** 12: 339.

18. D.-S. Young, H.-Y. Hung, L.K. Liu; An Easy and Rapid Method for Determination of Stability Constants by Electrospray Ionization Mass Spectrometry. *Rapid Commun. Mass Spectrom.* **1997,** 11: 769.

19. E. Leize, A. Jaffrezic, A. Van Dorsselaer; Correlation Between Solvation Energies and Electrospray Mass Spectrometric Response Factors. Study by Electrospray Mass Spectrometry of Supramolecular Complexes in Thermodynamic Equilibrium in Solution. *J. Mass Spectrom.* **1996,** 31: 537.

20. K. Wang, G.W. Gokel; Correlation of Solution and Gas Phase Complexation Assessed by Electrospray Ionization Mass Spectrometry : Application to One-, Two- and Three-Ring Macrocycles. *J. Org. Chem.* **1996,** 61: 4693.

21. F. Inokuchi, Y. Miyahara, T. Inazu, S. Shinkai; "Cation-Pi Interactions" Detected by Mass Spectrometry; Selective Recognition of Alkali Metal Cations by a Pi-Basic Molecular Cavity. *Angew. Chem. Int. Ed. Engl.* **1995,** 34: 1364.

22. T.M. Fyles, B. Zeng; On the Assessment of Complex Cation–Crown Ether Equilibria by Electrospray Mass Spectrometry. *Supramol. Chem.* **1998,** 10: 143.

23. S.M. Blair, E.C. Kempen, J.S. Brodbelt; Determination of Binding Selectivities in Host-Guest Complexation by Electrospray/Quadrupole Ion Trap Mass Spectrometry. *J. Am. Soc. Mass Spectrom.* **1998,** 9: 1049.

24. E.C. Kempen, J.S. Brodbelt, R.A. Bartsch, M.T. Blanda, D.B. Farmer; Screening Metal Binding Selectivities of Macrocycle Mixtures by HPLC-ESI-MS and Postcolumn Reactions. *Anal. Chem.* **2001,** 73: 384.

25. J.S. Brodbelt, E.C. Kempen, M. Reyzer; Determination of Binding Selectivities by Electrospray Ionization Mass Spectrometry. *Struct. Chem.* **1999,** 10: 213.

26. E.C. Kempen, J.S. Brodbelt, R.A. Bartsch, Y. Jang, J.S. Kim; Investigation of Alkali Metal Cation Selectivities of Lariat Crown Ethers by Electrospray Ionization Mass Spectrometry. *Anal. Chem.* **1999,** 71: 5493.

27. S.M. Blair, J.S. Brodbelt, A.P. Marchand, K.A. Kumar, H.-S. Chong; Evaluation of Binding Selectivities of Caged Crown Ligands Towards Heavy Metals by Electrospray Ionization/Quadrupole Ion Trap Mass Spectrometry. *Anal. Chem.* **2000,** 72: 2433.

28. M.L. Reyzer, J.S. Brodbelt, A.P. Marchand, Z. Chen, Z. Huang, I.N.N. Namboothiri; Determination of Alkali Metal Binding Selectivities of Caged Crown Ligands by Electrospray Ionization Quadrupole Ion Trap Mass Spectrometry. *Int. J. Mass Spectrom.* **2001,** 204: 133.

29. J. Gao, X. Cheng, R. Chen, G.B. Sigal, J.E. Bruce, B.L. Schwartz, S.A. Hofstadler, G.A. Anderson, R.D. Smith, G.M. Whitesides; Screening Derivatized Peptide Libraries for Tight Binding Inhibitors to Carbonic Anhydrase II by Electrospray Ionization Mass Spectrometry. *J. Med. Chem.* **1996,** 39: 1949.

30. D.-S. Young, H.-Y. Hung, L.K. Liu; Estimation of Selectivities and Relative Cationization Efficiencies of Different $[Crown+M]^+$ by Electrospray Mass Spectrometry. *J. Mass Spectrom.* **1997,** 32: 432.

31. E.C. Kempen, J.S. Brodbelt; A Method for the Determination of Binding Constants by Electrospray Ionization Mass Spectrometry. *Anal. Chem.* **2000,** 72: 5411.

32. R.J. Anderegg, D.S. Wagner; Mass Spectrometric Characterization of a Protein-Ligand Interaction. *J. Am. Chem. Soc.* **1995,** 117: 1374.

33. C.V. Robinson, M. Gross, S.J. Eyles, J.J. Ewbank, M.P. Mayhew, F.U. Hartl, C.M. Dobson, S.E. Radford; Conformation of GroEL-Bound α-Lactalbumin Probed by Mass Spectrometry. *Nature* **1994,** 372: 646.

34. I.-H. Chu, H. Zhang, D.V. Dearden; Macrocyclic Chemistry in the Gas Phase: Intrinsic Cation Affinities and Complexation Rates for Alkali Metal Cation Complexes of Crown Ethers and Glymes. *J. Am. Chem. Soc.* **1993,** 115: 5736.

35. Q. Chen, K. Cannell, J. Nicoll, D.V. Dearden; The Macrobicyclic Cryptate Effect in the Gas Phase. *J. Am. Chem. Soc.* **1996,** 118: 6335.

36. J.B. Nicoll, D.V. Dearden; Reactions of Multidentate Ligands With Ligated Alkali Cation Complexes: Self-Exchange and "Sandwich" Complex Formation Kinetics of Gas Phase Crown Ether–Alkali Cation Complexes. *Int. J. Mass Spectrom.* **2001,** 204: 171.

37. D.V. Dearden, Y. Liang, J.B. Nicoll, K. Kellersberger; Study of Gas-Phase Molecular Recognition Using Fourier-Transform Ion Cyclotron Resonance Mass Spectrometry. *J. Mass Spectrom.* **2001,** 36: 989.

38. M. Vincenti, C. Minero, E. Pelizzetti, A. Secchi, E. Dalcanale; Host-Guest Chemistry in the Gas Phase and at the Gas-Solid Interface: Fundamental Aspects and Practical Applications. *Pure Appl. Chem.* **1995,** 67: 1075.

39. M. Vincenti, E. Pelizzetti, E. Dalcanale, P. Soncini; Molecular Recognition in the Gas Phase. *Pure Appl. Chem.* **1993,** 65: 1507.

40. H. Rogniaux, A. Van Dorsselaer, P. Barth, J.F. Biellmann, J. Brabanton, M. van Zandt, B. Chevrier, E. Howard, A. Mitschler, N. Potier, L. Urzhumtseva, D. Moras, A. Podjarny; Binding of Aldose Reductase Inhibitors: Correlation of Crystallographic and Mass Spectrometric Studies. *J. Am. Soc. Mass Spectrom.* **1999,** 10: 635.

41. C.L. Hunter, A.G. Mauk, D.J. Douglas; Dissociation of Heme From Myoglobin and Cytochrome *b*5: Comparison of Behavior in Solution and in the Gas Phase. *Biochemistry* **2000,** 36: 1018.

42. A.A. Rostom, J.R.H. Tame, J.E. Ladbury, C.V. Robinson; Specificity and Interactions of the Protein OppA: Partitioning Solvent Binding Effects Using Mass Spectrometry. *J. Mol. Biol.* **2000,** 296: 269.

43. K.J. Light-Wahl, B.L. Schwartz, R.D. Smith; Observation of Non-Covalent Quaternary Associations of Proteins by Electrospray Ionization Mass Spectrometry. *J. Am. Chem. Soc.* **1994,** 116: 5271.

44. R. Ramanathan, L. Prokai; Electrospray Ionization Mass Spectrometric Study of Encapsulation of Amino Acids by Cyclodextrins. *J. Am. Soc. Mass Spectrom.* **1995,** 6: 866.

45. V. Nesatyy; Gas-Phase Binding of Non-Covalent Protein Complexes Between Bovine Pancreatic Trypsin Inhibitor and Its Target Enzymes Studied by Electrospray Ionization Tandem Mass Spectrometry. *J. Mass Spectrom.* **2001,** 36: 950.

46. J. Gao, Q. Wu, J.D. Carbeck, Q.P. Lei, R.D. Smith, G.M. Whitesides; Probing the Energetics of Dissociation of Carbonic Anhydrase-Ligand Complexes in the Gas Phase. *Biophys. J.* **1999,** 76: 3253.

47. Y.-T. Li, Y.L. Hsieh, J.D. Henion, T.D. Ocain, G.A. Schiehser, B. Ganem; Analysis of the Energetics of Gas-Phase Immunophilin-Ligand Complexes by Ionspray Mass Spectrometry. *J. Am. Chem. Soc.* **1994,** 116: 7487.

48. Q. Wu, J. Gao, D. Joseph-McCarthy, G.B. Sigal, J.E. Bruce, G.M. Whitesides, R.D. Smith; Carbonic Anhydrase-Inhibitor Binding: From Solution to Gas Phase. *J. Am. Chem. Soc.* **1997,** 119: 1157.

49. M.B. More, D. Ray, P.B. Armentrout; Intrinsic Affinities of Alkali Cations for 15-Crown-5 and 18-Crown-6: Bond Dissociation Energies of Gas-Phase M^+–Crown Ether Complexes. *J. Am. Chem. Soc.* **1999,** 121: 417.

50. P.B. Armentrout; Cation-Ether Complexes in the Gas Phase: Thermodynamic Insight into Molecular Recognition. *Int. J. Mass Spectrom.* **1999,** 193: 227.

51. M.T. Rodgers, P.B. Armentrout; Noncovalent Metal-Ligand Bond Energies As Studied by Threshold Collision-Induced Dissociation. *Mass Spectrom. Rev.* **2000,** 19: 215.

52. R.G. Cooks, J.S. Patrick, T. Kotiaho, S.A. McLuckey; Thermochemical Determinations by the Kinetic Method. *Mass Spectrom. Rev.* **1994,** 13: 287.

53. R.G. Cooks, P. Wong; Kinetic Method of Making Thermochemical Determinations: Advances and Applications. *Acc. Chem. Res.* **1998,** 31: 379.

54. C.-C. Liou, J.S. Brodbelt; Comparison of Gas-Phase Proton and Ammonium Ion Affinities of Crown Ethers and Related Acyclic Analogs. *J. Am. Chem. Soc.* **1992,** 114: 6761.

55. S. Maleknia, J.S. Brodbelt; Gas-Phase Selectivities of Crown Ethers for Alkali Metal Ion Complexation. *J. Am. Chem. Soc.* **1992,** 114: 4295.

56. C.-C. Liou, J.S. Brodbelt; Detremination of Orders of Relative Alkali Metal Ion Affinities of Crown Ethers and Acyclic Analogs by the Kinetic Method. *J. Am. Soc. Mass Spectrom.* **1992,** 3: 543.

57. D.S. Gross, Y. Zhao, E.R. Williams; Dissociation of Heme–Globin Complexes by BIRD: Molecular Specificity in the Gas Phase? *J. Am. Soc. Mass Spectrom.* **1997,** 8: 519.

58. P.D. Schnier, J.S. Klassen, E.F. Strittmatter, E.R. Williams; Activation Energies for Dissociation of Double Strand Oligonucleotide Anions: Evidence for Watson-Crick Base Pairing *in vacuo*. *J. Am. Chem. Soc.* **1998,** 120: 9605.

59. N. Felitsyn, E.N. Kitova, J.S. Klassen; Thermal Decomposition of a Gaseous Multiprotein Complex Studied by Blackbody Infrared Radiative Dissociation. Investigating the Origin of the Asymmetric Dissociation Behavior. *Anal. Chem.* **2001,** 73: 4647.

60. C. Versluis, A. van der Staaij, E. Stokvis, A.J.R. Heck, B. De Craene; Metastable Ion Formation and Disparate Charge Separation in the Gas Phase Dissection of Protein Assemblies Studied by Orthogonal Time-of-Flight Mass Spectrometry. *J. Am. Soc. Mass Spectrom.* **2001,** 12: 329.

61. C. Versluis, A.J.R. Heck; Gas-Phase Dissociation of Hemoglobin. *Int. J. Mass Spectrom.* **2001,** 210/211: 637.

62. S.G. Penn, F. He, C.B. Lebrilla; Peptides Complexed to Cyclodextrins Fragment Rather Than Dissociate When Subjected to Blackbody Infrared Radiation. *J. Phys. Chem. B* **1998,** 102: 9119.

63. A.L. Rockwood, M. Busman, H.R. Udseth, R.D. Smith; Thermally Induced Dissociation of Ions From Electrospray Mass Spectrometry. *Rapid Commun. Mass Spectrom.* **1991,** 5: 582.

64. M. Busman, A.L. Rockwood, D.L. Smith; Activation Energies of Gas Phase Dissociations of Multiply Charged Ions From Electrospray Ionization Mass Spectrometry. *J. Phys. Chem.* **1992,** 96: 2397.

65. M. Meot-Ner (Mautner), A. Dongré, A. Somogyi, V.H. Wysocki; Thermal Decomposition Kinetics of Protonated Peptides and Peptide Dimers, and Comparison With Surface Induced Dissociation. *Rapid Commun. Mass Spectrom.* **1995,** 9: 829.

66. S.G. Penn, F. He, M.K. Green, C.B. Lebrilla; The Use of Heated Capillary Dissociation and Collision-Induced Dissociation to Determine the Strength of Non-Covalent Bonding Interactions in Gas-Phase Peptide–Cyclodextrin Complexes. *J. Am. Soc. Mass Spectrom.* **1997,** 8: 244.

67. F. He, J. Ramirez, B.A. Garcia, C.B. Lebrilla; Differentially Heated Capillary for Thermal Dissociation of Noncovalently Bound Complexes Produced by Electrospray Ionization. *Int. J. Mass Spectrom.* **1999,** 182/183: 261.

68. B. Garcia, J. Ramirez, S. Wong, C.B. Lebrilla; Thermal Dissociation of Protonated Cyclodextrin-Amino Acid Complexes in the Gas Phase. *Int. J. Mass Spectrom.* **2001,** 210/211: 215.

69. D. Peiris, Y. Yang, R. Ramanathan, K.R. Williams, C.H. Watson, J.R. Eyler; Infrared Multiphoton Dissociation of Electrosprayed Crown Ether Complexes. *Int. J. Mass Spectrom. Ion. Proc.* **1996,** 157/158: 365.

70. A. van der Kerk-van Hoof, A.J.R. Heck; Covalent and Non-Covalent Dissociations of Gas-Phase Complexes of Avoparcin and Bacterial Receptor Mimicking Precursor Peptides Studied by CAD Mass Spectrometry. *J. Mass Spectrom.* **1999,** 34: 813.

71. D.E. Clemmer, R.R. Hudgins, M.F. Jarrold; Naked Protein Conformations: Cytochrome *c* in the Gas Phase. *J. Am. Chem. Soc.* **1995,** 117: 10141.

72. D.E. Clemmer, M.F. Jarrold; Ion Mobility Measurements and Their Applications to Clusters of Biomolecules. *J. Mass Spectrom.* **1997,** 32: 577.

73. Y. Liu, S.J. Valentine, A.E. Counterman, C.S. Hoaglund, D.E. Clemmer; Injected-Ion Mobility Analysis of Biomolecules. *Anal. Chem.* **1997,** 69: 728A.

74. J.I. Baumbach, G.A. Eiceman; Ion Mobility Spectrometry: Arriving on Site and Moving Beyond Low Profile. *Appl. Spectros.* **1999,** 53: 338A.

75. M.E. Hemling, J.J. Conboy, M.F. Bean, M. Mentzer, S.A. Carr; Gas Phase H/D Exchange in Electrospray Ionization Mass Spectrometry As a Practical Tool for Structure Elucidation. *J. Am. Soc. Mass Spectrom.* **1994,** 5: 434.

76. B.L. Schwartz, D.C. Gale, R.D. Smith; Noncovalent Interactions Observed Using Electrospray Ionization. *Methods Mol. Biol.* **1996,** 61: 115.

77. M.A. Freitas, C.L. Hendrickson, M.R. Emmett, A.G. Marshall; Gas-Phase Bovine Ubiquitin Cation Conformations Resolved by Gas-Phase H/D Exchange Rate and Extent. *Int. J. Mass Spectrom.* **1999,** 185/186/187: 565.

78. F. Wang, M.A. Freitas, A.G. Marshall, B.D. Sykes; Gas-Phase Memory of Solution-Phase Protein Conformation: H/D Exchange and Fourier Transform Ion Cyclotron Resonance Mass Spectrometry of the n-Terminal Domain of Cardiac Troponin C. *Int. J. Mass Spectrom.* **1999,** 192: 319.

79. F.W. Mc Lafferty, Z. Guan, U. Haupts, T.D. Wood, N.L. Kelleher; Gaseous Conformational Structure of Cytochrome *c*. *J. Am. Chem. Soc.* **1998,** 120: 4732.

80. P.G. Wolynes; Biomolecular Folding in Vacuo!!!(?). *Proc. Natl. Acad. Sci. USA* **1995,** 92: 2426.

5.
SCOPE OF THE THESIS

In the previous chapter, we have seen that a large variety of noncovalent complexes have already been studied by electrospray ionization mass spectrometry. Some reports indicate a good correlation between ES-MS and solution-phase results, but counter-examples can also be found. In the present work, the goal is to generalize (1) in which cases (for which complexes) and (2) how (experimental procedure and interpretation of the results) ES-MS can be used to obtain reliable information on the complexes.

To make some generalizations based on the nature of the interactions that are involved, model compounds have been chosen in which the contributions of the different interactions can be varied independently, in series of similar compounds. The studied complexes are described in detail in Chapter 6. For each series of complexes, different experimental procedures were undertaken, which are described in Chapter 7. The experimental work has therefore a grid-shaped architecture. The results could have been presented following the horizontal axis (by type of complex) or vertical axis (by type of experiment). Actually, a third kind of presentation was preferred, with emphasis on a global interpretation of the results.

The "Results and Discussion" section is separated in two distinct parts, in order to avoid any confusion between the two kinds of information that can be obtained:

Part I: The full scan mass spectra give information on the composition of the solution that is injected in electrospray, and therefore on the solution-phase stability of the complexes. Chapter 8 leads to a discussion of the criteria given by Smith *et*

al.[1,2] to assess the specificity of the observed complexes. In Chapter 9, a new method for determining simultaneously the binding constants and the relative electrospray response factors is presented, and the influence of the nature of the complex on these response factors is discussed.

Part II: The collision-induced dissociation of the complexes in the gas phase and the measurement of the amounts of fragments resulting from this dissociation give information on the gas-phase kinetic stability of the complexes. Chapter 10 explains the hows and whys of the gas-phase kinetic stability measurements. Chapter 11 shows that different collision regimes can give very different fragmentation pathways, and some rules to choose the adequate experimental conditions will be given. In Chapter 12, the conservation of different types of noncovalent interactions in the gas phase was studied, and the correlation with solution-phase data is discussed. Finally, in Chapter 13, we propose and discuss a dissociation mechanism for large noncovalent complexes in the gas phase.

---

[1] R.D. Smith, K.J. Light-Wahl; The Observation of Non-Covalent Interactions in Solution by Electrospray Ionization Mass Spectrometry : Promise, Pitfalls and Prognosis. *Biol. Mass Spectrom.* **1993,** 22: 493.

[2] R.D. Smith, J.E. Bruce, Q. Wu, Q.P. Lei; New Mass Spectrometric Methods for the Study of Non-Covalent Associations of Biopolymers. *Chem. Soc. Rev.* **1997,** 26: 191.

6.
THE STUDIED COMPLEXES

6.1. Duplex DNA

Structure and noncovalent interactions implied in solution

We will describe only the structure of the B-DNA, the most commonly found structure in aqueous solution[1-3]. This is the structure that will be assumed for all the duplexes that were investigated.

Hydrogen bonding in Watson-Crick base pairing

Hydrogen bonds are formed very specifically between the purine and pyrimidine bases: two H-bonds between adenine (A) and thymine (T) and three between guanine (G) and cytosine (C) (Figure 6-1). Therefore, for a duplex of given length, the larger the number of GC base pairs, the higher the stability of the duplex.

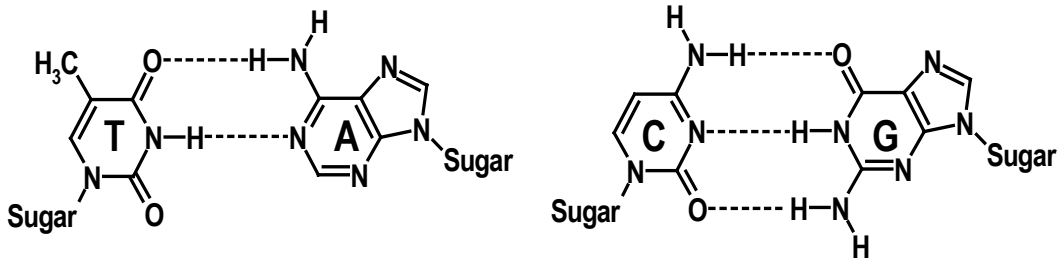

Figure 6-1. Hydrogen bonds between the Watson-Crick base pairs. Left: thymine-adenine. Right: cytosine-guanine.

Electrostatic repulsion

The phosphate groups on the uprights of the strands are negatively charged. In pure water, no duplex can form due to this repulsion. Duplexes are formed in physiological solutions thanks to the electrolytes present in solution: the negative charges of the phosphate groups are shielded by the counter-ionic atmosphere.

Hydrophobic interactions and the double-helix structure

If the double-stranded DNA had the structure of a straight ladder, the bases would be separated by 0.60 nm, and water molecules could be inserted between the adjacent bases. The bases are aromatic molecules which are hydrophobic. The formation of the double-helix structure is the simplest way of releasing these water molecules and to stabilize the structure, as the bases are now separated by 0.34 nm and are stacked on each other (Figure 6-2).

Base stacking

The driving force for the stacking of the base pairs is hydrophobicity, but the adjacent bases can also interact with each other electrostatically. The bases are multipoles that interact with each other. These short-range forces ($1/r^3$ to $1/r^5$) are favored in the double-helix for conformational reasons[4]. Note that base stacking also occurs in oligonucleotide single-strands.

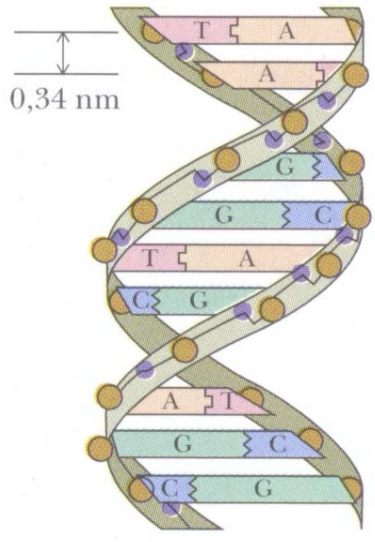

Figure 6-2. Double-helix structure of B-DNA

Stability in solution

The stability of a duplex in solution depends on the electrolyte, on the number of GC base pairs and on the base sequence. The stability has been determined by thermal denaturation, or calculated by "nearest neighbor models".

Thermal denaturation

In our thermal denaturation experiments in solution, the absorbance of the solution was measured with a Lambda 5 UV spectrophotometer (Perkin Elmer, Norwalk, CT, USA) interfaced with a PC XT for data acquisition. The quartz cells were heated by a Julabo F25 heating circulator (Kutztown, PA, USA). The melting temperature (T_m) of a species is defined as the temperature of half denaturation, i.e. the temperature corresponding to the inflexion point in the absorbance vs. temperature graph. All measurements were performed with duplex concentrations of 2.5 μM, in order to have an absorbance range between 0.2 and 0.8. The concentrations were carefully set to the same value for the different UV-melting experiments. By doing so, the relative T_m values directly indicate the relative stability of the analyzed species (otherwise the T_m's would also depend on the concentration[5]).

Nearest neighbor models

Nearest-neighbor (n-n) models[3] are established to calculate the sequence-dependent stability of short duplex DNA oligomers (20 base pairs or less). They are based on the statistical analysis of denaturation (melting) data and provide tables that can be used to calculate thermodynamic parameters for any sequence, by an incremental method. We used the tables given by Sugimoto et al.[6], which are reproduced in Table 6-1 (next page), to calculate the duplex melting enthalpy ($\Delta H_{n\text{-}n}$).

Sample preparation

Oligonucleotides were purchased from Eurogentec (Sart-Tilman, Belgium). Complementary single strands were first dissolved in water, then annealed (heated to 80 °C and cooled overnight) in 50 mM ammonium acetate to form the duplex. The NH_4OAc concentration was chosen on the basis of preliminary thermal denaturation experiments: a concentration of 50 mM ensures that duplexes with 12 base pairs or larger remain stable at room temperature. This concentration is easily tolerated by the

electrospray mass spectrometers. The duplexes were desalted with MICROCON3 filters (Amicon, Beverly, MA, USA) when the necessity was revealed by the mass spectra. The extinction coefficients of the duplexes were derived from thermal denaturation curves, the ε_{260} values for the single strands being given by the supplier. These extinction coefficients were used to determine the concentration by UV absorption spectroscopy.

Table 6-1. Nearest-neighbor parameters to calculate the duplex melting enthalpy[6]

Sequence (*ij*)	ΔH_{ij} (cal/mol)
AA/TT	-8.0
AG/CT	-6.6
AT/AT	-5.6
AC/GT	-9.4
GA/TC	-8.8
GG/CC	-10.9
GC/GC	-10.5
TA/TA	-6.6
TG/CA	-8.2
CG/CG	-11.8
Nucleation parameter	0.6

6.2. DNA complexes with minor groove binders

Structure and noncovalent interactions implied

B-DNA has multiple recognition sites: the edges of the base pairs exposed to the solvent have hydrogen bond donor and acceptor groups (Figure 6-3). The two grooves of DNA differ in size and in topology: the major groove is wider and is generally the recognition region for proteins. The minor groove is narrower and surrounded by the sugar-phosphate-sugar chains.

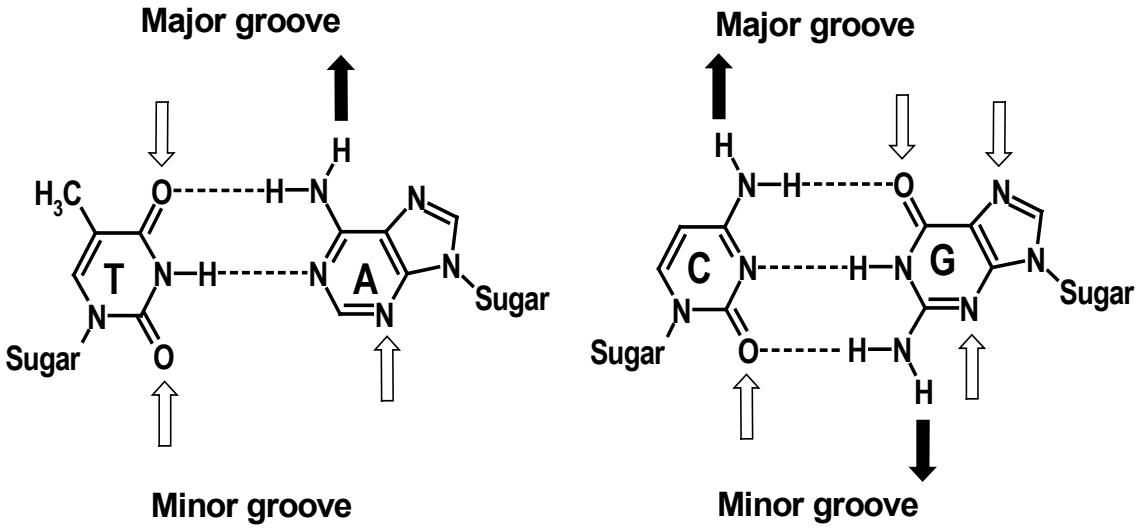

Figure 6-3. Hydrogen bond donor and acceptor groups in the grooves of DNA.

Minor groove binders are synthetic molecules (Figure 6-4) that interact with B-DNA in the minor groove. They have a crescent shape that fits nicely in the groove without distorting the double helix. Hydrogen bond donor groups at the inner edge make H-bonds with the base pairs of each strand.

The drugs we studied here all have a preference for AT-rich regions of DNA for three reasons: (i) the $-NH_2$ groups on guanines cause steric hindrance in the groove, (ii) the minor groove is narrower in AT-rich regions, which is favorable to van der Waals contacts with the sugars, and (iii) the AT regions have a more negative electrostatic potential, which is favorable for the binding of positively charged molecules[7,8]. Minor groove binders can form either 1:1 or 2:1 complexes like shown in Figure 6-5.

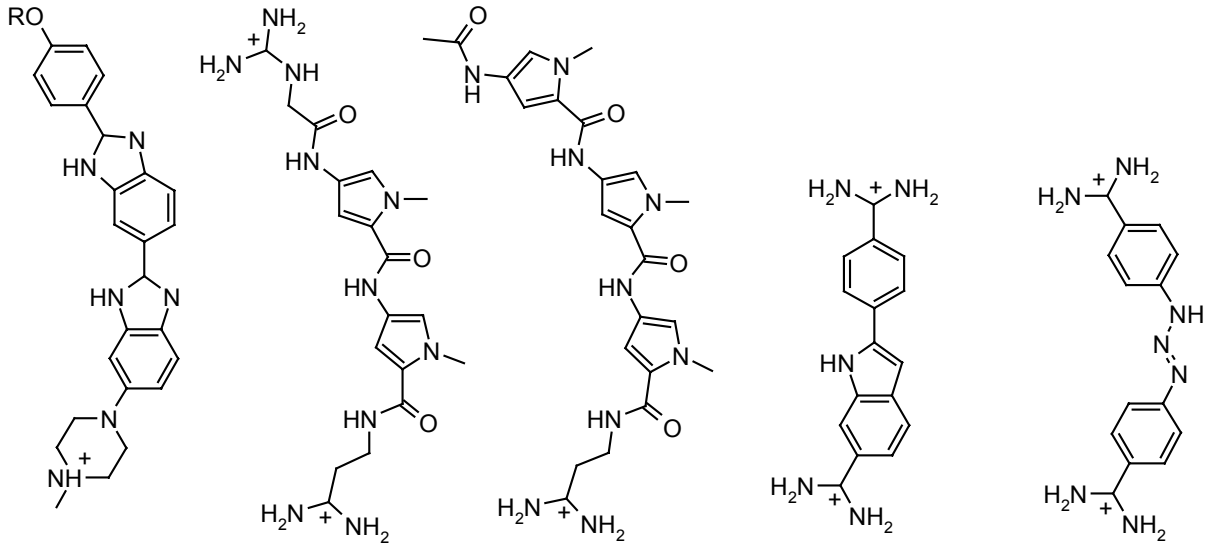

Figure 6-4. Structures and masses of the minor groove binders used in this study.

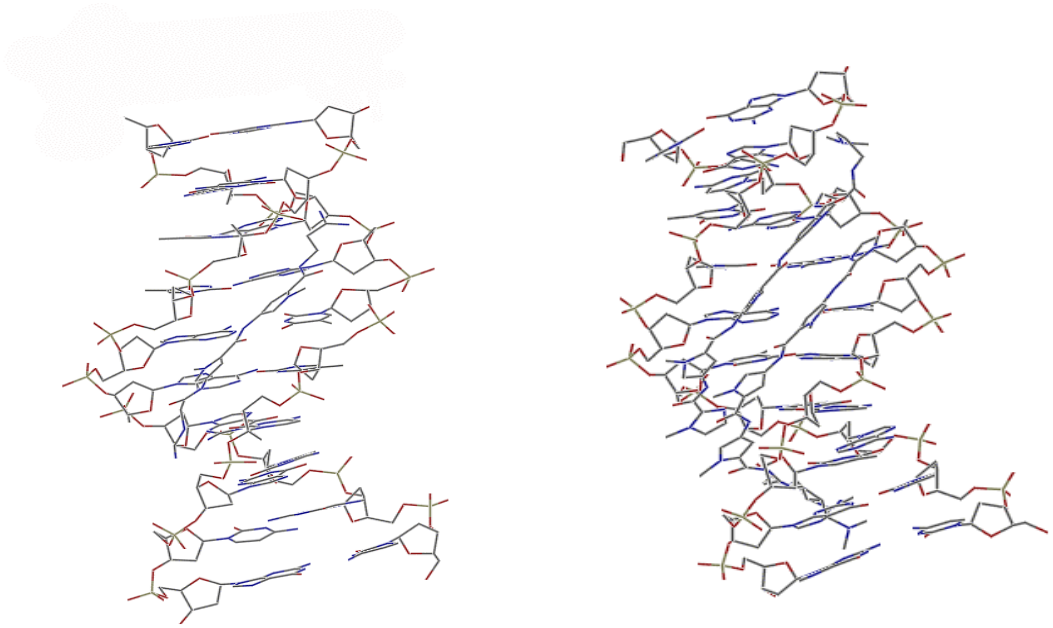

Figure 6-5. Structure of 1:1 and 2:1 complexes between minor groove binders and B-DNA (adapted from the Nucleic Acid Databank entries 121D and 407D respectively).

Sample preparation

The minor groove binders Hoechst 33258, ε_{338}* = 42,000 and Hoechst 33342, ε_{348} = 42,000 (Acros, Geel, Belgium), DAPI, ε_{342} = 27,000 (Fluka, Bornem, Belgium) netropsin, ε_{296} = 21,500 and distamycin A, ε_{302} = 35,000 (Serva, Heidelberg, Germany) and berenil, ε_{370} = 34,400 (kindly provided by C. Bailly, Inserm, Lille, France) were dissolved in aqueous NH_4OAc. The complexes were formed simply by mixing the drug and the duplex solutions.

* All extinction coefficients are given in $mol^{-1}cm^{-1}$.

6.3. DNA complexes with intercalators

Structure and noncovalent interactions implied

Intercalators bind to DNA by insertion of their planar aromatic chromophore between DNA base pairs[9,10]. Simple intercalators have few substituents, but others like amsacrine and actinomycin D (Figure 6-6) are more complex, and substituents can interact with the minor or the major groove and participate to a wide variety of intermolecular interactions.

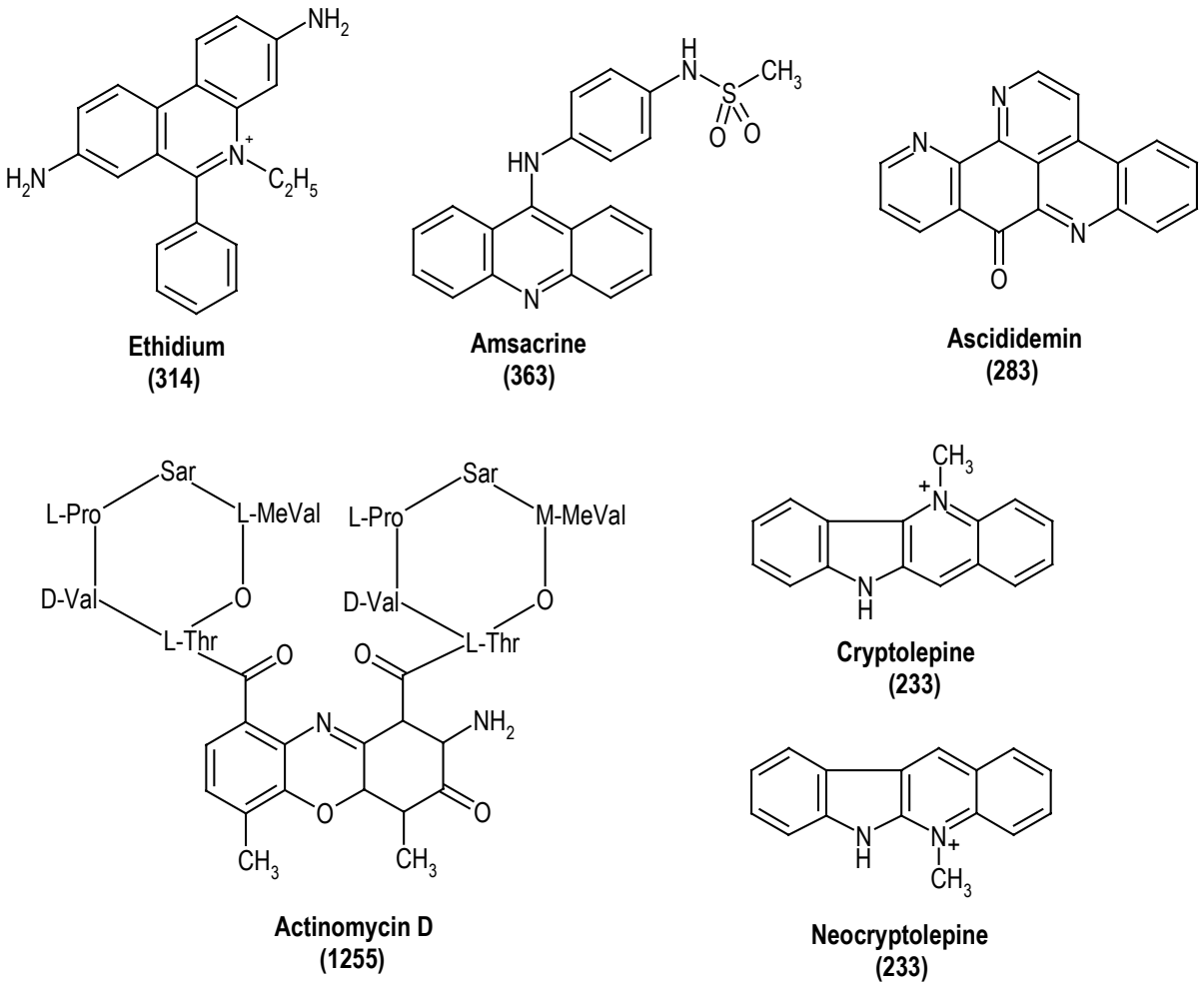

Figure 6-6. Structure of the intercalators used in this study.

A conceptual model for intercalation is shown in Figure 6-7[11]. First, DNA must undergo conformational transition (the double helix is unwound) to form the intercalation site (6-7a). Second, the transfer of the intercalator from the solution to the intercalation site is hydrophobic (6.7-b). Finaly, a variety of noncovalent molecular interactions can be formed (stacking of the aromatic ring, hydrogen bonding, van der Waals contacts,…) (6.7-c). The final structure with the distorted helix is presented in Figure 6-7d.

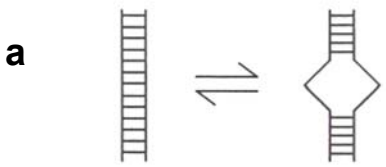

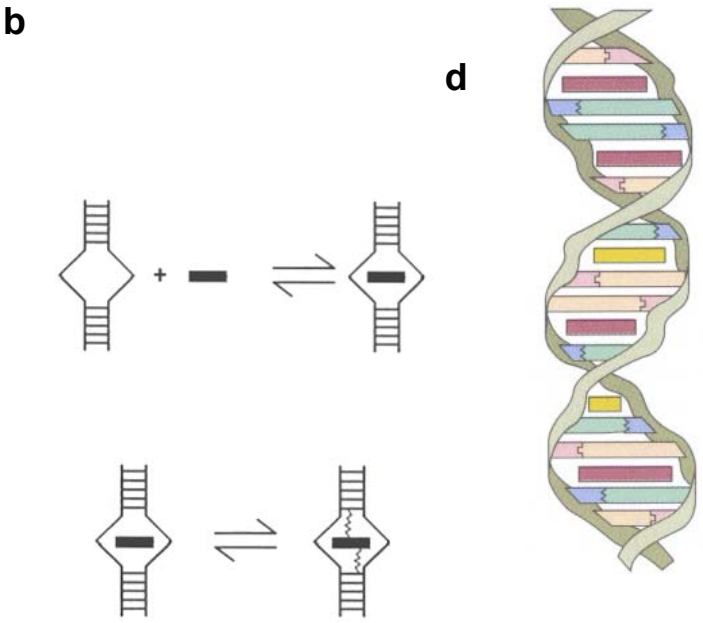

Figure 6-7. **a-c**: Intercalation mechanism[11] (see the text for a detailed description). **d**: Structure of the DNA with intercalators bound.

Sample preparation

Ethidium bromide, ε_{480} = 5,850 and actinomycin D, ε_{440} = 24,500 (Sigma, Bornem, Belgium) were dissolved in aqueous NH_4OAc. Amsacrine, ε_{434} = 12,000 (Sigma, Bornem, Belgium), ascididemin (kindly provided by C. Bailly), cryptolepine, ε_{369} = 28,600 and neocryptolepine ε_{334} = 12,200 (kindly provided by L. Pieters, Univ. Antwerpen, Belgium) were dissolved in methanol for the stock solution and then dissolved in aqueous ammonium acetate. The complexes were formed simply by mixing the drug and the duplex solutions.

6.4. Cyclodextrin complexes

Structure and noncovalent interactions implied

Cyclodextrins (CD's) are torus-like macro-rings built up from glucopyranose units. α-CD has six glucopyranose units, β-CD has seven glucopyranose units, and γ-CD has eight glucopyranose units[12,13]. The structure of α-CD is shown in Figure 6-8.

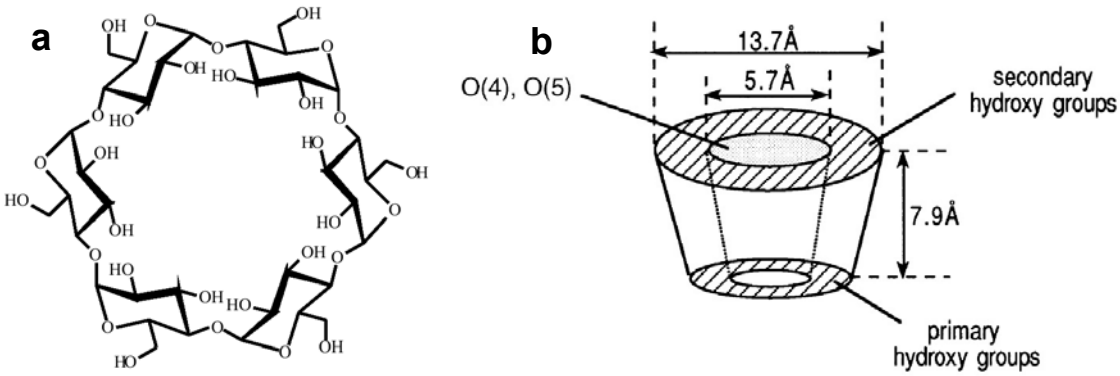

Figure 6-8. **a**: Structure of α-CD. **b**: Shape and dimensions of the molecule.

The exterior of the cavity is hydrophilic, making the molecule water-soluble, while the interior is semi-polar[14,15]. The most probable mode of binding involves the insertion of the less polar part of the guest molecule into the cavity, while the more polar groups of the guest remain exposed to the bulk solvent just outside the wider opening of the cavity[15]. As a general rule, the complex is strong when there is a size complementarity between the guest and the cavity of the CD. Molecules containing aliphatic chains can fit into the α-CD, while molecules containing phenyl groups fit better into β-CD. We have chosen to investigate the complexes between α-CD and aliphatic α,ω-dicarboxylic acids $^{-}OOC–(CH_2)_n–COO^{-}$. In solution, the binding constant increases when the aliphatic chain length increases, and this is attributed to the hydrophobic effect[16,17]. Comparisons have been made with maltohexaose, which is the linear analog of α-CD.

Sample preparation

All chemicals were purchased from Aldrich and used as received. A stock solution of α-CD (5.0×10^{-3} M) was prepared in doubly distilled water. All stock solutions of α,ω-dicarboxylic acids (5.0×10^{-3} M) were prepared in NH_4OH (pH = 9). The 2.0×10^{-3} M solutions of α-cyclodextrin complexes were prepared by mixing equimolar amounts of α-CD and α,ω-diacids. The stock solutions were diluted to their final

concentration with aqueous NH_4OH. The complexes with maltohexaose were prepared in the same way as complexes with α-CD.

References

1. K.A. Sharp, B. Honig; Salt Effects on Nucleic Acids. *Curr. Opin. Struct. Biol.* **1995,** 5: 323.

2. D.H. Turner; Thermodynamics of Base Pairing. *Curr. Opin. Struct. Biol.* **1996,** 6: 299.

3. R. Owczarzy, P.M. Vallone, F.J. Gallo, T.M. Paner, M.J. Lane, A.S. Benight; Predicting Sequence-Dependent Melting Stability of Short Duplex Oligomers. *Biopolymers* **1998,** 44: 217.

4. J. Sponer, J. Laszczynski, P. Hobza; Hydrogen Bonding and Stacking of DNA Bases: a Review of Quantum-Chemical *ab initio* Studies. *J. Biomol. Struct. Dyn.* **1996,** 14: 117.

5. K.J. Breslauer; Extracting Thermodynamic Data From Equilibrium Melting Curves for Oligonucleotide Order-Disorder Transition. *Methods Enzymol.* **1995,** 221.

6. N. Sugimoto, S.-I. Nakano, M. Yoneyama, K.-I. Honda; Improved Thermodynamic Parameters and Helix Initiation Factor to Predict Stability of DNA Duplex. *Nucl. Acid. Res.* **1996,** 24: 4501.

7. B.H. Geierstranger, D.E. Wemmer; Complexes of the Minor Groove of DNA. *Annu. Rev. Biomol. Struct.* **1995,** 24: 463.

8. J. Pindur, G. Fischer; DNA Complexing Minor Groove-Binding Ligands: Perspective in Antitumour and Antimicrobial Drug Design. *Curr. Med. Chem.* **1996,** 3: 379.

9. M.J. Waring, C. Bailly; DNA Recognition by Intercalators and Hybrid Molecules. *J. Mol. Recognit.* **1994,** 7: 109.

10. A.H.J. Wang; Intercalative Drug Binding to DNA. *Curr. Opin. Struct. Biol.* **1992,** 2: 361.

11. J.B. Chaires; Energetics of Drug-DNA Interactions. *Biopolymers* **1997,** 44: 201.

12. J. Szejtli; Introduction and General Overview of Cyclodextrin Chemistry. *Chem. Rev.* **1998,** 98: 1743.

13. W. Saenger; Cyclodextrin Inclusion Compounds in Research and Industry. *Angew. Chem. Int. Ed. Engl.* **1980,** 19: 344.

14. K.A. Connors; The Stability of Cyclodextrin Complexes in Solution. *Chem. Rev.* **1997,** 97: 1325.

15. M.V. Rekharsky, Y. Inoue; Complexation Thermodynamics of Cyclodextrins. *Chem. Rev.* **1998,** 1875.

16. I. Gomez-Orellana, D. Hallen, M. Stödeman; Microcalorimetric Titration of α-Cyclodextrin With Some Straight-Chain α,ω-Dicarboxylates in Aqueous Solution at Different Temperature. *J. Chem. Soc., Faraday Trans.* **1994,** 90: 3397.

17. G. Castronuovo, V. Elia, F. Velleca, G. Viscardi; Thermodynamics of the Interaction of α-Cyclodextrin With α,ω-Dicarboxylic Acids in Aqueous Solutions. A Calorimetric Study at 25°C. *Thermochimica Acta* **1997,** 292: 31.

7. MASS SPECTROMETERS USED

7.1. LCQ: electrospray quadruplole ion trap mass spectrometer

The LCQ is a commercial instrument by ThermoFinnigan (San Jose, CA, USA). It was used with its standard electrospray source. We used the software Xcalibur 1.0 with the advanced scan features. The mass range extends to 2000 m/z. Up to 10 MS/MS steps can be achieved in theory. The standard scan features allow to change the activation amplitude. The advanced scan features allow to change also the activation time.

Electrospray source

The electrospray source (standard on the LCQ instrument) is illustrated in Figure 7-1. The sample is infused, at flow rates typically in the range 1-5 μL/min, in the sample tube (0.1 mm ID, fused silica) to the ES needle. The ES nozzle directs the sheath gas and the auxiliary gas (nitrogen) to assist the formation of the spray. The needle is slightly off-axis compared to the heated capillary that is used as counter-electrode. This allows a better sampling of the ions. The ions are drawn into the heated capillary in the atmospheric pressure region and are transported to the capillary-skimmer region (1 Torr) by a decreasing pressure gradient. A potential (0 to ± 130 V) assists in repelling ions from the heated capillary to the skimmer.

Ions coming from the heated capillary enter the tube lens, which focuses the ions towards the skimmer during ion accumulation. It is also used as a gate to stop the injection of the ions to the mass analyzer: a potential of –200 V (+200 V) is used to deflect positive (negative) ions away from the skimmer. The skimmer acts as a vacuum baffle between the high pressure capillary-skimmer region (at 1 Torr) and the lower pressure first octapole region (at 10^{-3} Torr).

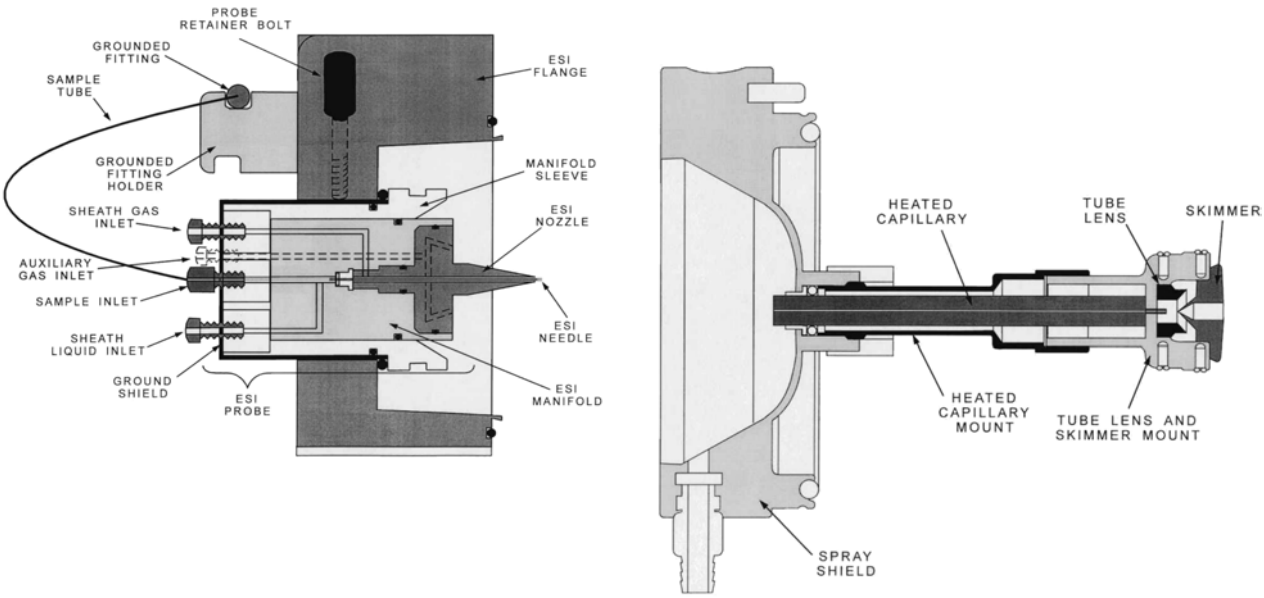

Figure 7-1. Cross sectional view of the electrospray source of the LCQ mass spectrometer (LCQ MS detector hardware manual pp. 2-13 and 2-17).

Sample requirements

It is very difficult to obtain a stable spray with a purely aqueous solution. It is therefore necessary to add 20% methanol to the infused solutions. For experiments on duplex DNA, methanol could be a problem. We have performed circular dichroism measurements that revealed that 20% methanol did not alter the B double helix structure (data not shown).

Source-CID

Three source parameters can be used to vary the internal energy given to the ions in the source region:

- **The heated capillary temperature (T_{cap})**. It can be raised up to 350 °C.
- **The capillary voltage (V_{CS})**. This voltage difference between the capillary and the skimmer causes the ions to accelerate in the 1 Torr region of the source, in which collisions occur.
- **The tube lens offset (TLO)**. The tube lens has a mass-dependent potential applied to it to focus the ions towards the skimmer. This potential can be modulated by an offset of between 0 and ± 60 V, called the tube lens offset. It can be applied to the tube lens. For positive ions, a positive offset causes the ions to travel faster towards the skimmer, and the collisions with the background gas are more energetic. For negative ions, a more negative tube lens offset causes more energetic collisions.

Ion optics

Ions enter the optics after passing through the skimmer. The ion optics consists of two octapoles and an interoctapole lens. The octapoles act as ion transmission devices. The interoctapole lens assists in the focusing and gating of the ions. It also serves as a vacuum baffle between the first octapole region and the analyzer region (2×10^{-5} Torr).

The quadrupole ion trap (QIT) mass analyzer

The quadrupole ion trap mass analyzer (Figure 7-2) includes three stainless steel electrodes: the entrance endcap electrode, the ring electrode, and the exit endcap electrode. The inner surfaces of the electrodes are hyperbolic. They form a cavity in which the mass analysis takes place. Ions enter the cavity through the entrance endcap electrode, and can be ejected through either endcap electrode during mass analysis. Ions that are ejected through the exit endcap electrode are focused towards the detection system. The cavity is filled with helium at a pressure of 10^{-3} Torr.

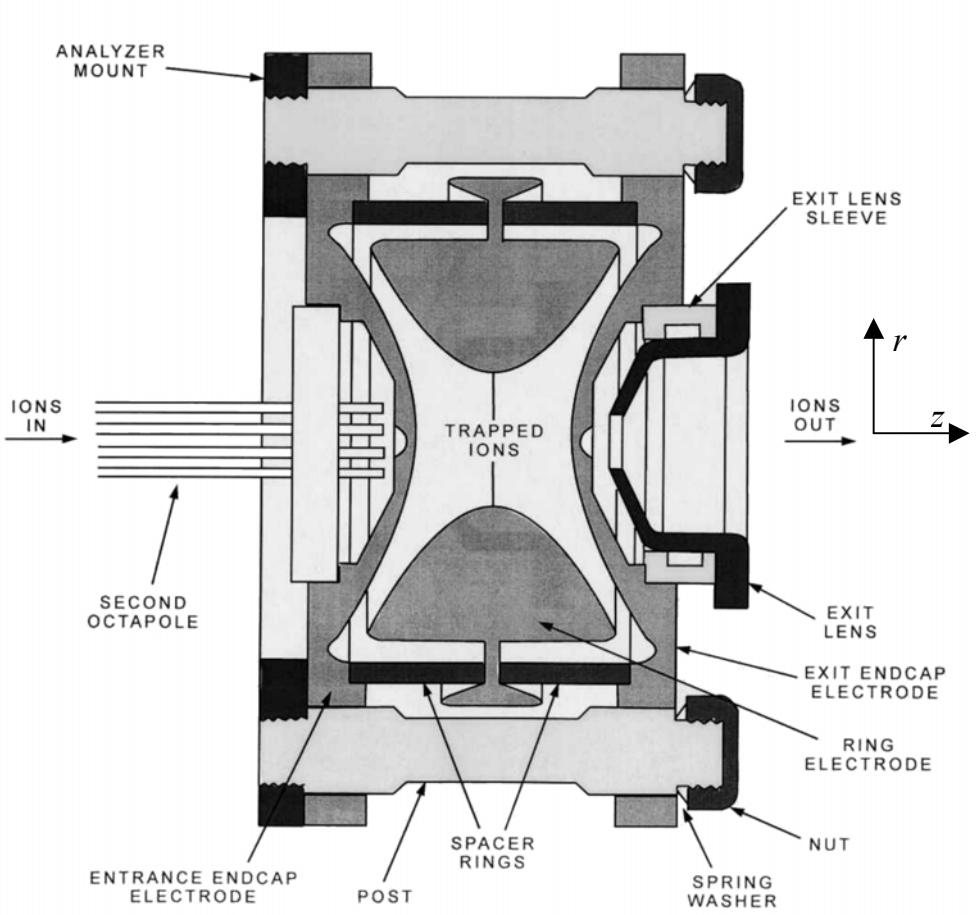

Figure 7-2. Cross sectional view of the ion trap mass analyzer (LCQ MS detector hardware manual p. 2-21).

An ac voltage of constant frequency (760 kHz – a radio-frequency (RF)) and variable amplitude (0 to 8500 V zero-to-peak) is applied to the ring electrode [$V_{rf}\cos(2\pi f_{rf}t)$]. This produces a three-dimensional quadrupole field within the mass analyzer cavity. Ions stored in the trap follow trajectories described by the Mathieu differential equation. The solution of this equation is expressed in terms of the Mathieu parameters a_z and q_z (equations 7.1 and 7.2) in the case of the ion trap[1-4].

$$a_z = -2a_r = \frac{-16zeU}{m\left(r_0^2 + 2z_0^2\right)\Omega^2} \tag{7.1}$$

$$q_z = -2q_r = \frac{-8zeV}{m\left(r_0^2 + 2z_0^2\right)\Omega^2} \tag{7.2}$$

$\vec{r}$ and $\vec{z}$ represent the radial and axial directions respectively. U is the dc amplitude, V is the RF amplitude, e is the charge of the electron, z is the charge of the ion, m is the mass of the ion, r_0 is the inner radius of the ring electrode, z_0 is the axial distance from the center of the device to the nearest point of the endcap electrodes, and $\Omega = 2\pi f_{rf}$ where f_{rf} is the frequency of the main RF voltage (760 kHz). a_z and q_z therefore depend inversely on the masse-to-charge ratio of the ion. Plotting these solutions in the (a,q) space for the $\vec{r}$ and $\vec{z}$ dimensions forms the QIT stability diagram (Figure 7-3). In order to remain trapped in the analyzer, the ions must have stable trajectories in both the axial and the radial direction. They must be located in the shaded region of Figure 7-3. In practice, as the dc voltage $U = 0$, the operating line is defined by $a_z = 0$.

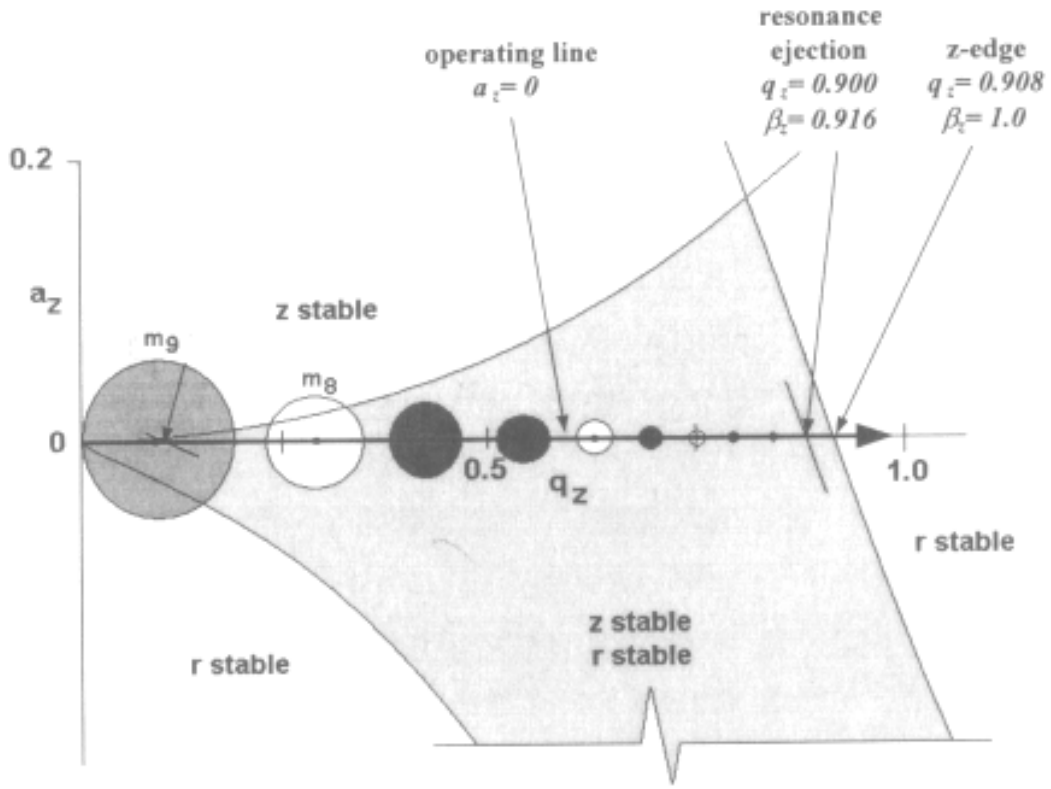

Figure 7-3. A portion of the QIT stability diagram (shaded region) showing the mass-selective instability operating line at $a_z = 0$. The circles represent ion q_z values on the operating line for various ions with different mass-to-charge ratios (e.g. $m_9 > m_8$). Adapted from reference 3.

The motion of ions confined in a quadrupole ion trap is characterized by an axial and a radial secular frequency. These frequencies depend on the q_z value of these ions (and therefore on their mass-to-charge ratio), which can be excited upon resonant irradiation at either frequency, or both of them. Typically such irradiation is effected by applying an oscillating potential across the endcap electrodes.

Ion trapping in the analyzer

In the case of electrospray-QIT instruments, the ions are formed outside the trap at atmospheric pressure and have to be injected in the mass analyzer. They therefore have some initial kinetic energy in the $\vec{z}$ direction, and enter the trap from a boundary (through the endcap). Both conditions disfavor storage[5].

To efficiently trap the axially injected ions, it is crucial to have an appropriate RF amplitude applied to the ring electrode and to have a helium bath gas at 1-2 mTorr[3,5,6]. Collisions with He kinetically cool the ions which eventually "fall" in the middle of the potential energy well, i.e. in the center of the trap. Concerning the amplitude of the RF trapping potential, an approximately linear relationship exists between the optimum RF amplitude and the *m/z* ratio of the ion. Because only one amplitude is applied during ion accumulation, the well depth decreases with *m/z*, which minimizes *m/z* discrimination.

In the trap, too few ions would result in a loss of sensitivity, and too many ions would cause space charge effects. Space charge effects are caused by the distortion of the applied trapping field owing to the presence of the electrostatic fields from the ions. Space charge effects may induce a significant deviation of the ion motion compared to the predicted trajectories. This causes a degradation of the resolution*, a reduction in peak heights, and mass shifts[3]. The amount of ions allowed to enter the trap is regulated by the automatic gain control of the instrument. A fast pre-scan is performed before the analytical scan to determine the optimum ion injection time, during which the ions are accumulated in the trap.

---

* The resolution of a peak at mass *m* is equal to $m/\Delta m$. Δm is the peak's full width at half maximum.

Mass-selective axial instability mode

This is the way full scan spectra are produced. For the mass-selective instability scan, the operating line in the QIT stability diagram (Figure 7-3) starts at $(a_z,q_z) = (0,0)$ and passes through $(a_z,q_z) = (0,0.908)$. Since q_z is inversely proportional to the mass (m), ions with a high mass-to-charge ratio have a lower q_z value than low mass-to-charge ratio ions. By increasing V, the RF amplitude applied to the ring electrode, ions positioned along the operating line move towards higher q_z values. At the edge of the stability diagram ($q_{z\text{-edge}} = 0.908$), instability ensues in the $\vec{z}$ direction and the ions leave the QIT through the holes in the endcaps. The RF amplitude ramp (from 0 to 8500 $V_{z\text{-p}}$) causes ions of increasing m/z ratios to be ejected consecutively from the trap.

Ideally, all ions of the same m/z must be ejected from the trap in a dense packet. The resolution is improved by the use of the helium bath gas. The ions are kinetically cooled in the center of the trap, and the ion packet is confined in space. The resolution is also improved by the use of a resonant ejection RF voltage applied on the endcap electrodes when ions approach the stability boundary. The resonance ejection RF voltage is applied at fixed frequency and increasing amplitude during the ramp of the ring electrode RF voltage.

Collision-induced dissociation in the trap

Ion trap instruments perform the tandem MS analyses in time: a sequence of events is applied to the ions that are stored in the trap. A typical MS/MS experiment consists in the following steps:

- **Ion accumulation and storage** (see above).
- **Isolation of the ion of interest**. A waveform voltage is applied to the endcap electrodes, in combination with the ring electrode RF voltage, to eject all ions except those of a selected mass-to-charge ratio (or narrow ranges of m/z ratios). The ion isolation waveform is calculated by the LCQ and applied automatically at the correct time.
- **Resonance excitation of the ion of interest**. An RF voltage that is resonant with the axial secular frequency of the ion is applied between the endcap electrodes. The maximum activation amplitude V_{max} is equal to 5 V (peak-to-peak), and the

amplitude can be varied from 0 to 100% of V_{max} by steps of 1%. The activation time can be varied from 1 to 10,000 ms with the advanced scan features of the Xcalibur 1.0 software. In all our experiments, the q_z of the selected ion has been kept at 0.250. During resonant excitation, the kinetic energy of the ions is increased. By collisions with the helium atoms, kinetic energy can be converted into internal energy of the ion.

- **Mass analysis of the resulting fragments**. A mass-selective instability scan is subsequently performed to detect the fragments formed upon collision-induced dissociation.

Such events can be combined in time to perform MS^n experiment (up to n = 10).

Detection system

A conversion dynode is located at a right angle with respect to the ion beam. A potential of -15 kV (+15 kV) is applied for the detection of positive (negative) ions. When an ion strikes the conversion dynode, secondary particles are emitted. The high voltage applied to the conversion dynode results in a high conversion efficiency and an increased signal. The increase in conversion efficiency is more pronounced for more massive ions than for less massive ones. These secondary particles strike the inner walls of the cathode of an electron multiplier with sufficient energy to eject electrons. The signal is amplified and a cascade of electrons is created that finally results in a measurable current at the end of the cathode where the electrons are collected by the anode.

7.2. Q-TOF2: Electrospray hybrid quadrupole – time-of-flight mass spectrometer

Electrospray source

In conventional electrospray sources, the trajectory of analyte ions is roughly a straight line between the inlet tube carrying the solution of interest and a skimmer orifice placed at a short distance away. The Q-TOF2 instrument is equipped with the so-called Z-spray source, which is an adaptation of electrospray. The Z-spray inlet source has a geometry such that the trajectory of the ions follows a sort of flattened Z-shape in going from the inlet tube to the final skimmer (Figure 7-4). Electrical potentials in the source cause the ion beam to bend towards the sample cone, and then to the extraction cone. However, the neutrals are not deflected and travel straight to the cleaning baffle.

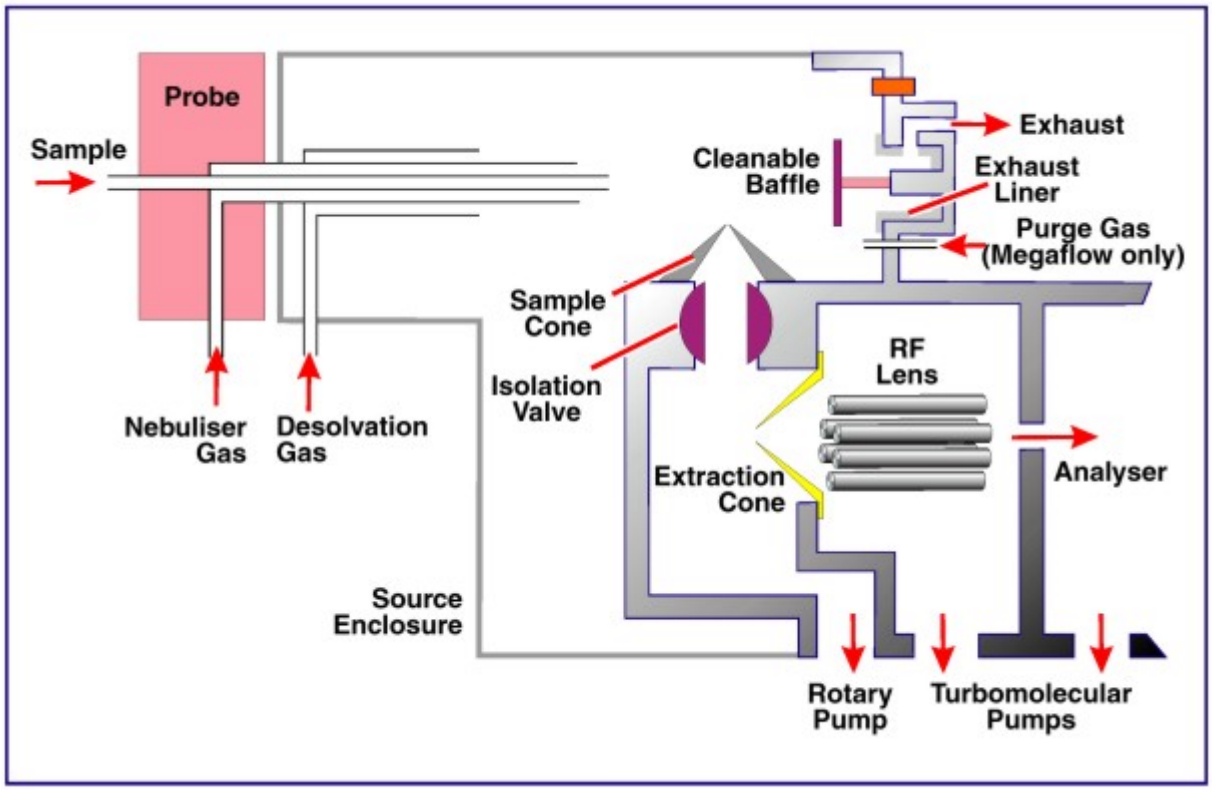

Figure 7-4. Schematic view of the electrospray source of the Q-TOF2 instrument (from the Micromass Z-spray manual).

Sample infusion

For the electrospray experiments, the solution is injected at a flow rate of typically 5 μL/min, with a Harvard (model 22) injector. The syringe is connected to a peek tubing, which is connected to a stainless steel capillary. For nanospray experiments, metal-coated medium glass capillaries (Protana, Odense, DK) were used.

Source-CID

Different source parameters can be used to vary the internal energy given to the ions in the source region: the source block temperature, the desolvation temperature (temperature of the gas infused near the sample cone), and the voltage difference between the sample cone and the extraction cone. In practice, the source block and desolvation temperatures were kept constant at 80 °C for all our experiments. Only the voltage difference between the two skimmers was varied.

Quadrupole devices

A quadrupole consists of four rods of circular cross-section on which opposite dc and ac voltages are applied, as shown in Figure 7-5. Theoretically the rods should have hyperbolic cross-sections, but in practice cylindrical rods work satisfactorily.

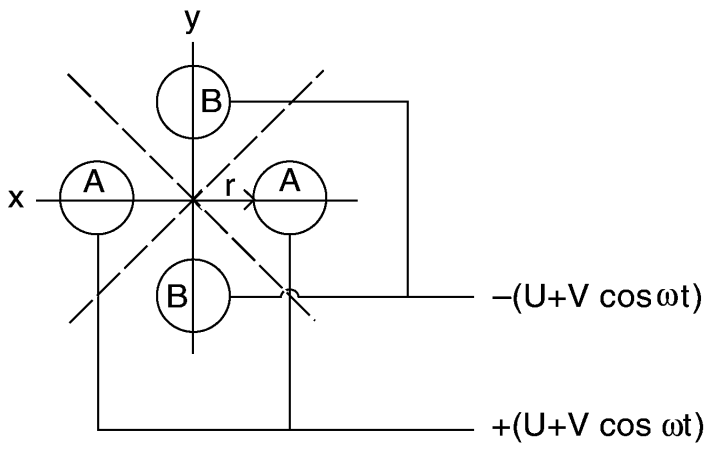

Figure 7-5. Cross-sectional view of a quadrupole assembly. A positive potential +[$U + V\cos(\Omega t)$] is applied to two opposite rods (A) and a negative potential –[$U + V\cos(\Omega t)$] on the other two (B). The dotted lines indicate planes of zero electric field. The dimension r is typically of about 5 mm. The $\vec{x}$ and $\vec{y}$ axes are indicated on the figure, the $\vec{z}$ axis being perpendicular to the plane of the paper. (Figure from reference 7, p. 386).

The resulting field in the $(\vec{x},\vec{y})$ plane causes the ions to be alternately attracted and repelled by the rod pairs. The movement of the ions in the quadrupole is oscillatory. As in the case of the quadrupole ion trap, the conditions to have stable trajectories for a given ion can be represented in a stability diagram (Figure 7-6). The a and q parameters are given by [1,7,8]:

$$a = \frac{8zeU}{mr^2\Omega^2} \tag{7.3}$$

$$q = \frac{4zeV}{mr^2\Omega^2} \tag{7.4}$$

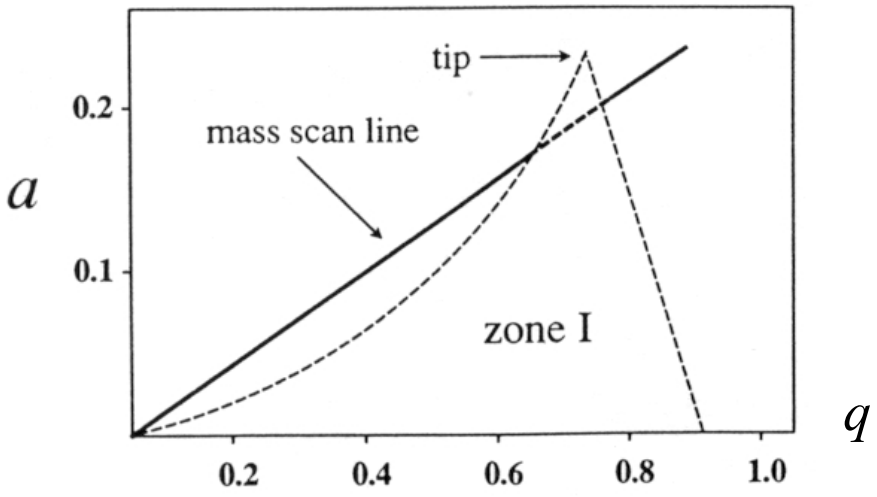

Figure 7-6. The operating region of the quadrupole stability diagram[8]. The zone I represents the area of stable ion motion, i.e. (a,q) values for which ions can be transmitted through the quadrupole. Other ions with non-stable trajectories eventually hit the rods and are lost.

In practice, the frequency (Ω) is fixed, typically in the range 1-2 MHz, and the operating line is defined by a fixed U/V ratio, and therefore a constant slope a/q. A quadrupole can be used for different purposes:

- To use the quadrupole as a mass scanning device, the slope is set to cross the stability region near the top (to have only ions of a small m/z range passing through

the quadrupole at the same time), the U/V ratio is constant and the magnitudes of U and V are varied to scan the desired mass range.

- To use the quadrupole as a mass filter, the U/V ratio is fixed at a value that allows only the ions of interest to pass through the quadrupole. This is also called the 'narrow-bandpass' mode.

- To use the quadrupole as an ion guide for ions of all masses, it is operated in the "RF only" mode ($U = 0$ and $a = 0$). This dos not mean that all ions are transmitted equally through the quadrupole[9,10]. All ions with m/z values below a certain cut-off corresponding to $q = 0.908$ are rejected. Although there is no sharp cut-off at the other end of the spectrum, transmission of ions with high m/z values suffers because of poor focusing. In the RF-only mode, ions covering approximately an order of magnitude in m/z are transmitted simultaneously.

Note also that the field has no effect along the direction of the central axis of the quadrupole assembly (the $\vec{z}$ axis). The ions must first be accelerated through an electric potential (typically 5-10 V) before entering the quadrupole.

Time-of-flight analyzers

In a time-of-flight (TOF) mass spectrometer, ions formed in the source are extracted and accelerated to a high velocity by an electric field into an analyzer consisting of a long 'drift tube'. After the initial acceleration phase, all ions have the same kinetic energy:

$$mv^2/2 = zeE \tag{7.5}$$

where m is the mass of the ion, v its velocity, z its charge, e the charge of the electron, and E the applied electric field. Equation (7.6) follows by simple rearrangement:

$$v = \sqrt{\frac{2zeE}{m}} \tag{7.6}$$

If the distance from the source to the detector is d, then the time t an ion takes to traverse the drift tube is given by equation (7.7).

$$t = \frac{d}{v} = d.\sqrt{\frac{m}{2zeE}} \tag{7.7}$$

The flight time is therefore proportional to the square root of the *m*/*z* ratio. Heavy ions travel more slowly to the detector than light ions (Figure 7-7). as all ions are injected in the TOF at the same time, TOF analyzers are not scanning devices.

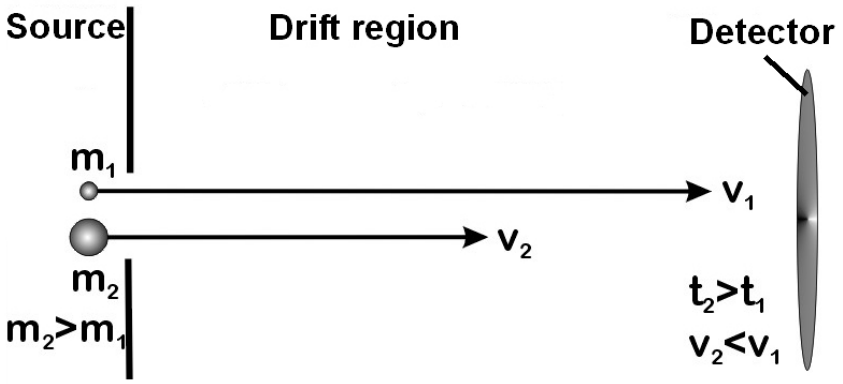

Figure 7-7. Principle of the time-of-flight mass analyzer.

Generally, the resolution attainable with a TOF analyzer is limited by two factors. First, as the flight time is proportional to the square root of *m*/*z*, the difference in the flight times for two ions separated by one mass unit decreases as the mass increases. The resolution is therefore lower for high-mass ions. Second, all ions of a given *m*/*z* do not have exactly the same velocity after acceleration in the source. They have a kinetic energy distribution. A technical means to correct for the initial kinetic energy distribution is to use an ion mirror (or reflectron).

A homogeneous electrostatic field is placed at the end of the flight path and has the same polarity as that of the ions. The ions come to a stop and are accelerated in the opposite direction (Figure 7-8). Consider two ions of a same *m*/*z* value, but with two different initial kinetic energies. The faster ions, having greater kinetic energy, travel further into the electrostatic field before being reflected. As a result, faster ions spend slightly more time within the reflectron than do the slower ones. The reflectron is tuned to focus the ions on the detector in terms of arrival time, thereby increasing resolution.

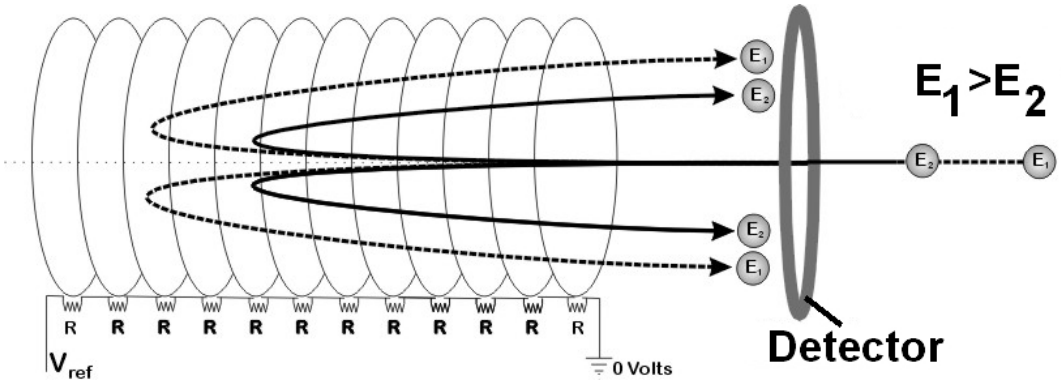

Figure 7-8. Principle of the reflectron. (adapted from the Micromass Tofspec manual).

The hybrid Q-TOF instrument

The term Q-TOF is used to describe a type of hybrid mass spectrometer system, in which a quadrupole analyzer (Q) is used in conjunction with a time-of-flight analyzer (TOF), as shown in Figure 7-9.

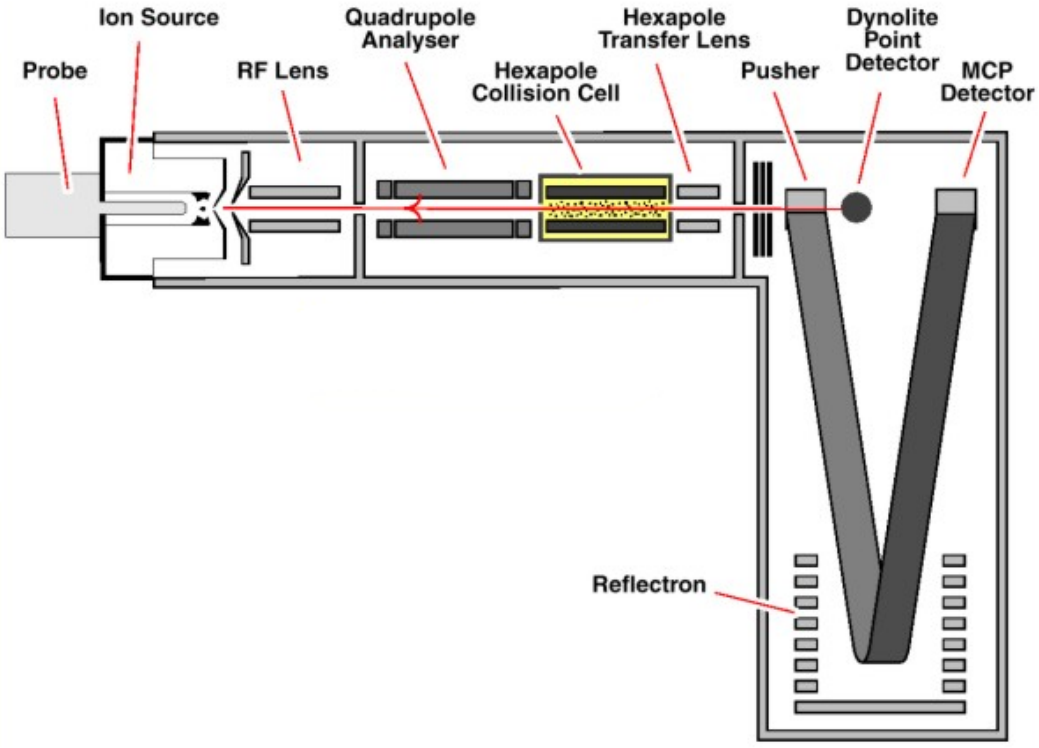

Figure 7-9. Schematic view of the Micromass Q-TOF2 instrument (from the Micromass Q-TOF manual).

The ions produced in the Z-spray source pass through the RF lens (hexapole used to confine the ion beam) before entering the quadrupole analyzer. The quadrupole can be used in the RF-only mode to allow all ions to go to the TOF, or in the narrow-bandpass mode to select an ion of given *m*/*z* for MS/MS (see below). The ions then pass through a hexapole that is enclosed in a collision gas cell filled with argon (about 10 mTorr) and through another hexapole RF lens before being transferred to the reflectron TOF analyzer.

The ions are produced continuously in the source, and a continuous beam of ions arrives in the TOF region. Orthogonal injection provides a high-efficiency interface for transferring ions from a continuous beam to a pulsed mode that can be coupled to a time-of-flight analyzer[10-12]. The ions are first slowed down, and an electrode is placed so that its pulsed electric field is at right angle with respect to the continuous beam. This is the pusher unit. The trajectory of the ions is shown in Figure 7-9. A section of the main beam is pulsed away, and ions in this pulsed set all start at the same moment and can be timed by the TOF analyzer. The flight times give *m*/*z* values and the number of ions give the abundances.

Single MS operation

For full scan MS spectra, the TOF is used as the analyzer because of its higher resolution compared to the quadrupole. The quadrupole is simply used in the RF-only mode, so that there is no ion selection. As mentioned before, this does not mean that all ions are equally well transmitted through the quadrupole. The *m*/*z* range of optimum transmission can be modified in the "MS profile" parameters of the instrument. The MS profile shown in Table 7-1 was used for all measurements, unless otherwise mentioned.

Table 7-1. MS profile used throughout this study.

Mass (*m*/*z*)	Dwell time (% of scan time)	Ramp time (% of scan time)
5	10	5
250	85	0

This means that the RF voltage is modulated during the spectrum acquisition to allow different mass ranges to be transmitted. The reason for scanning first at very low mass range during a short time is to purge the quadrupole from all possibly remaining unwanted ions.

In the Q-TOF2 instrument, even for single MS scans, argon is maintained in the collision hexapole, and the ions are accelerated through an electric potential of 10 V before entering this hexapole. It has been found by the manufacturer that collisions with the bath gas at relatively high pressure in the collision hexapole helped confining the ion beam. A well-defined ion beam is crucial for the operation of the pusher unit, and increases the instrument resolution.

MS/MS operation

For MS/MS experiments, the quadrupole analyzer is operated in the narrow bandpass mode. Ions of selected *m*/*z* can pass right through the inter pole space and pass out at the other end. Ions of other *m*/*z* values do not pass through, but strike the rods and are lost. This configuration effectively acts as an electronic gate.

The ions are injected in the hexapole collision cell with a higher kinetic energy than for the MS procedure. Typically, voltages of 15 to 40 V are used to accelerate the ions before entering the collision cell. By collisions with the argon atoms, pert of the relative kinetic energy can be converted into internal energy of the ion.

Detection system

The detector is a microchannel plate (MCP). It consists of a number of single point ion detection elements, which are very small electron multipliers. The MCP is designed to detect all ions of any single *m*/*z* value as they arrive separated in time. The pulse of electrons at the anode is about 1-2 ns in width. All the back ends of the detection elements are connected together electronically. This electronic pulse is used to trigger a timing pulse that is sent to the time-to-digital converter (TDC). The TDC registers the arrival time of the pulse (relative to the starting time given by the pusher), and the event and arrival time are stored in memory. Each TOF pulse results in a spectrum of

arrival times that is stored in memory. The dynamic range* of the TDC is limited by the counting dead time – the period after each ion event when the TDC itself is unable to record another count. Dead times are typically of several nanoseconds. The result is that intense mass peaks become distorted by depletion of the top right hand side of the peak, so that the peak intensity is decreased and the centroid** is shifted to the left. In the Q-TOF2 instrument, an empirical dead time correction can be applied to correct for such effect. In all our measurements, no dead time correction was necessary, as we always worked under the saturation level of the TDC (as a rule of thumb, below 200 counts per second).

References

1. W. Paul; Electromagnetic Traps for Charged and Neutral Particles (Nobel Lecture). *Angew. Chem. Int. Ed. Engl.* **1990,** 29: 739.

2. R.E. March; An Introduction to Quadrupole Ion Trap Mass Spectrometry. *J. Mass Spectrom.* **1997,** 32: 351.

3. M.E. Bier, J.C. Schwartz; Electrospray-Ionization Quadrupole Ion-Trap Mass Spectrometry. In *Electrospray Ionization Mass Spectrometry*; R.B. Cole, Ed.; John Wiley & Sons: New York, 1997; Chapter 7, pp. 235-289.

4. R.E. March; Advances in Quadrupole Ion Trap Mass Spectrometry. *Adv. Mass Spectrom.* **1998,** 14: 241.

---

* Dynamic range: the ratio of the overload level (the maximal signal power that the system can tolerate without distortion of the signal) to the noise level of the system.

** Centroid: center-of-gravity of the digitized signal for an ion.

5. S.A. McLuckey, G.J. Van Berkel, D.E. Goeringer, G.L. Glish; Ion Trap Mass Spectrometry of Externally Generated Ions. *Anal. Chem.* **1994,** 66: 689A.

6. J.N. Louris, J.W. Amy, T.Y. Ridley, R.G. Cooks; Injection of Ions into a Quadrupole Ion Trap Mass Spectrometer. *Int. J. Mass Spectrom. Ion. Proc.* **1989,** 88: 97.

7. Micromass: Back to Basics. *http://www.micromass.co.uk/basics/index.html*.

8. A.J. Reuben, G.B. Smith, P. Moses, A.V. Vagov, M.D. Woods, D.B. Gordon, R.W. Munn; Ion Trajectories in Exactly Determined Quadrupole Fields. *Int. J. Mass Spectrom. Ion. Proc.* **1996,** 154: 43.

9. L. Wojcik, K. Bederski; Determination of the Ion Transmission Coefficient for a Mass Spectrometer With a Quadrupole Ion Analyzer. *Int. J. Mass Spectrom. Ion. Proc.* **1996,** 153: 139.

10. I.V. Chernushevich, A.V. Loboda, B.A. Thomson; An Introduction to Quadrupole–Time-of-Flight Mass Spectrometry . *J. Mass Spectrom.* **2001,** 36: 865.

11. I. Chernushevich, W. Ens, K.G. Standing; Orthogonal Injection TOF MS for Analyzing Biomolecules. *Anal. Chem.* **1999,** 71: 452 A-461 A.

12. M. Guilhaus, D. Selby, V. Mlynski; Orthogonal Acceleration Time-of-Flight Mass Spectrometry. *Mass Spectrom. Rev.* **2000,** 19: 65.

8.
SPECIFICITY OF THE COMPLEXES

8.1. Double-stranded DNA

Introduction

Smith and Light-Wahl[1] have discussed the characteristics that allow to differentiate between specific associations observed by electrospray and nonspecific ones: these include persistence upon dilution, stability in the gas phase, and sensitivity to solution modifications (see Chapter 4). For double-stranded DNA, nonspecific aggregation translates in random associations of non-complementary strands. These nonspecific aggregations are often due to concentration effects. Ding and Anderegg[2] have shown that these effects could be avoided by working at low concentration (around 10 μM) with reasonably long strands (octamers or longer). This is in agreement with results reported earlier[3-5].

We studied the dodecamer duplex d(GGGGAATTGGGG)•d(CCCCAATTCCCC) (noted **GC**) by ES-MS on the Q-TOF instrument and studied the influence of the sample preparation and the electrospray conditions on the appearance of the spectra. The duplex is complementary, and the single strands have different masses and can be distinguished easily on the spectra (**G**: 3806.53 Da; **C**: 3486.34 Da).

Experimental

Electrospray mass spectra were acquired with a Micromass Q-TOF (first generation), equipped with a Z-Spray source. The first generation Q-TOF is similar to the Q-TOF2, except that no argon is used in the second quadrupole when performing single-stage MS measurements, and that the resolution is lower. A cone voltage of 50 V was used to optimize the observation of the charge state 5-. This cone voltage optimum is proper to this Q-TOF.

Influence of the electrolyte concentration

Thermal denaturation experiments monitor the separation of duplex into single strands by measuring the absorbance at 260 nm as a function of the solution temperature. The denaturation curves for duplex **GC** (concentration = 2.14×10^{-6} M) in NH_4OAc at 10 mM and 50 mM are displayed in Figure 8-1. The melting temperatures (T_m) are 35 °C and 48 °C respectively. The melting temperature is the temperature at which half the duplex is dissociated into single strands (if assuming a one-step dissociation). At higher concentration in NH_4OAc, the T_m does not increase significantly (T_m = 49 °C at [NH_4OAc] = 100 mM).

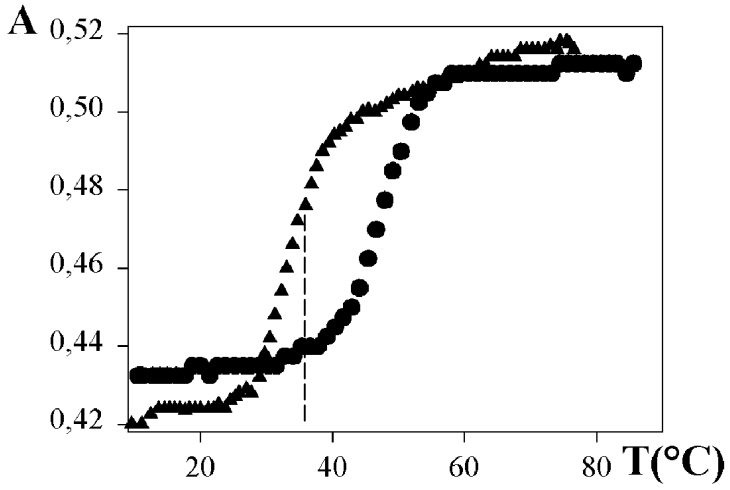

Figure 8-1. Thermal denaturation curves of the duplex in 10 mM (▲) and 50 mM NH_4OAc (●). The absorbance values have been normalized to allow a visual comparison of the curves.

To show how closely the mass spectra can be an image of the species present in the sprayed solution, we compared (a) a freshly annealed solution in 50 mM NH_4OAc with (b) a solution left overnight at 37 °C in a 10 mM NH_4OAc solution (T_m = 38 °C), sprayed immediately without cooling. The results are shown in Figure 8-2.

According to the denaturation curves (Figure 8-1), in solution (b), there should be approximately half the amount of duplex than in solution (a). The MS results (Figure 8-2) show that the relative intensity of the duplex compared to the single strands is indeed reduced by a factor of about two in the partially denatured sample. This indicates that the relative intensities of the noncovalent duplex is proportional to its concentration in solution. The amount of sodium adducts is lower in solution (a) than in solution (b). This indicates that high NH_4OAc concentrations help to displace the sodium from the negatively charged ions in solution.

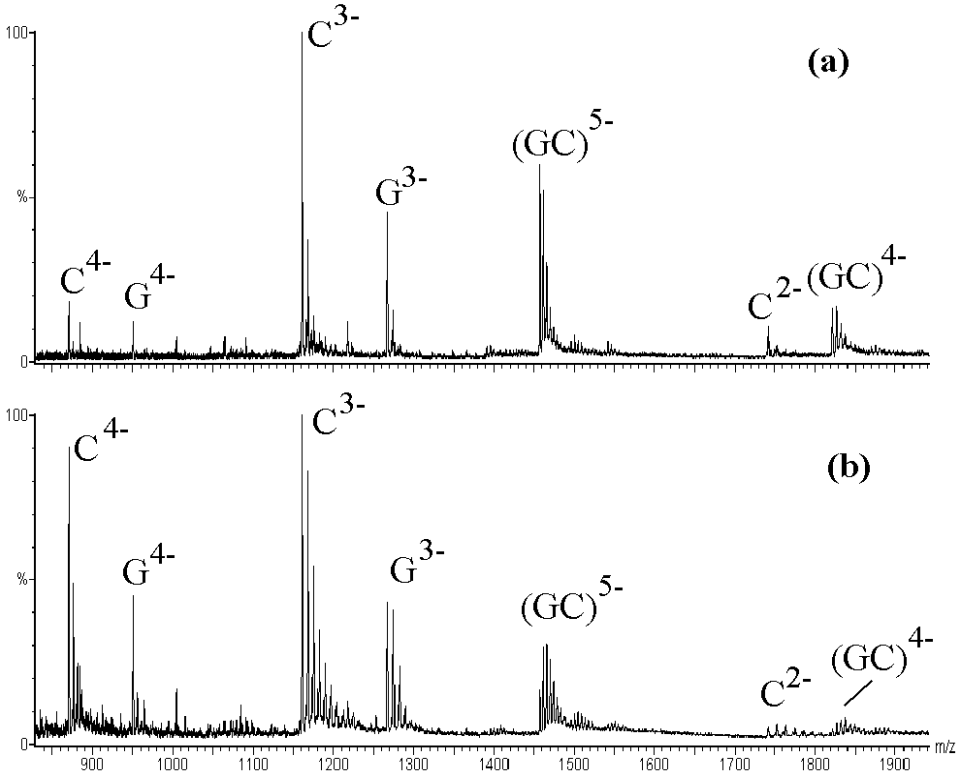

Figure 8-2. Compared full scan Q-TOF spectra of **(a)** a freshly prepared 10 µM duplex solution in 50 mM NH_4OAc and a **(b)** 10 µM solution partially denatured for 12 hours at 35 °C in 10 mM NH_4OAc.

Influence of the duplex concentration

The association of two oligonucleotide strands into a duplex is an equilibrium. The degree of association therefore depends on the concentration. Thermal denaturation experiments at different concentrations have been performed, and have shown that for duplex concentrations > 10^{-6} M, the duplex can be assumed to be quantitatively formed at room temperature.

Figure 8-3 shows the ES-MS spectra for duplex solutions at different concentrations. The nonspecific homodimers $(\mathbf{GG})^{5-}$ and $(\mathbf{CC})^{5-}$ are present at very low intensity at 20 μM concentration, but completely disappear at 10 μM concentration, while the relative intensity of the specific duplex $(\mathbf{GC})^{5-}$ increased compared to the single strands. An even more interesting feature of the dilution experiment is the partial suppression of sodium adducts when the duplex concentration is equal or lower than 10 μM (see the insets of Figure 8-3). This indicates that the Na^+ counterions are displaced by NH_4^+, and that a $[NH_4^+]$/[duplex] ratio of at least 5,000 is preferable. Ammonium adducts are readily eliminated by NH_3 loss during desolvation, which simplifies the spectra. The increase of the duplex/single strands ratio upon dilution of the sample is due to the elimination of most sodium adducts.

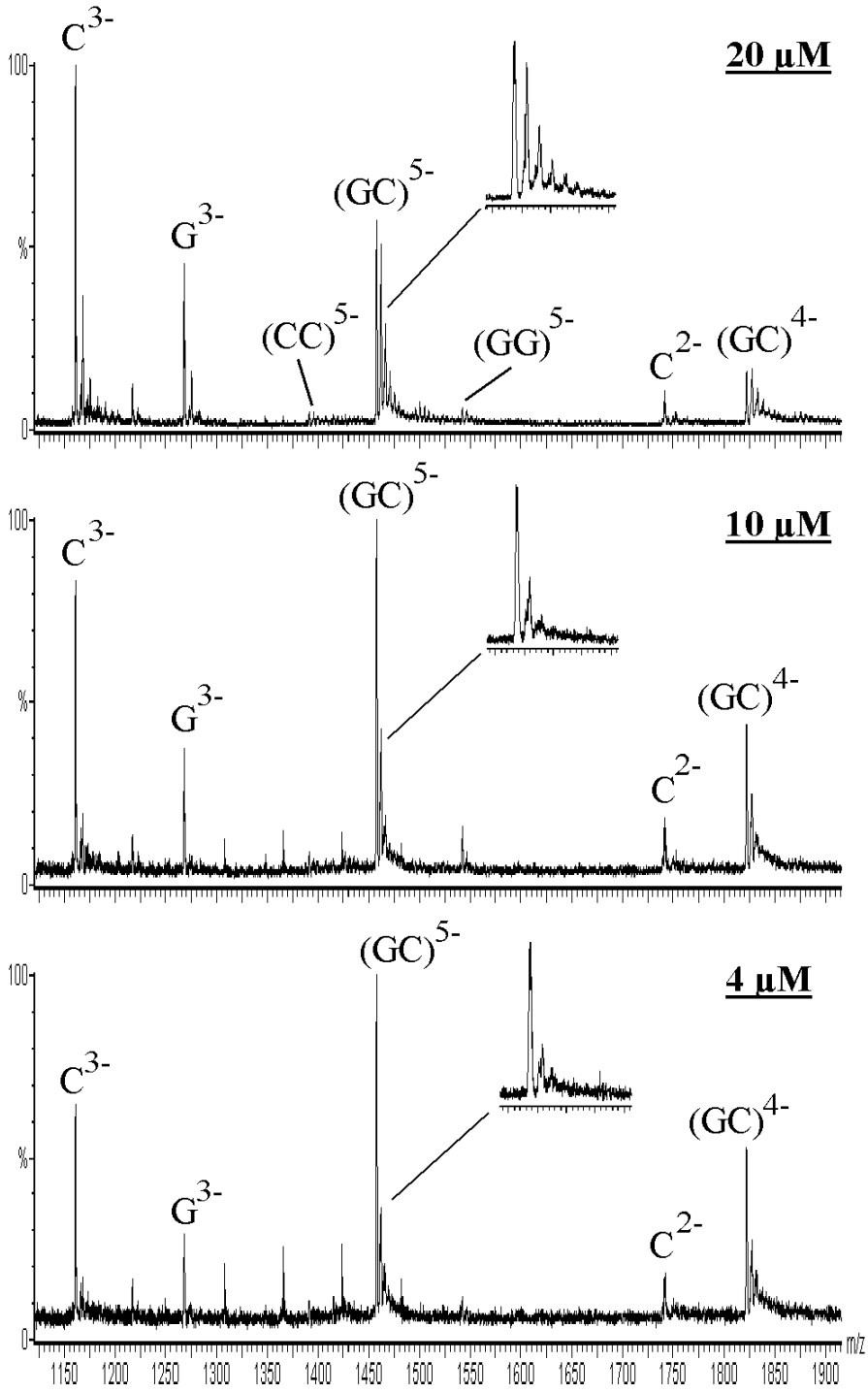

Figure 8-3. ES-MS spectra of duplex solutions recorded with a Q-TOF at different duplex concentrations, all in aqueous 50 mM NH_4OAc (no organic solvent added). The zoom on the (**GC**)$^{5-}$ species shows the distribution of sodium adducts in each case. The spectra obtained with a LCQ, using 20% methanol in water, are identical.

Influence of the cone voltage

This is illustrated with the full scan MS spectra of a 16-mer duplex recorded with the Q-TOF2 at different cone voltage values. This example has been chosen because all charge states from 5- to 8- can be detected on the spectra. The results are shown in Figure 8-4. Increasing the cone voltage has three effects: (1) an increase of the total intensity because ions are more effectively transmitted through the skimmer, (2) a stripping of the remaining NH_4^+ ions (NH_3 is lost, giving back a proton), and (3) a dissociation of the complex due to collisional activation. There is therefore an optimum voltage for each charge state. The higher the charge state, the lower the optimum voltage. The choice of a good working value of the cone voltage depends on the charge state that is selected*.

Next page:

Figure 8-4. Full MS spectra of duplex d(GGGCTATAATATCGGG)•d(CCCGATATTATAGCCC) recorded with the Q-TOF2 at different cone voltages (increasing upwards). For each spectrum 100 scans were summed. Scanning regions corresponding to the charge states 8- to 5- are shown from left to right. The number of counts on the detector corresponding to the 100% relative intensity is indicated in the top right hand corner of each small spectrum.

* There is no correspondence between the absolute values of the cone voltages on the Q-TOF1 and the Q-TOF2.

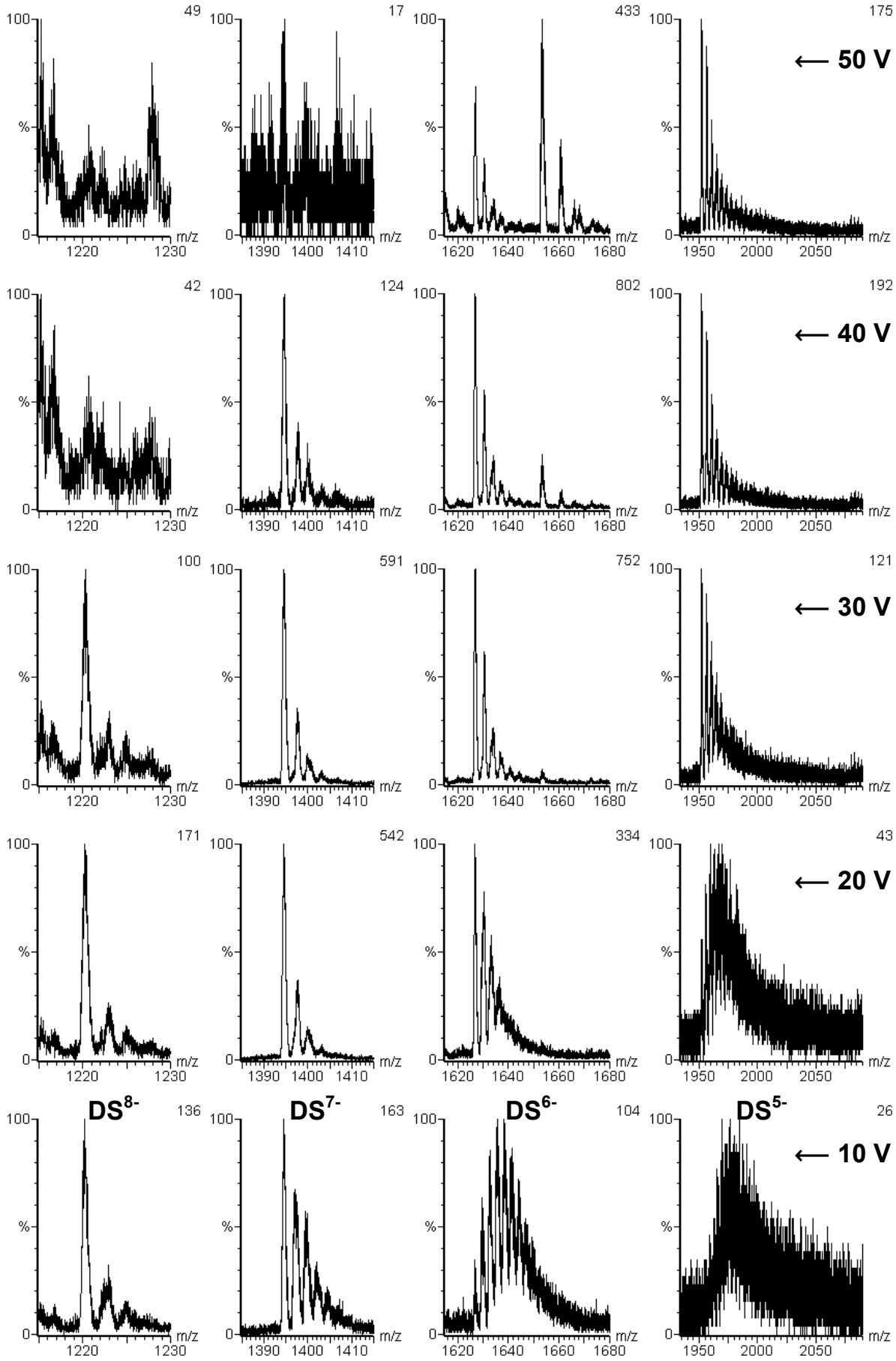
49
17
433
175
← 50 V
42
124
802
192
← 40 V
100
591
752
121
← 30 V
171
542
334
43
← 20 V
DS8-
DS7-
DS6-
DS5-
136
163
104
26
← 10 V
100
%
0
m/z
1220
1230
1390
1400
1410
1620
1640
1660
1680
1950
2000
2050

8.2. DNA complexes with drugs

Experimental

The ES-MS spectra were acquired with the LCQ. The electrospray source conditions were optimized to favor the observation of the fragile noncovalent species. This implies that the ions should have undergone just enough collisions in the high-pressure region of the source to be fully desolvated, keeping their internal energy low enough to avoid dissociation. We have chosen a heated capillary temperature of 190 °C, and a tube lens offset of 40 V. Although complexes survive to cone voltages up to -50 V, we used a constant value of -6 V to have a higher signal to noise ratio. The scanned mass range [1,000-2,000] was also kept constant in all experiments.

Complexes with minor groove binders

Figures 8-5 to 8-7 shows the spectra obtained with the LCQ for the 1:1 drug-duplex mixtures between the duplex **GC** (d(GGGGAATTGGGG)•d(CCCCAATTCCCC)) and the drugs netropsin (Fig. 8-5), Hoechst 33258 (Fig. 8-6) and distamycin A (Fig. 8-7). Regarding the stoichiometries of the complexes, different behaviors can be distinguished for the different drugs following their spectra. Netropsin shows exclusively the 1:1 complex, Hoechst 33258 shows a small amount of 1:2 complex in addition to the 1:1 one, and for distamycin A the 1:2 complex is the predominant species.

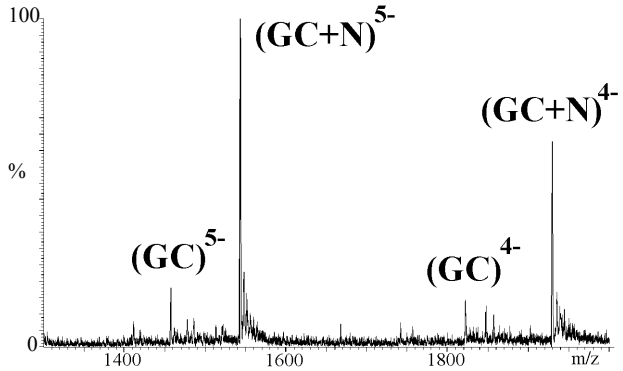

Figure 8-5. Full scan ES-ion trap MS spectra of an equimolar mixture (10-10 μM) of duplex **GC** and netropsin (**N**).

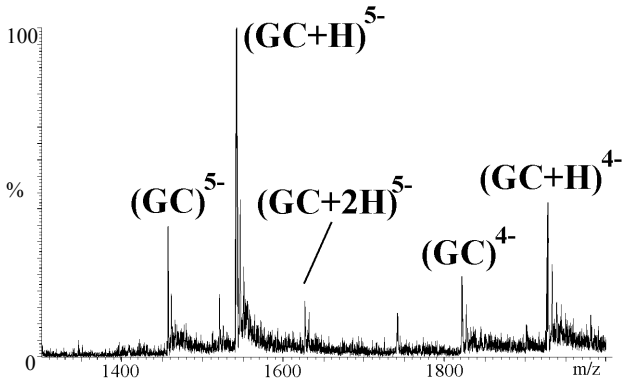

Figure 8-6. Full scan ES-ion trap MS spectra of an equimolar mixture (10-10 μM) of duplex **GC** and Hoechst 33258 (**H**).

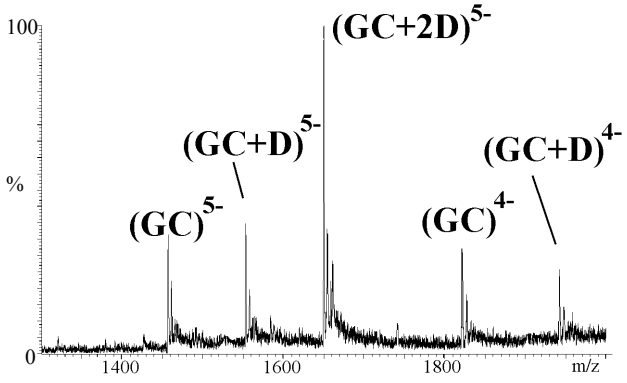

Figure 8-7. Full scan ES-ion trap MS spectra of an equimolar mixture (10-10 μM) of duplex **GC** and distamycin A (**D**).

To further characterize the formation of the 1:1 and 1:2 complexes, we studied the influence of the concentration of drug, from 2 μM to 20 μM, added to the 10 μM duplex solution in the case of netropsin, Hoechst 33258 and distamycin A. The data are summarized in Figure 8-8, where the relative intensities have been normalized to 100% for each spectrum. For netropsin, no 1:2 complex could be observed, even at the highest drug concentrations. For distamycin A, the 1:2 complex becomes rapidly predominant as the drug concentration increases, thereby indicating the preferential one-step formation of this 1:2 complex over the 1:1 complex, of which signal vanishes

progressively. The distinct behaviors of netropsin and distamycin A are well-known in the solution phase[6]. Distamycin forms a head-to-tail dimer which inserts in the AT-rich region, thereby widening the minor groove[7-9]. This 1:2 binding mode is favored by an alternating AT sequence compared to poly(A)-type ones because they naturally present a wider and more flexible minor groove[6,10]. In the case of netropsin, however, the positive charges at each end of the molecule prevent the formation of such dimers and the resulting complex with the AT-rich region is thus exclusively 1:1.

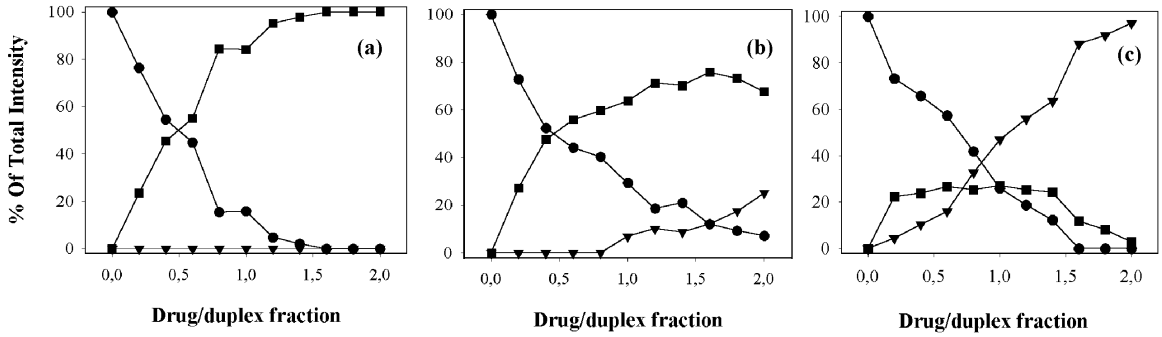

Figure 8-8. Plots of the relative intensities of the different species versus the drug molar fraction added to a 10 μM duplex solution for (a) netropsin, (b) Hoechst 33258 and (c) distamycin A. The circles (●) represent the intensity of the duplex (sum of the 5- and 4- charge states), the squares (■) represent the intensity of the 1:1 complex (sum of the 5- and 4- charge state) and the triangles (▼) represent the 1:2 complex (5- charge state only, due to the limited mass range). The symbols are bonded by a guideline.

In the case of Hoechst 33258, mass spectrometry is shedding a new light on a controversial problem: the possible existence of multiple stoichiometries for Hoechst binding to DNA[11-13]. With measurements in solution, in general, the presence of minor species of different stoichiometries is only suggested by clues. For example, a fluorescence measurement that can not be fitted with a 1:1 model may suggest that other complex species are present, but no clear cut can be made because the relative

contributions of the different complexes to the total fluorescence can not be separated. Our results suggest the formation of a 1:2 complex with a lower binding constant than for the 1:1 complex, which is the predominant one.

Complexes with intercalators

Influence of the polarity of the drug

The complexes between duplex **GC** and three intercalating ligands (ethidium, ascididemin and amsacrine) have been investigated by ES-MS on the LCQ. The experimental conditions were the same as for the complexes with the minor groove binders. Figures 8-9 to 8-11 show the spectra recorded for the three drugs at 10 µM and 30 µM concentration, the duplex concentration being kept at 10 µM. The spectra reveal a different behavior than for minor groove binders: instead of well-defined stoichiometries, the intercalators show multiple associations with a distribution suggesting a nonspecific addition on the duplex. For the different drugs, the relative intensities of the complexes compared to those of the duplexes parallels their polarity: peaks from complexes with the positively charged ethidium are far more intense than those with the polar neutral amsacrine, which are in turn more intense than those with the quasi non-polar neutral ascididemin molecule.

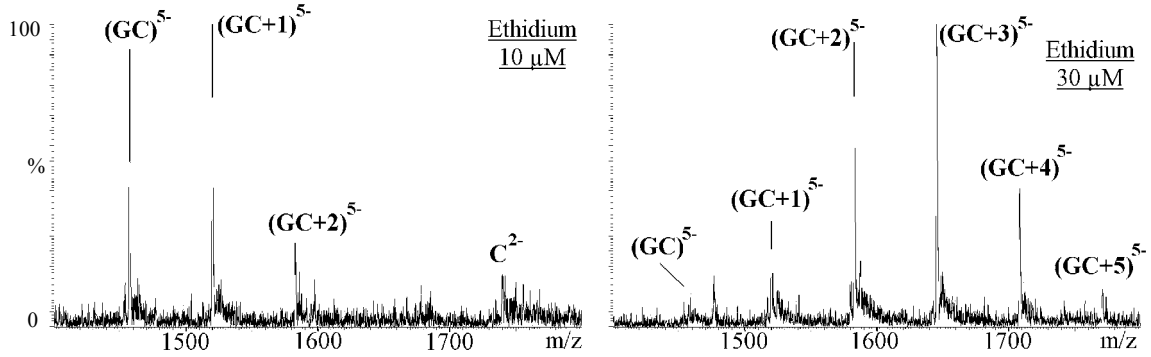

Figure 8-9. Full scan ES-ion trap MS spectra of duplex + ethidium mixtures. The duplex concentration was kept at 10 µM. The stoichiometries of the observed species are noted (GC+*n*), *n* being the number of added intercalator molecules.

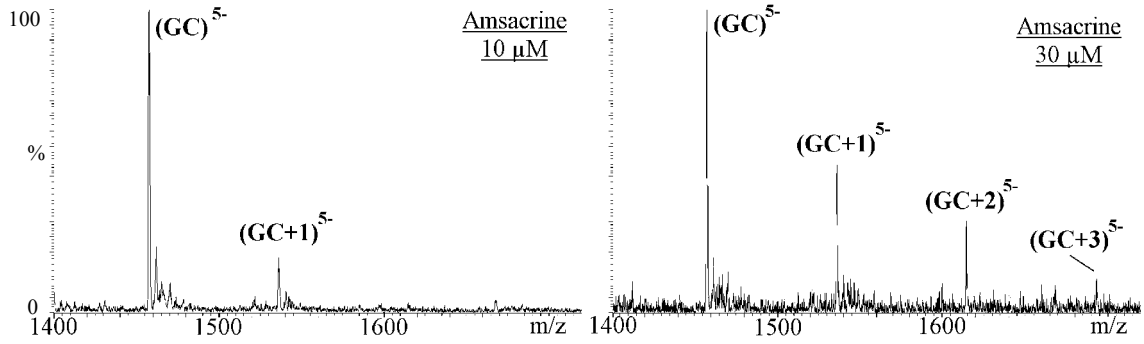

Figure 8-10. Full scan ES-ion trap MS spectra of duplex + amsacrine mixtures. The duplex concentration was kept at 10 µM. The stoichiometries of the observed species are noted (GC+*n*), *n* being the number of added intercalator molecules.

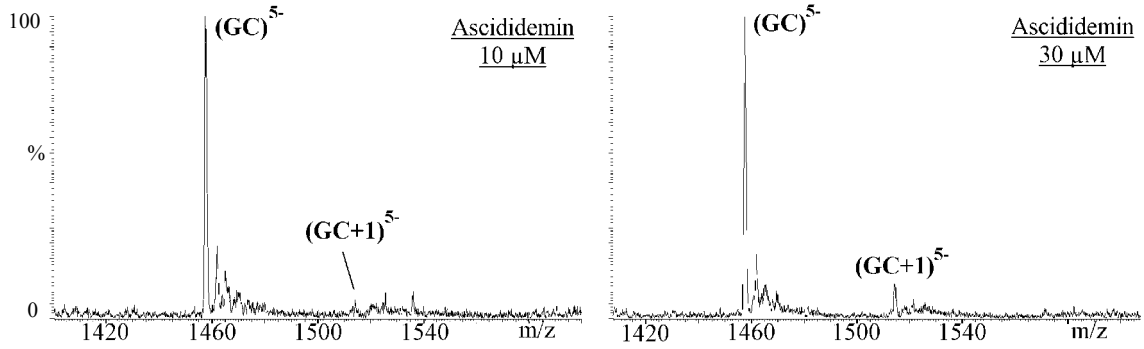

Figure 8-11. Full scan ES-ion trap MS spectra of duplex + ascididemin mixtures. The duplex concentration was kept at 10 µM. The stoichiometries of the observed species are noted (GC+*n*), *n* being the number of added intercalator molecules.

Complexes with cryptolepine and neocryptolepine

Cryptolepine and neocryptolepine are two indoloquinoline isomer alkaloids isolated from the roots of the African plant *Cryptolepis Sanguinolenta*[14]. They have been used in African folk medicine in the form of plant extracts for the treatment of multiple diseases. They have antibacterial, antiparasitic activities, and are strongly cytotoxic to tumor cells. The two drugs are structural isomers (Figure 6-6). Both drugs are known to intercalate in DNA, cryptolepine having a higher affinity than neocryptolepine[15].

This is supposed to be one of the causes of the higher cytotoxicity of cryptolepine[15,16]. Both drugs have a sequence preference for GC-rich regions of DNA.

These two compounds are similar in structure and polarity, but show a marked difference in DNA affinity in solution. This constitutes an excellent test system to solve the question of the specificity of the intercalating complexes observed by ES-MS.

The full scan mass spectra of the complexes between each drug and a series of duplexes with different GC content (duplex **A-C**, see Table 8-1) were recorded with the LCQ. The results are shown in Figure 8-12. We can see that a higher amount of complex is detected with cryptolepine than with neocryptolepine, and that the affinity increases with the GC content of duplexes. Both drugs also show a higher affinity for GC-rich duplexes. This parallels the behavior in solution.

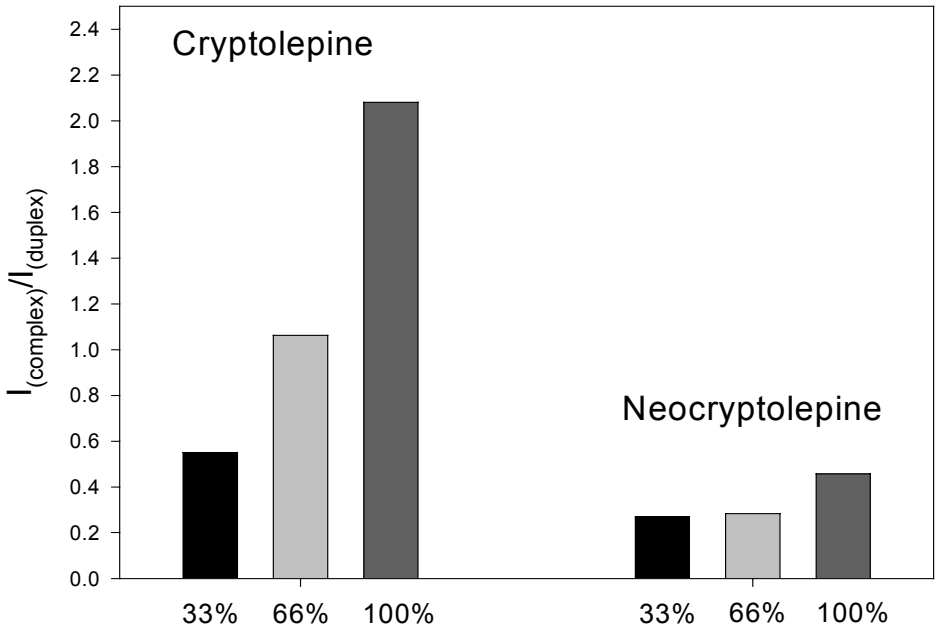

Figure 8-12. Comparison of the relative binding affinities for complexes of cryptolepine and neocryptolepine with duplexes of different percentages of GC base pairs. The DNA and drug concentrations were equal to 10 µM and 20 µM respectively.

Table 8-1. Base sequences of 12-mer duplexes **A**-**C**.

Duplex	Base sequence	% of CG base pairs
A	d(5'-CGTAAATTTACG-3')$_2$	33%
B	d(5'-CGCGAATTCGCG-3')$_2$	67%
C	d(5'-CGCGGGCCCGCG-3')$_2$	100%

Conclusions

Smith *et al.*[1,17] have provided criteria and tests to assess whether the complexes observed in electrospray mass spectrometry are specific or nonspecific (see chapter 4). One of these criteria is that specific complexes should be observed at defined (not random) stoichiometries.

The problem is the definition that is given to specificity. We have adopted the definition of Janin[18,19], who defines specificity in a context of competition in solution (see Chapter 1). However, in the mass spectrometry literature, specificity is sometimes used with another meaning. Complexes are said to be specific if they really exist in solution, and nonspecific if their signal results from artifacts of electrospray.

The chosen 12-mer duplex has one ATAT site that can accommodate minor groove binders, but many G/C consecutive base pair sites that can accommodate intercalators. For the complexes with minor groove binders, there is no ambiguity, as the stoichiometries are well-defined and correspond to the solution-phase behavior. For the complexes with the intercalators, random stoichiometries are observed, and it is therefore impossible from single measurements to assess whether this is due to random (nonspecific) association in solution, to random electrostatic aggregation during the solvent evaporation, or to both effects. This issue can be addressed by comparisons between very similar molecules, like cryptolepine and neocryptolepine. Our measurements indicate that the intercalating complexes formed with are specific in that case.

8.3. Cyclodextrin complexes

Introduction

Various studies of noncovalent complexes between β-cyclodextrins and aromatic molecules have shown that the complexes that were known to be present in solution could be detected by ES-MS[20-26]. In all these studies, the aromatic guest molecules were bearing at least one polar group. However, Cunniff and Vouros[27] have reported that ES-MS on β-CD complexes with aromatic non-polar molecules resulted in false negatives. Conversely, ES-MS on complexes with non-aromatic amines gave false positives. The authors concluded that the complexes observed were electrostatic adducts formed in the electrospray process rather than specific inclusion complexes. However, gas-phase studies on electrospray-produced complexes of β-CD and amino acids have shown that these complexes adopted an inclusion structure[28-30]. Molecular modeling calculations suggest that nonspecific complexes in the solution may convert to inclusion complexes in the gas phase. The evidence for gas-phase inclusion complexes does not necessarily confirm the presence of solution-phase inclusion complexes[30].

Here we report the ES-MS study of α-cyclodextrin complexes with α,ω-dicarboxylic acids of different chain length. In solution, the equilibrium binding constant of α-CD with aliphatic molecules increases with the chain length. This is attributed to the hydrophobic effect[31,32]. Our aim is to further investigate the origin of the cyclodextrin complexes that are observed in ES-MS. Are they formed only due to random electrostatic aggregation during the electrospray process, or do the hydrophobic interactions present in solution still play a role?

Experimental

All along the text, the diacids $^{-}OOC\text{-}(CH_2)_n\text{-}COO^{-}$ will be noted **1,n-da**, with **n** indicating the chain length. ES-MS analyses were performed on a Q-TOF2 mass spectrometer equipped with a Z-spray source. Electrospray ionization was achieved by application of -2.5 kV on the needle. For nanospray experiments, the capillary voltage was set to -700 V. Unless otherwise mentioned, the cone voltage was set to 10 V.

Results

The complexation of aliphatic diacids with α-CD was investigated in the negative ion mode for a concentration range from 4.0×10^{-4} M to 2.0×10^{-3} M. Figure 8-13 shows the MS spectra of equimolar mixtures (4.0×10^{-4} M) of (a) α-CD and 1,5-da and (b) α-CD and 1,10-da. The relative intensity of the singly charged free diacid depends dramatically on the chain length: the longer the chain, the larger the surface activity and the larger the electrospray response. The diacid could only be detected as a singly charged species. We can also see in the spectra the signals corresponding to the free α-CD (singly and doubly deprotonated). However, the complexes with diacids are predominantly doubly charged. One can see a major peak corresponding to the [1:1] complex, and a minor peak corresponding to a [2:1] complex (two cyclodextrins + one diacid). These observations hold for the whole concentration range.

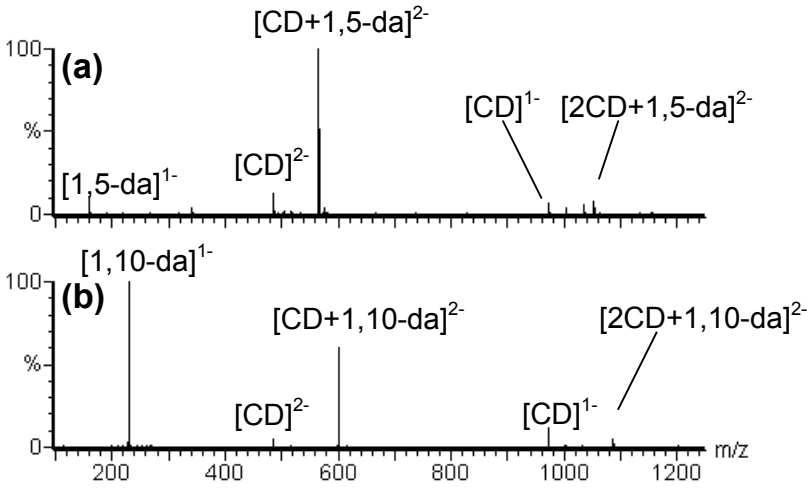

Figure 8-13. Full scan electrospray mass spectra obtained for equimolar mixtures (4×10^{-4} M) of (a) α-CD and 1,5-diacid and (b) α-CD and 1,10-diacid in water (pH = 9).

Charge states of free and complexed diacids

At the pH used in this study, the diacids are completely doubly deprotonated in solution. However, as already pointed out in other studies in methanol/water or acetonitile/water solvents[33,34], the full scan MS spectra of the pure diacids show signals from both the singly and the doubly charged species. We repeated these measurements in pure water and observed the same behavior. Figure 8-14 shows the relative intensity (RI) of the doubly charged species for the free diacid (filled circles). The relative intensity is calculated with equation (8.1):

$$\text{RI}\ (\%) = \frac{I_{(M^{2-})}}{I_{(M^{2-})} + I_{(M^{-})}} \cdot 100\% \qquad (8.1)$$

For all these experiments, the MS profile of the first quadrupole was set to have a maximum transmission at a m/z equal to a quarter of the mass of the singly charged species considered. This avoids any discrimination between the charge states due to the transmission of the quadrupole. In the MS spectra shown in Figure 8-13, the MS profile, set with the maximum transmission at m/z = 250, is responsible for the fact that we can not observe any doubly charged diacid. For the free diacids, the shorter the chain, the lower the relative intensity of doubly charged species. For the complexed diacids, we can see in Figure 8-14 (squares) that there is a very small influence of the chain length on the charge state. The complexes are almost only doubly deprotonated.

For the aliphatic diacids, the fact that the molecule is doubly charged in solution is not sufficient to ensure that only the doubly charged species is observed in the mass spectra. The charge state distribution depends on the size of the molecule rather than on its charge in solution. In the case of the complexed diacid, the fact that almost only the doubly charged species is observed can also be rationalized by considering the size of the molecule (the size of the whole complex).

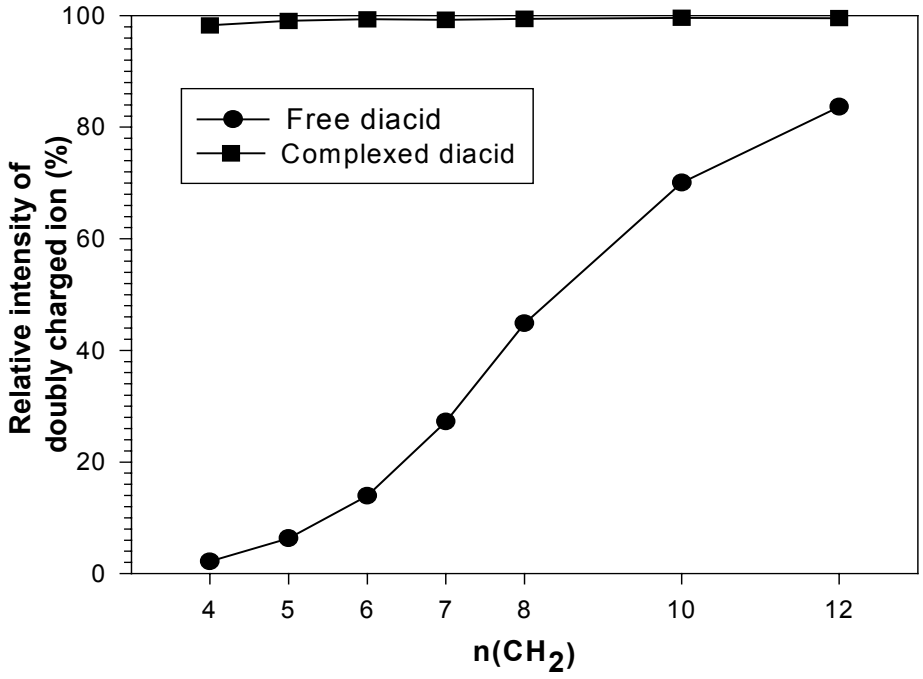

Figure 8-14. Relative intensity of doubly charged ion for (●) the free diacids (4×10^{-4} M) and (■) the complexed diacids ([diacids] = [cyclodextrin] = 1×10^{-3} M) as a function of the chain length *n*. The relative intensity is calculated using equation (8.1).

Influence of the chain length on the abundance of complex

The relative intensities of the α-CD, the [1:1] complex and the [2:1] complex are given in Table 8-2 for the equimolar mixtures of α-CD and diacids of different chain lengths. The intensities of the diacids were not taken into account because of the dependence of the response on the chain length. In solution, it is well known that the equilibrium association constant of the [α-CD+diacid] complex depends on the chain length of included diacid (the longer the chain, the larger the association constant[31,32]). However, in the mass spectra, the relative abundance of the signals from the [1:1] complex does not depend significantly on the chain length of dicarboxylic acids. Does it mean that the observed complexes are resulting from nonspecific associations? In order to get some more information on the nature of the complexes, we acquired MS spectra of all diacids with another ligand, maltohexaose.

Table 8-2. Relative intensities of α-CD and the complexes with diacids of different chain length for equimolar mixtures ([α -CD] = [1,n-da] = 4×10^{-4} M). The error on the relative intensities in between 0.1 and 0.2%.

n(CH_2)	α-CD (%)	$[1:1]^{2-}$ (%)	$[1:1]^{1-}$ (%)	$[2:1]^{2-}$ (%)
4	26.9	68.8	0.5	3.8
5	24.5	70.9	0.3	4.3
6	14.4	68.7	1.7	15.2
7	16.1	66.3	2.9	14.7
8	14.3	68.9	1.3	15.5
10	12.1	70.7	2.1	15.1
12	14.8	69.4	1.4	14.4

Comparison with maltohexaose

Maltohexaose is the linear analog of α-CD. It can not form inclusion complexes in solution, and is often used as a test for inclusion in solution by comparison with α-CD[31,32]. There should therefore be no signal corresponding to the complex in the MS spectra when mixing maltohexaose with aliphatic diacids. However, the MS spectra of the mixture of maltohexaose and dicarboxylic acids show signals corresponding to both $[1:1]^{2-}$ and $[2:1]^{2-}$ complexes (Figure 8-15). The relative intensities observed for the equimolar mixtures of maltohexaose and the different diacids are given in Table 8-3. On the contrary to the case of α-CD, the dependence of the relative intensities of the complexes on the chain length of the diacids is significant: the shorter the chain length, the larger the relative intensity of the complex with maltohexaose. These results suggest that in the case of the cyclodextrin, at least part of the observed complex species may result from nonspecific (non-inclusion) complex formation. Moreover, the shorter the diacid, the greater the tendency to form this kind of adduct.

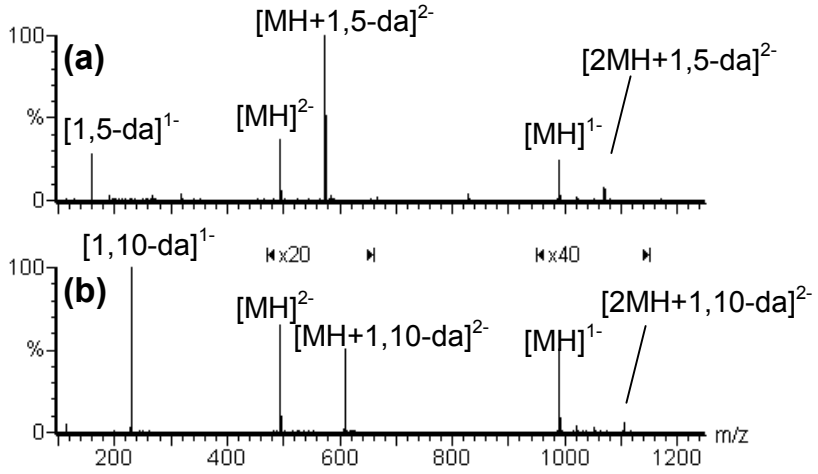

Figure 8-15. Full scan electrospray mass spectra obtained for equimolar mixtures (4×10^{-4} M) of (a) maltohexaose and 1,5-diacid and (b) maltohexaose and 1,10-diacid in water (pH = 9). Note the different magnification factors in spectrum (b).

Table 8-3. Relative intensities of maltohexaose and the complexes with diacids of different chain length for equimolar mixtures ([MH] = [1,n-da] = 4×10^{-4} M). The error on the relative intensities in between 0.1 and 0.2%.

n(CH_2)	MH (%)	$[1:1]^{2-}$ (%)	$[1:1]^{1-}$ (%)	$[2:1]^{2-}$ (%)
4	7.8	87.6	-	4.6
5	7.0	89.0	-	4.0
6	16.0	81.4	-	2.6
7	17.6	79.1	-	3.3
8	20.6	76.2	-	3.2
10	43.9	53.9	0.5	1.7
12	47.5	50.5	0.4	1.6

Lower concentration and flow rate

In order to investigate the origin of the observed complexes, we tried to find experimental conditions in which they would not be observed. It has been suggested that lowering the sample concentration and the electrospray flow rate helps to prevent the formation of nonspecific adducts[1,17]. To minimize aggregation, we first lowered the concentration close to the electrospray detection limit (4×10^{-5} M), and performed a comparison between electrospray and nanospray mass spectra for α-CD and maltohexaose complexes at that concentration. The relative intensities obtained for complexes with 1,10-da are summarized in Table 8-4.

Table 8-4. Relative intensities measured in the spectra of equimolar mixtures of α-cyclodextrin or maltohexaose with 1,10-diacid obtained by electrospray and nanospray for different concentrations. "Ligand" stands for either α-CD or MH (singly + doubly charged).

		Ligand (%)	$[1:1]^{2-}$ (%)	$[1:1]^{1-}$ (%)	$[2:1]^{2-}$ (%)
α-CD	Electrospray (4×10^{-4} M)	12.1	70.7	2.1	15.1
	Electrospray (4×10^{-5} M)	44.6	54.7	0.3	0.4
	Nanospray (4×10^{-5} M)	55.0	41.7	1.6	1.7
MH	Electrospray (4×10^{-4} M)	43.9	53.9	0.5	1.7
	Electrospray (4×10^{-5} M)	89.1	6.1	4.8	-
	Nanospray (4×10^{-5} M)	94.1	4.5	1.4	-

For the complex with α-CD, lowering the concentration moderately reduces the proportion of [1:1] complex, but dramatically reduces that of the [2:1] complex. In the case of MH, the intensity of all complexes is dramatically reduced upon dilution. The nanospray source offers the possibility to drastically decrease the flow rate (nL/min)

compared to electrospray conditions (μL/min). Nanospray gives much smaller initial droplets than electrospray. These smaller droplets therefore contain less molecules, and aggregation caused by solvent evaporation is minimized[35]. For example, it has been shown that much less salt adducts (which are electrostatic adducts) are observed with nanospray than with ionspray[36]. Here, surprisingly, the use of nanospray led only to a small reduction of the relative intensities of the complexes compared to electrospray, both for α-CD and maltohexaose.

MS/MS experiments

Tandem mass spectrometry experiments were performed on the doubly charged [1:1] complexes with α-cyclodextrin and maltohexaose. We used a cone voltage of 10 V, and monitored the fragmentation upon increasing the collision energy. Upon fragmentation one charge goes to the dextrin and one to the diacid. This partitioning of the charges upon fragmentation was quite unexpected, as in solution the dextrins are neutral[37] and diacids are present as doubly charged ions. We therefore performed MS/MS on singly charged [1:1] complexes with α-CD, and observed that the charge went exclusively to the dextrin upon fragmentation, so the α-CD actually seems more acidic than the diacid in the gas phase.

The following equation was used for the calculation of the relative intensity (RI) of a parent ion at each collision energy.

$$\mathrm{RI}\ (\%) = \frac{I_{(1:1)^{2-}}}{I_{(1:1)^{2-}} + \dfrac{I_{(da)^{1-}} + I_{(ligand)^{1-}}}{2}} \cdot 100\% \qquad (8.2)$$

Where “da” stands for the diacid and “ligand” stands for α-CD or MH. In the case of the complex with maltohexaose, at values of collision energy > 10 eV, there are signals from maltohexaose fragments. In order to be able to compare those results with MS/MS measurement with α-CD, we added the intensity of the fragments to the intensity of the free ligand.

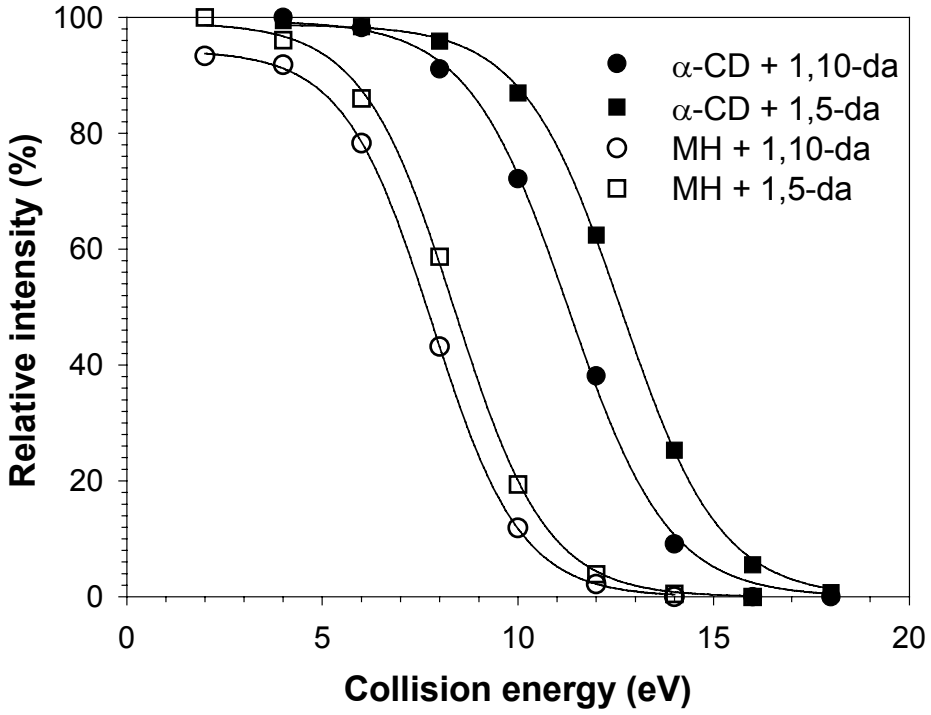

Figure 8-16. Relative intensity of complex as a function of the collision energy obtained in the MS/MS experiments on the $[1:1]^{2-}$ complexes between α-cyclodextrin or maltohexaose and 1,5- or 1,10-diacids. The relative intensity is calculated using equation (8.2).

The fragmentation curves (Fig. 8-16) indicate that the complexes with α-CD are more kinetically stable than the corresponding complexes with maltohexaose. The dependence of the gas-phase kinetic stability on the chain length is more intriguing. For both α-CD and maltohexaose complexes, a larger collision energy is needed for the dissociation of the complexes with the shorter diacids. This is exactly the reverse trend compared to the solution phase, where for α-CD more stable complexes are formed with the longer chains. No satisfactory explanation could be found to account for the higher gas-phase kinetic stability of the complexes with the shorter chains. The effect of the number of degrees of freedom on the dissociation kinetics would have given the opposite trend (see Section 3.4 and Chapter 10). The Coulombic repulsion between the charged fragments can not be invoked either, as a stronger repulsion is expected for the shorter diacids, due to the proximity of the charges.

Discussion

The complexes observed in the case of maltohexaose with linear diacids are nonspecific electrostatic adducts formed during the electrospray process. The fact that the relative intensity of the complexes with MH in the MS spectra is higher for the shorter diacids is in agreement with the MS/MS results: the complexes with shorter diacids are also more stable in the gas-phase. It has been shown by molecular modeling that, once transferred in the gas phase, linear oligosaccharides are sufficiently flexible to wrap around guest molecules and form "quasi-inclusion" complexes[29,30], but nothing is known about how and when these complexes are produced in the electrospray process. Upon dilution, the abundance of the complexes with maltohexaose in the MS spectra is greatly reduced, which is also an indication of their nonspecific character. For the same reason, the [2:1] complexes with α-CD can be considered as nonspecific.

The [1:1] complexes with α-CD have some characteristics of specific complexes (they are more resistant to dilution and to CID than the complexes with maltohexaose), and also show some characteristics of nonspecific complexes (the relative intensities of the complexes are not correlated with the abundances in solution). The observation of complexes with maltohexaose implies that, in similar conditions, nonspecific adducts can also form with α-CD. This suggests that the total intensity of the [1:1] complex results from two contributions: one from specific complexes and one from nonspecific adducts.

The spectra obtained with the linear analog maltohexaose can be used to evaluate the proportion of nonspecific adduct in the spectra of α-CD complexes. To be able to compare the relative intensities of the complexes in Tables 8-2 and 8-3, we have determined the ratio between the electrospray responses of α-CD and MH by measuring the intensity ratio in the MS spectrum of an equimolar mixture of those two compounds. The response of MH is 3.7 times lower than the response of α-CD. We then corrected the relative intensities in Table 8-3 with this factor. The results are reported in Figure 8-17. The total height of the bars is equal to the total relative intensity of the $[1:1]^{2-}$ complex observed for α-CD. In light gray is the relative intensity of nonspecific complex estimated as explained above. The remaining (in dark gray) therefore corresponds to the estimated contribution of specific complex to the total intensity. We can see that the proportion of specific complex is nil for n = 4 and n = 5, and then increases as the chain length increases. This behavior is in agreement with the solution behavior[31].

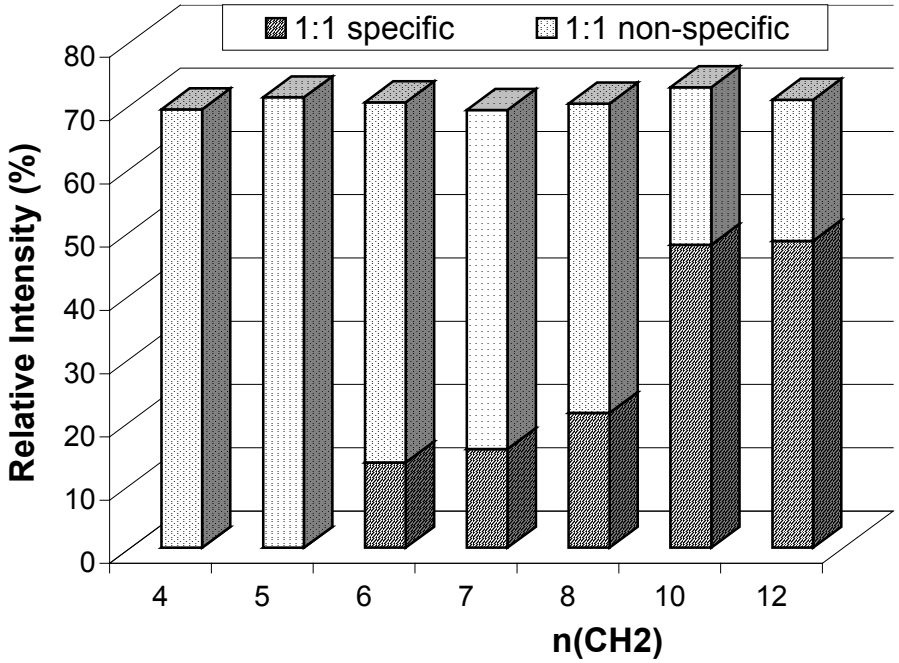

Figure 8-17. Estimated contribution of specific (dark grey) and nonspecific (light grey) complexes to the total intensity of complexes between α-cyclodextrin and the diacids of different chain lengths.

Conclusion

On the basis of these results on cyclodextrin complexes, it is possible to conclude that what is observed in the MS spectra of the complexes of α-CD with linear α,ω-dicarboxylic acids is the mixture of specific (inclusion) complexes which are present in solution and nonspecific (electrostatic) adducts formed during the electrospray process. Inclusion in solution is almost always driven by hydrophobic interactions, i.e. by the solvent reorganization upon complexation. The electrospray process consists in pulling ions out of the solution. This implies that solvophobic forces can not contribute anymore to the stabilization of the complex, but also that electrostatic interactions will play a larger role in the gas phase than in solution due to the change in the dielectric constant of the medium. Moreover, as we can only observe *ions* by MS, these electrostatic interactions are very strong (ion/ion or ion/multipole interactions). The transfer of ions from the solution to the gas phase induces a complete reversal of the scale of the interactions that are responsible for the stabilization of the complex. We will therefore inevitably be faced with the problem of nonspecificity and false positives when studying hydrophobic complexes by electrospray mass spectrometry.

References

1. R.D. Smith, K.J. Light-Wahl; The Observation of Non-Covalent Interactions in Solution by Electrospray Ionization Mass Spectrometry: Promise, Pitfalls and Prognosis. *Biol. Mass Spectrom.* **1993,** 22: 493.

2. J. Ding, R.J. Anderegg; Specific and Non-Specific Dimer Formation in the Electrospray Ionization Mass Spectrometry of Oligonucleotides. *J. Am. Soc. Mass Spectrom.* **1995,** 6: 159.

3. B. Ganem, Y.-T. Li, J.D. Henion; Detection of Oligonucleotide Duplex Forms by Ionspray Mass Spectrometry. *Tetrahedron Lett.* **1993,** 34: 1445.

4. K.J. Light-Wahl, D.L. Springer, B.E. Winger, C.G. Edmonds, D.G. Camp, B.D. Thrall, R.D. Smith; Observation of a Small Oligonucleotide Duplex by Electrospray Ionization Mass Spectrometry. *J. Am. Chem. Soc.* **1993,** 115: 803.

5. E. Bayer, T. Bauer, K. Schmeer, K. Bleicher, M. Maier, H.-J. Gaus; Analysis of Double-Stranded Oligonucleotides by Electrospray Mass Spectrometry. *Anal. Chem.* **1994,** 66: 3858.

6. B.H. Geierstranger, D.E. Wemmer; Complexes of the Minor Groove of DNA. *Annu. Rev. Biomol. Struct.* **1995,** 24: 463.

7. J.G. Pelton, D.E. Wemmer; Structural Characterization of a 2:1 Distamycin A:d(CGCAAATTGGC) Complex by Two-Dimensional NMR. *Proc. Natl. Acad. Sci. USA* **1989,** 86: 5723.

8. J.G. Pelton, D.E. Wemmer; Binding Modes of Distamycin A With $d(CGCAAATTTGCG)_2$ Determined by Two-Dimensional NMR. *J. Am. Chem. Soc.* **1990,** 112: 1393.

9. D.E. Wemmer, B.H. Geierstranger, P.A. Fagan, T.J. Dwyer, J.P. Jacobsen; Minor Groove Recognition of DNA by Distamycin and Its Analogs. In *Structural Biology: The State of the Art, Proc. Eighth Conversation on Biomolecular Stereodynamics*; S.M. Sarma, M.H. Sarma, Eds.; Adenine: 1994; Vol. 2, pp 301-323.

10. K.R. Fox; Probing the Conformations of Eight Cloned DNA Dodecamers; CGCGAATTCGCG, CGCGTTAACGCG, CGCGTATACGCG, CGCGATATCGCG, CGCAAATTTGCG, CGCTTTAAAGCG, CGCGGATCCGCG and CGCGGTACCGCG. *Nucl. Acid. Res.* **1992,** 20: 6487.

11. S. Frau, J. Bernadou, B. Meunier; Hoechst 33258, Un Agent De Reconnaissance Du Petit Sillon De L'ADN. *Bull. Soc. Chim. Fr.* **1996,** 133: 1053.

12. F.G. Loontiens, P. Regenfuss, A. Zechel, L. Dumortier, R.M. Clegg; Binding Characteristics of Hoechst 33258 With Calf Thymus DNA, Poly[d(A-T)], and $d(CCGGAATTCCGG)_2$: Multiple Stoichiometries and Determination of Tight Binding With a Wide Spectrum of Site Affinities. *Biochemistry* **1990,** 29: 9029.

13. I. Haq, J.E. Ladbury, B.Z. Chowdhry, T.C. Jenkins, J.B. Chaires; Specific Binding of Hoechst 33258 to the $d(CGCAAATTTGCG)_2$ Duplex: Calorimetric and Spectroscopic Studies. *J. Mol. Biol.* **1997,** 27: 244.

14. K. Cimanga, T. De Bruyne, L. Pieters, M. Claeys, A. Vlietinck; New Alkaloids From *Cryptolepis Sanguinolenta*. *Tetrahedron Lett.* **1996,** 37: 1703.

15. C. Bailly, W. Laine, B. Baldeyrou, M.-C. De Pauw-Gillet, P. Colson, C. Houssier, K. Cimanga, S. Van Miert, A.J. Vlietink, L. Pieters; DNA Intercalation, Topoisomerase II Inhibition and Cytotoxic Activity of the Plant Alkaloid Neocryptolepine. *Anti-cancer Drug Design* **2000,** 15: 191.

16. L. Dassonneville, A. Lansiaux, A. Wattelet, N. Wattez, C. Mahieu, S. Van Miert, L. Pieters, C. Bailly; Cytotoxicity and Cell Cycle Effects of the Plant Alkaloids Cryptolepine and Neocryptolepine: Relation to Drug-Induced Apoptosis. *Eur. J. Pharmacol.* **2000,** 409: 9.

17. R.D. Smith, J.E. Bruce, Q. Wu, Q.P. Lei; New Mass Spectrometric Methods for the Study of Non-Covalent Associations of Biopolymers. *Chem. Soc. Rev.* **1997,** 26: 191.

18. J. Janin; Protein-Protein Recognition. *Prog. Biophys. Mol. Biol.* **1995,** 64: 145.

19. J. Janin; Quantifying Biological Specificity: the Statistical Mechanics of Molecular Recognition. *Proteins* **1996,** 25: 438.

20. A. Selva, E. Redenti, M. Zanol, P. Ventura, B. Casetta; A Study of β-Cyclodextrin and Its Inclusion Complexes With Piroxicam and Tefenadrine by Ionspray Mass Spectrometry. *Org. Mass Spectrom.* **1993,** 28: 983.

21. P. Camilleri, N.J. Haskins, A.P. New, M.R. Saunders; Analysis of the Complexation of Amino Acids and Peptides With β-Cyclodextrin Using Electrospray Ionization Mass Spectrometry. *Rapid Commun. Mass Spectrom.* **1993,** 7: 949.

22. N.J. Haskins, M.R. Saunders, P. Camilleri; The Complexation and Chiral Selectivity of 2-Hydroxypropyl-β-Cyclodextrin With Guest Molecules As Studied by Electrospray Mass Spectrometry. *Rapid Commun. Mass Spectrom.* **1994,** 8: 423.

23. R. Ramanathan, L. Prokai; Electrospray Ionization Mass Spectrometric Study of Encapsulation of Amino Acids by Cyclodextrins. *J. Am. Soc. Mass Spectrom.* **1995,** 6: 866.

24. P. Cescutti, D. Garozzo, R. Rizzo; Study of the Inclusion Complexes of Aromatic Molecules With Cyclodextrins Using Ionspray Mass Spectrometry. *Carbohyd. Res.* **1996,** 290: 105.

25. P. Cescutti, D. Garozzo, R. Rizzo; Effect of Methylation of β-Cyclodextrin on the Formation of Inclusion Complexes With Aromatic Compounds. An Ionspray Mass Spectrometry Investigation. *Carbohyd. Res.* **1997,** 302: 1.

26. E. Lamcharfi, S. Chuilon, A. Kerbal, G. Kunesch, F. Libot, H. Virelizier; Electrospray Ionization Mass Spectrometry in Supramolecular Chemistry: Characterization of Non-Covalent Cyclodextrin Complexes. *J. Mass Spectrom.* **1996,** 31: 982.

27. J.B. Cunniff, P. Vouros; False Positives and the Detection of Cyclodextrin Inclusion Complexes by Electrospray Mass Spectrometry. *J. Am. Soc. Mass Spectrom.* **1995,** 6: 437.

28. J. Ramirez, S. Ahn, G. Grigorean, C.B. Lebrilla; Evidence for the Formation of Gas-Phase Inclusion Complexes With Cyclodextrins and Amino Acids. *J. Am. Chem. Soc.* **2000,** 122: 6884.

29. S. Ahn, J. Ramirez, G. Grigorean, C.B. Lebrilla; Chiral Recognition in Gas-Phase Cyclodextrin:Amino Acid Complexes - Is the Three Point Interaction Still Valid in the Gas Phase? *J. Am. Soc. Mass Spectrom.* **2001,** 12: 278.

30. C.B. Lebrilla; The Gas-Phase Chemistry of Cyclodextrin Inclusion Complexes. *Acc. Chem. Res.* **2001,** 34: 653.

31. I. Gomez-Orellana, D. Hallen, M. Stödeman; Microcalorimetric Titration of α-Cyclodextrin With Some Straight-Chain α,ω-Dicarboxylates in Aqueous Solution at Different Temperatures. *J. Chem. Soc., Faraday Trans.* **1994,** 90: 3397.

32. G. Castronuovo, V. Elia, F. Velleca, G. Viscardi; Thermodynamics of the Interaction of α-Cyclodextrin With α,ω-Dicarboxylic Acids in Aqueous Solutions. A Calorimetric Study at 25°C. *Thermochimica Acta* **1997,** 292: 31.

33. K.W.M. Siu, G.J. Gardner, S.S. Berman; Multiply Charged Ions in Ionspray Mass Spectrometry. *Org. Mass Spectrom.* **1989,** 24: 931.

34. R.T. Aplin, M.G. Moloney, R. Newby, E. Wright; Negative-Ion Electrospray Mass Spectrometric Analysis of Dicarboxylic Acids. *J. Mass Spectrom.* **1999,** 34: 60.

35. M. Karas, U. Bahr, T. Dülcks; Nano-Electrospray Ionization Mass Spectrometry: Addressing Analytical Problems Beyond Routine. *Fres. J. Anal. Chem.* **2000,** 366: 669.

36. R. Juraschek, T. Dülcks, M. Karas; Nanoelectrospray – More Than Just a Minimized-Flow Electrospray Ionization Source. *J. Am. Soc. Mass Spectrom.* **1999,** 10: 300.

37. J. Szejtli; Introduction and General Overview of Cyclodextrin Chemistry. *Chem. Rev.* **1998,** 98: 1743.

9.

DETERMINATION OF BINDING CONSTANTS: INFLUENCE OF THE RESPONSE FACTORS

9.1. Introduction

As explained in detail in Chapter 4, in the current literature, the determination of binding selectivities and of binding constants by electrospray mass spectrometry is very often based on the assumption that the relative intensities in the mass spectra reflect the relative abundances in the injected solution. For example, in the case of a competition experiment between guests B and C for the host A, it is assumed that:

$$\frac{I(AB)}{I(AC)} = \frac{[AB]}{[AC]} \tag{9.1}$$

We will describe in the first part of this chapter an application of this assumption for the determination of binding selectivities of DNA-binding drugs by competition experiments.

For the determination of binding constants, it is assumed that the responses of the complex and the free substrate are equal, and this gives equation (9.2):

$$\frac{I(AB)}{I(A)} = \frac{[AB]}{[A]} \tag{9.2}$$

In the second part of the chapter, we will test this hypothesis by measuring the factor *R*, defined as the ratio between the response factors of the complex and the substrate:

$$\frac{I(AB)}{I(A)} = \frac{R_{AB}}{R_A} \cdot \frac{[AB]}{[A]} = R \cdot \frac{[AB]}{[A]} \tag{9.3}$$

9.2. Competition experiments with DNA-binding drugs

Competition between minor groove binders

As explained before, for these experiments, we assume that the relative intensities observed by ES-MS reflect the relative abundances in solution. This argument has been used in various studies[1-4] and is thought to be valid when the observed complexes are stabilized in the gas phase compared to the solution phase, mainly by electrostatic and hydrogen bonding interactions[5,6]. This is indeed the case for the binding of minor groove ligands with double-stranded DNA. Competition experiments were undertaken: the duplex was mixed with equal amounts of two drugs in a 10-10-10 µM solution, and the spectra of the mixtures were recorded. Some are reported in Figure 9-1. The competition experiments performed on the LCQ were made for drugs of significantly different masses.

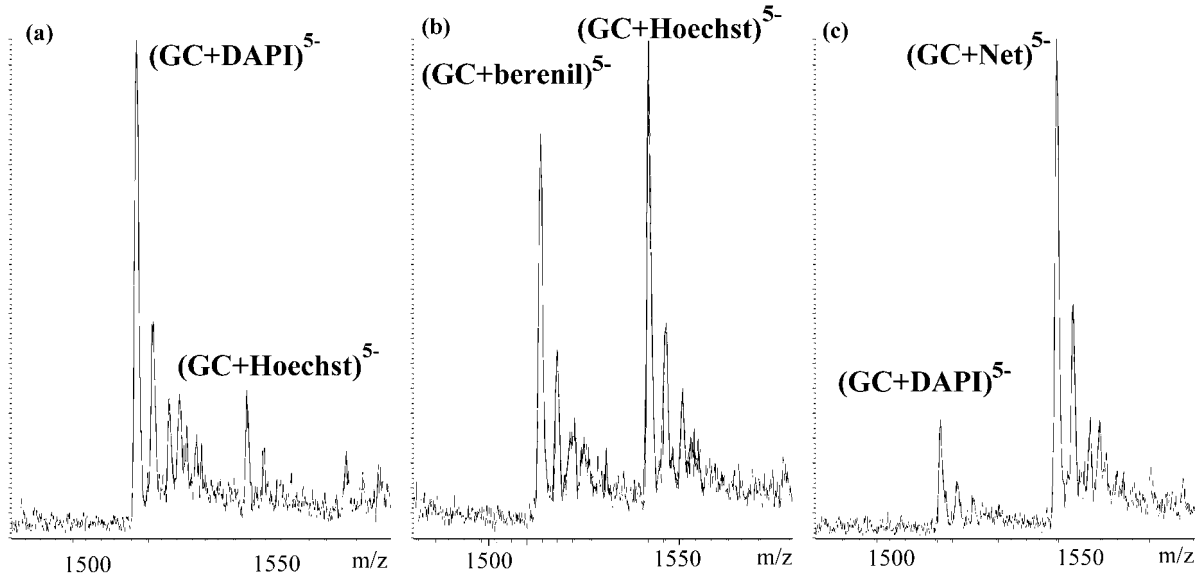

Figure 9-1. Full scan ES-MS spectra of equimolar (10-10-10 µM) mixtures of the duplex and two drugs which are thus in competition for binding to the DNA. Drug pairs are (a) DAPI/Hoechst 33258, (b) berenil/Hoechst 33258, and (c) DAPI/netropsin. The spectra have been recorded with the LCQ, with a constant mass range of [1,000-2,000] (for the clarity of the figure, only a portion of the spectra is shown).

These competition experiments allow the easy determination of which of the two drugs tested binds the duplex preferentially. For example, it is readily inferred from spectrum (a) that DAPI has a higher affinity than Hoechst 33258, and from (b) that berenil and Hoechst 33258 have approximately the same binding affinity. We can therefore establish step by step a relative affinity scale of drugs for a given duplex. In our case, we obtained the following scale: netropsin > DAPI > Hoechst 33258 ≃ berenil. Thermal denaturation experiments showed that the complex with netropsin is indeed more stable than the one with Hoechst 33258 (Fig. 9-2): the more stable the complex, the higher the denaturation temperature[7].

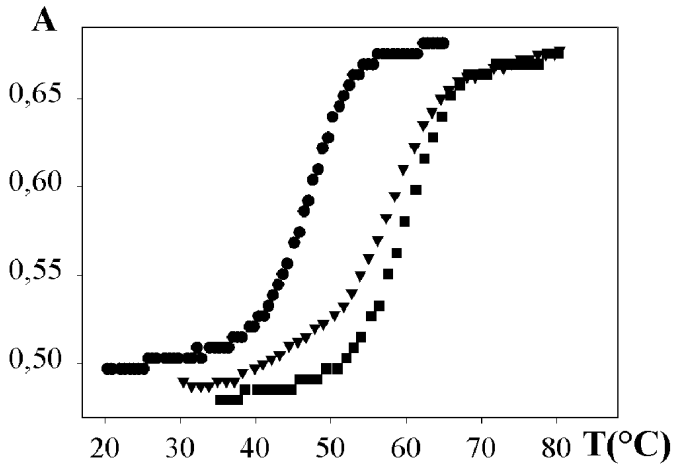

Figure 9-2. Thermal denaturation curves of the duplex (●), its complex with Hoechst 33258 (▼) and its complex with netropsin (■). All solutions were in 50 mM NH_4OAc. The absorbance values have been normalized to allow a visual comparison of the curves.

Competition between minor groove binders and ethidium

The concept of competition experiments has been applied to ethidium: a duplex-ethidium 10 μM-15 μM mixture has been allowed to react with various amounts (0 to 15 μM) of minor groove binder for at least 5 minutes (which turned out to be the minimum time to establish the equilibrium). The same kind of measurements are routinely achieved in the solution phase to determine the binding constant of the minor groove binder, provided that ethidium's one is known. The titration of the complex with ethidium by the other drug is monitored by fluorescence spectroscopy[8-12]. This experiment has been achieved with Hoechst 33258 and netropsin, to check for a

further confirmation of the greater affinity of netropsin to our duplex: netropsin should then replace the ethidium molecules more readily than Hoechst 33258. The results displayed in Figure 9-3 show that this is indeed the case.

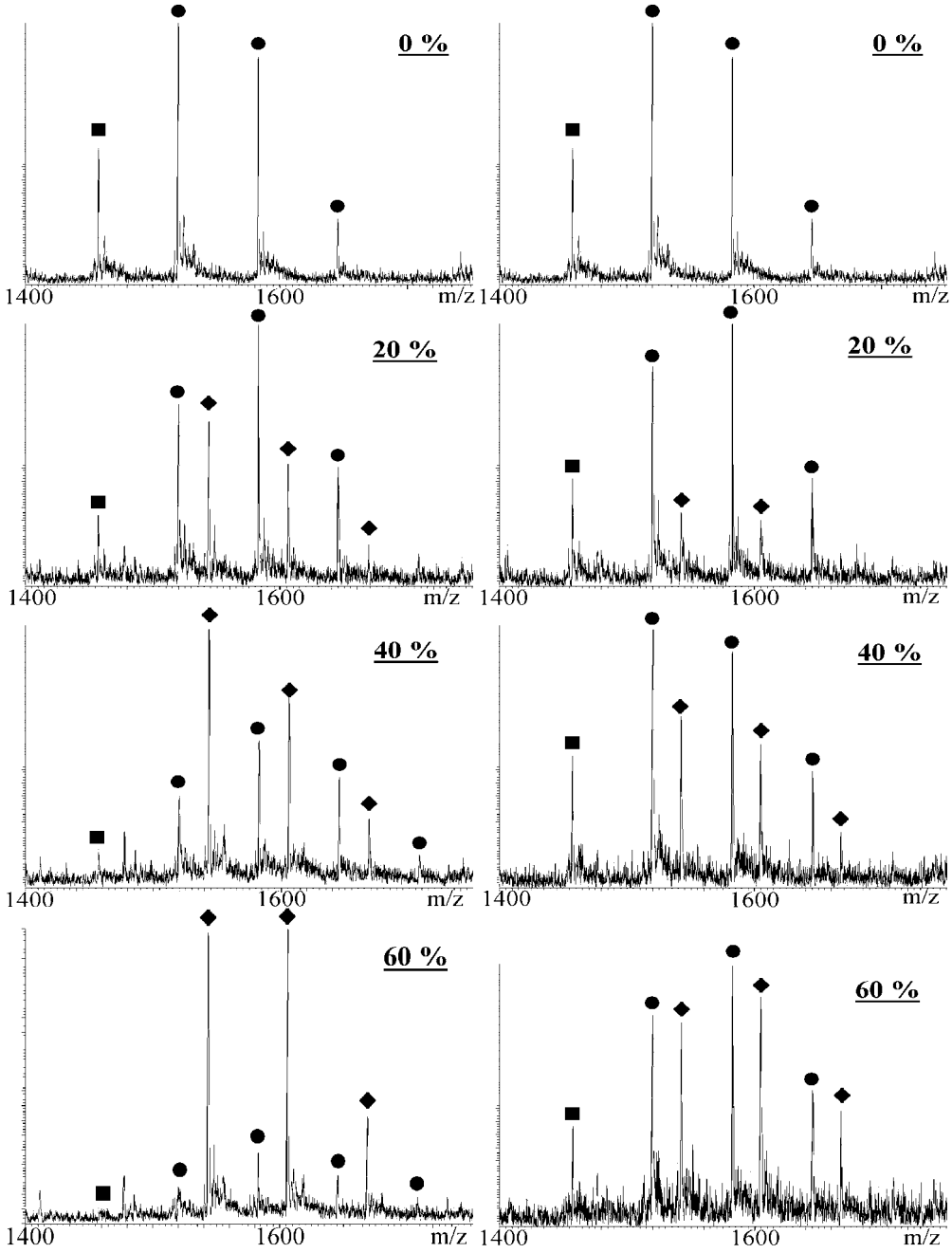

Figure 9-3. Full scan ES-MS spectra (LCQ) for the competition experiments between ethidium and netropsin (left) or Hoechst (right) at different minor groove binder molar fractions (noted in the top left hand corner of each spectra). The series are labeled as follows: ■ for the lone duplex, ● for the (duplex + n ethidium) series, and ◆ for the (duplex + minor groove binder + n ethidium) series.

The (duplex + netropsin + *n* ethidium) series takes more readily the precedence over the (duplex + *n* ethidium) series than does the (duplex + Hoechst + *n* ethidium) one. Furthermore, an observed contribution of the series (duplex + 2 Hoechst + *n* ethidium) at highest Hoechst concentrations (data not shown for clarity of the figure) is in agreement with the observation of the 2:1 complex noted above. The fact that the duplex is bound to intercalators and minor groove binders at the same time is compatible with the preference of the former for GC regions and of the latter for the ATAT site, although the possibility of nonspecific aggregation of ethidium on the (duplex + minor groove binder) complex during the electrospray process can not be ruled out.

9.3. Determination of the relative response factors

We established the equations to determine simultaneously the values of R and K_a. The value of K_a determined by the present method is automatically corrected for the relative response of the complexes and the substrates.

On the basic assumption

In equation (9.3), R is the ratio between the response factors of the complex and of the free substrate. A difference in the response of two species can be due to three factors: a difference in the efficiency of the electrospray process, a discrimination due to the transmission of the mass analyzer, and a difference in detection efficiency.

$R = 1$ represents the ideal case (equation 9.2) where the response factors are the same for A and AB. If R is assumed to be equal to unity when actually $R > 1$, (the response of the complex is higher than the response of the substrate), this leads to an overestimation of the association constant K_a. Conversely, if the actual R is lower than unity, this leads to an underestimation of K_a.

Equation (9.3) implies that the ratio between the response factors is constant over the whole concentration range. This is also an assumption. The electrospray response can

indeed deviate from linearity when working with concentrations varying in a very wide range. This approximation is anyway better than considering simply that $R = 1$. It is therefore recommended to use a concentration range of 1-2 orders of magnitude, carefully chosen to observe significant variations in the relative intensities of A and AB.

Fitting procedure to determine K_a *and* R *simultaneously*

Replacing equation (9.3) into the expression of K_a (1.2) gives:

$$K_a = \frac{[AB]}{[A].[B]} \tag{1.2}$$

$$K_a = \frac{1}{R}\frac{I(AB)}{I(A)}\frac{1}{[B]} \tag{9.4}$$

If the solution is equimolar in A and B ($[A]_0 = [B]_0 = C_0$), and if we define α as the fraction of bound ligand (equation 9.5)

$$\alpha = \frac{[AB]}{[AB]+[A]} = \frac{1}{1+\frac{[A]}{[AB]}} \tag{9.5}$$

as $C_0 = [A] + [AB] = [B] + [AB]$, we therefore have

$$[A] = [B] = C_0(1-\alpha) \tag{9.6}$$

and $[AB] = C_0\alpha$. Introducing successively equations (9.6), (9.5) and (9.3) in equation (9.4) gives:

$$K_a = \frac{1}{R}\frac{I(AB)}{I(A)}\frac{1}{C_0(1-\alpha)}$$

$$K_a = \frac{1}{R}\frac{I(AB)}{I(A)}\frac{1}{C_0\left(1-\frac{1}{1+\frac{[A]}{[AB]}}\right)}$$

$$K_a = \frac{1}{R}\frac{I(AB)}{I(A)}\frac{1}{C_0\left(1-\dfrac{1}{1+R\dfrac{I(A)}{I(AB)}}\right)}$$

$$K_a = \frac{1+R\dfrac{I(A)}{I(AB)}}{R^2\left(\dfrac{I(A)}{I(AB)}\right)^2 C_0} \tag{9.7}$$

The ratio of the intensities $I(A)/I(AB)$ is measured as a function of C_0 (the concentration of the equimolar solution). Equation (9.8) relating these two quantities can be found by taking the positive root of equation (9.7). The experimental results are fitted by a least squares procedure, introducing equation (9.8) into SigmaPlot 4.0. The two variable parameters are K_a and R.

$$\frac{I(A)}{I(AB)} = \frac{1+\sqrt{(1+4K_aC_0)}}{2RK_aC_0} \tag{9.8}$$

Robustness of the equation

Simulations with theoretical points were made to test the robustness of the equation and the influence of experimental errors on the determination of the constant by the method described above. Figure 9-4 shows plots of equation (9.8) obtained with three different couples of parameters (K_a,R). The curvature shows little sensitivity to the balance of K_a and R, and does not change dramatically although K_a can change over near two orders of magnitude. This indicates that large errors in $I(A)/I(AB)$ will result in large errors in the determination of K_a and R by fitting. Although this must be born in mind, the major source of error is not so much the experimental error on the determination of C_0 and $I(A)/I(AB)$ themselves, but stems from the fact that the solution may not be strictly equimolar. This is illustrated in Figure 9-5. The theoretical points were generated by calculating $I(A)/I(AB)$ for 12 values of C_0 in the range $2.0 \times 10^{-6} - 6.0 \times 10^{-5}$ M, with fixed values of K_a and R ($K_a = 10^6$ M^{-1}, $R = 0.2$). The following three datasets were generated: (i) truly equimolar solution, (ii) solution with

an excess of A and (iii) solution with a deficit of A. For the equimolar solution, the fitting gives the correct values of K_a and R. When A is in excess compared to B, the intensity ratio $I(A)/I(AB)$ does not sufficiently decrease at high concentration; the slope of the fitted curve is less steep than it should be and this results in an overestimation of K_a (and an underestimation of R). The opposite is true when A is in deficit compared to B. The whole procedure has been repeated for $R = 1$ and $R = 5$ (data not shown), and we observed that the smaller the value of R, the larger the effect of the non-equimolarity of the solution.

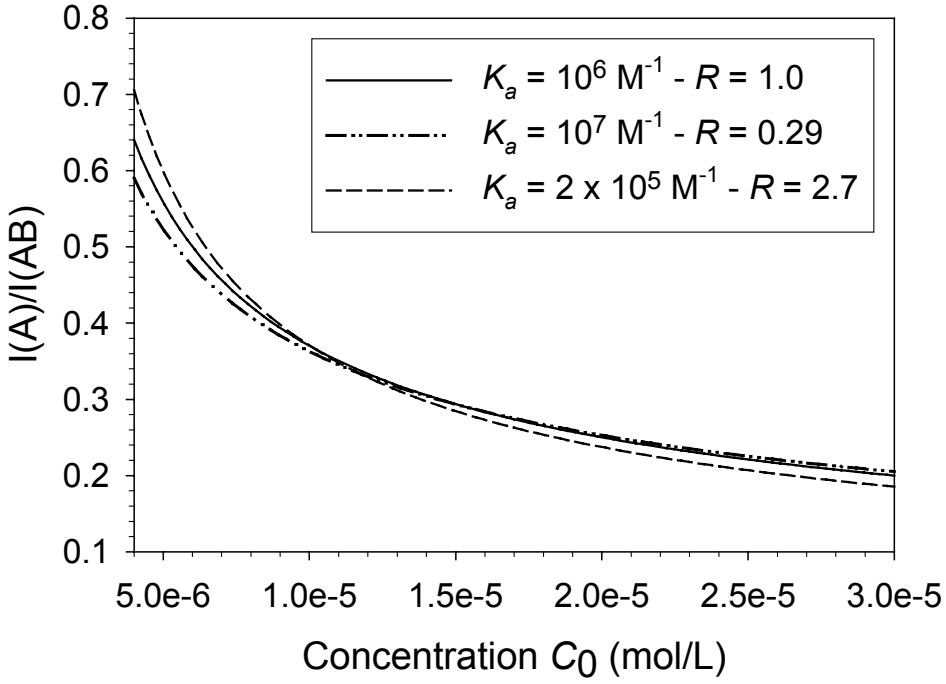

Figure 9-4. Plots of equation (9.8) with three different couples of (K_a,R) that superimpose in the selected concentration range.

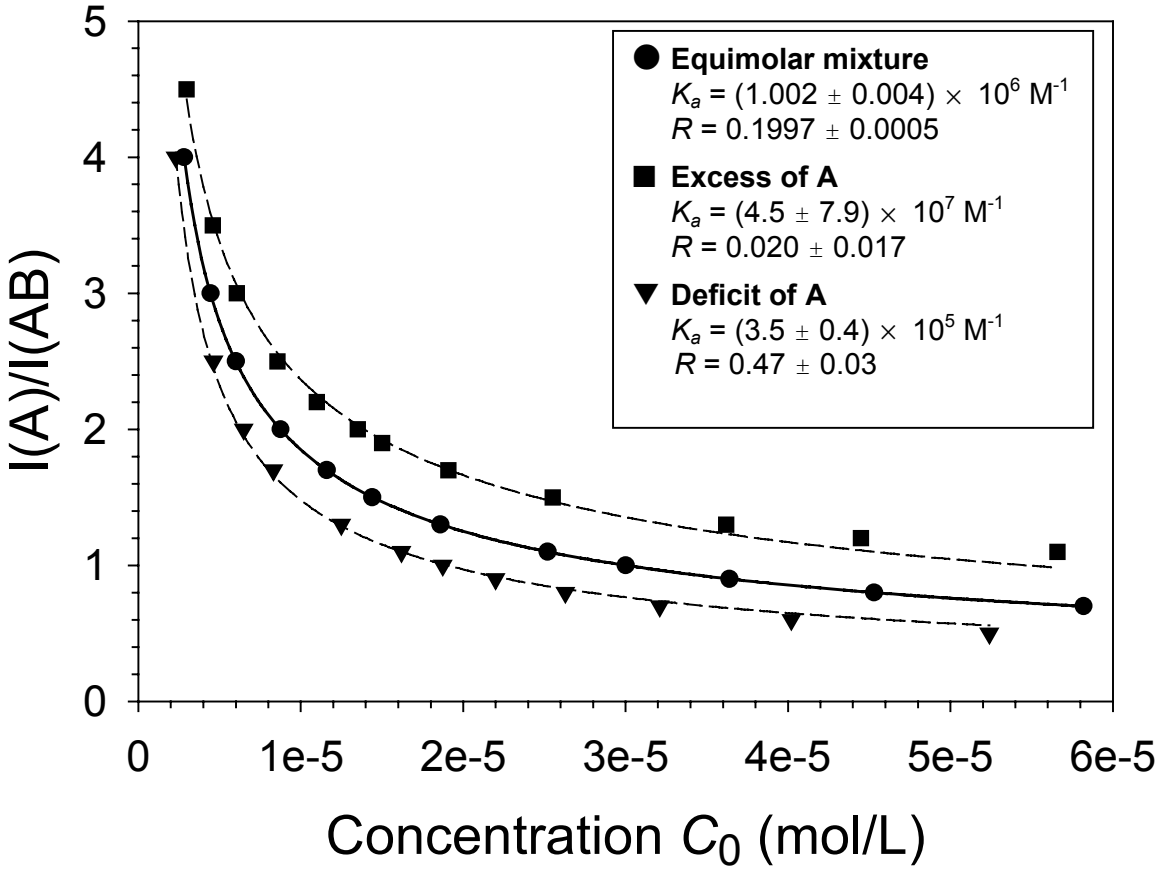

Figure 9-5. Results of the fitting procedure if the mixture is equimolar ($[A]_0 = [B]_0 = C_0$) (●), if there is an excess of A ($[A]_0 = C_0$ and $[B]_0 = 0.9 \times C_0$) (■), or if there is a deficit of A ($[A]_0 = C_0$ and $[B]_0 = 1.1 \times C_0$) (▼). 12 datapoints were generated for each case, considering $K_a = 10^6$ M^{-1} and $R = 0.2$. These datapoints are then fitted using equation (9.8) and values obtained for K_a and R are reported in the inset together with their standard errors.

The problem of the determination of the concentration is common to all methods for determining association constants, but it is clear that the present method is very sensitive to errors on the concentrations of A and B. It has been shown above that the solution has to be strictly equimolar in A and B to avoid systematic error on K_a. The advantage of the method is that this kind of systematic error can be detected and evaluated by a careful examination of the results of the fitting procedure. If the fitting curve goes systematically below the experimental points at high concentration, this

indicates that A is in excess, and that the value of K_a obtained by fitting is an upper bound to the real K_a. If however the fitting curve goes systematically above the experimental points at high concentration, A is in deficit, and the constant K_a obtained by fitting is a lower bound to the real K_a. When applying the above-described fitting procedure, it is recommended to work in a concentration range broad enough to detect whether equation (9.7) is applicable or not (at least for one order of magnitude). A kind of system for which the equimolarity problem is avoided is for dimerization reactions. We will present below the results obtained for two systems for which the concentrations of the partners could be determined accurately.

DNA-minor groove binder complexes

It has often been assumed in MS that complexes with small drugs that do not disturb the conformation of the substrate have the same electrospray response as the host[13]. Minor groove binders interact with the floor of the minor groove of DNA with Van der Waals, hydrogen bonding and electrostatic interactions, at AT-rich sites, with no dramatic change in the conformation of the DNA double helix[14-16]. We therefore tested these kind of complexes to verify the hypothesis according to which R should be close to 1.

Experimental section

Materials. Single stranded oligodeoxyribonucleotides d(GGGGAATTGGGG) (M = 3863.53 Da), d(CCCCAATTCCCC) (M = 3486.34 Da), d(GGGGAAAAGGGG) (M = 3824.56 Da), d(CCCCTTTTCCCC) (M = 3468.31 Da) and d(CGCGAATTCGCG) (M = 3646.44 Da) were purchased from Eurogentec (Angleur, Belgium). Complementary (or self-complementary) strands are annealed overnight in 100 mM NH_4OAc to form the duplexes.

Fluorescence Spectroscopy. Fluorescence titration of the oligonucleotide duplex by the Hoechst 33342 was performed on a SLM-AMINCO 8100 spectrofluorometer (Spectronic Unicam, Cambridge, UK) at 20 °C in an aqueous solution of 100 mM NH_4OAc (pH = 7.0). The concentration of duplex oligonucleotide was 8.1×10^{-9} M. Since thermal denaturation experiments in 100 mM NH_4OAc extrapolated to a concentration of 8.1 nM gives a melting temperature of 35 °C, the duplex can reasonably be assumed to be quantitatively formed at room temperature in the solution used for fluorescence titration experiments. The ligand concentration was varied from 0 to 1.1×10^{-6} M. The solution was excited at 354 nm, and fluorescence emission was measured at 485 nm after mixing for 4 minutes to equilibrate between each titrant addition. Each point is the mean value of four data collections. Background fluorescence intensity from the oligonucleotide solution before the addition of drug was subtracted from each point. Fluorescence titration data were fitted by a single site model[17].

Mass Spectrometry. The ES-MS spectra of oligonucleotide complexes were recorded with the LCQ mass spectrometer operated in the negative ion mode (needle voltage = -3.9 kV). The capillary was heated to 180 °C and the applied potential was -10 V. The skimmer was at ground potential. The tube lens offset was maintained at 40 V. The 80/20 (100 mM aqueous NH_4OAc/methanol) solution was injected at 5 μL/min. Full scan mass spectra were recorded in the range [1000-2000] *m*/*z*.

Results

Complexes with berenil. Figure 9-6 shows spectra of equimolar mixtures of the duplex d(GGGGAATTGGGG)•d(CCCCAATTCCCC) and berenil. A little amount of 2:1 complex is detected at high concentration, as previously reported (see Chapter 8). The contribution of other stoichiometries than 1:1 can not be taken into account with the present equations, so it must be assumed that the contribution of minor species of other stoichiometries is not significant enough to perturb the determination of K_a. Only the charge state 5- was considered for the determination of the intensity ratio. Fitting of the results obtained by varying the concentration from 2.0×10^{-6} to 2.0×10^{-5} M gives an association constant $K_a = (2.3 \pm 0.7) \times 10^5$ M^{-1} and a factor $R = 0.8 \pm 0.2$. With a similar duplex having a central sequence AAAA•TTTT, the fitting gives $K_a = (9 \pm 8) \times 10^4$ M^{-1} and $R = 1.6 \pm 1.0$. Within the errors given by the non-linear least squares fitting program, R can be considered to be close to unity.

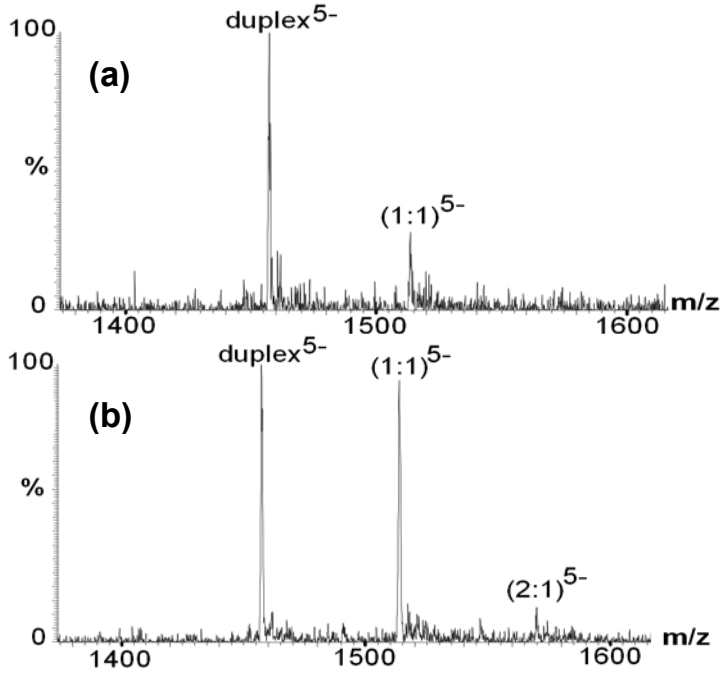

Figure 9-6. ES-MS spectra of equimolar mixtures of berenil and duplex d(GGGGAATTGGGG)•d(CCCCAATTCCCC) at (a) C_0 = 2.0 × 10^{-6} M and (b) C_0 = 10^{-5} M.

Complexes with Hoechst 33342 and comparison with fluorescence. In order to be able to make comparisons with constants measured in solution by an independent method, we have chosen the drug Hoechst 33342 which, unlike berenil, makes a fluorescent complex with DNA. The complex with the dodecamer $d(CGCGAATTCGCG)_2$ has been studied. MS spectra were recorded at different concentrations for equimolar drug/duplex mixtures in 80/20 (v:v) 100 mM NH_4OAc/methanol. 20% methanol does not change dramatically the dielectric constant of the medium, and it has been checked by circular dichroism that the B-form of the double helix was conserved. The fitting procedure was applied (Figure 9-7), considering the charge state 5-. The results obtained by fitting are K_a = (1.9 ± 0.4) × 10^8 M^{-1}, and R = 0.5 ± 0.2. Considering R = 1 would lead to an association constant K_a = (5.9 ± 0.6) × 10^7 M^{-1}. No data exist in the literature on association constants determined in ammonium acetate electrolyte, either for the present complex or for related drug-DNA complexes. To determine the association constant by an independent method in a solution with a composition close to the one used in ES-MS, we performed fluorescence titration in 100 mM NH_4OAc. The experiment could not

be conducted in the presence of methanol due to quenching effects. The fluorescence titration experiment had to be conducted with a starting concentration of duplex of 8.1 nM to ensure that the equations used are applicable[18]. The association constant measured by fluorescence titration is $K_a = (1.4 \pm 0.2) \times 10^8$ M^{-1}. Despite all the approximations made, this value is close to the one determined by the fitting method with the correction for the response factors. Assuming that $R = 1$ leads however to an underestimation of the constant.

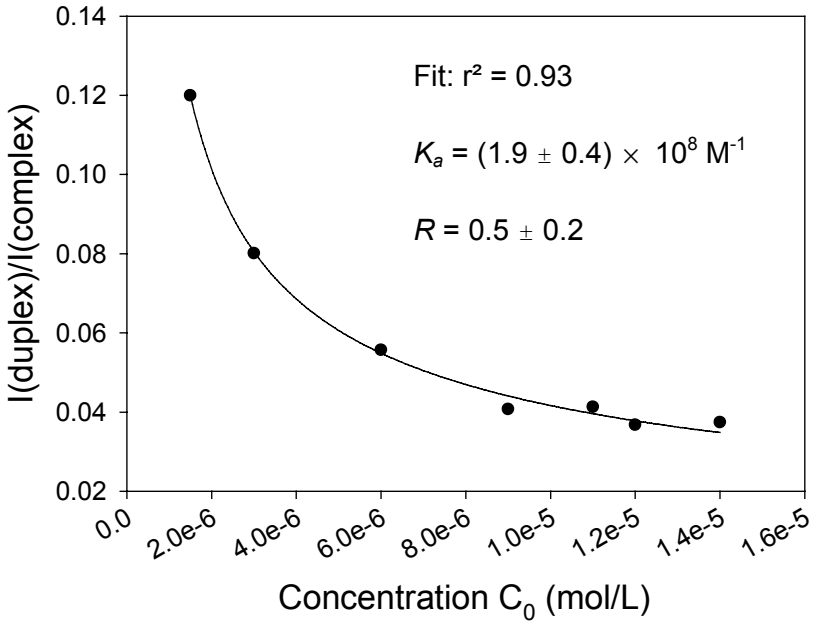

Figure 9-7. Determination of K_a and R for the complex between Hoechst 33342 and d(CGCGAATTCGCG)$_2$. Fitting of the experimental results using equation (9.8), considering $I(A)$ = intensity of the duplex^{5-} and $I(AB)$ = intensity of the complex [1:1]$^{5-}$.

Discussion

Meaning of *R*. The effect of the source conditions on the breaking of duplex DNA and complexes had been studied previously (see Chapters 11 and 12) on the LCQ mass spectrometer. The experimental conditions chosen here are soft enough to avoid breaking of the complex. The mass range used also prevents ion discrimination during trapping: the instrument automatically selects the RF amplitude that is necessary to

trap all ions of the chosen mass range. As the duplex and the complex have close values of m/z compared to the mass range, both of their trapping efficiencies can be assumed to be optimum. There is therefore no other discrimination on the intensities of the duplex and the complex than the different electrospray response factors, and R can be simply interpreted as the ratio between the electrospray response of the complex and that of the duplex.

Influence of the structure of the complex. For berenil, the duplex and the complex have the same response factor (within experimental error), and $R = 1$ is a reasonable approximation. For Hoechst 33342, the response of the complex is about twice lower than the response of the duplex. The difference in the response factors for the duplex and the complex may indicate a conformational change in the double helix upon drug binding. Indeed, crystallographic[19] and molecular modelling studies[20] on Hoechst analogs have shown that the structure of the dodecamer is slightly distorted in the complex compared to the free duplex, and the role of DNA plasticity in minor groove binding has been emphasized[19]. We have found out that the response of the complex was half that of the duplex. This implies that even a slight deformation of the molecule can change its electrosrpay response by a factor of two. If it had been assumed that $R = 1$, this would have led to an error on the constant by a factor of about two as well. The sensitivity of the electrospray response on the conformation has another major interest: the present method, besides the determination of the equilibrium association constants, could allow to detect substrate conformational changes upon ligand binding, but this point needs further investigation.

Implication for competition experiments. In the light of these measurements, we can now comment further on the competition experiments which are based on the assumption that all complexes had the same response factors. It must be mentioned that the competition experiments are quite early work compared to the present study including the R factor. We think that the scale of binding affinities established by the competition experiments could have been skewed by errors on the concentrations of the drugs: the solution may not have been strictly equimolar. As for the basic assumption on the equal response factors of the complexes, we now see that it may be wrong and that complexes with different drugs can have different response factors. Nevertheless, the differences in R are not so large and competition experiments can still be very useful to have a quick estimation of the relative binding affinities of drugs. Especially in a drug design approach consisting in the synthesis of series of analog molecules differing only by single substituents, competition experiments between

analogs (provided that they have different masses) can give reliable results. If the drugs are similar in shape, the complexes can be expected to be similar in shape as well, and their responses can be expected to be similar.

Cyclodextrin-diacid complexes

Experimental

The ES-MS spectra of α-cyclodextrin complexes were recorded with a Q-TOF2 mass spectrometer equipped with a Z-spray source. Electrospray ionization was achieved in the negative ion mode by application of -2.5 kV on the needle. Three different cone voltage values (10, 20 and 30 V) were used.

α-cyclodextrin + α,ω-nonanoic diacid: results and discussion

This system was studied to illustrate the use of the method in a more complicated case. Figure 9-8 shows a spectrum of an equimolar mixture (C_0 = 4.0 × 10^{-4} M) of α-cyclodextrin and α,ω-nonanoic diacid (1,7-da). The mass spectrum shows the singly and doubly deprotonated cyclodextrin (A), the singly charged acid (B), the doubly charged 1:1 complex (AB), and also a less abundant doubly charged A_2B complex.

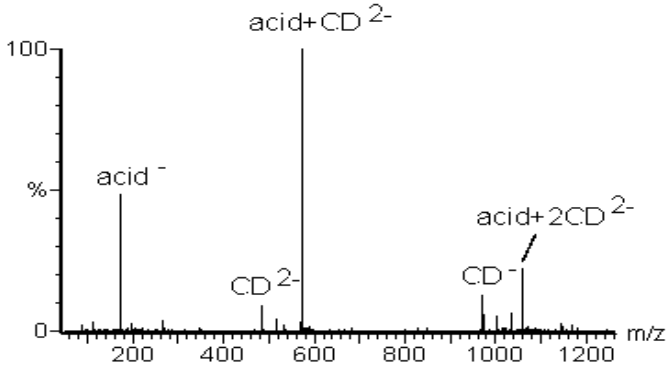

Figure 9-8. ES-MS spectrum obtained for an equimolar mixture (C_0 = 4 × 10^{-4} M) of α-cyclodextrin (CD) and α,ω-nonanoic acid. The cone voltage was set to 10 V.

A priori, the response factors of the cyclodextrin and the complex can not be predicted, but are very likely to differ for two reasons. First, cyclodextrin is neutral in solution, and looses one or two protons during the electrospray process to produce the CD^{1-} and CD^{2-} species. The complex, however, is "pre-charged" by the dianion that is complexed, and indeed appears only as a doubly charged species. The diacid chain length can be included in the cyclodextrin or not. Second, as will be shown below, collision-induced dissociation (CID) can occur in the electrospray source at the cone voltages used. The factor *R* therefore needs to be determined experimentally.

The fitting procedure was applied considering the cyclodextrin as A, and the 1:1 complex as AB. As for the drug-DNA system, the 2:1 complex A_2B was not taken into account. For the systems studied here these were only minor species, and a good fitting is obtained with this assumption. Figure 9-9 A-C shows three attempts of fitting, considering the different charge states of α-cyclodextrin, at a cone voltage of 10 V.

It can be seen from Figures 9-9A and 9-9B that considering only one charge state of the cyclodextrin at a time is not a successful approach. The quality of the fit is poor, and the errors on K_a and *R* are larger than K_a and *R* themselves. However, when considering the sum of the intensities corresponding to the two charge states of cyclodextrin $I(A) = I(CD^{1-}) + I(CD^{2-})$, the fit is of good quality and the errors on K_a and *R* are reasonable. Considering the charge states in an isolated manner causes problems for this system because the charge state distribution changes with the concentration. Figure 9-9D shows that the proportion of CD^{1-} compared to CD^{2-} increases when C_0 increases. We checked for the same effect in solutions containing only cyclodextrin, and found out no such behavior when increasing the cyclodextrin concentration. In the equimolar mixture, the increasing proportion of CD^{1-} is therefore due to the increasing concentration of acid in the solution, which is not buffered. The pH of the solution influences the charge state distribution of cyclodextrins. In Figure 9-9B, the experimental values of $I(CD^{1-})/I(complex)$ do not decrease steeply enough with the concentration. This results in an underestimation of the association constant. Conversely, considering CD^{2-} alone leads to an overestimation of the association constant. The association constant obtained by fitting in Figure 9-9C at a cone voltage of 10 V is $K_a = (2.6 \pm 0.6) \times 10^3\ M^{-1}$, and the factor $R = 6.6 \pm 1.0$.

As *R* is larger than 1, the response of the complex is larger than the response of the cyclodextrin. As the transmission of the quadrupole can not be responsible of such a discrimination in the considered mass range, this *R* value indicates a difference in the electrospray response, which can be due to two factors. First, as mentioned before, the

complex has two permanent charges in the solution. Cyclodextrin is neutral and has to exchange protons to get charged, so that negative ions of cyclodextrin may be more difficult to produce than a negatively charged complex. Second, the difference in response can come from the presence of the diacid in the complex.

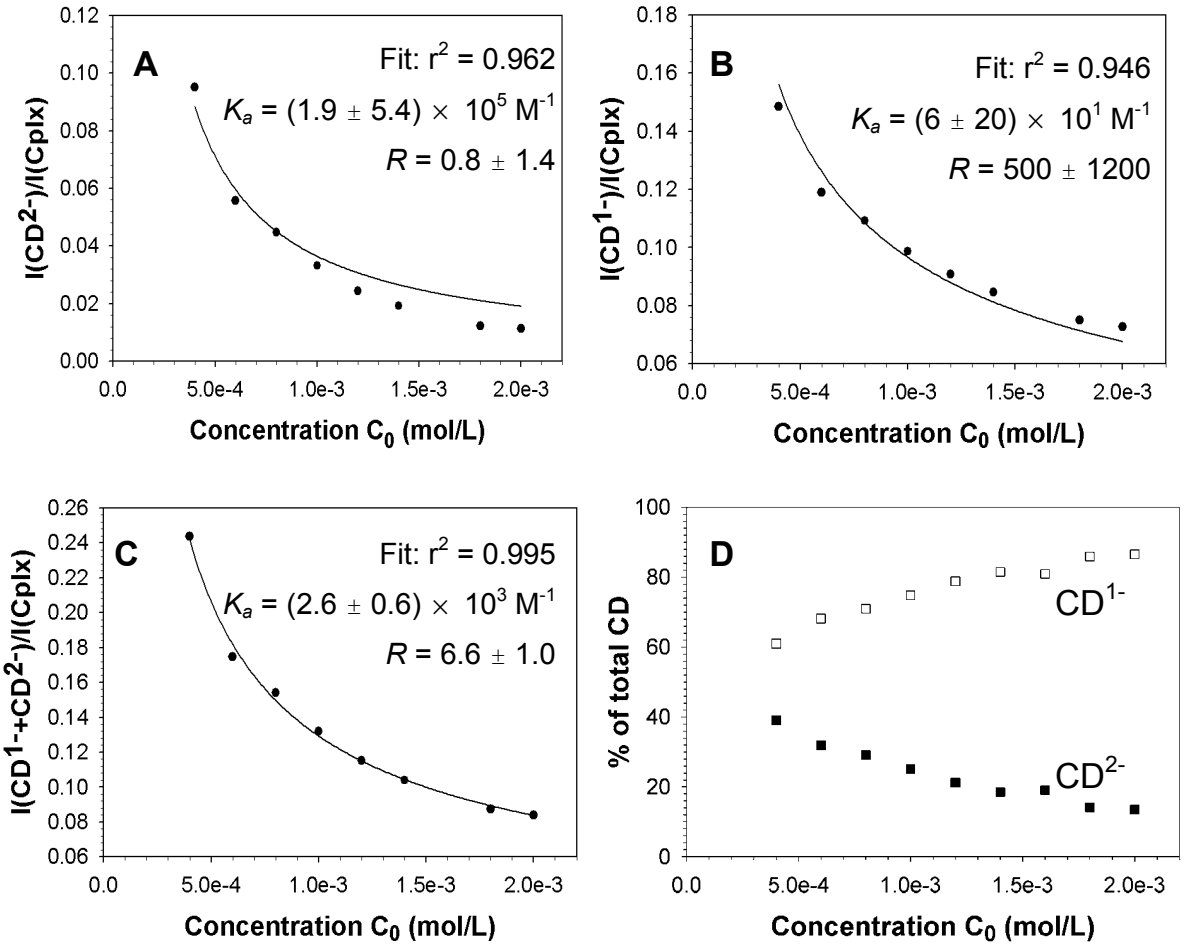

Figure 9-9. **A-C**: Determination of K_a and R for the complex between α-cyclodextrin (CD) and α,ω-nonanoic diacid considering (**A**) I(A) = I(CD^{1-}), (**B**) I(A) = I(CD^{2-}) and (**C**) I(A) = I(CD^{1-}) + I(CD^{2-}). Fittings were made using equation (9.8). **D**: Evolution of the relative intensity of the two charge states of α-cyclodextrin (CD) as a function of the concentration of the equimolar (CD:acid) mixture.

The effect of the cone voltage on the determination of the constants has also been investigated. The fitting procedure was applied to the same system, with a cone voltage of 20 V. The relative intensity of the complex is slightly smaller than at 10 V (data not shown). Fitting of the results at 20 V gives an association constant K_a = (4.2 ± 1.4) × 10^3 M^{-1}, consistent with the value obtained at 10 V within experimental error. The factor R has however decreased to a value of R = 4.0 ± 0.8, a significantly lower value than at 10 V. The response of the complex at 20 V is lower than at 10 V due to its partial dissociation. At 30 V, the abundance of the complex is largely reduced, but no good fitting of the results could be obtained. This illustrates that the above-described fitting method is also capable of correcting for moderate source-CID of the complex.

Influence of the diacid chain length

In Chapter 8, we reported qualitative results for the complexes of diacids of different chain lengths with α-cyclodextrin, and concluded that part of the observed complex was due to specific inclusion in solution, and part was due to nonspecific electrostatic aggregation induced by the electrospray process. Here we report the results obtained for the determination of the equilibrium association constants for these complexes.

The results are summarized in Table 9-1. The method described above successfully gave K_a and R values only for diacids with n = 6, 7 and 8. For the other diacids, the solutions were obviously not equimolar, and this resulted in too large errors.

For all diacids the factor R is larger than 1. The complex always responds better than the cyclodextrin. The factor R can give indications on the conformation of the complex when it escaped the electrospray droplet. If the diacid was included in the cavity, the chain length would be hidden from the solvent and the responses of all the complexes would be similar. The fact that R increases with the diacid chain length therefore suggests that a significant proportion of the complex has a non-inclusion geometry.

Table 9-1. Binding constants for complexes of 1,n-diacids and α-cyclodextrin determined by calorimetry and mass spectrometry. The mass spectrometric results are given for a cone voltage = 10 V.

n	K_a Calorimetry [a] (M^{-1})	K_a MS (M^{-1}) [b] (assuming R = 1)	MS (fitting method) K_a (M^{-1})	MS (fitting method) R
4	no complex	36,000 ± 6,000 [c]		
5	24 ± 1			
6	93 ± 1	53,000 ± 5,000	3300 ± 1000	5.0 ± 0.9
7	630 ± 20	67,000 ± 9,000	2600 ± 600	6.6 ± 1.0
8	1790 ± 80	81,000 ± 9,000	2000 ± 400	6.7 ± 0.9
10		100,000 ± 40,000 [d]		
12		91,000 ± 45,000 [d]		

(a) Data from reference 21.

(b) Mean value over the concentration range [4.0×10^{-4} – 2.0×10^{-3} M].

(c) Concentration dependence indicates a too low concentration of diacid, and hence an underestimation of the constant.

(d) Concentration dependence indicates a too high concentration of diacid, and hence an overestimation of the constant.

9.4. Conclusions

In summary, we reported the equations and methodology for simultaneous determination of the equilibrium association constant (K_a) of noncovalent complexes and the ratio between the response factors of the complex and the free substrate (R). The method neither requires the prior knowledge of any association constant, nor any calibration, nor the complete displacement of the equilibrium. The practical limitation is that the concentration of the reactants has to be determined precisely, but a careful examination of the results allows to detect and evaluate such a source of error. The method is also currently limited to 1:1 complexes (otherwise a different R factor would be needed for each complex of the mixture).

The possibility to determine R experimentally by electrospray mass spectrometry (not by comparison of the MS-determined constants with other methods) can become a very useful tool for fundamental studies of noncovalent interactions. The factor R corrects for any discrimination like differences in spectrometer transmission, in detection efficiency, different electrospray responses and moderate in-source CID of the complex. When the other discrimination factors are minimized by a careful selection of the experimental conditions, the factor R can reflect the different electrospray response factors of the complex and the substrate. As shown for a drug-DNA complex, the difference in electrospray response for the free DNA duplex and the complex could be used to get some insight into the effect of complexation on the conformation of the substrate. In the case of the cyclodextrin complexes, R gives indications on the conformation of the complex, i.e. whether or not the ligand is included in the cyclodextrin cavity.

References

1. J.A. Loo, D.D. Holsworth, R.S. Root-Bernstein; Use of Electrospray Ionization Mass Spectrometry to Probe Antisense Peptide Interactions. *Biol. Mass Spectrom.* **1994,** 23: 6.

2. J.A. Loo, P. Hu, P. McConnell, W.T. Mueller, T.K. Sawyer, V. Thanabal; A Study of SH2 Domain Protein-Phosphopeptide Binding Interactions by Electrospray Ionization Mass Spectrometry. *J. Am. Soc. Mass Spectrom.* **1997,** 8: 234.

3. Y.-L. Chen, J.M. Campbell, B.A. Collings, L. Koenermann, D.J. Douglas; Stability of a Highly Charged Non-Covalent Complex in the Gas Phase: Holomyoglobin. *Rapid Commun. Mass Spectrom.* **1998,** 12: 1003.

4. H.-K. Lim, Y.L. Hsieh, B. Ganem, J.D. Henion; Recognition of Cell-Wall Peptide Ligands by Vancomycin Group Antibiotics: Studies Using Ionspray Mass Spectrometry. *J. Mass Spectrom.* **1995,** 30: 708.

5. C.V. Robinson, E.W. Chung, B.B. Kragelund, J. Knudsen, R.T. Aplin, F.M. Poulsen, C.M. Dobson; Probing the Nature of Noncovalent Interactions by Mass Spectrometry. A Study of Protein-CoA Ligand Binding and Assembly. *J. Am. Chem. Soc.* **1996,** 118: 8646.

6. T.J.D. Jorgensen, P. Roepstorff, A.J.R. Heck; Direct Determination of Solution Binding Constants for Noncovalent Complexes Between Bacterial Cell Wall Peptide Analogues and Vancomycin Group Antibiotics by Electrospray Ionization Mass Spectrometry. *Anal. Chem.* **1998,** 70: 4427.

7. D.M. Crothers; Statistical Thermodynamics of Nucleic Acid Melting Transitions With Coupled Binding Equilibria. *Biopolymers* **1971,** 2147.

8. M. Lee, A.L. Rhodes, M.D. Wyatt, S. Forrow, J.A. Hartley; GC Base Sequence Recognition by Oligo(Imidazolecarboxamide) and C-Terminus-Modified Analogues of Distamycin Deduced From Circular Dichroism, Proton NMR, and Methylpropylethylenediaminetetraacetate-Iron(II) Footprinting Studies. *Biochemistry* **1993,** 32: 4237.

9. F.A. Tanious, J. Spychala, A. Kumar, K. Greene, D.W. Boykin, W.D. Wilson; Different Binding Mode in AT and GC Sequences for Unfused-Aromatic Dications. *J. Biomol. Struct. Dyn.* **1994,** 11: 1063.

10. D.L. Boger, B.E. Fink, S.R. Brunette, W.C. Tse, M.P. Hedrick; A Simple, High-Resolution Method for Establishing DNA Binding Affinity and Sequence Selectivity. *J. Am. Chem. Soc.* **2001,** 123: 5878.

11. F.J. Meyer-Almes, D. Porschke; Mechanism of Intercalation into the DNA Double Helix by Ethidium. *Biochemistry* **1993,** 32: 4246.

12. D. Rentzeperis, M. Medero, L.A. Marky; Thermodynamic Investigation of the Association of Ethidium, Propidium and Bis-Ethidium to DNA Hairpins. *Bioorg. Med. Chem.* **1995,** 3: 751.

13. K.A. Sannes-Lowery, R.H. Griffey, S.A. Hofstadler; Measuring Dissociation Constants of RNA and Aminoglycoside Antibiotics by Electrospray Ionization Mass Spectrometry. *Anal. Biochem.* **2000,** 280: 264.

14. J.B. Chaires; Energetics of Drug-DNA Interactions. *Biopolymers* **1997,** 44: 201.

15. J. Pindur, G. Fischer; DNA Complexing Minor Groove-Binding Ligands: Perspective in Antitumour and Antimicrobial Drug Design. *Curr. Med. Chem.* **1996,** 3: 379.

16. S. Neidle; Crystallographic Insights into DNA Minor Groove Recognition by Drugs. *Biopolymers* **1997,** 44: 105.

17. M.R. Eftink; Fluorescence Methods for Studying Equilibrium Macromolecule-Ligand Interactions. *Methods Enzymol.* **1997,** 278: 221.

18. J. Ren, J.B. Chaires; Sequence and Structural Selectivity of Nucleic Acid Binding Ligands. *Biochemistry* **1999,** 16067.

19. M.A.A.F. de CT Carrondo, M. Coll, J. Aymani, A.H.J. Wang, G.A. Van der Marel, J.H. Van Boom, A. Rich; Binding of Hoechst Dye to $d(CGCGATATCGCG)_2$ and Its Influence on the Conformation of the DNA Fragment. *Biochemistry* **1989,** 28: 7849.

20. M.C. Vega, M. Coll, C. Aleman; Intrinsic Conformational Preferences of the Hoechst Dye Family and Their Influence on DNA Binding. *Eur. J. Biochem.* **1996,** 239: 383.

21. G. Castronuovo, V. Elia, F. Velleca, G. Viscardi; Thermodynamics of the Interaction of α-Cyclodextrin With α,ω-Dicarboxylic Acids in Aqueous Solutions. A Calorimetric Study at 25°C. *Thermochimica Acta* **1997,** 292: 31.

10.

HOW TO EXTRACT RELEVANT INFORMATION FROM DISSOCIATION EXPERIMENTS

10.1. Introduction

One often finds in the literature statements like: “the voltage required to dissociate ions of the (…) complexes in the orifice-skimmer region of an electrospray mass spectrometer, a measure of the complex stability,…”[1], “Increasing the internal energy of the gas-phase complex led to dissociation of the complex. The ease of dissociation is interpreted in terms of intrinsic stability of the complex…”[2] or “the *Vc* (acceleration voltage) value needed to dissociate 50% of the noncovalent complex initially present (Vc_{50}) was taken as a gas-phase stability parameter of the (…) complex.”[3]. What is the physical basis for such relationship between the dissociation efficiency and the gas-phase stability of a complex?

In the present work, we used source-CID, heated capillary dissociation and collisional activation in MS/MS to induce the fragmentation of the complexes. In this short chapter, we will comment on what kind of information can be deduced from such experiments, what precautions have to be taken, and how the results have to be interpreted. This will be done on the basis of the theory of dissociation kinetics in mass spectrometry (see Chapter 3).

10.2. On the comparison between dissociation efficiencies

First, it must be emphasized that the relative intensity of the fragments compared to that of the intact complex depends on the dissociation rate of the complex.

The complex exits the source with a certain amount of internal energy, and can be further activated by collisional activation in the case of MS/MS experiments. The unimolecular dissociation can proceed until the complex reaches the detector.

The dissociation kinetics depends on the internal energy

The dependence of the unimolecular dissociation rate constant on the internal energy is given by the RRKM formula (equation 3.6). One can only compare the fragmentation efficiencies of complexes when the same amount of internal energy is given to all the members of the series. It may seem superfluous to insist on that point, but in many publications the comparison is made between ions that have been given the same laboratory kinetic energy for collisions[1-7]. This is not sufficient to ensure that the ions have the same internal energy. Few papers report the comparison in terms of center-of-mass kinetic energy[8,9], which is mass-dependent. And even if the center-of-mass kinetic energy is the same, the efficiency of the conversion of kinetic energy into internal energy can differ, depending again on the mass of the ion and also on the degrees of freedom of the ion and the target gas[10,11].

The dissociation kinetics depends on the number of degrees of freedom

This arises directly from the statistical theory of unimolecular dissociation: the rate constant depends on the fraction of the total internal energy that is located in the particular degree(s) of freedom corresponding to the reaction coordinate. For a given total internal energy, the larger the total number of degrees of freedom, the lower the probability of the energy to be in the reaction coordinate, and the lower the rate constant (see Chapter 3). The consequence is that one can not compare the fragmentation efficiency of two complexes having different sizes to infer directly information on the reaction energetics.

This is illustrated by a example selected from our work. Figure 10-1 shows the relative intensity of intact duplex for two DNA duplexes as a function of the capillary-skimmer voltage in the source of the LCQ instrument. The duplexes have the same base pairs, so they have the same binding interface and therefore the same interaction energy, but

they have different sizes (see Table 10-1). The relative intensities are calculated using equation (10.1).

$$\%Duplex = \frac{I_{Dup^{6-}}}{I_{Dup^{6-}} + \frac{I_{A^{3-}} + I_{B^{3-}}}{2}} \cdot 100\% \qquad (10.1)$$

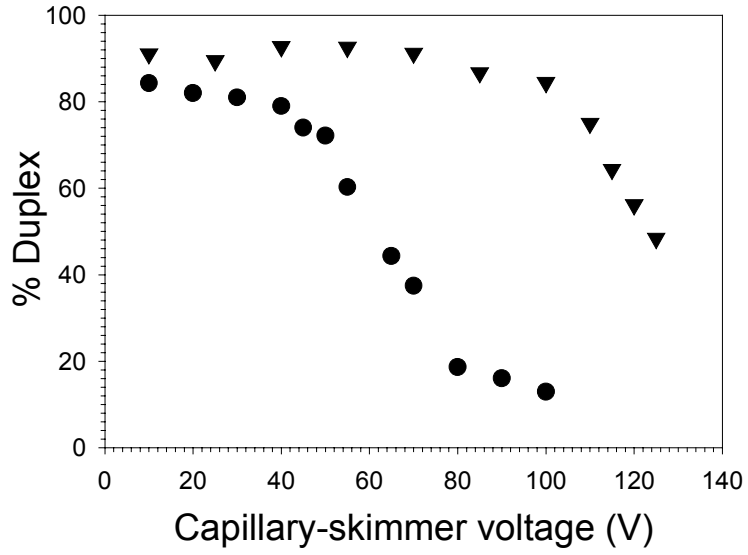

Figure 10-1. Dissociation curves of two duplexes with the same interaction interface between the two strands, but of different sizes. The base sequences are given in Table 10-1.

Table 10-1. Summary of the study of the influence of the complex size: complete base sequence and voltages of half dissociation.

		Base sequence	$V_{1/2}$
1:	●	GGGCTATAATATCGGG CCCGATATTATAGCCC	68 V
2:	▼	TTTGGGCTATAATATCGGGTTT CCCGATATTATAGCCC	125 V

It can be seen in Figure 10-1 that, although the two duplexes are expected to have the same activation energy and the same reaction mechanism, the longer one clearly requires a larger laboratory kinetic energy to achieve fragmentation. Even if we correct the $V_{1/2}$ (the voltage at which 50% of the duplex is dissociated) of duplex **2** for the center-of-mass energy, we obtain $V_{1/2}$ = 105 V instead of 125 V. This is still much larger than for duplex **1**. This difference is due to the degree-of-freedom effect. A higher number of degrees of freedom slows down the reaction rate, and a higher energy is required to achieve the same fragmentation yield.

Actually, in the RRKM formula (3.6), it is the density of states of the reactant and of the transition state that are implied. The density of states directly depends on the number of degrees of freedom, but the distribution of the vibrational frequencies is also important. Molecules of similar structures are likely to have a similar distribution of frequencies.

The dissociation kinetics depends on the activation enthalpy and the activation entropy

Any equation expressing the internal energy dependence of a rate constant contains an enthalpic term (E_0 in the RRKM formula, E_a in the Arrhenius formula) which is related to the height of the barrier to be crossed in the potential energy surface for the dissociation of the molecule, and an entropic term. In the RRKM formula, the entropic term is the ratio between the number of states of the transition state and the density of states of the reactant. In the Arrhenius formula, it is the pre-exponential factor A. The entropic term corresponds to the change in the flexibility of the molecule between the reactant and the transition state. Only the study of the internal energy dependence of the dissociation rate (for example in BIRD experiments) can give access to both the enthalpic and the entropic terms.

Conclusions

If we want the dissociation rate constants of a series of complexes to reflect their relative activation barriers in non-thermal activation like BIRD, we must:

- give the complexes the same internal energy distribution,

- compare complexes of similar structure and same size (this also ensures that the center-of-mass kinetic energies are the same), and
- compare reactions for which the activation entropy for dissociation is the same. The transition states must have the same frequency distribution, and therefore the dissociation mechanism have to be the same.

10.3. Comparison between thermodynamic and kinetic data

Except in the rare cases where equilibrium measurements are possible, mass spectrometry only provides access to the dissociation reaction of the complex:

[Ligand-Substrate] $\rightarrow$ Ligand + Substrate (10.2)

We therefore do not have access to the dissociation *equilibrium constant*, but only to the dissociation *rate*. Such experimental conditions allow to probe the *lability* (kinetic connotation) of the complex, but not its *stability* (thermodynamic connotation).

Figure 10-2 presents a section in the potential energy surface of the complex along the reaction coordinate leading to the dissociation. The dissociation of the complex into its subunits requires the overcoming of the activation barrier E_0. The rate constant depends on E_0 (see RRKM formula), which is related to $\Delta H^{\ddagger\circ}_{diss}$. If the reaction proceeds via path **1**, the loose transition state resembles the products of dissociation and $\Delta H^{\ddagger\circ}_{diss} = \Delta H^{\circ}_{diss}$. If reaction proceeds via path **2**, there is a reverse energy barrier E_r that makes $\Delta H^{\ddagger\circ}_{diss} \neq \Delta H^{\circ}_{diss}$. This demonstrates the difficulty of relating the kinetic data obtained in mass spectrometry and thermodynamic data in the gas phase, obtained from calculations. It is important to note that the relative *labilities* of complexes will be indicative of their relative *stabilities* (ΔH°_{diss} in the gas phase) only if their reverse activation barriers are proportional.

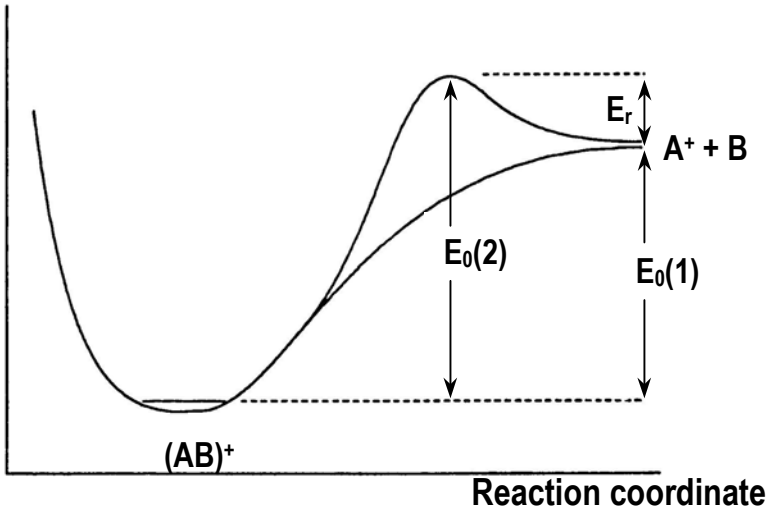

Figure 10-2. Simplified potential energy diagram for the dissociation of a complex $(AB)^+$. In the case of path **1**, the barrier E_0 is equal to the difference between the zero point energy of the product and that of the reactant. Path **2** involves a reverse energy barrier E_r.

References

1. C.L. Hunter, A.G. Mauk, D.J. Douglas; Dissociation of Heme From Myoglobin and Cytochrome B5: Comparison of Behavior in Solution and in the Gas Phase. *Biochemistry* **2000,** 36: 1018.

2. A.A. Rostom, J.R.H. Tame, J.E. Ladbury, C.V. Robinson; Specificity and Interactions of the Protein OppA: Partitioning Solvent Binding Effects Using Mass Spectrometry. *J. Mol. Biol.* **2000,** 296: 269.

3. H. Rogniaux, A. Van Dorsselaer, P. Barth, J.F. Biellmann, J. Brabanton, M. van Zandt, B. Chevrier, E. Howard, A. Mitschler, N. Potier, L. Urzhumtseva, D. Moras, A. Podjarny; Binding of Aldose Reductase Inhibitors: Correlation of Crystallographic and Mass Spectrometric Studies. *J. Am. Soc. Mass Spectrom.* **1999,** 10: 635.

4. K.J. Light-Wahl, B.L. Schwartz, R.D. Smith; Observation of Non-Covalent Quaternary Associations of Proteins by Electrospray Ionization Mass Spectrometry. *J. Am. Chem. Soc.* **1994,** 116: 5271.

5. J. Gao, Q. Wu, J.D. Carbeck, Q.P. Lei, R.D. Smith, G.M. Whitesides; Probing the Energetics of Dissociation of Carbonic Anhydrase-Ligand Complexes in the Gas Phase. *Biophys. J.* **1999,** 76: 3253.

6. Y.-T. Li, Y.L. Hsieh, J.D. Henion, T.D. Ocain, G.A. Schiehser, B. Ganem; Analysis of the Energetics of Gas-Phase Immunophilin-Ligand Complexes by Ionspray Mass Spectrometry. *J. Am. Chem. Soc.* **1994,** 116: 7487.

7. Q. Wu, J. Gao, D. Joseph-McCarthy, G.B. Sigal, J.E. Bruce, G.M. Whitesides, R.D. Smith; Carbonic Anhydrase-Inhibitor Binding: From Solution to Gas Phase. *J. Am. Chem. Soc.* **1997,** 119: 1157.

8. R. Ramanathan, L. Prokai; Electrospray Ionization Mass Spectrometric Study of Encapsulation of Amino Acids by Cyclodextrins. *J. Am. Soc. Mass Spectrom.* **1995,** 6: 866.

9. V. Nesatyy; Gas-Phase Binding of Non-Covalent Protein Complexes Between Bovine Pancreatic Trypsin Inhibitor and Its Target Enzymes Studied by Electrospray Ionization Tandem Mass Spectrometry. *J. Mass Spectrom.* **2001,** 36: 950.

10. S.A. McLuckey; Principles of Collisional Activation in Analytical Mass Spectrometry. *J. Am. Soc. Mass Spectrom.* **1991,** 3: 599.

11. A. Hoxha, C. Collette, E. De Pauw, B. Leyh; Mechanism of Collisional Heating in Electrospray Mass Spectrometry: Ion Trajectory Calculations. *J. Phys. Chem. A* **2001,** 105: 7326.

11.

EFFECT OF THE COLLISION REGIME ON THE DISSOCIATION OF THE COMPLEXES

11.1. Introduction

In order to investigate the strength of noncovalent interactions in the gas phase, one usually compares the energy required to dissociate the complex into its constitutive parts. This is the noncovalent dissociation channel. The usual way to obtain comparative data for different complexes is to measure the appearance of the fragments upon increase of the collision energy, and to compare the energies at which 50% of the complex is dissociated. The present chapter is dedicated to a discussion of the effect of the experimental MS/MS conditions on such measurements. That is why we do not report such breakdown curves, but rather show the spectra obtained in different typical activation conditions. In this chapter, we report the study of duplex DNA. The noncovalent dissociation channel corresponds to the breaking of the duplex into the single strands.

11.2. Comparison of MS/MS on the Q-TOF and on the LCQ

Experimental

CID in the quadrupole collision cell of the Q-TOF2

MS/MS experiments were performed on the Q-TOF2 electrospray mass spectrometer, and the source was operated in the negative ion mode (capillary voltage = -2350 V).

The source block temperature was 80 °C and the desolvation gas (N_2) temperature was 100 °C. The cone voltage was set to 20 V.

CID in the LCQ

The needle voltage was set to –3.9 kV, the capillary voltage to –20 V and the heated capillary temperature to 180 °C. MS/MS was performed during different activation times with the advanced scan parameters of Xcalibur 1.0 software. The activation time can be varied from 1 ms to 10 s. The longer the activation, the smaller the activation amplitude necessary to fragment the parent ion to a given extent.

MS/MS of 12-mer duplexes with different hydrogen bond content at different collision regimes

The studied duplexes

The base sequences of the studied duplexes are given in Table 11-1. In the full scan MS spectra the most intense signal comes from the duplex^{5-} on both instruments.

Table 11-1. Base sequences of 12-mer duplexes **A**-**C**.

Duplex	Base sequence	% of CG base pairs
A	d(5'-CGTAAATTTACG-3')$_2$	33%
B	d(5'-CGCGAATTCGCG-3')$_2$	67%
C	d(5'-CGCGGGCCCGCG-3')$_2$	100%

MS/MS results

Figure 11-1 shows four MS/MS spectra of duplex **A**, obtained by using slower activation conditions from (a) to (d). CID of the duplex^{5-} (noted **DS**, for double-stranded) in the quadrupole collision cell of the Q-TOF2 produces the single strands

(noted **ss**) which share the available charges. In the ion trap, the main fragmentation pathway is also the noncovalent dissociation into single strands, but another fragment appears in slow heating conditions, namely the duplex that has lost a neutral base (noted **DS-B** or **-B**), either adenine or guanine.

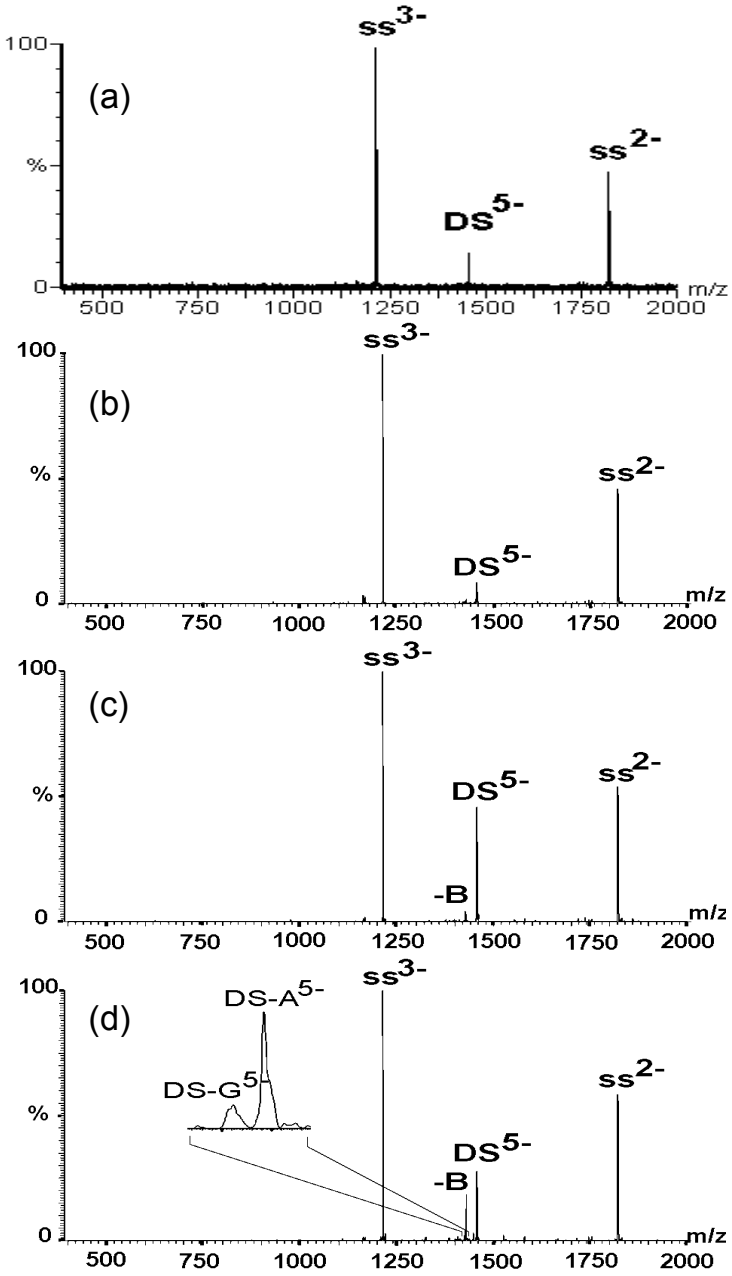

Figure 11-1. MS/MS spectra of duplex **A** recorded under different collision regimes, fastest to slowest activation from top to bottom. (a) Q-TOF2, collision energy = 16 eV. (b) LCQ, activation time = 3 ms, activation amplitude = 22%. (c) LCQ, activation time = 30 ms, activation amplitude = 10%. (d) LCQ, activation time = 300 ms, activation amplitude = 8%. The annotations are described in the text.

Figure 11-2 shows the MS/MS spectra of duplex **B** recorded for the same reaction times as in Figure 11-1.

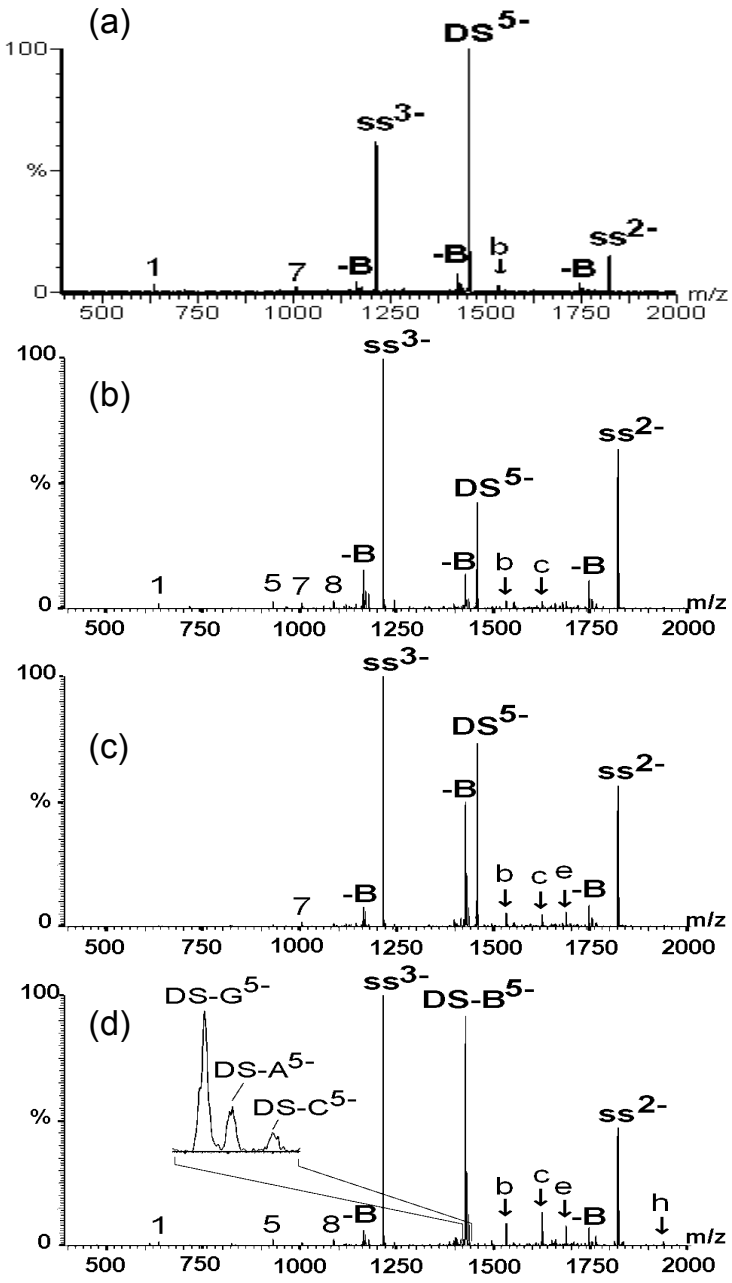

Figure 11-2. MS/MS spectra of duplex **B** recorded under different collision regimes, fastest to slowest activation from top to bottom. (a) Q-TOF2, collision energy = 22 eV. (b) LCQ, activation time = 3 ms, activation amplitude = 24%. (c) LCQ, activation time = 30 ms, activation amplitude = 12%. (d) LCQ, activation time = 300 ms, activation amplitude = 10%. The annotations are described in the text.

At the highest collision energy regimes (Figs. 11-2a and 11-2b), the main fragmentation pathway is the noncovalent dissociation into single strands. At the lowest collision energy regimes (Figs. 11-2c and 11-2d), the neutral base loss from the duplex becomes more important. In addition to these major peaks, other fragments appear in the spectra. Table 11-2 summarizes the fragments that have been observed throughout this study.

Table 11-2. Identification of the observed fragments, following the nomenclature of McLuckey, Van Berkel and Glish[1].

Type I				Type II	
1:	w_2^-	**7:**	$a_4\text{-}B^-$	**a:**	$(DS\text{-}a_5)^{4-}$
2:	$a_5\text{-}B^{2-}$	**8:**	w_7^{2-}	**b:**	$(DS\text{-}a_4)^{4-}$
3:	$a_3\text{-}B^-$	**9:**	w_8^{2-}	**c:**	$(DS\text{-}d_2\text{-}G)^{4-}$
4:	$a_6\text{-}B^{2-}$	**10:**	w_4^-	**d:**	$(DS\text{-}x_7\text{-}G)^{3-}$
5:	w_6^{2-}	**11:**	$a_5\text{-}B^-$	**e:**	$(DS\text{-}a_2)^{4-}$
6:	w_3^-	**12:**	w_{10}^{2-}	**f:**	$(DS\text{-}x_6\text{-}G)^{3-}$
				g:	$(DS\text{-}a_6)^{3-}$
				h:	$(DS\text{-}a_5)^{3-}$

Two categories of fragments can be distinguished: Type I fragments (noted **1**, **2**, **3**,…) are defined as backbone fragments of single strands and Type II fragments (noted **a**, **b**, **c**,…) are defined as duplexes which have lost a fragment of one of the strands. The relative abundance of Type II fragments increases when slow activation conditions are used.

In Figure 11-3, we see that the abundance of Type I and Type II fragments is even higher for duplex **C**. Like for duplex **A** and **B**, the neutral base loss channel is highly

favored by slow activation conditions. Two bases can even be lost. Type I fragments are however favored when CID is performed in the quadrupole collision cell of the Q-TOF2 (Fig. 11-3a).

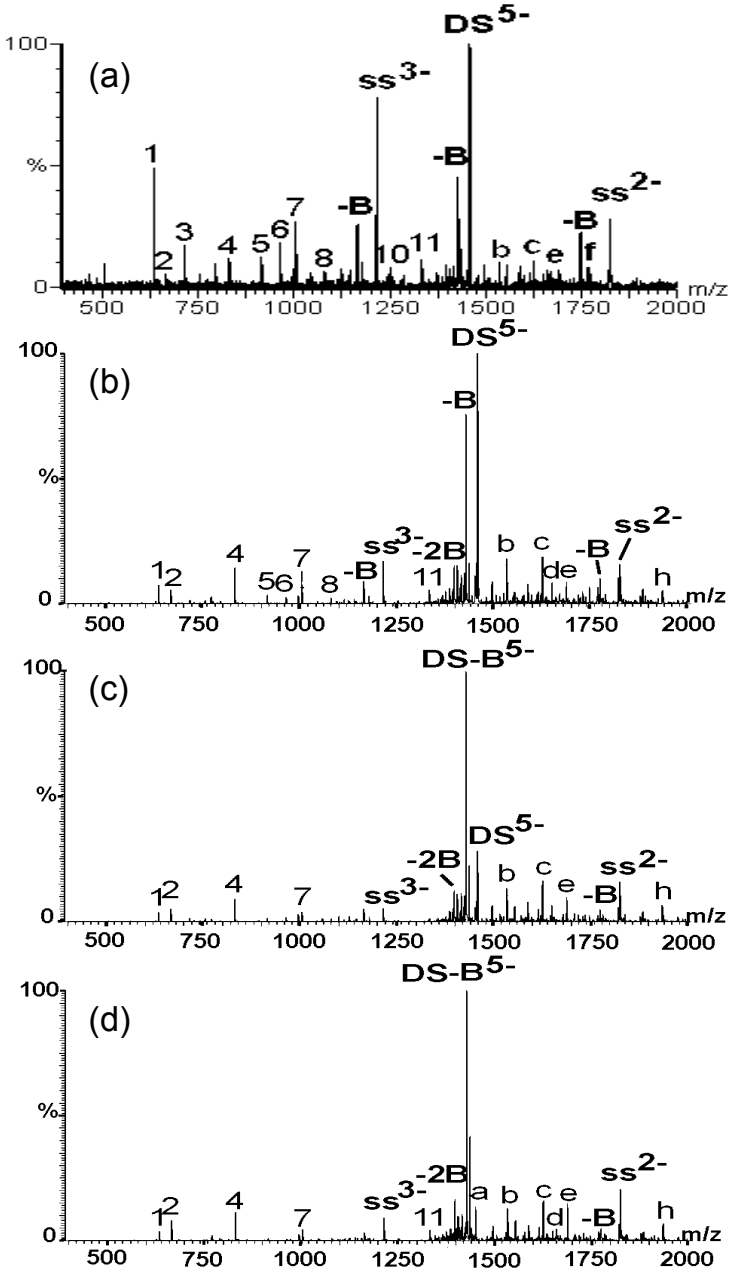

Figure 11-3. MS/MS spectra of duplex **C** recorded under different collision regimes, fastest to slowest activation from top to bottom. (a) Q-TOF2, collision energy = 30 eV. (b) LCQ, activation time = 3 ms, activation amplitude = 24%. (c) LCQ, activation time = 30 ms, activation amplitude = 12%. (d) LCQ, activation time = 300 ms, activation amplitude = 11%. The annotations are described in the text.

Competition between noncovalent dissociation and covalent fragmentation

Besides the dissociation channel of interest corresponding to the noncovalent dissociation of the complex into its components, there can be side processes like the fragmentation of covalent bonds that, if predominant, complicate the comparison with solution-phase data, and are therefore not desirable. It has been reported that cyclodextrin-peptide complexes underwent noncovalent dissociation in CID and heated-capillary dissociation[2], so that the relative kinetic stabilities of the complexes could be determined and correlated with the binding affinities in solution. However, in BIRD experiments on the same complexes, covalent fragmentation of the peptide occurred instead, and no activation energy could be determined for the noncovalent dissociation reaction[3].

Competition between the noncovalent dissociation of the complex and different covalent fragmentation reactions have also been reported for DNA duplexes[4,5]. The neutral base loss is the predominant channel competing with the noncovalent dissociation. For single strands[6,7] and for non-complementary duplexes[4], it has been reported that the base loss initiated the backbone fragmentation. To investigate whether the Type II fragments observed in Figures 11-2 and 11-3 are also initiated by base loss, we performed MS^3 experiments on the $[DS\text{-}B]^{5-}$ species isolated from the fragmentation of duplex **B**, which was isolated by a first MS/MS step in slow heating conditions (activation time = 300 ms). MS^3 results are displayed in Figure 11-4. When comparing Fig. 11-2b with Fig. 11-4a, and Fig. 11-2d with Fig. 11-4b (same activation times for DS^{5-} and $[DS\text{-}B]^{5-}$ respectively), we see that Type II fragments are more abundant when CID is undertaken on the [DS-B] species. Although this is not a definite proof, this suggests that [DS-B] species are the precursors of Type II fragments. Type I fragments can be produced either by fragmentation of [DS-B] into Type II and the complementary Type I fragments or by fragmentation of single strands that contain excess energy.

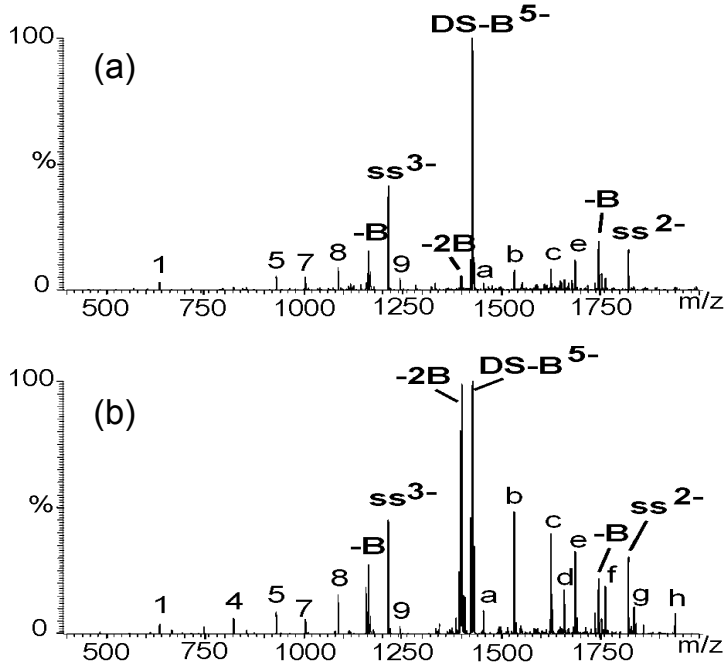

Figure 11-4. MS^3 experiment on duplex **B**. $[DS\text{-}B]^{5-}$ was isolated from duplex **B**, which is produced like in Figure 11-2d. (a) Activation time = 3 ms, activation amplitude = 23%. (b) Activation time = 300 ms, activation amplitude = 9%. The annotations are described in the text.

Influence of the collision regime on the observed reaction channels

Entropy-favored noncovalent dissociation

Figures 11-1 to 11-3 all show that a fast activation regime favors the noncovalent dissociation channel compared to the neutral base loss, which is the major competing covalent fragmentation channel. Typical $k(E)$ curves reflecting the observed situation are shown in Figure 11-5. The fact that the relative proportion of noncovalent dissociation and neutral base loss varies with the collision regime indicates that the activation entropy of these two channels is different. Indeed, the $k(E)$ curves can cross only if the steepness of the curves is different, and it is the activation entropy that is responsible for the steepness of the curve. As previously reported[8], the transition state for base loss is tight; it involves a complex rearrangement mechanism. This is an entropy-disfavored process: the rate constant for base loss increases less steeply with

internal energy than the rate constant of an entropy-favored process. Noncovalent dissociation is however a highly entropy-favored process. No complex rearrangements with constrained conformations are involved. As a matter of fact, the gain in conformational freedom is enormous, especially for complexes with a large interaction interface like in the present case (see Chapter 13). The rate constant therefore raises much more steeply with internal energy.

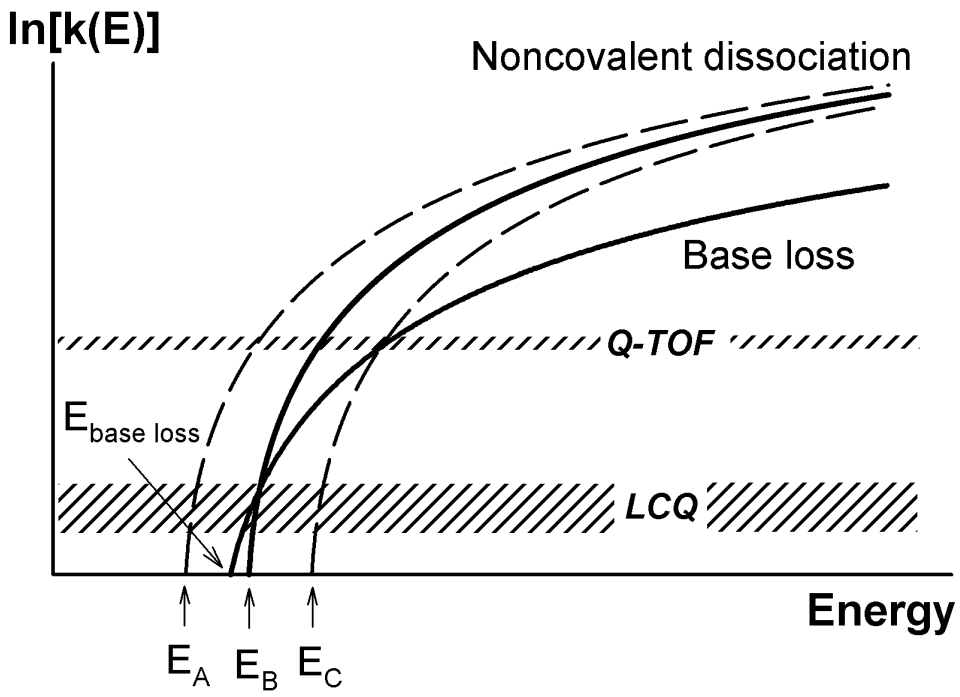

Figure 11-5. Scheme depicting the internal energy dependence of global rate constants for neutral base loss and noncovalent dissociation. Base loss (a rearrangement) has a low energy threshold, but the rate constant increases less steeply with the energy. Noncovalent dissociation reactions have increasing thresholds from duplex **A** to **C**, and are entropy-favored processes: the rate constant increases more steeply with energy. In the LCQ (slow activation), the reaction times are varied from 3 ms to 300 ms, and the observed rate constants are small. In the Q-TOF2 (fast activation), the reaction time is in the microsecond range and more energy is required to obtain larger rate constants. The kinetic shift is larger for fast heating conditions.

Kinetic shift effect

The critical energy E_0 for the noncovalent dissociation assumed to depend on the strength of the intermolecular interactions. The experimental threshold for the observation of the dissociation increases with the number of hydrogen bonds in the duplex[4,5,9] (see Chapter 12). The larger the number of GC base pairs (and hence the number of hydrogen bonds between the strands), the higher the collision energy necessary to reach noncovalent dissociation. For duplexes **A**, **B** and **C**, the $k(E)$ curves are assumed to be parallel, as the dissociation mechanisms are likely to be the same.

When low threshold, entropy-disfavored processes are in competition with entropy-favored processes, it can happen that the respective $k(E)$ curves cross at a given energy. In a typical energy-dependent MS/MS experiment, the reaction time is fixed, and the internal energy is increased progressively. This corresponds to a movement from left to right on a horizontal line in Figure 11-5. The order of appearance of the different dissociation channels depends on the order in which the $k(E)$ curves are crossed by that horizontal line. In the case of an infinitely long reaction time, the order of occurrence of the reactions when increasing the energy would depend only on the critical energy E_0, (no kinetic shift). As the time allowed for reaction diminishes, the kinetic shift increases: the apparent threshold is higher than the true threshold E_0 and the order of appearance of the different reaction channels can change.

In the LCQ, three different reaction times were studied, from 3 to 300 ms. In such slow activation conditions, the internal energy rises by small increments, and slow processes are observed (see parts (c) and (d) in Figures 11-1 to 11-3). For duplex **A**, the apparent threshold for noncovalent dissociation is low and this is the main channel observed. For duplex **B**, the apparent thresholds for base loss and noncovalent dissociation must be close, and both channels are almost equally important. For duplex **C** (100% of GC base pairs), the rate constant for base loss is highly favored due to its lower apparent threshold. For the duplex **C**, the only way to obtain significant amounts of single strands is to perform MS/MS in a quadrupole (Fig. 11-3a). This illustrates that for very strong complexes, it can be very difficult to find suitable experimental conditions to observe only the noncovalent dissociation channel.

In the Q-TOF2 instrument, the internal energy uptake per collision is higher than in the slow activation conditions of the LCQ, and the reaction time is in the order of the microsecond time scale. The kinetic shift is therefore higher than in the LCQ. This faster activation regime favors the noncovalent dissociation channels (see Figure 11-5). Competition between base loss and noncovalent dissociation is also observed when

isolating $[DS\text{-}B]^{5-}$ of duplex **B** (Figure 11-4): in fast heating conditions (Fig. 11-4a) the noncovalent dissociation of [DS-B] into the single strands (one of which with a missing base) is predominant, while in slow heating conditions (Fig. 11-4b) a second base loss occurs. Type II fragments are also favored by a slow heating of $[DS\text{-}B]^{5-}$.

MS/MS on oligonucleotide complexes with drugs

To illustrate the influence of the collision regime on the appearance of the MS/MS spectra of complexes between double-stranded DNA and different drugs, we report here MS/MS experiments on the $[1{:}1]^{5-}$ complexes between duplex **B** and three drugs.

Hoechst 33258 (minor groove binder)

Figure 11-6 shows the MS/MS spectra of the complex in three different conditions: (a) on the Q-TOF2, (b) on the LCQ with activation during 3 ms and (c) on the LCQ with activation during 300 ms. MS/MS on the Q-TOF2 instrument shows the predominant noncovalent dissociation of the complex into the single strands or the single strands with a drug bound. In the LCQ, the base loss from the duplex becomes more important when the activation time increases and the activation energy decreases. Moreover, Type II fragments are present in the LCQ MS/MS spectra. This is in agreement with the report of Wan *et al*.[5] who performed MS/MS of a complex with distamycin on an LCQ instrument with the standard activation time of 30 ms. They observed the predominant covalent fragmentation of the complex (neutral base loss and formation of Type II fragments) and the minor noncovalent dissociation channel (into one nude single strand and one single strand with a drug bound).

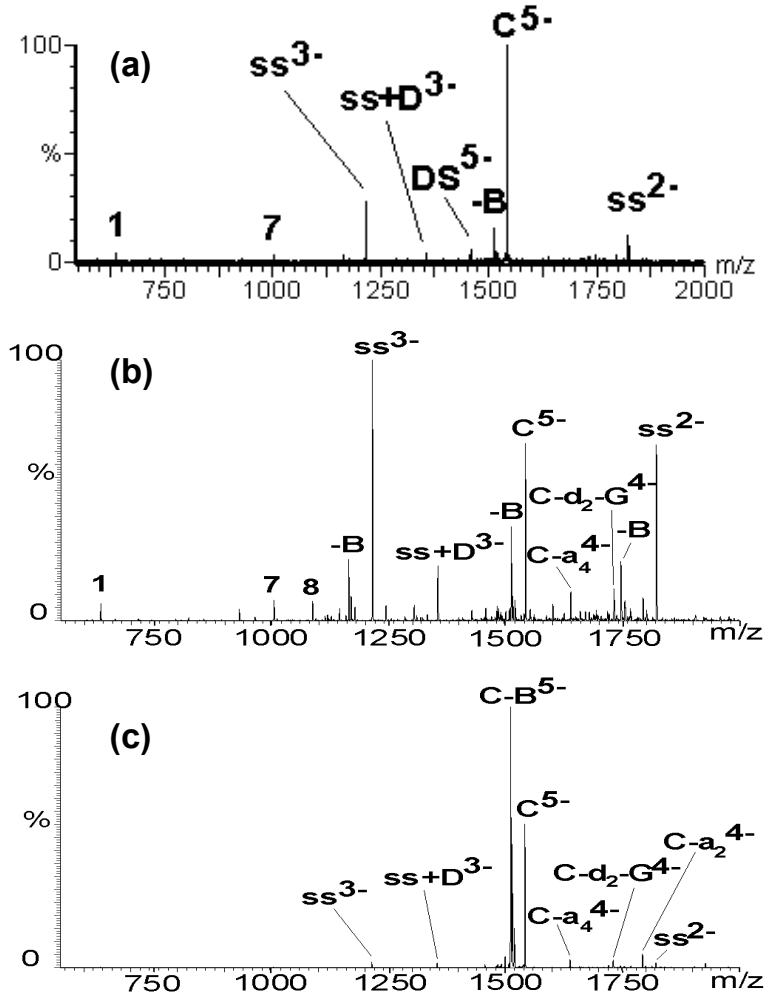

Figure 11-6. MS/MS spectra of the complex $\mathbf{C^{5-}}$ between duplex **B** and Hoechst 33258. The complex is noted **C** and the drug is noted **D**. Other conventions are the same as before. Spectra were recorded with **(a)** the Q-TOF2, collision energy = 30 eV. **(b)** the LCQ, activation time = 3 ms, activation amplitude = 23% and **(c)** the LCQ, activation time = 300 ms, activation amplitude = 9%.

Minor groove binders bridge the duplex by forming hydrogen bonds with both strands, and the threshold energy for noncovalent dissociation is higher than for the duplex. Slow heating conditions induce the terminal unzipping of the duplex (the drug is bound to the central AT sequence), the threshold for neutral base loss is reached first and covalent fragmentation occurs. In fast heating conditions, the entropy-favored noncovalent dissociation channel has a larger rate constant, which is actually observed.

Actinomycin D (intercalator with major groove binding substituents)

Figure 11-7 shows the MS/MS spectra of the complex between duplex **B** and actinomycin D at three different activation regimes. In all the spectra, the main fragmentation pathway is the noncovalent dissociation of the $[complex]^{5-}$ into the $[duplex]^{4-}$ and the negatively charged drug. The direct base loss from the complex is favored at low activation energies. At higher energies, one can observe $[DS\text{-}B]^{4-}$, which implies the loss of both the drug and a neutral base.

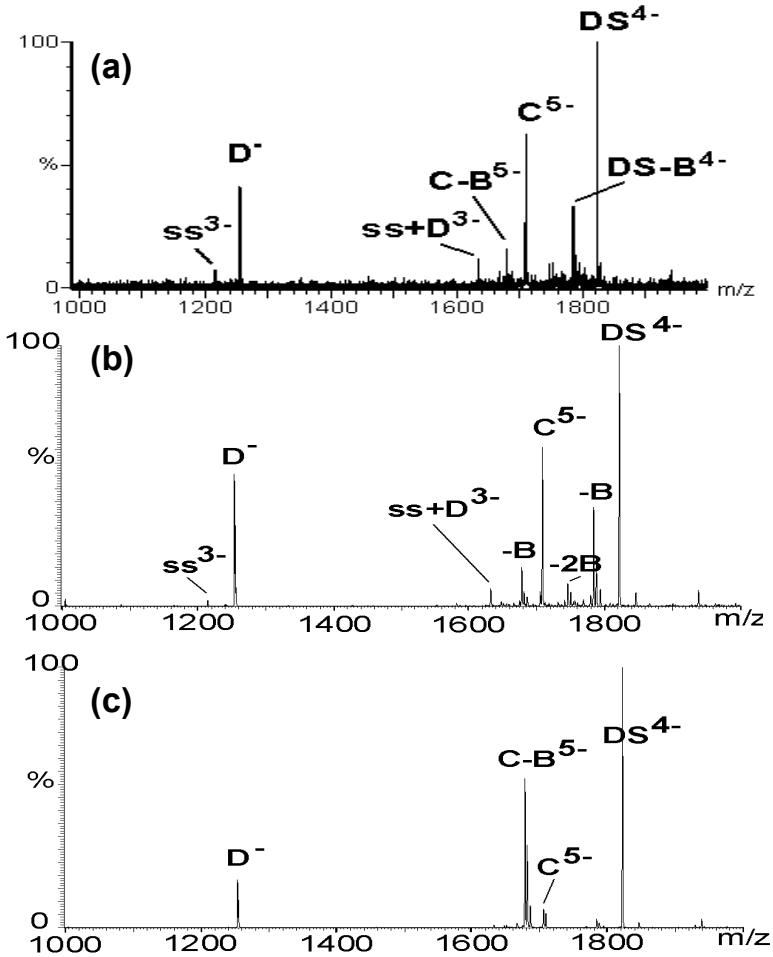

Figure 11-7. MS/MS spectra of the complex $\mathbf{C}^{5-}$ between duplex **B** and actinomycin D. The complex is noted **C** and the drug is noted **D**. Other conventions are the same as before. Spectra were recorded with **(a)** the Q-TOF2, collision energy = 30 eV. **(b)** the LCQ, activation time = 3 ms, activation amplitude = 22% and **(c)** the LCQ, activation time = 300 ms, activation amplitude = 9%.

Amsacrine (intercalator)

Figure 11-8 shows the MS/MS spectra of the complex between duplex **B** and amsacrine at different collision regimes. The complex with amsacrine is much less kinetically stable than the complex with actinomycin D. The loss of the neutral drug occurs at a lower collision energy than the loss of neutral base at all collision regimes, even after a reaction time of 10 s (Fig. 11-8c). The true threshold E_0 for the noncovalent dissociation is therefore lower than the E_0 for the base loss.

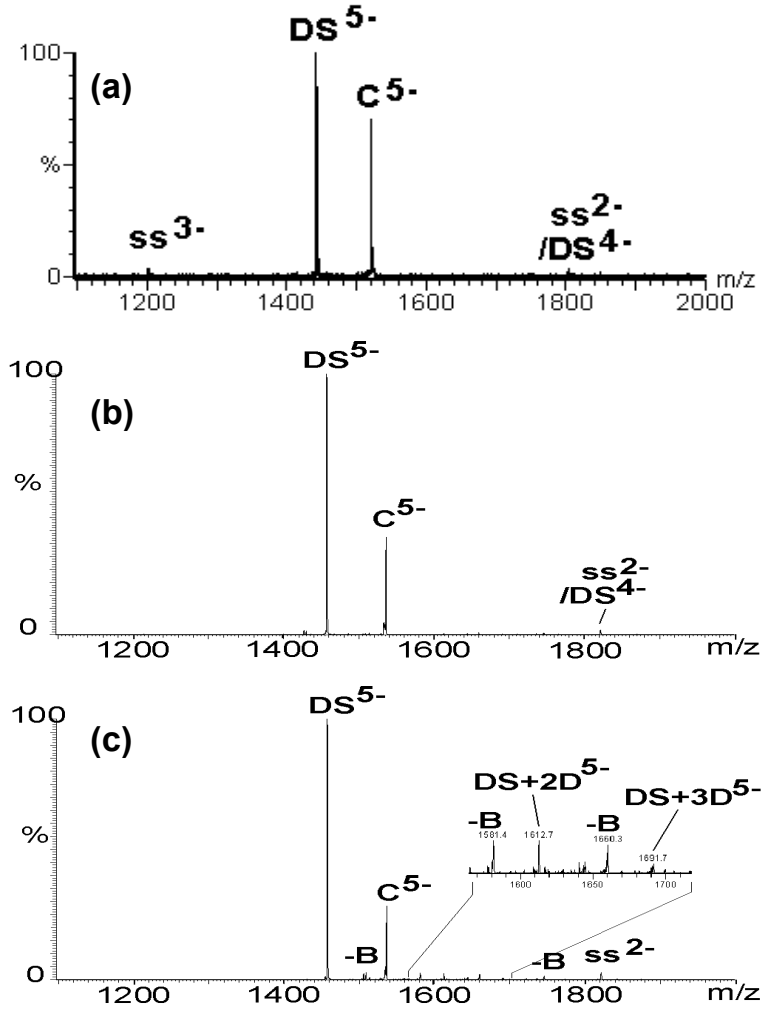

Figure 11-8. MS/MS spectra of the complex $\mathbf{C}^{5-}$ between duplex **B** and amsacrine. The complex is noted **C** and the drug is noted **D**. Other conventions are the same as before. Spectra were recorded with **(a)** the Q-TOF2, collision energy = 14 eV. **(b)** the LCQ, activation time = 3 ms, activation amplitude = 18% and **(c)** the LCQ, activation time = 10 s, activation amplitude = 6%.

An interesting phenomenon appeared in the CID of the complex at very long activation times. Small peaks appear that can be attributed unambiguously to the [duplex + 2 drugs]$^{5-}$ and the [duplex + 3 drugs]$^{5-}$ species, and to these complexes with a base lost (Fig. 11-8c). This indicates that some neutral drug is present in the trap*. It can come either from the dissociation of the [1:1] complex, or from direct leakage from the source.

Conclusions

The choice of the MS/MS experimental conditions is critical for the study of the dissociation of noncovalent complexes. The choice of the collision regime (and therefore the choice of the instrument) can have a great influence on the observed dissociation channels when some low-energy (enthalpy-driven) covalent bond cleavages can compete with the noncovalent dissociation channel. As noncovalent dissociation is an entropy-driven process, its observation can be favored by high energy, fast activation conditions.

11.3. Comparison with source-CID

We also wanted to characterize the activation regime when performing source-CID experiments. We therefore have chosen to compare the source-CID spectra of duplex **C** with the MS/MS spectra of the same duplex that were obtained with different activation times (Figure 11-3).

Figure 11-9 shows the source-CID spectrum obtained on the Q-TOF2 instrument compared to the spectrum obtained with soft source conditions. In the electrospray source of the Q-TOF instruments, the most direct way to change the amount of internal

* The neutrals are not expelled from the trap at each mass analysis cycle, but are only eliminated by pumping.

energy imparted to the ions is to change the cone voltage. The source-CID spectrum (top) shows Type I fragments and base loss from the duplex. As there is no mass selection, all single stranded and double stranded species that are present in the bottom spectrum are collisionally activated. It is therefore not very reliable to compare the respective amounts of Type I fragments between source-CID and MS/MS spectra. It is actually better to compare the relative amounts of DS^{5-} and $[DS\text{-}B]^{5-}$. The source-CID spectrum shows a relatively small amount of base loss, thereby indicating a fast activation regime, similar to the MS/MS collision regime in the quadrupole collision cell.

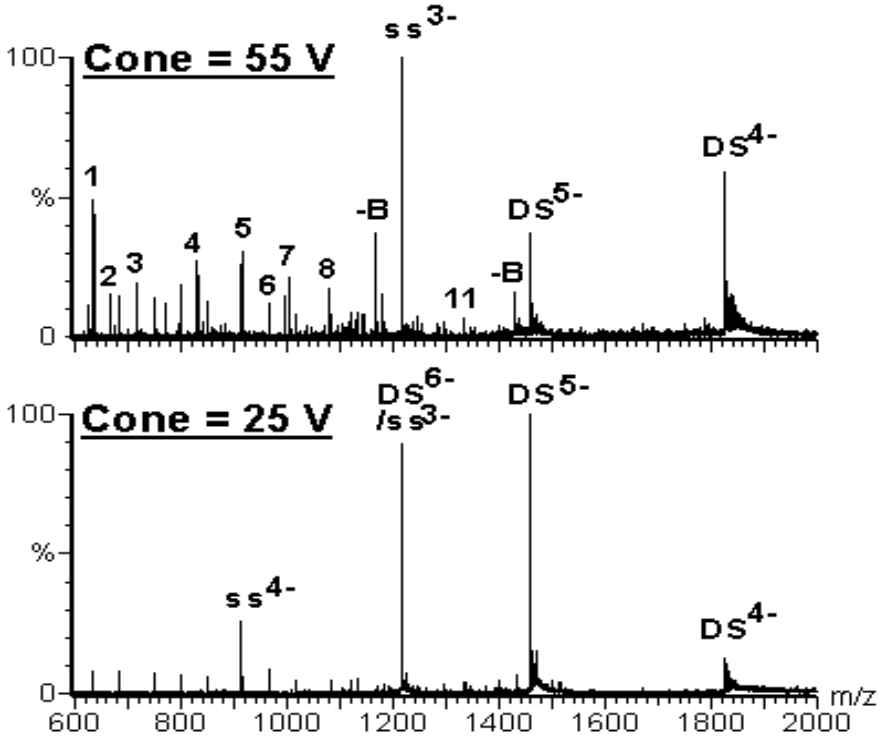

Figure 11-9. Full scan MS spectra of duplex **C** obtained with the Q-TOF2 under hard source conditions (cone voltage = 55 V) and under soft conditions (cone voltage = 25 V). In the bottom spectrum small peaks other than those corresponding to the duplex and the single strands result from undesirable contamination.

In the electrospray source of the LCQ, the amount of internal energy of the ions can be varied in three different ways. Acceleration in the capillary-skimmer region can cause collisional energy transfer and can be modulated by the capillary voltage and by the tube lens offset voltage, or the heated capillary temperature can be raised. Figure 11-

10 shows the source-CID spectra obtained by varying each one of these experimental parameters separately, compared to the spectrum obtained in soft conditions.

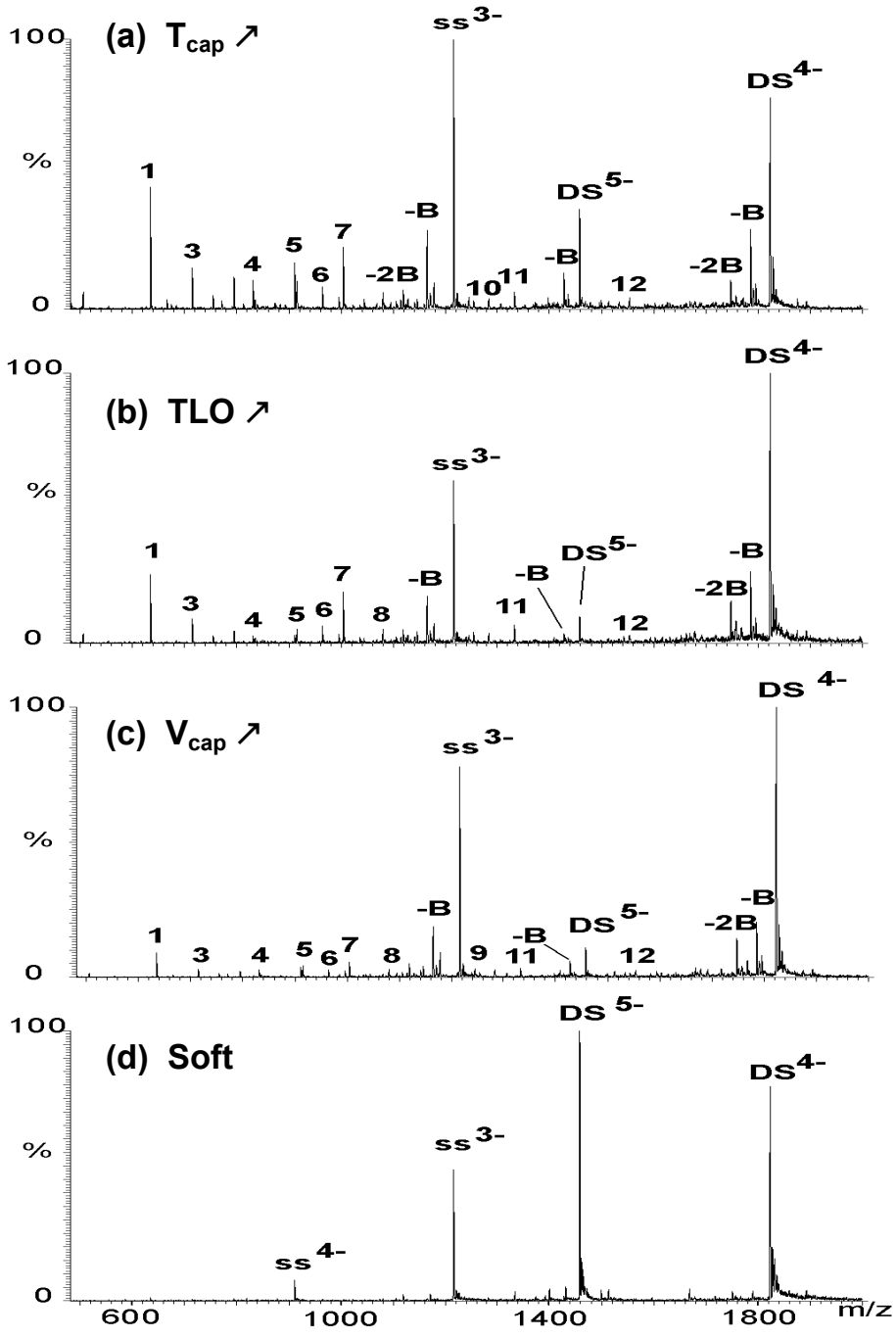

Figure 11-10. Full scan MS spectra of duplex **C** obtained with the LCQ under hard source conditions achieved in three different ways and in soft conditions. **(a)** The capillary temperature is increased to 300 °C. **(b)** The tube lens offset is decreased to –30 V. **(c)** The capillary voltage is decreased to -130 V. **(d)** The soft source conditions are: capillary temperature = 170 °C, capillary voltage = -30 V and tube lens offset = 40 V.

We can immediately see that all three source-CID spectra are very similar to each other, are similar to the source-CID spectrum obtained on the Q-TOF2, and also similar to the MS/MS spectrum obtained with fast activation conditions on the Q-TOF2. This suggests that the time scales of all these experiments are similar: the ions need a few microseconds to fragment. For source-CID, this corresponds to the time spent between the activation and the entrance into the analyzer (TOF or trap). This also implies that "heated capillary dissociation" is more comparable with source-CID (fast activation) than with BIRD (thermal, slow) activation. With a very small residence time in the heated capillary (10 μs[10]), the establishment of a rapid energy exchange regime is doubtful, and we therefore believe that the Arrhenius treatment of heated capillary dissociation data is meaningless.

References

1. S.A. McLuckey, G.J. Van Berkel, G.L. Glish; Tandem Mass Spectrometry of Small, Multiply Charged Oligonucleotides. *J. Am. Soc. Mass Spectrom.* **1992,** 3: 60.

2. S.G. Penn, F. He, M.K. Green, C.B. Lebrilla; The Use of Heated Capillary Dissociation and Collision-Induced Dissociation to Determine the Strength of Non-Covalent Bonding Interactions in Gas-Phase Peptide–Cyclodextrin Complexes. *J. Am. Soc. Mass Spectrom.* **1997,** 8: 244.

3. S.G. Penn, F. He, C.B. Lebrilla; Peptides Complexed to Cyclodextrins Fragment Rather Than Dissociate When Subjected to Blackbody Infrared Radiation. *J. Phys. Chem. B* **1998,** 102: 9119.

4. P.D. Schnier, J.S. Klassen, E.F. Strittmatter, E.R. Williams; Activation Energies for Dissociation of Double Strand Oligonucleotide Anions: Evidence for Watson-Crick Base Pairing *in vacuo*. *J. Am. Chem. Soc.* **1998,** 120: 9605.

5. K.X. Wan, T. Shibue, M.L. Gross; Gas-Phase Stability of Double-Stranded Oligodeoxynucleotide and Their Noncovalent Complexes With DNA-Binding Drugs Is Revealed by Collisional Activation in an Ion Trap. *J. Am. Soc. Mass Spectrom.* **2000,** 11: 450.

6. S.A. McLuckey, G. Vaidyanathan, S. Habibi-Goudarzi; Charged vs. Neutral Nucleobase Loss From Multiply Charged Oligonucleotide Anions. *J. Mass Spectrom.* **1995,** 30: 1222.

7. E. Nordhoff, F. Kirpekar, P. Roepstorff; Mass Spectrometry of Nucleic Acids. *Mass Spectrom. Rev.* **1996,** 15: 67.

8. J.S. Klassen, P.D. Schnier, E.R. Williams; Blackbody Infrared Radiative Dissociation of Oligonucleotide Anions. *J. Am. Soc. Mass Spectrom.* **1998,** 9: 1117.

9. J. Ding, R.J. Anderegg; Specific and Non-Specific Dimer Formation in the Electrospray Ionization Mass Spectrometry of Oligonucleotides. *J. Am. Soc. Mass Spectrom.* **1995,** 6: 159.

10. F. He, J. Ramirez, B.A. Garcia, C.B. Lebrilla; Differentially Heated Capillary for Thermal Dissociation of Noncovalently Bound Complexes Produced by Electrospray Ionization. *Int. J. Mass Spectrom.* **1999,** 182/183: 261.

12.

INTERACTIONS THAT ARE CONSERVED IN THE GAS PHASE

12.1. Introduction

On the basis of the discussions of Chapters 10 and 11, our study of the noncovalent interactions in the gas phase is based on the following principles:

(1) The dissociation of the complexes is studied in fast activation conditions (source-CID on any instrument, or MS/MS on the Q-TOF) to favor the noncovalent dissociation channel.

(2) Only series of complexes of the same masses and same structures were compared. This is the best way to ensure that their relative internal energy is proportional to the laboratory kinetic energy of the complexes. For this reason, we can report the dissociation efficiency as a function of the instrumental parameters (cone voltage, capillary temperature, collision energy given by the instrument,…).

(3) This also ensures that there is no degree-of-freedom effect on the unimolecular rate constants (k_{uni} in the Lindemann-Hinshelwood mechanism (3.3)).

(4) Finally, we will compare only the same dissociation channels for the complexes, and assume that the dissociation mechanisms are identical. In other words, we assume that the activation entropies are the same.

In these conditions, we can reasonably assume that the relative fragmentation efficiencies do reflect the relative activation energies of the unimolecular dissociation of the complexes.

12.2. Hydrogen bonding in duplex DNA

In order to investigate the lone contribution of hydrogen bonding to the gas phase kinetic stability of the DNA double helix, we performed source-CID experiments on the LCQ instrument on a series of 16-mer duplexes with variable percentages of GC base pairs (varying number of H-bonds). Symmetrical base sequences were chosen to avoid the formation of homodimers, and to minimize mismatches in base pairing. Table 12-1 summarizes the sequences of the studied duplexes, and the main results. As base stacking effects on stability are smaller than hydrogen bonding effects, their influence will be hidden in this series of comparisons. Moreover, all the duplexes have the same purine/pyrimidine sequence (adenines are replaced by guanines, and thymines are replaced by cytosines), and only 4 bases have been changed at a time.

Table 12-1. Summary of the study of the hydrogen bonding in duplex DNA: base sequences, GC percentage, measured values of T_m (temperature of half-denaturation in solution in 50 mM NH_4OAc) and V_m (voltage of half-fragmentation in source-CID experiments) at two different capillary temperatures T_{cap}.

	Base sequence[(a)]	% G≡C	T_m (°C)	V_m (V) (T_{cap} = 160°C)	V_m (V) (T_{cap} = 180°C)
1	AAATTATAATATTAAA	0	34	32	-
2	GGATTATAATATTAGG	25	43	60	37
3	GGGCTATAATATCGGG	50	54	80	65
4	GGGCCGTAATGCCGGG	75	64.5	118	91
5	GGGCCGCGGCGCCGGG	100	76	-	> 105

(a) only the sequence of strand A (5'-3') is indicated. Strand B is the complementary of strand A.

Figure 12-1 shows the solution thermal denaturation experiments on duplexes **1-5**, containing different percentages of GC base pairs. In solution, a temperature increase induces the denaturation of the duplex, which manifests itself in a hyperchromism measured by UV-spectrophotometry (single strands have a higher extinction coefficient ε than the duplex). The melting temperature T_m is defined as the temperature at which half of the duplex is denatured, or melted. The higher the melting temperature, the greater the stability of the duplex in the solution.

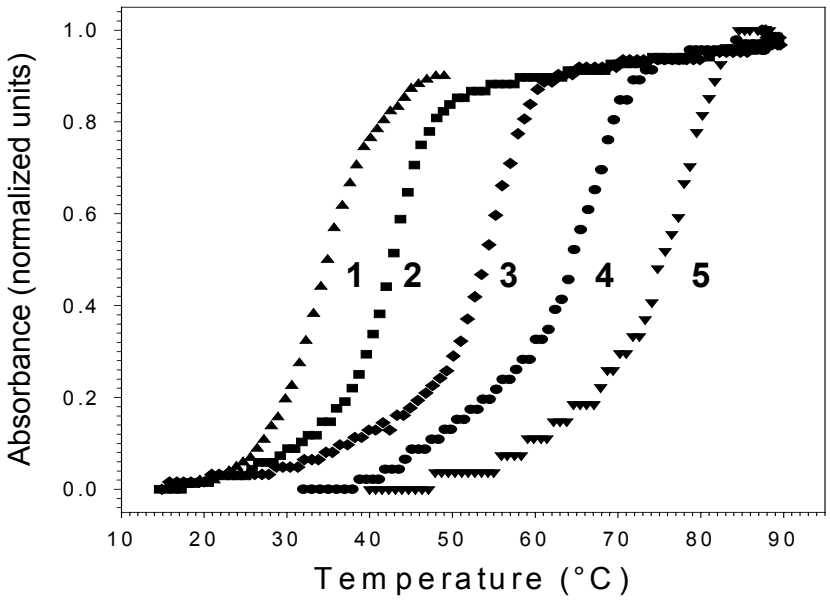

Figure 12-1. Thermal denaturation curves of duplexes **1-5** in solution (NH_4OAc 50 mM) measured by UV-spectrophotometry. The absorbance ranges have been scaled from 0 to 1 (arbitrary units) for all duplexes.

Figure 12-2 shows the evolution of the percentage of $[duplex]^{6-}$ in the spectra as a function of the capillary voltage V_{CS}, for duplexes **1-4**, at two different capillary temperatures. These four duplex species are dissociating into their constitutive triply charged single strands exclusively. The percentage of duplex in each mass spectrum was calculated with equation (12.1).

$$\%Duplex = \frac{I_{Dup^{6-}}}{I_{Dup^{6-}} + \frac{I_{A^{3-}} + I_{B^{3-}}}{2}} \cdot 100\% \qquad (12.1)$$

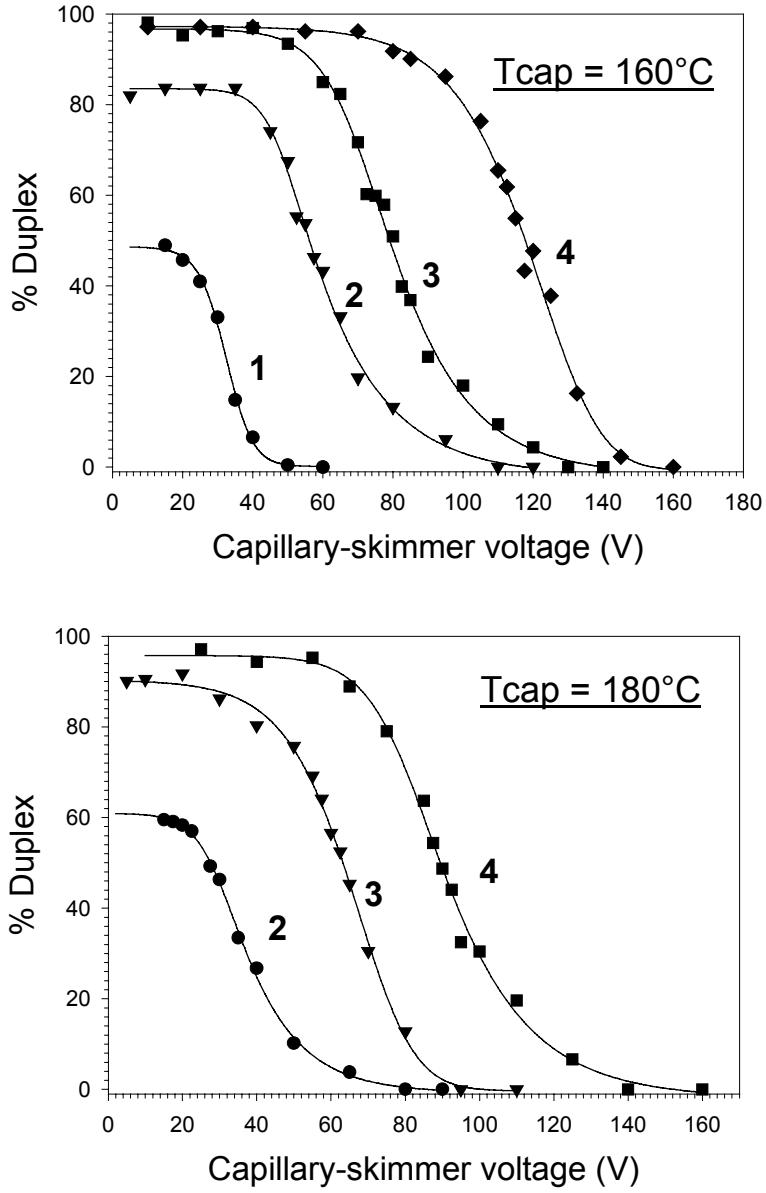

Figure 12-2. Source-CID experiments on duplexes **1-4**, at two capillary temperatures (160°C and 180°C). The duplex percentage was calculated using equation (12.1) for each spectrum recorded at a different capillary-skimmer voltage (or V_{CS}).

No major covalent fragmentation is observed for duplexes **1-4**. In the case of the duplex **5** with 100% GC, extensive breaking of covalent bonds occurs before breaking of all the hydrogen bonds. Resulting spectra are highly noisy, and sequence-informative fragments can not be sorted out. That is why no dissociation curve for that particular duplex is shown.

Figure 12-2 clearly shows that the gas phase kinetic stability of a duplex is dramatically dependent on the number of hydrogen bonds between the two strands. By analogy with the melting temperature T_m, we can define the melting voltage V_m as the voltage at which half of the duplex is fragmented. The V_m values obtained are also summarized in Table 12-1. Similar approaches have already been described for source-CID[1] (V_m was called Vc_{50}), or MS/MS[2,3] (the collision energy of half fragmentation was called E_{50} or $E_{1/2}$).

It can be seen in Figure 12-2 that at capillary voltages below 30 V, a kind of plateau is reached. We believe that, although the capillary voltage is set by the software to a value between 0 and 30 V, the actual acceleration in the capillary-skimmer region of the source remains equivalent to that achieved at a capillary voltage of about 30 V. This phenomenon is not uncommon and has been noticed also on other sources[4]. On the Q-TOF2 the same happens for cone voltages below 10 V, due to source design.

Figure 12-3 summarizes the V_m values that have been obtained for duplexes **1-5** at different capillary temperatures. If more internal energy is already given by thermal heating in the capillary, less is remaining to be added by acceleration in order to achieve 50% of fragmentation. The linear relationship between T and V indicates that the two activation methods are equivalent: increasing V_{CS} by 10 V has the same effect as increasing the capillary temperature by about 10 °C. Changing the capillary temperature just shifts the internal energy range available when varying the V_{CS} from the minimum to the maximum value (0 to 135 V). When the ions undergo collisional activation in the capillary-skimmer region, they have a memory of the thermal energy they received in the capillary, and this is reflected in the rate constant.

The variation of activation energy as a function of the number of hydrogen bonds between DNA strands has already been studied by BIRD[5] and by MS/MS[3]. The phenomenological trend is confirmed by this source-CID study on duplexes **1-4**: the activation barrier E_0 depends on the percentage of GC base pairs in the DNA strands. This parallels the stability scale in solution, where T_m strongly depends on the number of hydrogen bonds between the strands.

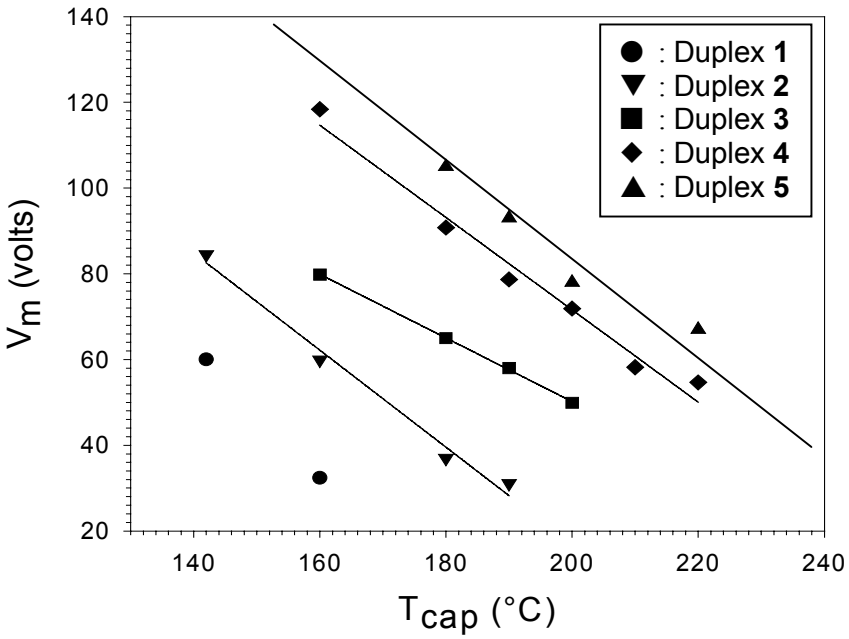

Figure 12-3. Voltages of half-fragmentation (V_m) for duplexes **1-4** at different capillary temperatures T_{cap}. For duplex **5**, the points represent the onset of the covalent bond fragmentation. These (V_m,T_{cap}) values can be considered as the upper limit for the source-CID method to be applicable.

12.3. Base stacking in duplex DNA

Base stacking interactions in solution translate into a sequence-dependent stability of oligonucleotide duplexes. We used the nearest-neighbor tables given by Sugimoto *et al*.[6] to calculate the duplex melting enthalpy ($\Delta H_{n\text{-}n}$) that will be correlated with the gas-phase kinetic stability measured by MS/MS. In order to study the effect of this type of interaction independently, we compared the behavior of a series of 16-mer duplexes, all with the same amount of GC base pairs, but with different base sequences. The MS/MS experiments were performed on a Q-TOF2. The kinetic stability has been measured for duplexes 6- and 7-. For all duplexes the tendency was the same with the two charge states.

The percentage of surviving $[duplex]^{6-}$ is determined by using equation (12.1) and is plotted against the collision energy in Figures 12-4 to 12-6, for duplexes containing different percentages of GC base pairs.

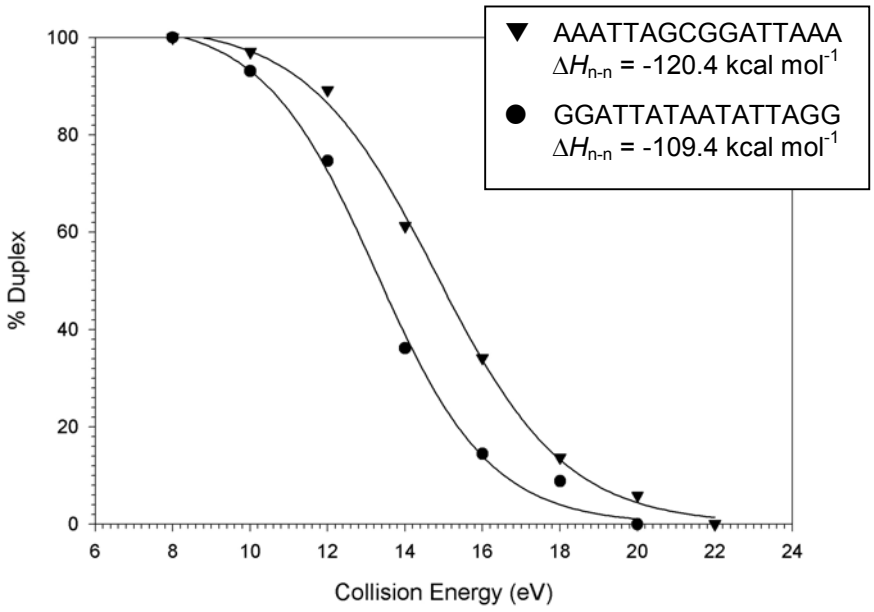

Figure 12-4. Dissociation curves for two duplexes containing 25% of GC base pairs. The % Duplex is calculated using equation (12.1) for each collision energy. The cone voltage was set to 20 V. The base sequence of one of the strands is given (5'-3'). The other one is the complementary. The corresponding solution melting enthalpies are given in the inset.

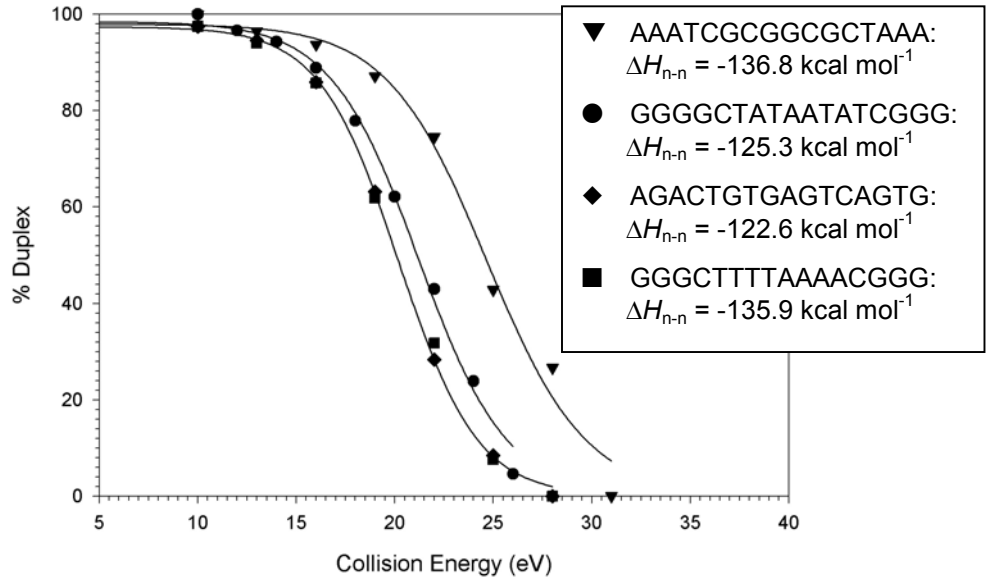

Figure 12-5. Dissociation curves for four duplexes containing 50% of GC base pairs. The % Duplex is calculated using equation (12-1) for each collision energy. The cone voltage was set to 20 V. The base sequence of one of the strands is given (5'-3'). The other one is the complementary. The corresponding solution melting enthalpies are given in the inset.

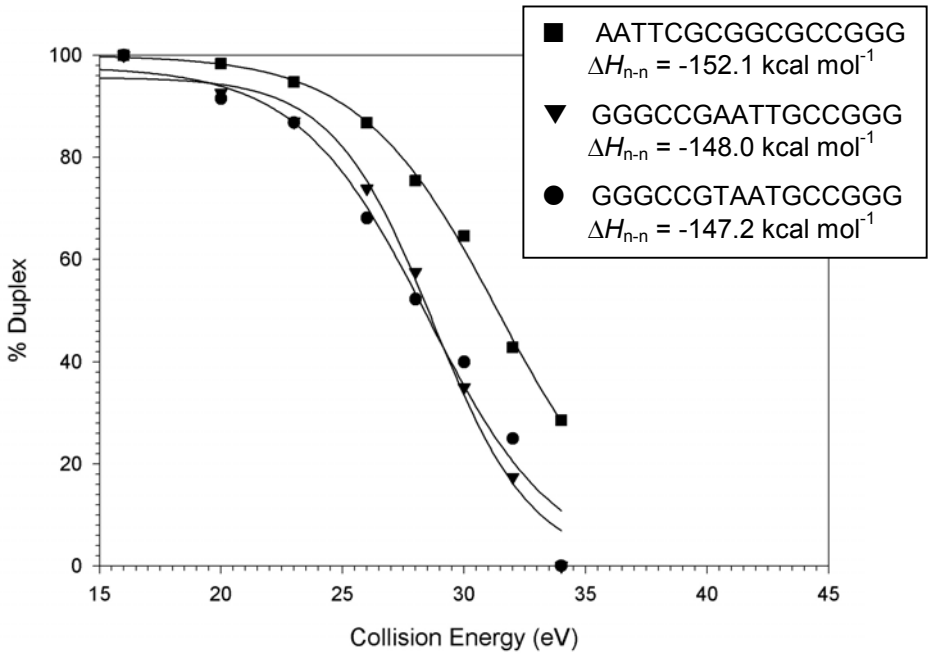

Figure 12-6. Dissociation curves for three duplexes containing 75% of GC base pairs. The % Duplex is calculated using equation (12-1) for each collision energy. The cone voltage was set to 20 V. The base sequence of one of the strands is given (5'-3'). The other one is the complementary. The corresponding solution melting enthalpies are given in the inset.

Figure 12-4 displays the results obtained for the two duplexes with 25% of GC base pairs. There is a marked difference in their gas-phase kinetic stabilities that parallels their respective stabilities in solution.

Figure 12-5 gathers the results for four duplexes with 50% GC. For the first three duplexes the gas-phase stabilities also parallel those calculated by nearest-neighbor models. Only duplex 50%-4 (sequence d(GGGCTTTTAAAACGGG)) does not obey this rule. This exception can be explained by the fact that, in solution, A-tract sequences cause significant curvature of the B-DNA structure that is locally distorted[7-10]. The nearest-neighbor models, that are applicable to B-DNA only, are therefore not appropriate to calculate the solution-phase stability of these special structures that are less stable than if they were B-DNA's. The lower gas-phase kinetic stability observed for this duplex may indicate that this distorted structure is conserved in the gas phase.

For the three duplexes with 75% GC base pairs (Figure 12-6), the correlation between the solution and gas-phase stabilities is also qualitatively excellent, but two of the curves are crossing. It must be noted that for this high GC percentage, there is a significant amount of base loss. Therefore the %Duplex calculated using equation (12.1) is approximate for collision energies equal or higher than 30 eV.

12.4. Drug-DNA interactions

MS/MS

We studied the interaction between the two minor groove binders (netropsin and Hoechst 33258) and the duplex d(GGGGATATGGGG)•d(CCCCATATCCCC). The duplex is noted **GC** (**G** is the guanine-rich strand and **C** is the cytosine-rich strand) The MS/MS experiments were performed with a Q-TOF (first generation). The 5- charge state was chosen for the MS/MS experiments. For the $[duplex]^{5-}$, the single strands start to appear at a collision energy of 25 eV. For the complexes, at 25 eV, no fragment could be detected yet. The collision energy had to be raised to about 30 eV* to see the fragments. The results are shown in Figure 12-7.

The CID of the complexes shows a different behavior from drug to drug. The complex $[GC+Hoechst]^{5-}$ dissociates into the duplex and the single strands, with release of the neutral drug. The complex with netropsin $[GC+Net]^{5-}$, however, dissociates at the same collision energy into the single strands with the netropsin drug remaining attached selectively on strand **G**. Hoechst 33258 can loose a proton and leave the $complex^{5-}$ as a neutral. Netropsin, however, is a carbocationic species which has to remain attached to the negatively charged DNA strands. The fact that netropsin remains attached exclusively onto strand **G** indicates that the interactions with that strand are greater than with strand **C**.

---

* For practical reasons, the collision energy for the MS/MS of the complexes is not well defined. One should therefore not look close at the relative intensities in Figure 12-7. More precise gas-phase kinetic stabilities will be measured by source-CID (see below).

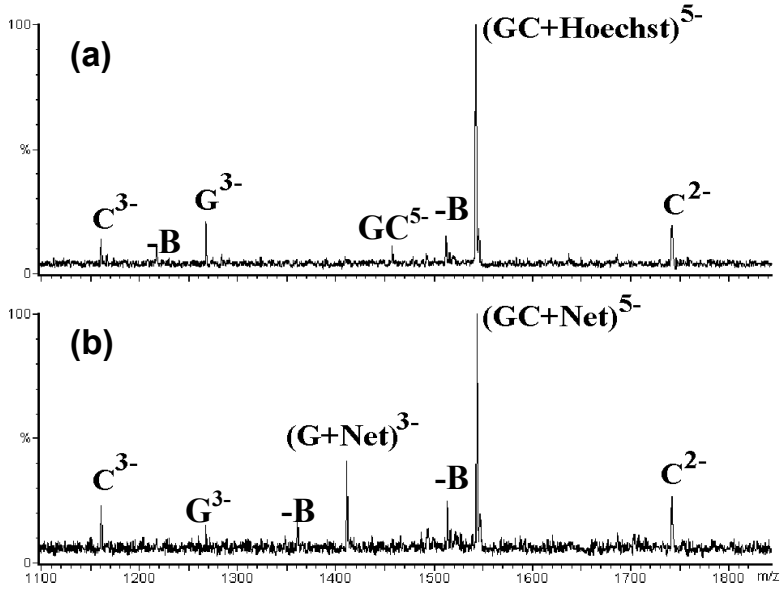

Figure 12-7. MS/MS spectra on **(a)** [duplex + Hoechst]$^{5-}$ and **(b)** [duplex + netropsin]$^{5-}$, both recorded at about 30 eV collision energy.

Source-CID

The source-CID experiments were performed on the LCQ by varying the capillary voltage. The relative intensities measured for the duplex^{5-} and the complexes^{5-} are nearly 100% at capillary voltages < 20 V. The charge state 5- has been chosen because the relative intensity of these peaks varies from 100% to 0% when varying the acceleration voltage from 0 to -135 V. The heated capillary temperature was set at 190 °C. As previously noted for MS/MS experiments on the same complexes, the nature of the fragments differs with the drug, netropsin remaining attached on strand **G**.

Source-CID results for the duplex^{5-} and complex^{5-} species are summarized in Figure 12-8 in such a way that the visual comparison with the solution thermal denaturation curves (Figure 9-2) is made easier. The percentage of relative intensity (RI) of the parent ion (duplex or complex) is calculated as follows:

$$RI(\%) = \frac{I(parent^{5-})}{I(parent^{5-}) + \frac{\sum I(strands)}{2}} \cdot 100\% \qquad (12.2)$$

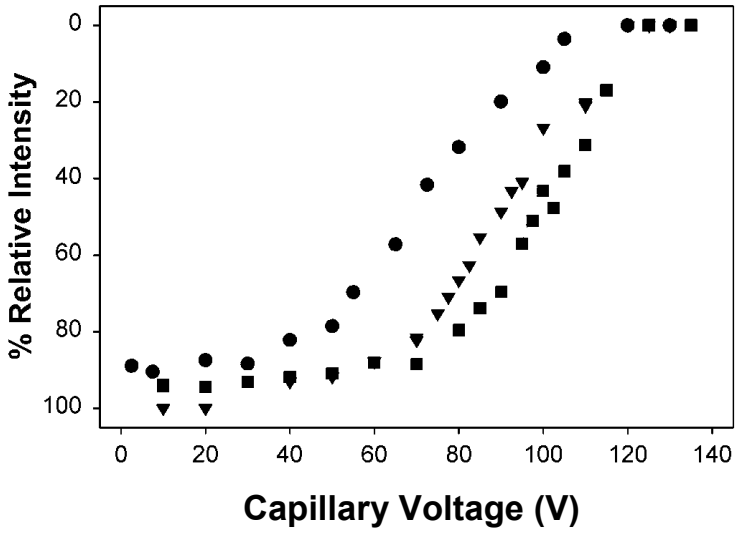

Figure 12-8. Gas phase dissociation curves obtained by mass spectrometry for the duplex GC^{5-} (●) and for the complexes $[GC+Hoechst]^{5-}$ (▼) and $[GC+Netropsin]^{5-}$ (■). The $\vec{y}$ axis is scaled from 100 to 0 to make easier a visual comparison with Figure 9-2.

Correlation with thermal denaturation and crystallographic data

The magnitude of the collision energy needed to fragment the $[GC+drug]^{5-}$ complexes reveals that they are more stable than the duplex alone. The magnitude of the difference in V_m can not be accounted for by the mass difference between the duplex and the complexes. This parallels the feature, well-known in the solution phase, that minor groove binders stabilize the double helix structure by forming hydrogen and Van der Waals bonds with both strands[11,12].

Moreover, the complex with netropsin was found to be more kinetically stable in the gas phase than the complex with Hoechst 33258. As the two complexes have the same mass and a similar structure, we can assume that the activation barrier for the dissociation is higher for the complex with netropsin. The curves of Figures 12-8 and 9-2 are strikingly similar, and although the nature of the experiments is fundamentally

different, the gas-phase dissociation curves parallels the solution-phase thermal denaturation curve. The T_m and V_m values are reported in Table 12-2.

Table 12-2. Denaturation temperatures (T_m) and denaturation voltages (V_m) for the duplex GC and the complexes with the minor groove binders.

	T_m (°C)	V_m (V)
Duplex	48.2	68
Duplex + Hoechst 33258	58.5	89
Duplex + netropsin	60.5	99

In solution, the forces that are involved in the molecular recognition of the ATAT central sequence by the minor groove binders are electrostatic interactions, hydrogen bonding with both strands, and van der Waals interactions with the edges of the minor groove[13]. Crystallographic structures of the complexes between the self-complementary dodecamer d(CGCGATATCGCG)$_2$ and netropsin[14] or Hoechst[15] have been published and hydrogen bond lengths have been calculated (Figure 12-9).

Hoechst forms three NH···O or NH···N hydrogen bonds (of which one is short: 2.9 Å) plus one weak CH_2···O interaction with the duplex. In contrast, netropsin has four NH···O or NH···N hydrogen bonds with the duplex, of which one is very short (2.6 Å). This simple count of the hydrogen bonds in the crystallographic structure of an analog dodecamer with the same binding region (ATAT) provides an explanation for the relative stabilities of the two complexes: complex with netropsin is more stable than complex with Hoechst because it forms more hydrogen bonds with the duplex. Our ES-MS measurements indicate that the stability scale is the same in the gas phase, and on this basis the hydrogen bonding interactions are thus believed to be conserved.

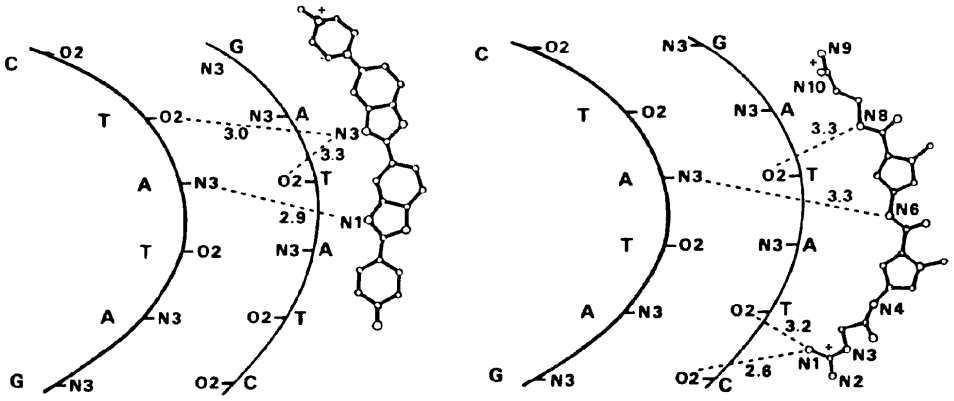

Figure 12-9. Drawings illustrating the interactions between Hoechst 33258 (left) and netropsin (right) with the self-complementary d(CGCGATATCGCG)$_2$ dodecamer. The hydrogen bonding interactions between the drug and the dodecamers are shown by dotted lines and the bond distances are given in Angströms. (Crystallographic data reproduced from references 14 and 15)

Complexes with cryptolepine and neocryptolepine

We saw in Chapter 8 that the relative intensities of the complexes with cryptolepine and neocryptolepine in the full scan MS spectra were proportional to their affinity in solution. We then performed MS/MS experiments on the Q-TOF2 on the $[1:1]^{5-}$ complexes with duplex **B**. Figure 12-10 shows the spectra obtained for both complexes at the same collision energy (10 eV). The neutral drug is lost to give back the intact duplex^{5-}. The complex with neocryptolepine fragments much faster than the complex with cryptolepine. These results undoubtedly indicate that in the complexes produced by electrospray, the drug is still intercalated in the DNA. If the complex was a simple nonspecific electrostatic adduct, the energy dependence of the dissociation would be the same. In the present case, the difference in gas phase stability must be due to stacking interactions, which seem stronger when the N^+–CH_3 group is on the opposite side of the ring compared to the N–H group of the indoloquinoline ring.

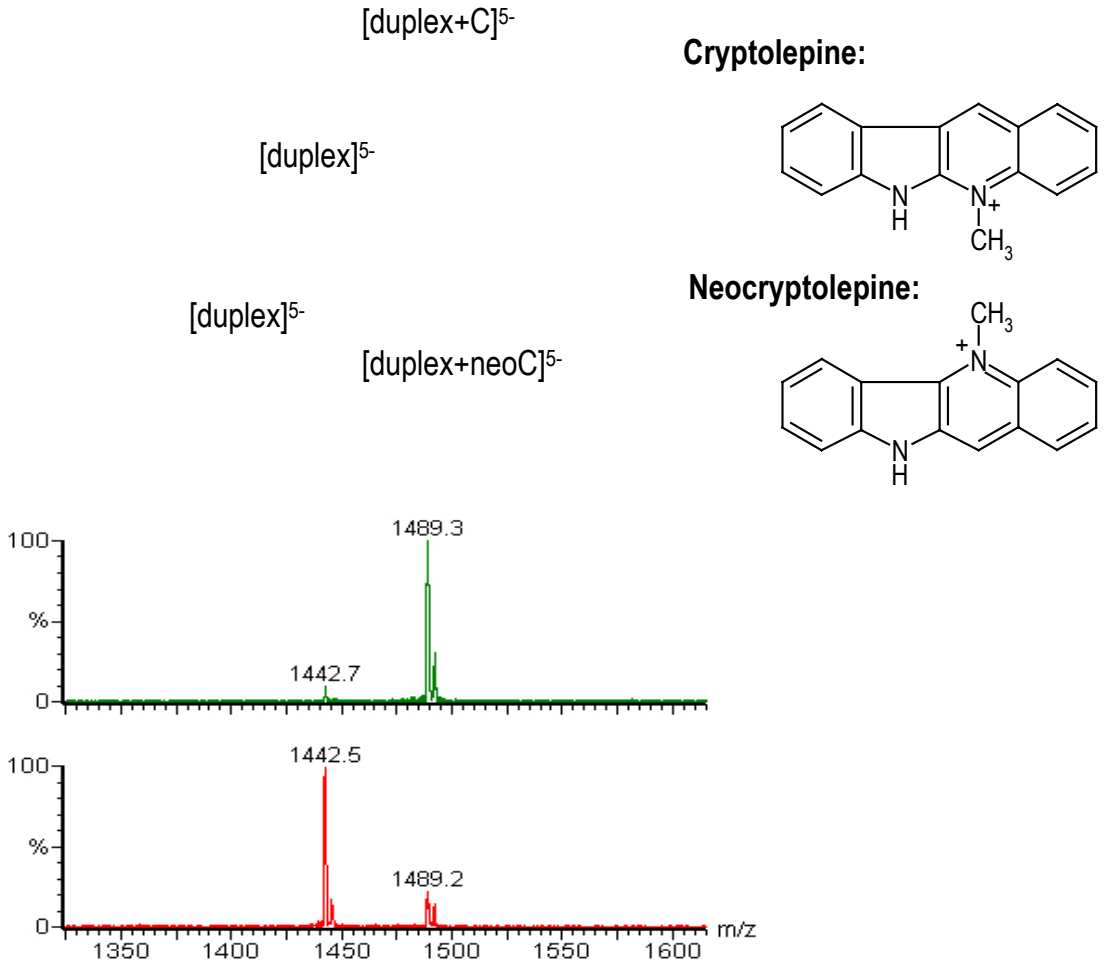

Figure 12-10. MS/MS spectra of the complex (m/z = 1489.2) with the two drugs at the same collision energy (10 eV): the resulting fragment is the duplex (m/z = 1442.5). The complex with neocryptolepine is less kinetically stable than the complex with cryptolepine.

12.5. Conclusions

The results on the gas-phase kinetic stability of duplex DNA clearly suggest that hydrogen bonding and base stacking interactions are conserved in the gas phase. Base stacking interactions are short-range and very conformation-dependent. We therefore believe that the double helix conformation must not be perturbed during the electrospray transfer process in order for these interactions to be kept in the gas phase.

Hydrogen bonding interactions also seem to be conserved in the case of the complexes with minor groove binders.

The case of complexes with intercalators is particularly interesting. In solution, the main driving force for the complexation is the hydrophobic transfer of the drug to the DNA interior. This kind of force becomes meaningless in the gas phase. However, the complexes can still be observed, and the kinetic stability scale in the gas-phase parallels the stability scale in solution. This implies that interactions other than hydrophobicity (electrostatic and Van der Waals interactions) are responsible for the difference in affinity of these complexes, both in solution and in the gas-phase. The MS/MS experiments are therefore a unique way to measure the sole contribution of the DNA-drug interactions in the absence of the effect of the solvent.

References

1. H. Rogniaux, A. Van Dorsselaer, P. Barth, J.F. Biellmann, J. Brabanton, M. van Zandt, B. Chevrier, E. Howard, A. Mitschler, N. Potier, L. Urzhumtseva, D. Moras, A. Podjarny; Binding of Aldose Reductase Inhibitors: Correlation of Crystallographic and Mass Spectrometric Studies. *J. Am. Soc. Mass Spectrom.* **1999,** 10: 635.

2. J. Gao, Q. Wu, J.D. Carbeck, Q.P. Lei, R.D. Smith, G.M. Whitesides; Probing the Energetics of Dissociation of Carbonic Anhydrase-Ligand Complexes in the Gas Phase. *Biophys. J.* **1999,** 76: 3253.

3. K.X. Wan, T. Shibue, M.L. Gross; Gas-Phase Stability of Double-Stranded Oligodeoxynucleotide and Their Noncovalent Complexes With DNA-Binding Drugs Is Revealed by Collisional Activation in an Ion Trap. *J. Am. Soc. Mass Spectrom.* **2000,** 11: 450.

4. L. Drahos, R.M.A. Heeren, C. Collette, E. De Pauw, K. Vékey; Thermal Energy Distributions Observed in Electrospray Ionization. *J. Mass Spectrom.* **1999,** 34: 1373.

5. P.D. Schnier, J.S. Klassen, E.F. Strittmatter, E.R. Williams; Activation Energies for Dissociation of Double Strand Oligonucleotide Anions: Evidence for Watson-Crick Base Pairing *in vacuo*. *J. Am. Chem. Soc.* **1998,** 120: 9605.

6. N. Sugimoto, S.-I. Nakano, M. Yoneyama, K.-I. Honda; Improved Thermodynamic Parameters and Helix Initiation Factor to Predict Stability of DNA Duplex. *Nucl. Acid. Res.* **1996,** 24: 4501.

7. D. MacDonald, K. Herbert, X. Zhang, T. Polgruto, P. Lu; Solution Structure of an A-Tract DNA Bend. *J. Mol. Biol.* **2001,** 306: 1081.

8. D. Strahs, T. Schlick; A-Tract Bending: Insights into Experimental Structures by Computational Models. *J. Mol. Biol.* **2000,** 301: 643.

9. R.P. Ojha, M.M. Dhingra, M.H. Sarma, M. Shibata, M. Farrar, C.J. Turner, R.H. Sarma; DNA Bending and Sequence-Dependent Backbone Conformation NMR and Computer Experiments. *Eur. J. Biochem.* **1999,** 265: 35.

10. M.A. Young, J. Srinivasan, I. Goljer, S. Kumar, D.L. Beveridge, P.H. Bolton; Structure Determination and Analysis of Local Bending in an A-Tract DNA Duplex: Comparison of Results From Crystallography, NMR, and Molecular Dynamics Simulation on $d(CGCAAAAATGCG)_2$. *Methods Enzymol.* **1995,** 261: 121.

11. B.H. Geierstranger, D.E. Wemmer; Complexes of the Minor Groove of DNA. *Annu. Rev. Biomol. Struct.* **1995,** 24: 463.

12. J. Pindur, G. Fischer; DNA Complexing Minor Groove-Binding Ligands: Perspective in Antitumour and Antimicrobial Drug Design. *Curr. Med. Chem.* **1996,** 3: 379.

13. M.L. Kopka, C. Yiin, D. Goodsell, P. Pjura, R.E. Dickerson; The Molecular Origin of DNA-Drug Specificity in Netropsin and Distamycin. *Proc. Natl. Acad. Sci. USA* **1985,** 1376.

14. M. Coll, J. Aymani, G.A. Van der Marel, J.H. Van Boom, A. Rich, A.H.J. Wang; Molecular Structure of the Netropsin–$d(CGCGATATCGCG)_2$ Complex: DNA Conformation in an Alternating AT Segment. *Biochemistry* **1989,** 28: 310.

15. M.A.A.F. de CT Carrondo, M. Coll, J. Aymani, A.H.J. Wang, G.A. Van der Marel, J.H. Van Boom, A. Rich; Binding of Hoechst Dye to $d(CGCGATATCGCG)_2$ and Its Influence on the Conformation of the DNA Fragment. *Biochemistry* **1989,** 28: 7849.

13.

DISSOCIATION MECHANISM OF DOUBLE-STRANDED DNA

13.1. Effect of the charge on the fragmentation pathway

Figure 13-1 shows the MS/MS spectra of a 16-mer duplex with 50% of GC base pairs for the charge states 8-, 7-, 6- and 5-. The $[duplex]^{8-}$ fragments in three competing ways:

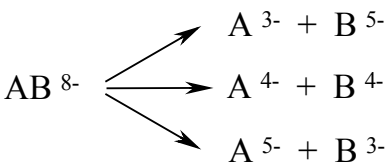

For the $[duplex]^{7-}$, the charges are spread on the two strands, and there are two possible dissociation channels, which will be called **a** and **b**:

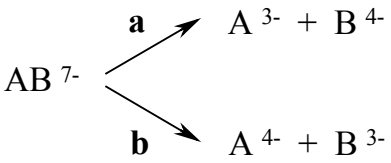

For both of these parent ion charge states, the two strands do not have the same tendency to keep the negative charges. This feature will be discussed in the next section. For the $[duplex]^{6-}$, the charges are evenly distributed ($AB^{6-} \rightarrow A^{3-} + B^{3-}$). For the $[duplex]^{5-}$, covalent fragmentation of the single strands and base loss occur instead of the noncovalent dissociation of the duplex into the single strands.

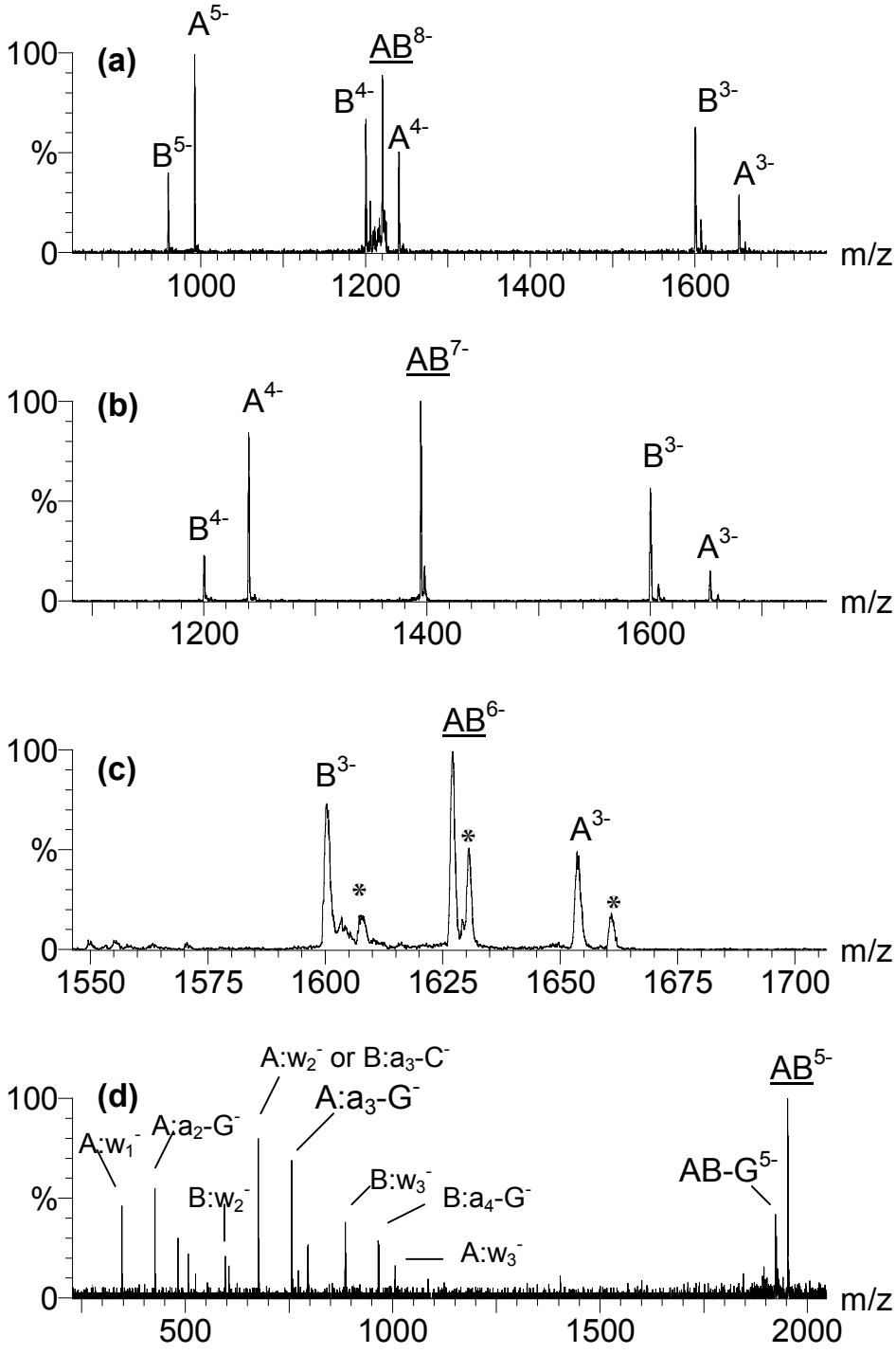

Figure 13-1. MS/MS on different charge states of a 16-mer duplex. The duplex is noted AB. Strand A: GGGCTATAATATCGGG. Strand B: CCCGATATTATAGCCC. **(a)** MS/MS on $[duplex]^{8-}$ with 12 eV collision energy (cone voltage = 17 V), **(b)** on $[duplex]^{7-}$ with 14 eV collision energy (cone voltage = 20 V), **(c)** on $[duplex]^{6-}$ with 20 eV collision energy (cone voltage = 30 V) and **(d)** on $[duplex]^{5-}$ with 30 eV collision energy (cone voltage = 45 V). The peaks marked with stars are sodium adducts.

As already mentioned in Chapter 8, higher values of the cone voltage are required to isolate duplex species of lower charge state (see Figure 8-4). We can see here that higher collision energies (as set on the instrument) are required to fragment duplexes of lower charge states. That energy (in eV) corresponds to the energy of a singly charged species. For multiply charged species, the indicated collision energy has to be multiplied by the charge of the ion to obtain the true laboratory kinetic energy. Nevertheless, even with this correction, it turns out that duplexes of lower charge states require a larger laboratory kinetic energy to start to fragment or dissociate. This is due to the Coulombic repulsion between the charges and will be discussed in section 13.4.

13.2. Charge distribution on the fragments

The uneven distribution of the charges was studied in detail for 11 duplexes (see Table 13-1 for the base sequences) by performing MS/MS on the complexes with seven negative charges. This charge state has been chosen because of the simplicity of the resulting spectra: only the two dissociation channels of interest are seen, and no fragmentation of the single strands occurs. Figure 13-2 shows the MS/MS spectra of two duplexes containing 25% of GC base pairs, each differing only in the position of the bases.

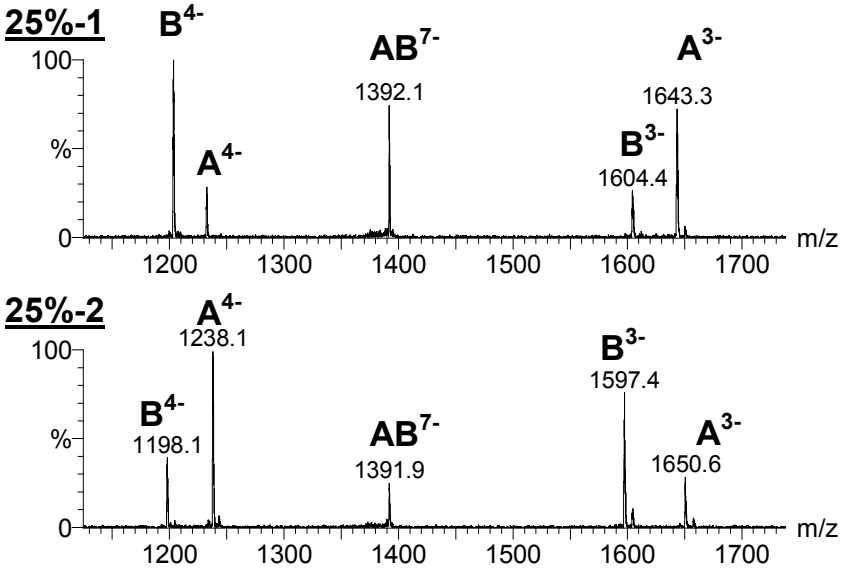

Figure 13-2. MS/MS spectra of duplexes 25%-1 (top) and 25%-2 (bottom) (see Table 13-1 for detailed base sequences) at 12 eV collision energy.

For duplex 25%-1, strand B has a greater tendency to keep negative charges, whereas for duplex 25%-2, it is strand A that has a tendency to keep more negative charges. The same measurements have been performed for all duplexes. For all of them the proportion of the two dissociation channels does not change when increasing the collision energy. The mean proportion of channel **a** ($AB^{7-} \rightarrow A^{3-} + B^{4-}$) is calculated using equation (13.1). The results are summarized in Table 13-1.

$$\% \text{ Channel } \mathbf{a} = \frac{I(A^{3-}) + I(B^{4-})}{I(A^{3-}) + I(B^{4-}) + I(A^{4-}) + I(B^{3-})}.100\% \qquad (13.1)$$

Table 13-1. Base sequences of the studied duplexes, and measured proportion of dissociation channel **a** ($AB^{7-} \rightarrow A^{3-} + B^{4-}$).

No.	Strand	Sequence	Proportion of channel a
0%-1	A: B:	5'-AAATTATAATATTAAA-3' 3'-TTTAATATTATAATTT-5'	83%
25%-1	A: B:	5'-AAATTAGCGGATTAAA-3' 3'-TTTAATCGCCTAATTT-5'	75%
25%-2	A: B:	5'-GGATTATAATATTAGG-3' 3'-CCTAATATTATAATCC-5'	30%
50%-1	A: B:	5'-AAATCGCGGCGCTAAA-3' 3'-TTTAGCGCCGCGATTT-5'	71%
50%-2	A: B:	5'-GGGCTATAATATCGGG-3' 3'-CCCGATATTATAGCCC-5'	21%
50%-3	A: B:	5'-AGACTGTGAGTCAGTG-3' 3'-TCTGACACTCAGTCAC-5'	53%
50%-4	A: B:	5'-GGGCTTTTAAAACGGG-3' 3'-CCCGAAAATTTTGCCC-5'	34%
75%-1	A: B:	5'-AATTCGCGGCGCCGGG-3' 3'-TTAAGCGCCGCGGCCC-5'	55%
75%-2	A: B:	5'-GGGCCGAATTGCCGGG-3' 3'-CCCGGCTTAACGGCCC-5'	48%
75%-3	A: B:	5'-GGGCCGTAATGCCGGG-3' 3'-CCCGGCATTACGGCCC-5'	35%
100%-1	A: B:	5'-GGGCCGCGGCGCCGGG-3' 3'-CCCGGCGCCGCGGCCC-5'	41%

When examining Table 13-1 in detail, we can not find any direct correlation between the propensity to take more negative charges and the number of a particular base contained in the strands. In fact, terminal bases are those that seem to govern the fragmentation channel. If strand A (B) has an adenine (thymine) at each end, channel **a** is preferred (see duplex 0%-1, 25%-1 and 50%-1). If strand A (B) has a guanine (cytosine) on each end, channel **b** is preferred (see duplex 25%-2, 50%-2, 50%-4, 75%-3, 100%-1). Two duplexes (50%-3 and 73%-1) have a guanine at one end of strand A and an adenine at the other end. In this case, no dissociation channel is markedly preferred. With the set of sequences studied here, it is not possible to assess whether the 5' or 3' location of the bases is a key factor for determining the distribution of the charges on the strands.

As a general rule, the negative charges therefore remain preferentially on the strands that bear guanine rather than cytosine, or thymine rather than adenine at the extremities. First, a correlation was sought with the pKa's (or better, the gas-phase acidities) of the bases, but this could not account for the adenine/thymine preference. However, a good agreement with our observations is found if the gas phase acidities of the [sugar-phosphate-sugar-base] species are considered (see Table 13-2), as the charge is located on the phosphate groups of the strands, not on the bases.

Table 13-2. Relative gas phase acidities of the [sugar-phosphate-sugar-base] species for the different bases[1]. The gas phase acidity of a species is its enthalpy of protonation. The authors used the kinetic method to determine the difference of the gas phase acidities of pairs of species, and related all their data to the gas-phase acidity of adenine (which has a $\Delta\Delta H_{acid} = 0$).

Species	$\Delta\Delta H_{acid}$ (kcal/mol)
$sugar_1$-Ⓟ-$sugar_2$-**G**	-2.4
$sugar_1$-Ⓟ-$sugar_2$-**T**	-0.4
$sugar_1$-Ⓟ-$sugar_2$-**C**	0.1
$sugar_1$-Ⓟ-$sugar_2$-**A**	1.0

We can therefore assume that the charges are distributed all along the chain, and tend to stay away from each other. This picture implies at least one charge at each extremity of the strands, and the others evenly distributed in between. The fact that the terminal base pairs are of prime importance for the distribution of the charges on the fragments is consistent with the Coulombic repulsion that forces the charges to stay apart from each other. Thereby two of them stay on the terminal phosphodiester groups[2].

Only the difference between duplexes 75%-2 and 75%-3 could not be accounted for by considering only the terminal bases. Although these two duplex differ only by the sequence of the four central base pairs, channel **b** is markedly preferred in the case of duplex 73%-3. This can be explained by considering that the charges are distributed alternatively on one strand and on the other along the duplex chain. Figure 13-3 shows that channel **b** could be favored in the case of the second duplex because the central charge is located in the vicinity of two thymines, which stabilize negative charges. In this simple picture, the distribution of the charges (which repel each other) on the duplex prior to dissociation conditions the charge distribution on the fragments.

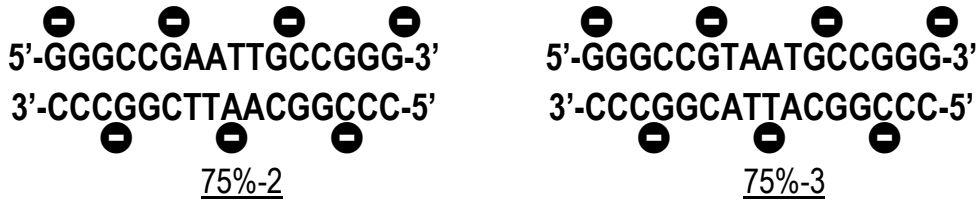

Figure 13-3. Model for the distribution of the negative charges in the case of channel **b** for duplexes 75%-2 and 75%-3.

13.3. Dissociation mechanism

Terminal unzipping of the duplex

We have seen in Chapter 11 that the duplexes can undergo neutral base loss, which is favored in slow heating conditions. The base loss from the duplex has also driven our attention for another reason: in order for the duplex to loose a base, both a covalent bond (sugar-base) and noncovalent bonds (base-base hydrogen bonds) must be broken. The duplex must therefore be in a partially unzipped state for the base loss to occur. To investigate the preferential unzipping sites, a series of 16-mer duplexes, each one containing 8 AT and 8 GC base pairs, but different sequences, has been studied. MS/MS was performed on the duplex DS^{6-} with the LCQ mass spectrometer with 8% activation amplitude during 1 s (slow heating conditions). The relative abundances of $[DS\text{-}G]^{6-}$ and $[DS\text{-}A]^{6-}$ have been measured. The results are summarized in Table 13-3. The duplex which has the A/T base pairs at terminal positions looses more readily adenine bases than a duplex with A/T and G/C base pairs equally distributed throughout the chain, and the duplex with the terminal G/C base pairs looses more readily guanines. Clearly, terminal bases are more readily lost than internal base pairs. Control experiments have confirmed that for single strands there is no such dependence on the position (data not shown). Unzipping, which is essential for base loss, therefore seems to occur preferentially at terminal base pairs.

Table 13-3. Relative intensities of adenine and guanine loss from the duplex DS^{6-} upon slow heating conditions (LCQ, 8%, 1 s). The error on the relative intensities is 2%.

Base sequence	A loss	G loss
5'-AAATCGCGGCGCTAAA-3' 3'-TTTAGCGCCGCGATTT-5'	55%	45%
5'-AGACTGTGAGTCAGTG-3' 3'-TCTGACACTCAGTCAC-5'	45%	55%
5'-GGGCTATAATATCGGG-3' 3'-CCCGATATTATAGCCC-5'	33%	67%

Proposed reaction mechanism

The separation of the duplex into its single strands is therefore not a single-step process. From a purely statistical point of view, the one-step dissociation of the duplex is highly improbable: the simultaneous breaking of dozens of hydrogen bonds would result in a very high energy activation barrier. A multi-step process, with each base pair opening requiring a small activation energy, is a more realistic hypothesis.

Assembling of all the above depicted pieces of information leads us to propose a detailed mechanism describing the collision-induced dissociation of duplex DNA (Figure 13-4).

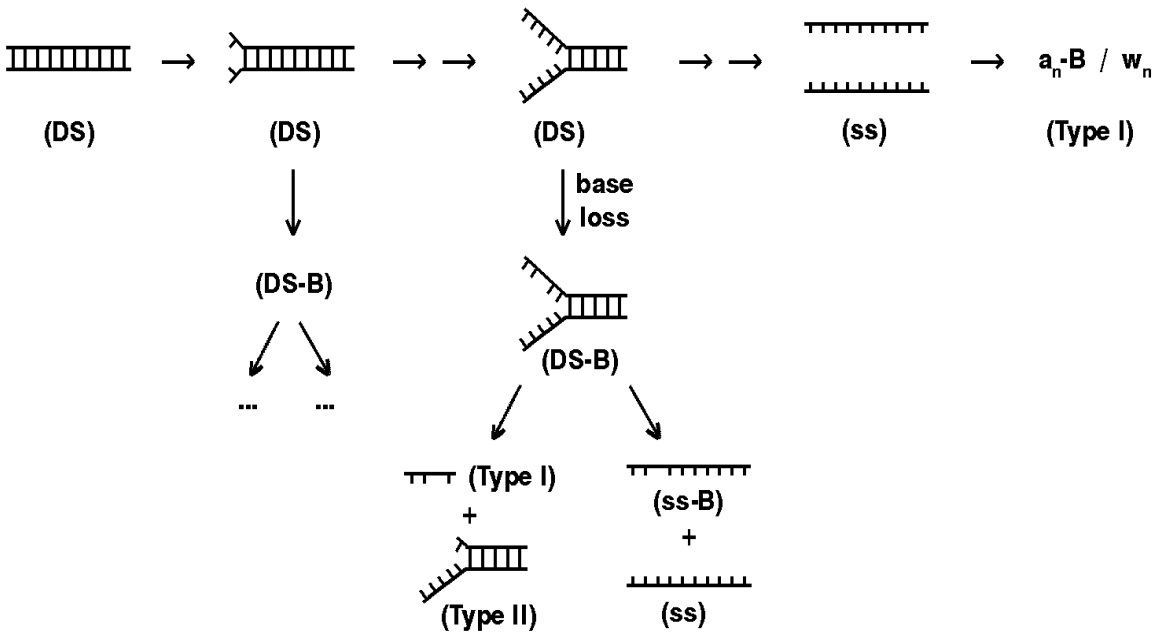

Figure 13-4. Proposed dissociation mechanism for complementary duplex DNA. Each partially unzipped state could possibly undergo base loss and subsequent fragmentation steps that are described in detail for one of the species. Base loss can occur anywhere on the partially unzipped part of the single strands (the base loss site on the figure has been chosen arbitrarily for illustration).

The duplex fragments into single strands through a multistep (preferentially terminal) unzipping process. This noncovalent dissociation channel is favored by fast activation conditions. If the single strands contain excess energy, they can fragment to produce the Type I fragments. In the course of unzipping, bases can be lost from the duplex. This is favored in slow activation conditions. This can in turn induce the backbone fragmentation of one of the single strands to produce Type II fragments, a process which is also favored by slow heating conditions. Alternatively, the [DS-B] species can carry on unzipping to produce the single strands, one of which having a missing base.

Type I fragments can be produced by two different reaction routes: (i) fragmentation of [DS-B] into Type II and the complementary Type I fragments and (ii) fragmentation of the single strands that contain excess energy. The former route is favored by slow heating conditions, while the latter is favored by fast heating conditions.

The observed dependence of the dissociation channel on the collision regime is not easy to understand. On the one hand, it may seem strange that, under slow heating conditions, a covalent bond cleavage channel is favored over the noncovalent dissociation. One would indeed expect that the threshold for the noncovalent dissociation of a base pair would be lower than the threshold for the base loss (which is in the order of 1 eV for adenine and 1.3 eV for cytosine and guanine[3]). At each branching junction of the mechanism, slow heating of the duplex should therefore favor the noncovalent dissociation. But this is not the case.

On the other hand, it must be recognized that the total amount of each type of fragment is the resultant of a complex process. The appearance of the intact single strands results from the unzipping of the duplex (consecutive reactions), while the appearance of the duplex with a base lost results from all the possible base loss channels from the partially unzipped duplex species (parallel reactions). To interpret the collision regime dependence of the dissociation channel, we must therefore consider the whole process.

The noncovalent dissociation of the duplex into the single strands is favored when the consecutive unzipping process is favored compared to the base loss branching reactions. Therefore the noncovalent dissociation channel is favored by fast heating conditions (1) because of the entropic reasons discussed before and (2) because the higher the internal energy, the faster the process, and the lesser the time spent in the partially unzipped states from which base loss can occur. Conversely, the base loss is

favored at slow activation regimes because the probability for base loss to occur increases with the time spent in the partially unzipped states. Similarly, slow heating conditions extend the time spent in partially unzipped states and thereby favor the neutral base loss and the formation of Type II fragments.

13.4. Role of the Coulombic repulsion

At this stage, it is not clear whether the unzipping is irreversible or whether the duplex can "breathe" reversibly. Nevertheless, two effects will favor the irreversible separation into the single strands: the entropy gain (see above) and the Coulombic repulsion. The latter has to be taken into account for any system dissociating into charged products. The potential energy surface for a simple bond cleavage is often represented with no reverse energy barrier, as the transition state is supposed to be loose. But this picture is valid only for the cleavage of an ion-neutral complex. When the complex dissociates into two charged species, the fragments repel each other. The extent of the repulsion depends on the charge of the fragments. The Coulombic repulsion between the fragments induces a reverse energy barrier in the section of the potential energy surface along the dissociation coordinate. This barrier is responsible for the irreversibility of the dissociation into fragments that bear charges of the same sign.

As shown above, the duplex dissociates by a multistep unzipping mechanism. For the potential energy surface, we will assume that this translates into a small energy barrier for each step (Figure 13-5). This is in agreement with recent results obtained by force spectroscopy[4,5]: experiments on streptavidin-biotin interactions (several streptavidin molecules were fixed on the cantilever) showed a force-distance curve with multiple small barriers. The entropy of the system increases after each step.

Collisional activation is necessary to pass over the barriers for the opening of the first base pairs, but as soon as the Coulombic repulsion is large enough to provide the driving force for the opening of the last base pairs, the dissociation reaction can continue even without further internal energy input. The higher the charge of the parent ion, the larger the Coulombic repulsion, and the earlier in the dissociation pathway does the irreversible separation of the fragments take place. Figure 13-5 helps

to understand the influence of the charge of the parent ion on the dissociation pathway.

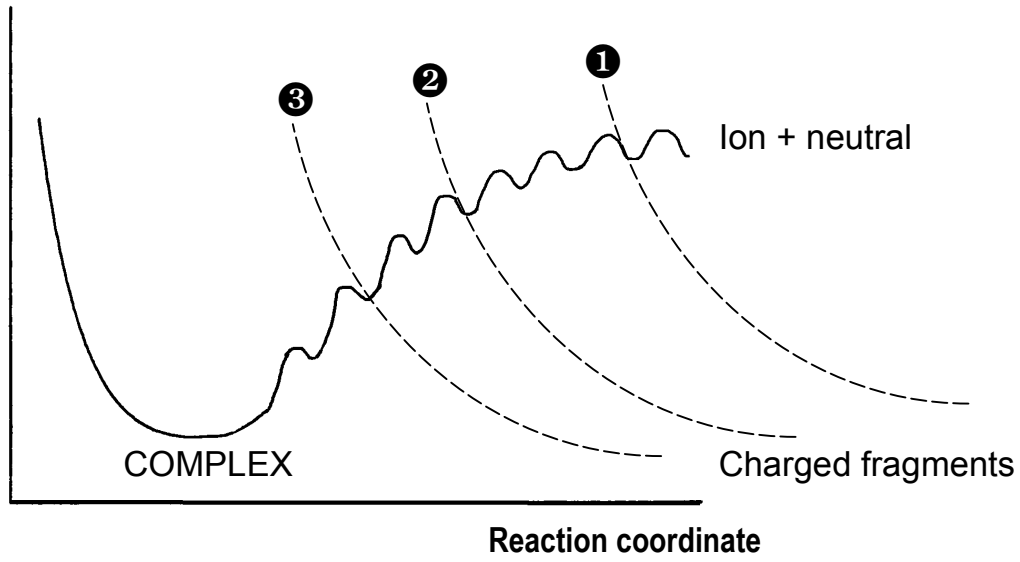

Figure 13-5. Scheme representing a hypothetical section in the potential energy surface for the dissociation of a noncovalent complex. For a DNA duplex, each small barrier corresponds to the opening of one base pair. Three Coulombic repulsion curves are shown, with the charge increasing from (1) to (3).

If the charge of the complex is low (curve 1), the Coulombic repulsion between the fragments occurs when they are almost completely separated already. Conversely, if the charge of the complex is high (curve 3), after the breaking of a few noncovalent bonds, the repulsion can be high enough to provide the driving force for the opening of the rest of the complex. This implies that the activation energy for the noncovalent dissociation decreases when the charge state increases. The noncovalent dissociation channel is enthalpically favored for the high charge states. However, the entropy of the complex increases progressively when the complex opens. The activation entropy (entropy difference between the transition state and the bound complex) increases when the charge state decreases. The noncovalent dissociation channel is therefore entropically favored for the low charge states. This quite simple picture explains the enthalpy-entropy compensation that has been observed in BIRD experiments on protein complexes of different charge states[6]. The dissociation of high charge state complexes is enthalpically favored and entropically disfavored (low E_a and low A) compared to the dissociation of low charge state complexes (which have a high E_a and a high A).

This has two major consequences for the dissociation of noncovalent complexes. The first one concerns the choice of the parent ion charge state to favor the noncovalent dissociation channel for a given collision regime. The charge state has to be high enough for the apparent threshold of the noncovalent dissociation channel to be lower than the apparent threshold for the competing covalent bond cleavages. This is illustrated for a DNA duplex in Figure 13-1: for a given collision regime (collisions in the quadrupole cell in the Q-TOF2), the noncovalent dissociation pathway is the only one observed for charge states 6- to 8-, but the covalent bond cleavages are predominant for the charge state 5-. As the apparent thresholds depend on the kinetic shift, the choice of the charge state depends on the collision regime and on the reaction time. For the same duplex, base loss already occurs when performing MS/MS in the LCQ (activation time = 1 s) on the charge state 6- (see Table 13-3).

The proposed dissociation model has another important implication. The apparent total activation energy depends on the sum of the small energy barriers that have to be overcome before reaching the transition state. On the section in the potential energy surface for the dissociation, the transition state is defined as the point that irreversibly separates the reactant from the products. If the Coulombic repulsion becomes predominant after the breaking of all the individual noncovalent interactions, then the apparent activation energy depends on all the small energy barriers, and therefore on the total contribution of the interactions implied in the complex. However, if the Coulombic repulsion becomes predominant after the breaking of the first few interactions, the transition state is closer to the reactants. The apparent activation energy only depends on the few interactions that have to be broken before the repulsion becomes the driving force of the dissociation reaction. In that case, the dissociation rate would depend not on all the interactions at the interface of the complex, but only on the few interactions that need to be broken before the irreversible dissociation occurs. This implies that the reaction rate is more likely to reflect the total contribution of the noncovalent interactions at the interface of the complex when performing MS/MS on low charge states than on high charge states.

This hypothesis is still to be confirmed, but a piece of evidence is shown in the MS/MS results on the DNA 16-mer duplexes. MS/MS was performed on the charge states 6- and 7- for duplexes of different percentages of GC base pairs (Figure 13-6).

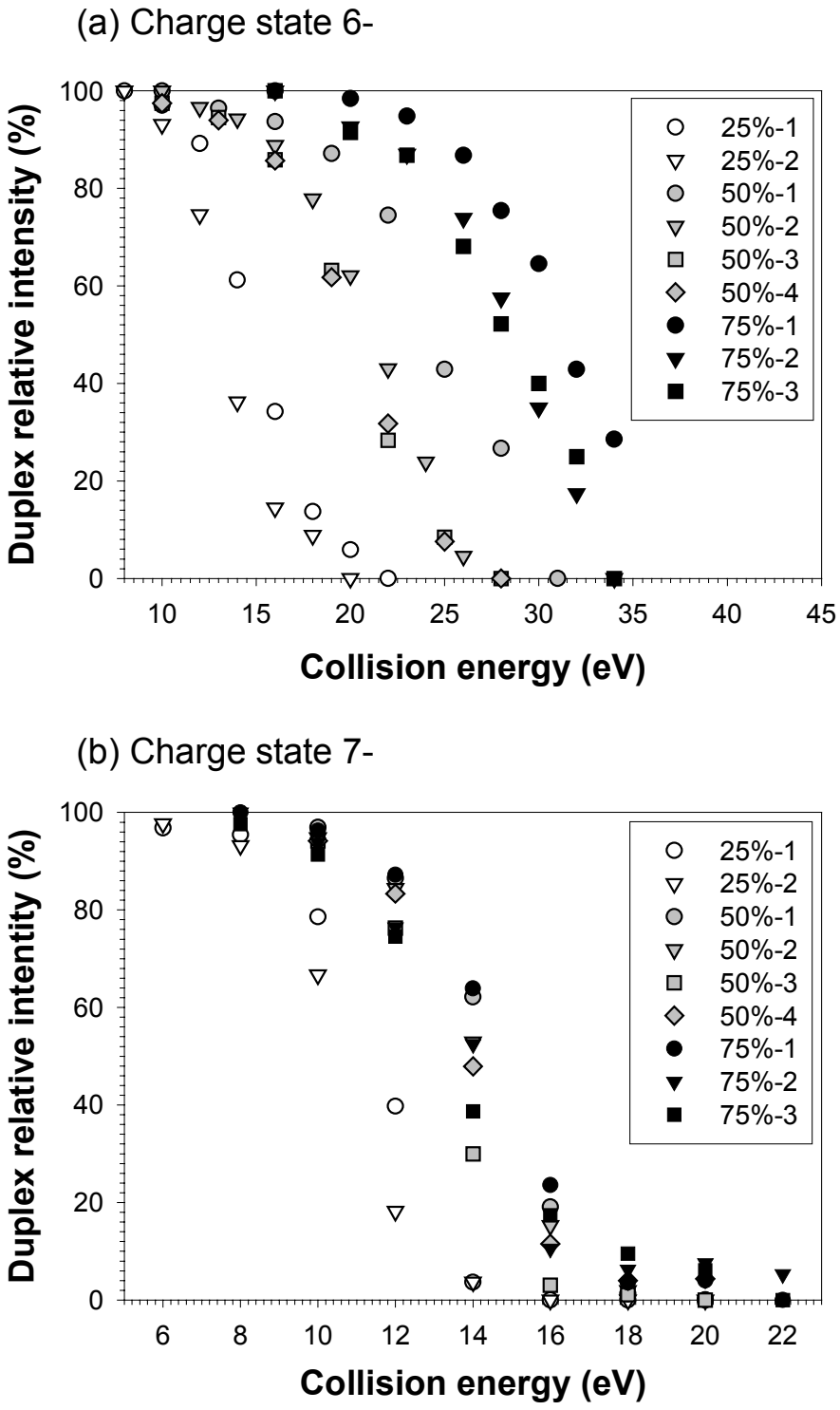

Figure 13-6. Superimposed dissociation curves for 16-mer duplex of different percentages of GC base pairs (see Table 13-1 for the base sequences). Experiments were performed on the Q-TOF2 for **(a)** the charge state 6- (cone voltage = 30 V) and **(b)** the charge state 7- (cone voltage = 20 V).

In the dissociation curves of the $[duplex]^{6-}$, there is a marked difference in the collision energy necessary to dissociate the complexes with 25% GC (white symbols), 50% GC (gray symbols) and 75% GC base pairs (black symbols). The differences between the duplexes of the same GC percentage is due to base stacking. In the case of $[duplex]^{7-}$, however, the dissociation curves are much closer to each other. The dissociation rate is therefore not so much dependent on the total number of hydrogen bonds in the duplex in the MS/MS experiments than on the higher charge state.

References

1. S. Habibi-Goudarzi, S.A. McLuckey; Ion Trap Collisional Activation of the Deprotonated Deoxymononucleoside and Deoxydinucleoside Monophosphates. *J. Am. Soc. Mass Spectrom.* **1995,** 6: 102.

2. A. Favre, F. Gonnet, J.C. Tabet; Location of the Negative Charge(s) on the Backbone of Single-Stranded Deoxyribonucleic Acid in the Gas Phase. *Eur. J. Mass Spectrom.* **2000,** 6: 389.

3. J.S. Klassen, P.D. Schnier, E.R. Williams; Blackbody Infrared Radiative Dissociation of Oligonucleotide Anions. *J. Am. Soc. Mass Spectrom.* **1998,** 9: 1117.

4. A. Janshoff, M. Neitzert, Y. Oberdörfer, H. Fuchs; Force Spectroscopy of Molecular Systems - Single Molecule Spectroscopy of Polymers and Biomolecules. *Angew. Chem. Int. Ed. Engl.* **2000,** 39: 3212.

5. A. Janshoff, C. Steinem; Energy Landscapes of Ligand-Receptor Couples Probed by Dynamic Force Spectroscopy. *Chem. Phys. Chem.* **2001,** 2: 577.

6. N. Felitsyn, E.N. Kitova, J.S. Klassen; Thermal Decomposition of a Gaseous Multiprotein Complex Studied by Blackbody Infrared Radiative Dissociation. Investigating the Origin of the Asymmetric Dissociation Behavior. *Anal. Chem.* **2001,** 73: 4647.

14.

GENERAL DISCUSSION AND CONCLUSIONS

The goal of our work was to contribute to the study of noncovalent interactions by electrospray mass spectrometry (ES-MS). We focused on two fundamental questions:

1. Do the species detected by ES-MS reflect the composition of the injected solution?

2. What kind of information can be extracted from the gas-phase measurements?

We therefore studied some simple model complexes for which the stoichiometries, structures and thermodynamic stabilities in solution had been well studied already: DNA duplexes, duplex-drug complexes, and cyclodextrin complexes with aliphatic acids. The mass spectrometric experiments were carried out on a Finnigan LCQ (electrospray quadrupole ion trap instrument) and a Micromass Q-TOF (electrospray hybrid quadrupole time-of-flight instrument).

14.1. Do the species detected by ES-MS reflect the composition of the injected solution?

Compromise between desolvation and stability

To maximize the chances for the mass spectra to reflect the composition of the solution, the electrospray source conditions must be as soft as possible. This means that the instrumental parameters are tuned to transfer little internal energy to the complex to reduce its dissociation. In practice, this is a compromise between giving enough energy to desolvate the complex and not giving too much energy so that complex remains intact. This means that when the complex undergoes the last desolvation steps, there is a competition between the breaking of the noncovalent bonds between the complex and the very last solvent molecules and the breaking of the noncovalent bonds of the complex itself. It can therefore be concluded that the intact desolvated complex can only be observed if the intermolecular interactions in the complex are stronger than the interactions with the solvent.

Hydrophobic complexes

The interaction between cyclodextrins and their guest molecules is mainly a hydrophobic interaction in solution. Upon removal of the solvent, the main driving force for the inclusion of the diacid in the cyclodextrin disappears. At the best, some weak van der Waals interaction may persist at the contact region between the interior of the cyclodextrin and the guest. However, it must not be forgotten that the mass spectrometer analyses charged species, and therefore charged complexes. This means that any complex detected by ES-MS is stabilized by ion-neutral and/or ion-ion interactions, which are by nature very strong. In the case of the cyclodextrin complexes, the ion-neutral interactions between the polar groups of the cyclodextrin and the diacid do certainly surpass the contact interactions between the polar groups of the two molecules. This implies that the removal of the solvent causes a complete reversal of the relative scale of the interactions. In solution, electrostatic interactions are shielded by the dielectric constant of the solvent and hydrophobic interactions are favorable. In the gas phase, the dielectric constant drops to unity, and there is no kind

of entropically favorable medium effect. It is therefore not surprising that some nonspecific (non-inclusion) complexes formed due to the electrospray process could be observed in the case of the cyclodextrin complexes.

Biological complexes

The problem of nonspecific aggregation due to electrostatic interactions is believed to be widely encountered when investigating hydrophobic complexes by mass spectrometry. What can therefore be predicted for the study of biological complexes in general? In molecular biology, there is a long and lively debate about how important are the relative interactions for the formation of complexes. Hydrophobic interactions usually contribute greatly to the stability of the complexes: there is often a nice correlation between the binding constant and the contact surface area between the partners of the complex. It may therefore appear relatively tricky to study these complexes by electrospray. Nevertheless, it must be kept in mind that hydrophobic interactions are not local, but constitute a global entropic effect that favors the bringing together of nonpolar surfaces. However, the specificity of a complex, which is essential for its function, is induced by directional interactions (ion-ion, ion-dipole, hydrogen bonds,…) between complementary donor-acceptor sites at the interface. As explained above, these interactions are maintained, and even reinforced when the solvent is removed. We can therefore reasonably expect that electrospray mass spectrometry will be convenient for the specific detection of most biological complexes, with, as exception, the complexes that are stabilized almost only by hydrophobic interactions.

Quantitative aspects

The quantitative aspects of the ES-MS technique regarding the exactness of the determination of equilibrium binding constants were also studied. The quickest method to determine binding constants by ES-MS is to assume that the relative intensities of the complex and the free ligand are directly proportional to the relative abundance of these species in the injected solution. Another possibility is to compare the binding of different ligands for a given substrate by handling competition experiments, assuming that the intensity recorded for the different complexes is

proportional to their relative abundance in solution. This competition approach has been applied to drug-DNA complexes. Whether the amount of ions detected is proportional to the concentration in solution depends on many factors: the distribution of the analytes in the charged electrospray droplets, the efficiency of ion emission from the droplets, the transmission of the mass analyzer, and the efficiency of the detector. For the relative intensities of two species to be exactly proportional to their concentration in solution, all these factors have to be identical. It is often possible to modify the transmission of the analyzer by a careful selection of the experimental parameters so as to ensure that there is no discrimination between the species of interest. The discrimination due to the efficiency of the detector is more difficult to avoid. In general, this discrimination is slightly dependent on the mass, but much more dependent on the charge of the ion. Comparing the relative intensities of the species of the same charge state is therefore recommended.

Influence of the electrospray process on the response factors

The last discrimination factor is related to the electrospray process itself: the analytes present in solution have to become ions in the gas phase. The equilibrium partitioning model states that the response of an analyte is proportional to its affinity for the surface of the droplet. The surface affinity can vary with the size of the molecule, its conformation, its charge, and mostly with the distribution of polar/nonpolar groups on the surface. On the basis of theoretical considerations, we can therefore infer some general rules concerning the feasibility of the determination of absolute and relative binding constants by ES-MS. We also developed a method that allows us to determine experimentally the equilibrium association constant for [1:1] complexes and the ratio of the responses of the complex and the free ligand. In the case of the DNA complexes with minor groove binders, the response factors of the complexes and of the duplex were found to be similar. This can be attributed to the fact that the conformation of the double helix of DNA is little disturbed by the small drug that fits almost exactly into the minor groove, and small changes in the response factors could indicate small changes in the duplex conformation upon ligand binding. In the case of cyclodextrin complexes, the response of the cyclodextrin and of the complexes differ greatly. This can be due to two factors. First, we compare the response of the doubly charged complex to the response of the cyclodextrin (singly + doubly charged). Second, the

diacid aliphatic chain may not be included in the cavity of the cyclodextrin, and the exposure of the nonpolar chain to the solvent increases the surface activity of the complex. The latter hypothesis is in agreement with our observation that the response of the complex increases with the diacid chain length.

Charge state distributions

The problem of correlation between the charge state distribution in solution and the charge state distribution observed in the electrospray mass spectra deserves some special attention. Our observations on the diacids and on the cyclodextrin complexes tend to indicate that the charge state in solution has a very little (if any) influence on the ES-MS charge state distribution. The case of the DNA complexes is also intriguing. At first sight it might seem strange that, in the negative ion mode, the complexes with positively charged drugs show a charge state distribution analog to that of the free duplex. If the most intense charge state for the free duplex is 5-, it is the same for the complex, even if the drug has two permanent positive charges. This means that in the $[complex]^{5-}$, there are seven negative charges located on the phosphate groups of the DNA and two positive charges on the drug. Even so, the response factors of the $[duplex]^{5-}$ and the $[complex]^{5-}$ are very similar. If we consider the ion evaporation model (equation 2.2), this means that the transition state is late enough so that only the total charge influences the activation energy for taking the ion out of the droplet. In conclusion, although the maximum charge states is conditioned by the total number of basic or acidic sites in the positive or negative ion mode respectively, the observed charge state distribution merely depends on the size of the molecule. This is in agreement with the model proposed by J.B. Fenn[1]: "…the spacing of the charges on a desorbed ion must relate to the spacing of the charges on the surface of the droplet…". In other words, the larger the surface of the droplet occupied by the molecule, the higher the number of charges that can be fixed when the molecule leaves the droplet.

---

[1] J.B. Fenn; Ion Formation From Charged Droplets: Roles of Geometry, Energy and Time. *J. Am. Soc. Mass Spectrom.* **1993,** 4: 524.

14.2. What kind of information can be extracted from the gas-phase measurements?

The CID method

In the second part of our work, we focused on the collision-induced dissociation of the complexes in the gas phase. The relative intensities of the intact complex and of the fragments depend on the dissociation kinetics of the complex. It is currently impossible to determine the amount of internal energy transferred to large molecules in collisional activation (multiple collisions conditions). Quantitative values of the activation energy and the activation entropy can only be obtained with the BIRD method, by an Arrhenius treatment of the temperature dependence of the rate constant. In CID, only qualitative results can be obtained by comparing series of homologous complexes. To ensure that the same internal energy is given to all the members of a series under given experimental conditions, only complexes of the same mass and same number of degrees of freedom were compared.

Activation energy and activation entropy

In the current literature, the interpretation of ion dissociation is based on the concepts of the RRKM statistical theory of unimolecular dissociation. The microcanonical rate constant $k(E)$ depends on an enthalpic term (the critical energy E_0, which is the energy difference between the reactant and the transition state), and on the activation entropy (through a degeneracy factor σ and the density of states of the reactant and the transition state). The transition state is defined as the point on the section in the potential energy surface that irreversibly separates the reactant from the products. At a given internal energy, the dissociation rate (and therefore the fragmentation ratio) depends on an enthalpic factor and an entropic factor. The enthalpic factor is supposed to reflect the strength of the noncovalent interactions. However, the role of the activation entropy is poorly understood, and is currently neglected to some extent. When performing comparisons between complexes, the activation entropies can be assumed to be the same if the reaction mechanisms are the same. Only complexes dissociating via the same reaction channel can therefore be compared.

Duplex DNA: competition between noncovalent dissociation and covalent fragmentation

We then studied the collision-induced dissociation of DNA duplexes in detail, and performed CID measurements at different collision regimes. We could observe a competition between two reaction channels: the noncovalent dissociation of the duplex into single strands, and the neutral base loss from the duplex (a covalent bond cleavage). The noncovalent dissociation is entropically favored compared to the covalent fragmentation, and is therefore favored at high internal energies (fast reaction times). However, the base loss proceeds by a rearrangement mechanism, and is therefore entropically disfavored. This implies that, in order to favor the noncovalent dissociation channel, it is preferable to use fast activation conditions instead of slow heating methods. This was also observed in the CID of DNA complexes with different drugs. As a result, BIRD, which is a slow heating method, is not applicable for complexes that undergo low-threshold fragmentation.

Strength of noncovalent interactions in the gas phase

We further studied the CID of series of homologous complexes (always of the same mass) in fast activation conditions (MS/MS on the Q-TOF, or source-CID). It was assumed that the activation entropies were the same, and therefore that the abundance of the fragments was proportional to the activation energy. The activation energy is supposed to reflect the strength of the noncovalent interactions in the gas phase (this point is discussed further below). With these assumptions, the relative strength of the intermolecular interactions in the gas phase could be compared to their strength in solution. The correlation between the number of hydrogen bonds and the resistance to CID was found to be excellent, both in the case of DNA duplexes and their complexes with minor groove binders. There is also a nice correlation between the sequence-dependence of the stability of the duplexes in solution and in the gas phase. This suggests that the base stacking interactions, which are responsible for that sequence dependence, are maintained in the gas-phase complexes. This is a very important result because stacking interactions are short range interactions. If they remain in the gas phase, this indicates that the conformation of the double helix is little disturbed compared to its conformation in solution. The helix seems not to unwind in the gas phase, at least on the time scale of our experiments. Nevertheless, this does not necessarily mean that this corresponds to the most stable structure in the gas phase (the

global minimum in the potential energy landscape). It has recently be suggested that electrospray-produced ions could be trapped in a local minimum, due to the softness of the ionization method[2]. This concept is particularly interesting. As the complexes can be produced from quasi-native solutions by electrospray, it means that the conformation of these species trapped in local minima may be closer to the conformation in solution than if they were in the global minimum.

The gas phase dissociation experiments that can be performed in mass spectrometry can be very useful as a complementary tool for the study of the noncovalent interactions between molecules. However, one should not especially expect a correlation between the stability in solution and the relative energy required for the gas-phase dissociation to occur. Actually, gas phase dissociation experiments allow to probe the contribution of the intermolecular interactions between the partners. This is particularly useful if the structure of the complex in the gas phase is close to the structure in solution.

MS/MS experiments give an important insight in one of the most important issues of molecular biology, namely the relative contribution of the different interactions to the stability and the specificity of complexes. This was illustrated by our results on the DNA complexes with the isomers cryptolepine and neocryptolepine. The driving force in solution for the intercalation of theses nonpolar molecules between the bases of the DNA is certainly the hydrophobic effect, but our results show that the difference in affinity is due to intermolecular interactions (electrostatic, Van der Waals,…). This kind of contribution is difficult to sort out by performing studies in solution only.

Dissociation mechanism of noncovalent complexes with a large interaction interface

Multistep dissociation

In Chapter 13, we proposed a general model for the dissociation of noncovalent complexes. The usual picture supposes that the dissociation of large complexes is a

---

[2] A.S. Danell, G.L. Glish; Evidence for Ionization-Related Conformational Differences of Peptide Ions in a Quadrupole Ion Trap. *J. Am. Soc. Mass Spectrom.* **2001,** 12: 1331.

one-step process, characterized by an energy barrier E_0 and an activation entropy. This simplistic view based on the RRKM theory is inherited from earlier studies on small molecules. We propose that the dissociation mechanism involves multiple intermediates, and that a one-step scheme may be too simplistic. Supramolecular assemblies are usually held together by multiple co-operating interactions (hydrogen bonds, Coulombic or shorter range electrostatic interactions, Van der Waals bonds,…). Each interaction alone would be insufficient to stabilize the complex, but together they can lead to a very strong complex provided that the constitutive ligands are adequately arranged in space. From a purely statistical point of view, the simultaneous breaking of all the noncovalent bonds at the same time is highly improbable, and the dissociation of noncovalent complexes involving multiple interaction sites is therefore more likely to proceed via a multi-step dissociation process. Evidence for this multistep unzipping has been provided for the dissociation of duplex DNA, by the study of the competition between the noncovalent dissociation and the neutral base loss. For double-stranded DNA, the unzipping starts preferentially at the terminal base pairs. In terms of potential energy surface, the consequence of a multistep dissociation is the formation of intermediates between the intact complex and the fragments corresponding to partially unzipped states. These intermediates are separated by small energy barriers corresponding to the breaking of individual noncovalent interactions. Moreover, the entropy of the complex increases after the breaking of each noncovalent interaction.

Role of the charge repulsion between the fragments

Another important feature of the noncovalent dissociation of large multiply charged complexes is that they dissociate into charged fragments which repel each other. This repulsion has to be taken into account in the dissociation mechanism and in the potential energy surface. On the basis of our results on the charge distribution on the DNA single strands, and of our discussion of the charge states produced by electrospray, we assume that the charge is distributed homogeneously on the whole complex. During the multistep dissociation, there is a critical point where the Coulombic repulsion between the strands becomes sufficiently large to provide the driving force that separates the fragments irreversibly. This critical point is, by definition, the transition state. If the Coulombic repulsion becomes predominant only after the breaking of all the individual noncovalent interactions, this corresponds to a late transition state. The activation enthalpy is high (unfavorable), and depends on the sum of the contributions of all the noncovalent interactions at the interface of the complex. The activation entropy is also high (favorable), as the complex has already

gained much conformational freedom at the transition state. However, if the Coulombic repulsion is high enough to become predominant after the breaking of only a few noncovalent bonds, then both the activation enthalpy and entropy are lower than in the previous case. More importantly, the dissociation rate may not reflect the contribution of all the interactions, but only the contribution of those of which the breaking constitutes the rate limiting step in the dissociation. This is supposed to be more probable for more highly charged complexes. Our hypothesis is to be checked further, but preliminary results on duplex DNA 16-mers of charge state 6- and 7- tend to indicate that the higher the charge state, the lesser the dissociation reflects the contribution of all base pairs.

Outlook

As a general conclusion, this work has shown current applications, limitations and perspectives of the use of electrospray mass spectrometry for the study of noncovalent interactions. In particular, mass spectrometry is the only method allowing an experimental study of complexes in the absence of solvent. In that respect, it would be very useful to provide experimental data that can eventually be correlated with theoretical calculations. In order to achieve that goal, mass spectrometric measurements badly need to become more quantitative, and one step in that direction would be the characterization of the internal energy distribution the ions acquire upon collision-induced dissociation, which is by far the most extensively used activation method. Bringing together theory and experiment will ultimately, we hope, give rise to a new approach for studying the dissociation of noncovalent complexes, and thereby getting some more insight into the fascinating mechanisms of molecular recognition.

15.
FURTHER READING

1. V. Gabelica, F. Rosu, E. De Pauw; The Interaction between Antitumor Drugs and a Double-stranded Oligonucleotide Studied by Electrospray Ionization Mass Spectrometry, *J. Mass. Spectrom* **1999,** 34: 1328-1337.

2. V. Gabelica, F. Rosu, C. Houssier, E. De Pauw; Gas Phase Thermal Denaturation of Oligonucleotide Duplex and Complexes with Minor Groove Binders, *Rapid Commun. Mass Spectrom.* **2000,** 14: 464-467.

3. V. Gabelica, E. De Pauw; Comparison between Solution Phase Stability and Gas Phase Kinetic Stability of Oligodeoxynucleotide Duplexes, *J. Mass Spectrom*. **2001**, 36: 397-402.

4. V. Gabelica, E. De Pauw; Comparison of the Collision-Induced Dissociation of Duplex DNA at Different Collision Regimes: Evidence for a Multistep Dissociation Mechanism, *J. Am. Soc. Mass Spectrom.* **2002**, 13: 91-98.

5. V. Gabelica, E. De Pauw; Collision-induced dissociation of 16-mer DNA duplexes with various sequences: evidence for conervation of the double helix conformation in the gas phase, *Int. J. Mass Spectrom.*, in press.

6. V. Gabelica, N. Galic, F. Rosu, C. Houssier, E. De Pauw; Determination of Equilibrium Association Constants of Noncovalent Complexes by Electrospray Ionization Mass Spectrometry with No Approximation on the Response Factors, submitted.

7. N. Galic, V. Gabelica, E. De Pauw; On the Specificity of Cyclodextrin Complexes Detected by Electrospray Mass Spectrometry, submitted.